ADVANCES IN MANAGEMENT AND TREATMENT OF HIGH MYOPIA AND ITS COMPLICATIONS

EDITED BY: Xiangjia Zhu, Yi Lu, Xiangtian Zhou, Xingchao Shentu and Quan V. Hoang

PUBLISHED IN: Frontiers in Medicine

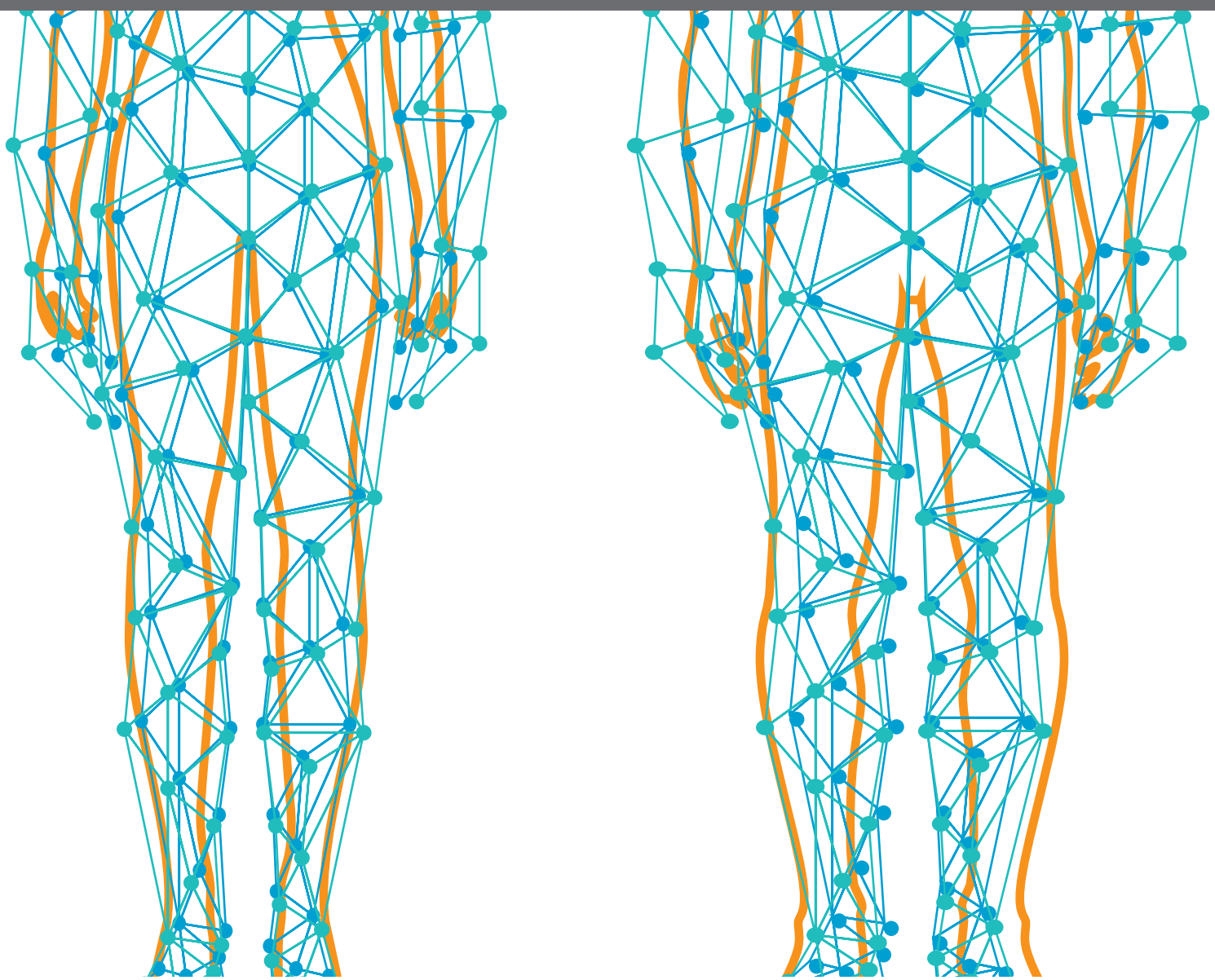

frontiers Research Topics

ISSN 1664-8714
ISBN 978-2-88974-819-8
DOI 10.3389/978-2-88974-819-8

About Frontiers

Frontiers is more than just an open-access publisher of scholarly articles: it is a pioneering approach to the world of academia, radically improving the way scholarly research is managed. The grand vision of Frontiers is a world where all people have an equal opportunity to seek, share and generate knowledge. Frontiers provides immediate and permanent online open access to all its publications, but this alone is not enough to realize our grand goals.

Frontiers Journal Series

The Frontiers Journal Series is a multi-tier and interdisciplinary set of open-access, online journals, promising a paradigm shift from the current review, selection and dissemination processes in academic publishing. All Frontiers journals are driven by researchers for researchers; therefore, they constitute a service to the scholarly community. At the same time, the Frontiers Journal Series operates on a revolutionary invention, the tiered publishing system, initially addressing specific communities of scholars, and gradually climbing up to broader public understanding, thus serving the interests of the lay society, too.

Dedication to Quality

Each Frontiers article is a landmark of the highest quality, thanks to genuinely collaborative interactions between authors and review editors, who include some of the world's best academicians. Research must be certified by peers before entering a stream of knowledge that may eventually reach the public - and shape society; therefore, Frontiers only applies the most rigorous and unbiased reviews.
Frontiers revolutionizes research publishing by freely delivering the most outstanding research, evaluated with no bias from both the academic and social point of view. By applying the most advanced information technologies, Frontiers is catapulting scholarly publishing into a new generation.

What are Frontiers Research Topics?

Frontiers Research Topics are very popular trademarks of the Frontiers Journals Series: they are collections of at least ten articles, all centered on a particular subject. With their unique mix of varied contributions from Original Research to Review Articles, Frontiers Research Topics unify the most influential researchers, the latest key findings and historical advances in a hot research area! Find out more on how to host your own Frontiers Research Topic or contribute to one as an author by contacting the Frontiers Editorial Office: frontiersin.org/about/contact

ADVANCES IN MANAGEMENT AND TREATMENT OF HIGH MYOPIA AND ITS COMPLICATIONS

Topic Editors:
Xiangjia Zhu, Fudan University, China
Yi Lu, Fudan University, China
Xiangtian Zhou, Wenzhou Medical University, China
Xingchao Shentu, Zhejiang University, China
Quan V. Hoang, Duke-NUS Medical School, Singapore

Citation: Zhu, X., Lu, Y., Zhou, X., Shentu, X., Hoang, Q. V., eds. (2022). Advances in Management and Treatment of High Myopia and Its Complications. Lausanne: Frontiers Media SA. doi: 10.3389/978-2-88974-819-8

Table of Contents

frontiers in Medicine

EDITORIAL
published: 10 March 2022
doi: 10.3389/fmed.2022.846540

Editorial: Advances in Management and Treatment of High Myopia and Its Complications

Quan V. Hoang[1,2,3], Xavier Chan[1], Xiangjia Zhu[4], Xiangtian Zhou[5], Xiangchao Shentu[6] and Yi Lu[4]*

[1] Singapore Eye Research Institute, Singapore National Eye Centre, Duke-NUS, Singapore, Singapore, [2] Department of Ophthalmology, Yong Loo Lin School of Medicine, National University of Singapore, Singapore, Singapore, [3] Department of Ophthalmology, Edward S. Harkness Eye Institute, Columbia University College of Physicians and Surgeons, New York, NY, United States, [4] Eye Institute, Eye & ENT Hospital, Fudan University, Shanghai, China, [5] School of Optometry and Ophthalmology and Eye Hospital, Wenzhou Medical University, Wenzhou, China, [6] Department of Ophthalmology, The Second Affiliated Hospital of Zhejiang University, College of Medicine, Hangzhou, China

Keywords: high myopia (HM), pathologic myopia, refractive surgery, cataract surgery, highly myopic cataract (HMC), myopic traction maculopathy (MTM), myopic macular degeneration, myopic choroidal neovascularization (mCNV)

Editorial on the Research Topic

Advances in Management and Treatment of High Myopia and Its Complications

High myopia (HM), or extreme near-sightedness, is a leading cause of blindness worldwide. By 2050, it is estimated that 4.8 billion people will have myopia worldwide, of which almost a billion will have HM (1). HM is due to progressive, lifelong and extreme eye elongation with subsequent eye wall (sclera) thinning; which may lead to localized, posterior eye shape changes (focal, ectatic outpouchings called *staphyloma*), which often precede or are concurrent with the onset of degenerative myopic macular degeneration (MMD) (2, 3). The main threats to vision in a HM patient are the development of MMD, staphyloma and macular traction maculopathy (MTM), and myopic choroidal neovascularization (mCNV) (4–8). The treatment options for the non-neovascular posterior segment manifestations of PM are scarce, but include novel approaches to achieve posterior scleral reinforcement such as with macular buckles, scleral allografts and various scleral collagen crosslinking agents (2, 8). In terms of anterior segment changes, cataract surgery and refractive surgeries in HM eyes has less predictable outcomes vs. emmetropic eyes, and require more careful pre-operative assessment and planning. Over the past decades, several groups of clinicians and scientists have investigated the pathologies, governing mechanisms, diagnostic and therapeutic options for high myopia and documented complications in tandem. In this issue of Frontiers in Medicine, advancements in the management and treatment of both the posterior and anterior segment manifestations of high myopia (HM) were investigated.

In terms of posterior segment manifestations, pathologic myopia (PM) tends to come in three main forms, the degenerative myopic atrophy maculopathy (MAM, including MMD), the tractional MTM, and the neovascular myopic neovascular maculopathy (or mCNV). Tey et al. demonstrated in the Myopic and Pathologic Eyes in Singapore (MyoPES) cohort that greater prevalences of degenerative forms of pathologic myopia (PM) occurred in eyes longer than 27.5 mm and prevalences of tractional forms of PM were greater in eyes longer than 29.0 mm (Ky et al.). Tian et al. investigated the association between the tractional and degenerative forms of PM in eyes and found that over 72% of their cohort with definite myopic retinoschisis also displayed diffuse chorioretinal atrophy.

Edited and reviewed by:
Jodhbir Mehta, Singapore National Eye Center, Singapore

****Correspondence:***
Quan V. Hoang
donny.hoang@singhealth.com.sg

Specialty section:
This article was submitted to Ophthalmology, a section of the journal Frontiers in Medicine

Received: *31 December 2021*
Accepted: *07 February 2022*
Published: *10 March 2022*

Citation:
Hoang QV, Chan X, Zhu X, Zhou X, Shentu X and Lu Y (2022) Editorial: Advances in Management and Treatment of High Myopia and Its Complications. Front. Med. 9:846540. doi: 10.3389/fmed.2022.846540

In terms of degenerative forms of PM, Shi et al. employed non-invasive quantitative and qualitative measurements of retinal and choroidal microvasculature using optical coherence tomographic angiography (OCTA) and found that a longer baseline AL was associated with larger changes of macular vessel density in the inner-inferior, inner-temporal and outer-temporal sectors (Shi et al.). Specifically, on swept source OCTA, in a Singaporean case-control study, Wong et al. report lower macular vessel density (VD) and smaller superficial FAZ area were found in adolescent and young adults with HM compared to those without. Moreover, in a cross-sectional, population-based study of young adults focused on fundus tessellation, Lyu et al. report that tessellation was found to be significantly correlated with AL, scleral thinning and choroidal thinning (particularly in the macula-papillary region). Early indicators for choroidal thickness in young myopic patients were also investigated by Sun et al. who used a machine learning approach with quantifiable models of imaging features and early changes of optic disc and peripapillary region were found to be significantly correlated with choroidal thickness. Meng et al. observed in a retrospective study of 1,692 patients that cilioretinal arteries were found to be associated with MMD, and proposed a photographic classification system and suggested cilioretinal arteries may afford a protective effect (e.g., better visual acuity) when present in HM eyes in a retrospective study.

In patients who develop mCNV, Xie et al. performed a study to assess the relationship between mCNV presence with choroidal thickness and scleral thickness. Intriguingly, over 78% of their cohort of 88 mCNV eyes had nearby scleral perforated vessels detected. For mCNV eyes undergoing treatment with anti-vascular endothelial growth factor (VEGF), Wang, Hu, et al. used an OCTA-based analysis and highlighted vessel junctions as a potential predictive biomarker for early therapeutic response to anti-VEGF therapy.

The treatment options for the non-neovascular posterior segment manifestations of PM are scarce. In terms of posterior scleral reinforcement (PSR) of the posterior pole, Zhang et al. reported short-term improvements in choroidal thickness and choroidal blood flow 1 month post-PSR. Recently, a novel approach to target the sclera by weakening, thinning, and expanding the sclera *via* scleral collagen cross-linking (SXL) have been proposed to halt the progression of myopia, thereby preventing aberrant scleral remodeling (Wang, Corpuz, et al.). For patients who develop myopic foveoschisis (MF) with foveal detachment, Yao et al. employed pars plana vitrectomy with silicone oil (SO) tamponade but without internal limiting membrane peeling, which was found to result in complete MF resolution and foveal re-attachment with no macular hole formation in a case series of 3 patients.

In terms of advancements in the management of anterior segment manifestations of HM, Zhao et al. reported greater variation in peripheral ACD and anterior chamber angle (ACA) after toric vs. non-toric implantable collamer lenses (ICL) and suggest that pre-operative anterior chamber structure and value affect postoperative peripheral ACD and ACA. Moreover, He et al. reported that risk of low vision post-cataract surgery, when treatment was performed by a junior surgeon, is greater in eyes with known macular complications, higher corneal astigmatism, longer axial length and thinner subfoveal choroidal thickness. In an attempt to improve the accuracy of intraocular lens (IOL) power prediction for cataract surgery with IOL implantation in HM eyes, Wei et al. developed a machine learning-based XGBoost calculator in order to improve the accuracy of IOL power predictions in highly myopic cataract (HMC) patients. Zhu et al. demonstrated that among their cohort of 142 HM eyes with cataracts, those with anterior chamber depth (ACD) $>$ 3 mm benefited from femtosecond laser capsultomy in terms of superior capsulorrhexis sizing and long-term IOL centration.

In summary, this issue on Advances in Management and Treatment of High Myopia and Its Complications highlights advancements in the management and treatment of both the posterior and anterior segment manifestations of high myopia. While several novel approaches have been proposed, findings will undoubtedly need to be further validated before widespread adoption.

AUTHOR CONTRIBUTIONS

QH and XC drafted the manuscript. QH, XC, XZhu, XZhou, XS, and YL critically proofread and edited the manuscript. All authors contributed to the article and approved the submitted version.

REFERENCES

1. Holden BA, Fricke TR, Wilson DA, Jong M, Naidoo KS, Sankaridurg P, et al. Global prevalence of myopia and high myopia and temporal trends from 2000 through 2050. *Ophthalmology.* (2016) 123:1036–42. doi: 10.1016/j.ophtha.2016.01.006
2. Saw S-M, Matsumura S, Hoang Q V. Prevention and management of myopia and myopic pathology. *Invest Ophthalmol Vis Sci.* (2019) 60:488–99. doi: 10.1167/iovs.18-25221
3. Wong YL, Sabanayagam C, Wong CW, Yeo AC, Cheung YB, Cheung GC, et al. Six-year changes in myopic macular degeneration in adults of the singapore epidemiology of eye diseases study. *Invest Ophthalmol Vis Sci.* (2020) 61:14. doi: 10.1167/iovs.61.4.14
4. Ang M, Wong CW, Hoang QV, Cheung CMG, Lee SY, Chia A, et al. Imaging in myopia – potential biomarkers, current challenges and future developments. *Br J Ophthalmol.* (2019) 103:855–62. doi: 10.1136/bjophthalmol-2018-312866
5. Matsumura S, Sabanayagam C, Wong CW, Tan CS, Kuo A, et al. Characteristics of myopic traction maculopathy in myopic Singaporean adults. *Br J Ophthalmol.* (2020) 20:182. doi: 10.1136/bjophthalmol-2020-316182
6. Zheng F, Wong CW, Sabanayagam C, Cheung YB, Matsumura S, Chua J, et al. Prevalence, risk factors and impact of posterior staphyloma diagnosed from wide-field optical coherence tomography in Singapore adults with high myopia. *Acta Ophthalmol.* (2021) 99:e144–53. doi: 10.1111/aos.14527

7. Tey KY, Qong QY, Dan YS, Tsai ASH. T DSW, Ang M, et al. Association of aberrant posterior vitreous detachment and pathologic tractional forces with myopic macular degeneratio.n *Invest Ophthalmol Vis Sci.* (2021) 62:7. doi: 10.1167/iovs.62.7.7
8. Hoang QV, Chang S, Yu DJG, Yannuzzi LA, Freund KB, Grinband J. 3-D Assessment of Gaze-Induced Eye Shape Deformations and Downgaze-Induced Vitreous Chamber Volume Increase in Highly Myopic Eyes with Staphyloma. *Br J Ophthalmol.* (2021) 105:1149–54. doi: 10.1136/bjophthalmol-2020-316084

Conflict of Interest: The authors declare that the research was conducted in the absence of any commercial or financial relationships that could be construed as a potential conflict of interest.

Publisher's Note: All claims expressed in this article are solely those of the authors and do not necessarily represent those of their affiliated organizations, or those of the publisher, the editors and the reviewers. Any product that may be evaluated in this article, or claim that may be made by its manufacturer, is not guaranteed or endorsed by the publisher.

frontiers in Medicine

ORIGINAL RESEARCH
published: 02 December 2020
doi: 10.3389/fmed.2020.595544

Cilioretinal Arteries in Highly Myopic Eyes: A Photographic Classification System and Its Association With Myopic Macular Degeneration

Jiaqi Meng[1†], *Ling Wei*[1†], *Keke Zhang*[1,2,3,4], *Wenwen He*[1,2,3,4], *Yi Lu*[1,2,3,4*] and *Xiangjia Zhu*[1,2,3,4*]

[1] Eye Institute and Department of Ophthalmology, Eye and ENT Hospital, Fudan University, Shanghai, China, [2] National Health Commission Key Laboratory of Myopia (Fudan University), Shanghai, China, [3] Key Laboratory of Myopia, Chinese Academy of Medical Sciences, Shanghai, China, [4] Shanghai Key Laboratory of Visual Impairment and Restoration, Shanghai, China

OPEN ACCESS

Edited by:
Daniel Ting,
Singapore National Eye Center, Singapore

Reviewed by:
Xinyi Su,
National University of Singapore, Singapore
Yasuo Yanagi,
Asahikawa Medical University, Japan

***Correspondence:**
Xiangjia Zhu
zhuxiangjia1982@126.com
Yi Lu
luyieent@163.com

[†] These authors have contributed equally to this work

Specialty section:
This article was submitted to Ophthalmology, a section of the journal Frontiers in Medicine

Received: 17 August 2020
Accepted: 09 November 2020
Published: 02 December 2020

Citation:
Meng J, Wei L, Zhang K, He W, Lu Y and Zhu X (2020) Cilioretinal Arteries in Highly Myopic Eyes: A Photographic Classification System and Its Association With Myopic Macular Degeneration. Front. Med. 7:595544. doi: 10.3389/fmed.2020.595544

Purpose: To develop a photographic classification for cilioretinal arteries and to investigate its association with myopic macular degeneration (MMD).

Methods: One thousand six hundred ninety-two highly myopic eyes of 1,692 patients were included. The presence of a cilioretinal artery was determined by fundus photographs, and a photographic classification was proposed. MMD was classified according to the International META-PM Classification. Associations of the cilioretinal artery and its classifications with MMD and visual acuity were analyzed.

Results: Of the eyes tested, 245 (14.5%) had a cilioretinal artery. The cilioretinal arteries were classified into four categories (temporal "cake-fork," 35.92%; temporal "ribbon," 53.47%; "multiple," 6.53%; "nasal," 4.08%) and 3 distributions based on whether its visible branches reached the central foveal area. Eyes with cilioretinal arteries had significantly less MMD of grade ≥3 and better visual acuity than those without ($P < 0.01$). Multiple linear regression analysis showed that younger age, male sex, shorter axial length, and the presence of a cilioretinal artery were associated with better visual acuity in highly myopic eyes (all $P < 0.05$). The "nasal" category presented more MMD with grade ≥3 and worse visual acuity than the other categories ($P < 0.05$), whereas the "multiple" category contained no eyes with MMD grade ≥3. The cilioretinal arteries reaching the central foveal area showed less MMD of grade ≥3 and better visual acuity than those not ($P < 0.05$).

Conclusions: We propose a photographic classification for cilioretinal arteries that has good clinical relevance to visual functions. The cilioretinal artery may potentially afford protection against MMD.

Keywords: cilioretinal artery, myopic macular degeneration, high myopia, fundus photography, visual acuity

INTRODUCTION

With the increasing prevalence of high myopia (1), myopic macular degeneration (MMD) has become one of the major causes of visual impairment worldwide (2, 3). It is characterized by a range of degenerative lesions in the retina and choroid, secondary to the increase in axial length (AL) and the formation of staphyloma (4). According to the International Meta-Analysis for Pathologic Myopia (META-PM) Classification System (5), the severity of MMD can be classified into four grades: tessellated fundus only (grade 1), diffuse chorioretinal atrophy (grade 2), patchy chorioretinal atrophy (grade 3), and macular atrophy (grade 4). With increasing MMD severity, the prognosis of visual acuity becomes worse (6, 7). However, the pathogenesis of MMD remains largely unknown.

Oxygen is delivered to the retina from both the retinal and choroidal circulation (8). The balance between retinal and choroidal perfusion plays an important role in several macular diseases (9). Previous studies have shown that the retinal circulation changes with increasing AL, including a reduction in the density of retinal capillary microvasculature and capillary non-perfusion (10, 11). Therefore, in high myopia, MMD caused by chorioretinal atrophy may be associated with a reduced delivery of oxygen caused by the reduced perfusion of the retina.

Cilioretinal arteries, which have a reported prevalence of 20–40% in the normal population, originate from the short posterior ciliary arteries or directly from the choroidal circulation, and usually extend to the macula (12–14). The presence of a cilioretinal artery may afford protection against late age-related macular degeneration (AMD), preventing the development of choroidal neovascularization (15). Therefore, we speculated that cilioretinal arteries, which effectively replace the contribution from central retinal artery (CRA) to the macula area, may also compensate for the reduced blood supply in highly myopic eyes and play a protective role against the development of MMD. However, few relevant studies have been reported.

In the present study, based on fundus photographs taken with an Optos-200Tx device (Optos, Dunfermline, UK), we describe a classification system for cilioretinal arteries that is clinically relevant to the visual function of highly myopic eyes, and demonstrate the protective role of cilioretinal arteries in MMD.

MATERIALS AND METHODS

The protocols for this retrospective observational study were approved by the Institutional Review Board of the Eye and Ear, Nose, Throat (EENT) Hospital of Fudan University, Shanghai, China. The study adhered to the tenets of the Declaration of Helsinki. It was affiliated with the Shanghai High Myopia Study, launched at the EENT Hospital of Fudan University in October 2015 (registered at www.clinicaltrials.gov under accession number NCT03062085). Written informed consent for the use of clinical data was obtained from each patient before participation in the study.

Patients

The Shanghai High Myopia Study is a hospital-based prospective cohort study that continuously includes highly myopic patients aged 18 years or older scheduled for cataract surgery in the EENT Hospital of Fudan University since October 2015. All subjects underwent detailed preoperative examinations and post-operative follow-ups. The medical records of patients included in the Shanghai High Myopia Study database were reviewed. Highly myopic eyes (AL $\geq$26.0 mm) with clear fundus photographs were included in the study. Eyes with corneal opacity, glaucoma, uveitis, optic nerve disease, fundus pathology other than high-myopia-related changes, previous trauma or vitrectomy, or diabetes were excluded from the study. When both eyes of a patient met the criteria, we randomly selected one eye from each patient. For patients in whom only one eye met the criteria, that eye was included. Ultimately, a total of 1,692 highly myopic eyes of 1,692 patients were included in the study.

Routine Ophthalmic Examinations

All the eyes included in the study underwent routine ophthalmic examinations, including a slit-lamp examination, funduscopy, fundus photography, B-scan ultrasonography, AL measurement (IOLMaster 700, Carl Zeiss AG, Oberkochen, Germany), and corneal topography. The best-corrected visual acuity [BCVA, logarithm of the minimum angle of resolution (logMAR)] was recorded for each eye included in the study.

Determination of the Presence of Cilioretinal Arteries and Their Classification

Fundus photographs were collected with the Optos-200Tx ultra-widefield retinal imaging device. Two experienced doctors (WH and JM) independently read all the images to determine the presence of a cilioretinal artery and its classification, before accessing any clinical information. If there was any discrepancy between the two doctors, a senior eye specialist (XZ) gave the final adjudication. A cilioretinal artery was defined as a visible retinal vessel emerging from the border of the optic disc and making a hook-like bend before reaching the retina, with no clear communication with any branches of the central retinal artery. After confirmation of the presence of cilioretinal arteries, their courses, the number of arteries, and distributions were carefully classified.

The cilioretinal arteries were classified into four categories based on the course and number of vessels: Category 1, temporal "cake-fork," refers to a vessel arising from the temporal disc border and extending like a "cake-fork" with two main branches (**Figure 1A**); Category 2, temporal "ribbon," refers to a vessel arising from the temporal border of the disc and extending like a "ribbon" with no obvious branches (**Figure 1B**); Category 3, "multiple," refers to two or more cilioretinal arteries per eye (**Figure 1C**); Category 4, "nasal," refers to a cilioretinal artery that emerges from the nasal border of the optic disc (**Figure 1D**). Based on whether it reached the central area within 500 μm of the foveal center (the central circle of the macula grid used in the International META-PM Classification System) (5), the

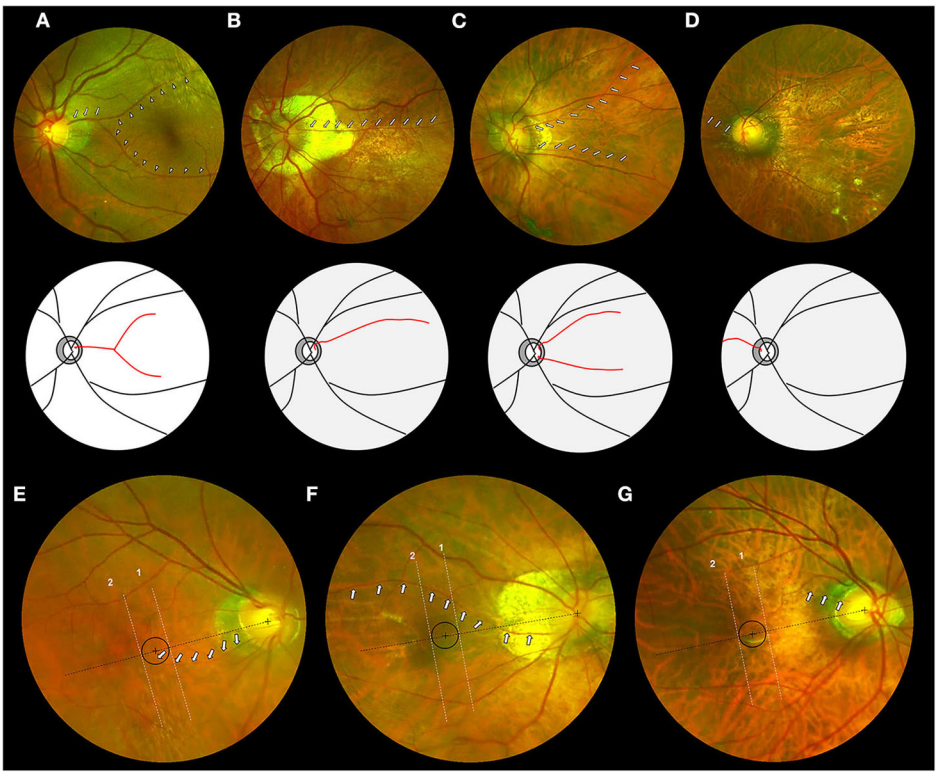

FIGURE 1 | Photographic classification system for cilioretinal arteries in highly myopic eyes. (Top row) Fundus photographs of four categories of cilioretinal arteries. **(A)** Category 1: eyes with a temporal "cake-fork" cilioretinal artery *(white arrows)* with two main branches (*white arrowheads*). **(B)** Category 2: eyes with a temporal "ribbon" cilioretinal artery *(white arrows)*. **(C)** Category 3: eyes with multiple cilioretinal arteries *(white arrows)*. **(D)** Category 4: eyes with a nasal cilioretinal artery *(white arrows)*. (Middle row) Schematic diagrams of four categories of cilioretinal arteries (*red lines*) corresponding to the top row. (Bottom row) Fundus photographs of three distributions of cilioretinal arteries. Black circle represents the area within 500 μm of the foveal center. Lines 1 and 2, both vertical to the dashed black line that connects the centers of the fovea and the optic disc, are used to differentiate the types of distribution. **(E)** Type A: eyes with a cilioretinal artery *(white arrows)* whose path (or visible branches) reaches the area within 500 μm of the foveal center. **(F)** Type B: eyes with a cilioretinal artery *(white arrows)* whose path (or visible branches) extends across the central region. **(G)** Type C: eyes with a cilioretinal artery *(white arrows)* whose path (or visible branches) does not reach the central region.

cilioretinal artery was assigned to one of three distributions: Type A (vessel reaching the central area, **Figure 1E**), Type B (vessel extending across the central area, **Figure 1F**), or Type C (vessel not reaching the central area, **Figure 1G**).

Grading of MMD

The fundus photographs were reviewed and graded by two doctors (WH and JM) according to the International META-PM Classification System (5), without access to any clinical information. Discrepancies were adjudicated by the senior eye specialist (XZ). MMD of grade ≥3 was regarded as severe MMD.

Statistical Analyses

The results are presented as means ± standard deviations for continuous data and as proportions (%) for categorical data. Interobserver agreement was assessed with the kappa (κ) statistic, and Landis and Koch's (16) guidelines for the interpretation of the κ statistics were applied. Student's *t*-test was used to assess between-group differences in continuous data and a χ^2-test or Fisher's exact probability test was used to compare categorical data. Analysis of covariance was used to assess the between-group differences in BCVA, with adjustment for AL. Multivariate logistic regression was used to evaluate the contribution of cilioretinal arteries to the MMD grade, with adjustment for AL. A stepwise multivariate linear regression analysis was used to identify the effects of age, sex, eye laterality, AL, and the presence of a cilioretinal artery on BCVA. By using the stepwise regression mode, eye laterality was removed from the model while the other independent variables were included in the regression model. For eyes with cilioretinal arteries, one-way ANOVA with Tukey's *post-hoc* test was used to compare continuous data among different categories or distributions. All statistical analyses were performed with SPSS version 22 (SPSS, Chicago, IL, USA). Two-sided $P < 0.05$ were considered statistically significant in all analyses.

RESULTS

Characteristics

The mean age of the 1,692 patients analyzed was 61.19 ± 9.12 years, and 42.7% (723/1,692) were male. The mean AL was 29.35 ± 2.30 mm, with a range of 26.01–36.50 mm. Of all

the eyes included, 14.5% (245/1,692) had a cilioretinal artery (interobserver agreement was 98.05% and κ was 0.92 [95% confidence interval: 0.90–0.95]). **Table 1** lists the characteristics of the highly myopic eyes with and without cilioretinal arteries. No significant differences in age, sex, or eye laterality were detected between the two groups (Student's *t*-test for age and χ^2-test for sex and eye laterality; all $P > 0.05$). Eyes with cilioretinal arteries were shorter than those without (cilioretinal artery present vs. absent: 28.86 ± 2.16 vs. 29.43 ± 2.31 mm, respectively; Student's *t*-test, $P < 0.001$). With increasing AL, the prevalence of cilioretinal arteries in the highly myopic eyes decreased, from 19.1% in the 26–28 mm AL group to 10.7% in the >30 mm AL group (**Figure 2**).

Photographic Classification System for Cilioretinal Arteries in Highly Myopic Eyes

As to the photographic classification, the percentages of the temporal "cake fork," the temporal "ribbon," the "multiple," and the "nasal" categories were 35.92% (88/245), 53.47% (131/245), 6.53% (16/245), and 4.08% (10/245), respectively. The cilioretinal artery had three main types of distribution, based on whether its path or visible branches reached the area within 500 μm of the central fovea. The percentage of Type A (arteries whose paths or visible branches reached the area within 500 μm of the foveal center), Type B (long vessels whose paths or visible branches extended across the central region), and Type C (vessels whose paths or visible branches did not reach the central region) were 37.96% (93/245), 24.49% (60/245), and 37.55%(92/245), respectively. Excellent agreement between the observers was observed, with κ ≥ 0.87 (see **Supplementary Table 1**).

Association Between the Presence of a Cilioretinal Artery and MMD or Visual Acuity

Of all the eyes, 76.5% (1,295/1,692) were classified with grade 1 or grade 2 MMD, 17.7% (299/1,692) had grade 3, and 5.8% (98/1,692) had grade 4. The interobserver agreement in the

TABLE 1 | Baseline characteristics.

	Cilioretinal artery present ($n = 245$)	Cilioretinal artery absent ($n = 1,447$)	*P*-value
Age*, years	61.71 ± 9.03	61.10 ± 9.13	0.328
Sex†, male/female	116/129	607/840	0.114
Eye laterality†, right/left	113/132	738/709	0.158
AL*, mm	28.86 ± 2.16	29.43 ± 2.31	<0.001

AL, axial length.
**Student's t-test.*
† χ^2-test.

TABLE 2 | MMD grading of highly myopic eyes with and without cilioretinal arteries.

Grade	Cilioretinal artery present, *N* (%)	Cilioretinal artery absent, *N* (%)	*P*-value*
Grade 1	148 (60.41%)	582 (40.22%)	<0.001
Grade 2	73 (29.79%)	492 (34.00%)	0.494
Grade 3	22 (8.98%)	277 (19.14%)	0.003
Grade 4	2 (0.82%)	96 (6.64%)	0.006

MMD, myopic macular degeneration; N, number.
**Multivariate logistic regression with adjustment for axial length.*

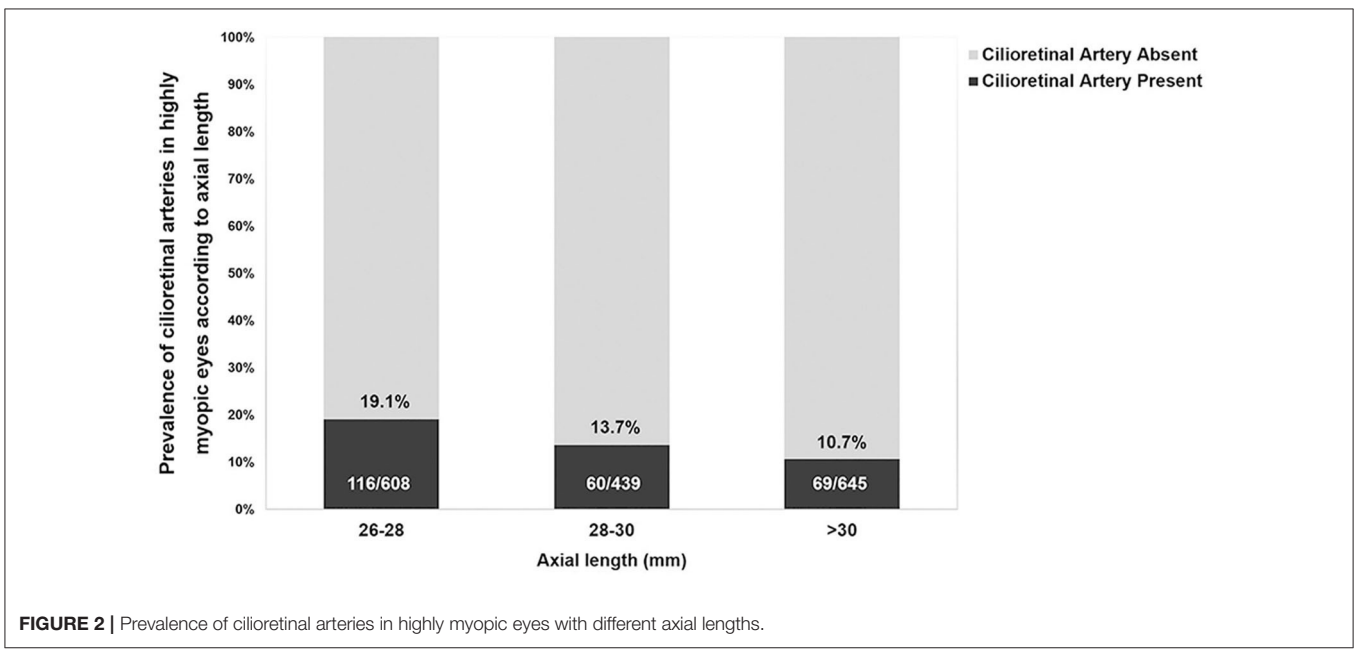

FIGURE 2 | Prevalence of cilioretinal arteries in highly myopic eyes with different axial lengths.

MMD grading was excellent, with κ-values of 0.88–0.96 (see **Supplementary Table 1**). **Table 2** lists the MMD grades for the highly myopic eyes with and without cilioretinal arteries. Because of the possible correlations between AL and MMD grade, we used a multivariate logistic regression analysis adjusted for AL and found that significantly more eyes with grade 1 MMD were found in eyes with cilioretinal arteries than in those without ($P < 0.001$). Both rates of grade 3 and grade 4 MMD were significantly lower in eyes with cilioretinal arteries than in those without after adjustment for AL ($P = 0.003$ and $P = 0.006$, respectively).

We used a covariance analysis for BCVA because of the possible correlation between AL and visual acuity, and found that eyes with cilioretinal arteries showed better BCVA than those without, after adjustment for AL (cilioretinal artery present vs. absent: 0.16 ± 0.21 logMAR [Snellen 20/29] vs. 0.24 ± 0.33 logMAR [Snellen 20/35], respectively; $P = 0.007$). A backwards stepwise multiple linear regression analysis showed that younger age ($\beta = 0.004$, $P < 0.001$), male sex ($\beta = 0.045$, $P = 0.002$), shorter AL ($\beta = 0.044$, $P < 0.001$), and the presence of a cilioretinal artery ($\beta = -0.055$, $P = 0.007$) were all associated with better BCVA in highly myopic eyes.

TABLE 3 | MMD grading and BCVAs in eyes with different categories and distributions of cilioretinal artery.

Classification	MMD grading*			BCVA†, logMAR
	Grades ≤2, *N* (%)	Grade 3, *N* (%)	Grade 4, *N* (%)	
Category				
Category 1	83 (94.32%)	5 (5.68%)	0 (0%)	0.12 ± 0.14
Category 2	117 (89.31%)	14 (10.69%)	0 (0%)	0.16 ± 0.20
Category 3	16 (100%)	0 (0%)	0 (0%)	0.12 ± 0.17
Category 4	5 (50.00%)	3 (30.00%)	2 (20.00%)	0.59 ± 0.43
P value	0.002	0.051	–	<0.001
Distribution				
Type A	89 (95.70%)	4 (4.30%)	0 (0%)	0.12 ± 0.17
Type B	54 (90.00%)	6 (10.00%)	0 (0%)	0.16 ± 0.20
Type C	78 (84.78%)	12 (13.04%)	2 (2.18%)	0.20 ± 0.25
P-value	0.044	0.109	–	0.035
Cilioretinal artery absent	1,074 (74.22%)	277 (19.14%)	96 (6.64%)	0.24 ± 0.43

MMD, myopic macular degeneration; BCVA, best-corrected visual acuities; logMAR, logarithm of the minimum angle of resolution; N, number.

*χ^2-test or Fisher's exact probability test.

†*One-way ANOVA with Tukey's post-hoc test.*

Associations Between the Classification of Cilioretinal Arteries and MMD or Visual Acuity

Table 3 lists the MMD grades and BCVAs for the highly myopic eyes in different categories and with different distributions of cilioretinal arteries. AL did not differ among the four categories or among the three distributions. Among the eyes with cilioretinal arteries, the "nasal" category (Category 4) presented more MMD with grade ≥3 than the other categories (χ^2-test, $p = 0.002$; **Table 3**). No difference was identified in severe MMD between eyes with nasal cilioretinal arteries and those without a cilioretinal artery (χ^2-test, $p = 0.138$). No eyes with a Category 3 cilioretinal artery had MMD grade ≥3. In terms of visual acuity, the "nasal" category (Category 4) had worse BCVA than those in the other categories (one-way ANOVA with Tukey's *post-hoc* test, $P < 0.001$; **Table 3**). **Figure 3** shows that eyes without a cilioretinal artery or with a nasal cilioretinal artery were more likely to display macular atrophy than those with temporal or multiple cilioretinal arteries. In terms of the distribution of cilioretinal arteries, significantly fewer eyes with severe MMD (grade ≥3) were identified as Type A than as Type C. The percentage of eyes with MMD grade ≥3 was 4.30% for Type A and 15.22% for Type C (χ^2-test, $P = 0.012$). Type A also had significantly better BCVA than Type C (0.12 ± 0.17 logMAR [Snellen 20/26] vs. 0.20 ± 0.25 logMAR [Snellen 20/32], respectively; one-way ANOVA with Tukey's *post-hoc* test, $P = 0.026$).

DISCUSSION

In recent years, MMD has become one of the major threats to visual health worldwide (17–19). MMD is aggravated by the reduced retinal microvasculature that occurs with elongation of the eyeball (20–22), suggesting a role for reduced retinal perfusion in the development of MMD. The cilioretinal artery may contribute to the blood supply to the macula and can prevent the progression of fundus diseases such as AMD (15). However, there have been few observations on the role of cilioretinal artery in MMD of highly myopic eyes and its classifications as well. Therefore, in the present study we first presented a classification system for cilioretinal arteries in highly myopic eyes based on a large sample of fundus photographs, and then analyzed its associations with MMD and visual acuity and found that the cilioretinal artery is a protective factor against MMD.

The cilioretinal artery, initially described by Mueller (23), is a retinal artery that may have a protective effect in fundus diseases (15, 24–26). In central retinal artery occlusion, eyes with cilioretinal arteries can show macular sparing and gain an intact central island field (24). The presence of a cilioretinal artery is also recognized as a protective factor in AMD (15). However, little is known about the effect of this vessel on MMD. To our knowledge, this study is the largest investigation until now of cilioretinal arteries in highly myopic eyes, and reports a prevalence of 14.5%. The prevalence of cilioretinal arteries decreases as AL increases, suggesting that the contribution from cilioretinal arteries to the macula tends to be weaker in longer eyes.

Because the anatomical features of the fundus are complex in highly myopic eyes (5, 27), the courses of cilioretinal arteries vary greatly. Therefore, a standard classification system is required to facilitate clinical and epidemiological studies of cilioretinal arteries. Based on the course, number, and distribution of cilioretinal arteries in highly myopic eyes, we propose a photographic classification system that includes four categories and three distributions. In highly myopic eyes, the most frequent category was the temporal "ribbon," followed by the temporal

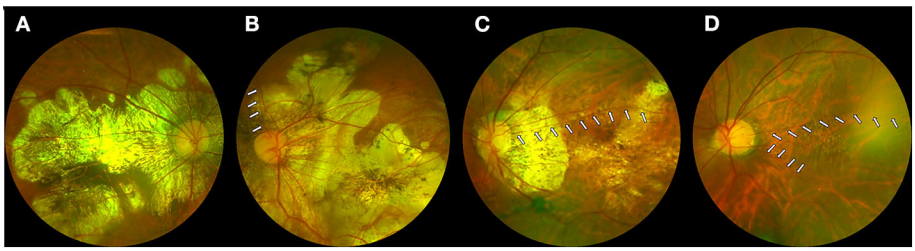

FIGURE 3 | Myopic macular degeneration in eyes with or without cilioretinal arteries. **(A)** Eyes without a cilioretinal artery. **(B)** Eyes with a nasal cilioretinal artery (*white arrows*). **(C)** Eyes with a temporal cilioretinal artery (*white arrows*). **(D)** Eyes with multiple cilioretinal arteries (*white arrows*).

"cake-fork." The percentages of eyes in the "multiple" and "nasal" categories in our study were 6.53 and 4.08%, respectively, which are similar to the 7 and 6%, respectively, in the normal population (28).

In this study, a protective role for the cilioretinal artery in high myopia was identified for the first time. After adjustment for AL, the eyes with cilioretinal arteries had a lower prevalence of severe MMD, especially vision-threatening macular atrophy. Moreover, the severity of MMD and the function of the macula are directly related to the visual acuity of patients with high myopia (6, 7). Generally, eyes with cilioretinal arteries showed better visual acuity than those without, and our multivariate regression analysis confirmed that the presence of a cilioretinal artery had a significantly favorable effect on visual acuity.

On the one hand, the cilioretinal artery may protect the macula by compensate for the hemodynamic imbalance of the retina. In high myopia, the main clinical features occur at the level of RPE and choroid (5), which may influence the perfusion from the choroid to the macula and disrupt the hemodynamic balance between the retinal and choroidal circulation. The cilioretinal artery may partly compensate for the hemodynamic imbalance and prevent the development of macular degeneration (15). On the other hand, retina vessels (irrespective of their origin from the CRA or cilioretinal artery) are basically end arteries with no anastomosis between them. Besides, the CRA and cilioretinal vessels supply distinct areas within the macula, which is supported by the clinical observation that the cilioretinal artery occlusion usually shows the same degree of retinal disability as the occlusion of a branch of CRA (24). Thus, the cilioretinal arteries do not increase the blood supply but effectively replace the contribution from the CRA to a variable segment of the retina. We understand that the ciliary circulation is influenced by sympathetic innervation while the retinal circulation has the autoregulatory mechanism (29). Also, different clinical features between eyes with cilioretinal arteries and those without have been reported in some fundus diseases, such as choroidal neovascularization, giant cell arteritis, and retinal angiomatous proliferation (15, 30, 31). Yet, it remains unclear whether in highly myopic eyes, the area of retina perfused by cilioretinal arteries behaves different from that perfused by the CRA. Therefore, future observation is needed to definitely map the area supplied by the cilioretinal artery and determine its correlation with the area of MMD based on OCT angiography.

Our photographic classification system also showed good clinical relevance to the patients' visual function. We found that nasal cilioretinal arteries presented more severe MMD than the other categories of cilioretinal arteries, but no difference was identified in severe MMD between eyes with nasal cilioretinal arteries and those without a cilioretinal artery. This indicated that the "nasal" category may have little influence on the development of MMD. On the contrary, in eyes in the "multiple" category, more protection seemed to be provided to the macula insofar as no eye in this category was identified with severe MMD. The temporal "cake-fork" which includes superior and inferior branches and provides perfusion to a wider area than the temporal "ribbon," may take second place. In terms of the distributions of the arteries, whether the end of the cilioretinal artery reaches the key area within 500 μm of the central fovea may be highly clinically significant. In Type A, the rate of severe MMD was low (4.30%), and no macular atrophy was identified. In contrast, the protective effect of the artery decreased if the vessel was either too short or too long. Although the long Type B vessels extended across the macula, the actual area of effective perfusion may have been located at the far end of the vessel.

In this study, fundus photography was used to determine the presence of cilioretinal arteries and their classifications. Although fluorescence angiography was recognized as a more precise way to evaluate the cilioretinal arteries, fundus photography may be more convenient for the rapid screening and daily clinical application. Most importantly, it is non-invasive. However, to further validate the results obtained from the fundus photo, future study based on non-invasive imaging modalities like OCT angiography are still needed. In addition, reaching central 500 microns area is not the same as actually participating in the peri FAZ ring of capillaries. Very often that decides the macular sparing effect of cilioretinal artery during CRVO. Therefore, based on OCT angiography analysis, the role of the cilioretinal artery participating in the peri FAZ ring of capillaries should be analyzed. Another limitation of this study is the retrospective design including only one single institution. Further prospective studies are needed to confirm the generalizability of the current results.

In conclusion, based on fundus photographs, we propose a classification system for cilioretinal arteries that has good clinical relevance to visual functions, and have demonstrated that the cilioretinal artery is a potentially protective

factor against MMD and loss of visual acuity in highly myopic eyes.

DATA AVAILABILITY STATEMENT

The raw data supporting the conclusions of this article will be made available by the authors, without undue reservation.

ETHICS STATEMENT

The studies involving human participants were reviewed and approved by the Institutional Review Board of the Eye and Ear, Nose, Throat (EENT) Hospital of Fudan University, Shanghai, China. The patients/participants provided their written informed consent to participate in this study.

AUTHOR CONTRIBUTIONS

XZ and YL: conception and design. XZ, JM, and LW: analysis and interpretation of data and manuscript preparation. JM, LW, KZ, and WH: data collection. All authors contributed to the article and approved the submitted version.

FUNDING

Publication of this article was supported by research grants from the Chinese National Natural Science Foundation (Grant No. 81870642, 81970780, 81670835, Beijing, China), the Shanghai High Myopia Study Group, the Shanghai Talent Development Fund (Grant No. 201604, Shanghai, China), the Outstanding Youth Medical Talents Program of Shanghai Health and Family Planning Commission (Grant No. 2017YQ011, Shanghai, China). The sponsor or funding organization had no role in the design or conduct of this research.

SUPPLEMENTARY MATERIAL

The Supplementary Material for this article can be found online at: https://www.frontiersin.org/articles/10.3389/fmed.2020.595544/full#supplementary-material

REFERENCES

1. Holden BA, Fricke TR, Wilson DA, Jong M, Naidoo KS, Sankaridurg P, et al. Global prevalence of myopia and high myopia and temporal trends from 2000 through 2050. *Ophthalmology.* (2016) 123:1036–42. doi: 10.1016/j.ophtha.2016.01.006
2. Xu L, Wang Y, Li Y, Wang Y, Cui T, Li J, et al. Causes of blindness and visual impairment in urban and rural areas in Beijing: the Beijing Eye Study. *Ophthalmology.* (2006) 113:1134.e1–11. doi: 10.1016/j.ophtha.2006.01.035
3. Cotter SA, Varma R, Ying-Lai M, Azen SP, Klein R, Los Angeles Latino Eye Study Group. Causes of low vision and blindness in adult Latinos: the Los Angeles Latino Eye Study. *Ophthalmology.* (2006) 113:1574–82. doi: 10.1016/j.ophtha.2006.05.002
4. Hayashi K, Ohno-Matsui K, Shimada N, Moriyama M, Kojima A, Hayashi W, et al. Long-term pattern of progression of myopic maculopathy: a natural history study. *Ophthalmology.* (2010) 117:1595–611. doi: 10.1016/j.ophtha.2009.11.003
5. Ohno-Matsui K, Kawasaki R, Jonas JB, Cheung CM, Saw SM, Verhoeven VJ, et al. International photographic classification and grading system for myopic maculopathy. *Am J Ophthalmol.* (2015) 159:877–83.e7. doi: 10.1016/j.ajo.2015.01.022
6. Koh V, Tan C, Tan PT, Tan M, Balla V, Nah G, et al. Myopic maculopathy and optic disc changes in highly myopic young Asian eyes and impact on visual acuity. *Am J Ophthalmol.* (2016) 164:69–79. doi: 10.1016/j.ajo.2016.01.005
7. Zhao X, Ding X, Lyu C, Li S, Liu B, Li T, et al. Morphological characteristics and visual acuity of highly myopic eyes with different severities of myopic maculopathy. *Retina.* (2020) 40:461–7. doi: 10.1097/IAE.0000000000002418
8. Dollery CT, Bulpitt CJ, Kohner EM. Oxygen supply to the retina from the retinal and choroidal circulations at normal and increased arterial oxygen tensions. *Invest Ophthalmol.* (1969) 8:588–94.
9. Blumenthal M, Best M, Galin MA, Gitter KA. Ocular circulation: analysis of the effect of induced ocular hypertension on reginal and choroidal blood flow in man. *Am J Ophthalmol.* (1971) 71:819–25. doi: 10.1016/0002-9394(71)90247-9
10. Li M, Yang Y, Jiang H, Gregori G, Roisman L, Zheng F, et al. Retinal microvascular network and microcirculation assessments in high myopia. *Am J Ophthalmol.* (2017) 174:56–67. doi: 10.1016/j.ajo.2016.10.018
11. Kaneko Y, Moriyama M, Hirahara S, Ogura Y, Ohno-Matsui K. Areas of nonperfusion in peripheral retina of eyes with pathologic myopia detected by ultra-widefield fluorescein angiography. *Invest Ophthalmol Vis Sci.* (2014) 55:1432–9. doi: 10.1167/iovs.13-13706
12. Randall BA. Cilio-retinal or aberrant vessels. *Trans Am Ophthalmol Soc.* (1887) 4:511–7.
13. Jackson E. Cilio-retinal and other anomalous retinal vessels. *Ophthal Rev.* (1911) 30:264–96.
14. Justice J Jr., Lehmann RP. Cilioretinal arteries. A study based on review of stereo fundus photographs and fluorescein angiographic findings. *Arch Ophthalmol.* (1976) 94:1355–8. doi: 10.1001/archopht.1976.03910040227015
15. Snyder K, Yazdanyar A, Mahajan A, Yiu G. Association between the cilioretinal artery and choroidal neovascularization in age-related macular degeneration: a secondary analysis from the age-related eye disease study. *JAMA Ophthalmol.* (2018) 136:1008–14. doi: 10.1001/jamaophthalmol.2018.2650
16. Landis JR, Koch GG. The measurement of observer agreement for categorical data. *Biometrics.* (1977) 33:159–74. doi: 10.2307/2529310
17. Fricke TR, Jong M, Naidoo KS, Sankaridurg P, Naduvilath TJ, Ho SM, et al. Global prevalence of visual impairment associated with myopic macular degeneration and temporal trends from 2000 through 2050: systematic review, meta-analysis and modelling. *Br J Ophthalmol.* (2018) 102:855–62. doi: 10.1136/bjophthalmol-2017-311266
18. Wong YL, Sabanayagam C, Ding Y, Wong CW, Yeo AC, Cheung YB, et al. Prevalence, risk factors, and impact of myopic macular degeneration on visual impairment and functioning among adults in Singapore. *Invest Ophthalmol Vis Sci.* (2018) 59:4603–13. doi: 10.1167/iovs.18-24032
19. Iwase A, Araie M, Tomidokoro A, Yamamoto T, Shimizu H, Kitazawa Y, et al. Prevalence and causes of low vision and blindness in a Japanese adult population: the Tajimi Study. *Ophthalmology.* (2006) 113:1354–62. doi: 10.1016/j.ophtha.2006.04.022
20. Li H, Mitchell P, Rochtchina E, Burlutsky G, Wong TY, Wang JJ. Retinal vessel caliber and myopic retinopathy: the blue mountains eye study. *Ophthalmic Epidemiol.* (2011) 18:275–80. doi: 10.3109/09286586.2011.602508
21. Yang Y, Wang J, Jiang H, Yang X, Feng L, Hu L, et al. Retinal microvasculature alteration in high myopia. *Invest Ophthalmol Vis Sci.* (2016) 57:6020–30. doi: 10.1167/iovs.16-19542
22. Spaide RF, Klancnik JM Jr., Cooney MJ. Retinal vascular layers imaged by fluorescein angiography and optical coherence tomography angiography. *JAMA Ophthalmol.* (2015) 133:45–50. doi: 10.1001/jamaophthalmol.2014.3616
23. Mueller H. Anatomisch-physiologische Untersuchungen über die Retina des Menschen und der Wirbelthiere. *Zeitschrift Fur Wissenschaftliche Zoologie.* (1856) 8:1–22.

24. Hayreh SS. Ocular vascular occlusive disorders: natural history of visual outcome. *Prog Retin Eye Res.* (2014) 41:1–25. doi: 10.1016/j.preteyeres.2014.04.001
25. Inan UU, Yavaş G, Oztürk F. Does the cilioretinal artery affect age-related macular degeneration? *Klin Monatsbl Augenheilkd.* (2007) 224:127–8. doi: 10.1055/s-2006-927316
26. Lee SS, Schwartz B. Role of the temporal cilioretinal artery in retaining central visual field in open-angle glaucoma. *Ophthalmology.* (1992) 99:696–9. doi: 10.1016/S0161-6420(92)31908-6
27. Ikuno Y. Overview of the complications of high myopia. *Retina.* (2017) 37:2347–51. doi: 10.1097/IAE.0000000000001489
28. Lorentzen SE. Incidence of cilioretinal arteries. *Acta Ophthalmol.* (1970) 48:518–24. doi: 10.1111/j.1755-3768.1970.tb03753.x
29. Delaey C, Van De Voorde J. Regulatory mechanisms in the retinal and choroidal circulation. *Ophthalmic Res.* (2000) 32:249–56. doi: 10.1159/000055622
30. Hayreh SS. Acute retinal arterial occlusive disorders. *Prog Retin Eye Res.* (2011) 30:359–94. doi: 10.1016/j.preteyeres.2011.05.001
31. Ghazi NG, Conway BP. Retinal angiomatous proliferation with a cilioretinal artery anastomosis: an unusual presentation. *Graefes Arch Clin Exp Ophthalmol.* (2005) 243:493–6. doi: 10.1007/s00417-004-1034-4

Conflict of Interest: The authors declare that the research was conducted in the absence of any commercial or financial relationships that could be construed as a potential conflict of interest.

frontiers in Medicine

ORIGINAL RESEARCH
published: 23 December 2020
doi: 10.3389/fmed.2020.592663

Accuracy Improvement of IOL Power Prediction for Highly Myopic Eyes With an XGBoost Machine Learning-Based Calculator

Ling Wei[1,2,3,4], *Yunxiao Song*[5], *Wenwen He*[1,2,3,4], *Xu Chen*[6], *Bo Ma*[7], *Yi Lu*[1,2,3,4] *and Xiangjia Zhu*[1,2,3,4*]

[1] Department of Ophthalmology and Eye Institute, Eye & ENT Hospital, Fudan University, Shanghai, China, [2] National Health Commission Key Laboratory of Myopia, Fudan University, Shanghai, China, [3] Key Laboratory of Myopia, Chinese Academy of Medical Science, Shanghai, China, [4] Shanghai Key Laboratory of Visual Impairment and Restoration, Shanghai, China, [5] New York University Shanghai, Shanghai, China, [6] Shanghai Aier Eye Hospital, Shanghai, China, [7] Department of Ophthalmology, Ninth People's Hospital of Shanghai Jiaotong University, Shanghai, China

OPEN ACCESS

Edited by:
Daniel Ting,
Singapore National Eye Center, Singapore

Reviewed by:
Christopher Kai-Shun Leung, The Chinese University of Hong Kong, China
Chee Wai Wong, Singapore National Eye Center, Singapore

***Correspondence:**
Xiangjia Zhu
zhuxiangjia1982@126.com

Specialty section:
This article was submitted to Ophthalmology, a section of the journal Frontiers in Medicine

Received: 07 August 2020
Accepted: 04 December 2020
Published: 23 December 2020

Citation:
Wei L, Song Y, He W, Chen X, Ma B, Lu Y and Zhu X (2020) Accuracy Improvement of IOL Power Prediction for Highly Myopic Eyes With an XGBoost Machine Learning-Based Calculator. Front. Med. 7:592663. doi: 10.3389/fmed.2020.592663

Purpose: To develop a machine learning-based calculator to improve the accuracy of IOL power predictions for highly myopic eyes.

Methods: Data of 1,450 highly myopic eyes from 1,450 patients who had cataract surgeries at our hospital were used as internal dataset (train and validate). Another 114 highly myopic eyes from other hospitals were used as external test dataset. A new calculator was developed using XGBoost regression model based on features including demographics, biometrics, IOL powers, A constants, and the predicted refractions by Barrett Universal II (BUII) formula. The accuracies were compared between our calculator and BUII formula, and axial length (AL) subgroup analysis (26.0–28.0, 28.0–30.0, or ≥30.0 mm) was further conducted.

Results: The median absolute errors (MedAEs) and median squared errors (MedSEs) were lower with the XGBoost calculator (internal: 0.25 D and 0.06 D^2; external: 0.29 D and 0.09 D^2) vs. the BUII formula (all $P \leq 0.001$). The mean absolute errors and were 0.33 ± 0.28 vs. 0.45 ± 0.31 (internal), and 0.35 ± 0.24 vs. 0.43 ± 0.29 D (external). The mean squared errors were 0.19 ± 0.32 vs. 0.30 ± 0.36 (internal), and 0.18 ± 0.21 vs. 0.27 ± 0.29 D^2 (external). The percentages of eyes within ±0.25 D of the prediction errors were significantly greater with the XGBoost calculator (internal: 49.66 vs. 29.66%; external: 78.28 vs. 60.34%; both $P < 0.05$). The same trend was in MedAEs and MedSEs in all subgroups (internal) and in AL ≥30.0 mm subgroup (external) (all $P < 0.001$).

Conclusions: The new XGBoost calculator showed promising accuracy for highly or extremely myopic eyes.

Keywords: machine learning, refractive error, myopia, intraocular lens, IOL power calculation

INTRODUCTION

High myopia has become a worldwide epidemic, with a predicted prevalence of 10% of the world population by the year 2050 (1). It often leads to significant visual impairment or even blindness (2). Patients with high myopia also have a higher risk of developing cataracts and undergo cataract surgeries at an earlier age (3–5). Therefore, the accurate IOL power calculation for these eyes is an important issue.

However, highly myopic eyes often experience hyperopic refractive surprise after cataract surgery (6, 7), despite the use of partial coherence interferometry, which could eliminate biometric errors (8, 9). Therefore, choosing appropriate formulas to reduce refractive errors becomes crucial in these eyes.

Fourth-generation formulas, such as the Barrett Universal II (BUII) (10), Olsen, and Hill-Radial Basis Function (RBF) formulas, offered promising outcomes for highly myopic eyes (11, 12). In particular, the BUII formula may show the greatest accuracy for myopic eyes (13–15). For eyes with ALs > 24.5 mm, the BUII formula presented the highest percentage of eyes within ±0.50 D of the prediction error (PE) (82.1% on average) (16). However, the accuracy of the BUII formula decreased sharply when we included more eyes with extreme myopia (AL > 28.0 mm), as the percentage of eyes within ±0.50 D of the PE decreased to 70%, and the percentage within ±0.25 D of the PE was only 25% (17). Therefore, accurate prediction of IOL power for eyes with high or extreme myopia remains challenging.

The purpose of this study was to develop a new calculator using the XGBoost machine learning regression technique that incorporates several clinical features, including the BUII formula results, to improve the accuracy of IOL power prediction for highly or extremely myopic eyes.

METHODS

Patients

The Institutional Review Board of the Eye and Ear, Nose, and Throat (ENT) Hospital of Fudan University (Shanghai, China) approved this study. The study adhered to the tenets of the Declaration of Helsinki and was registered at www.clinicaltrials.gov (accession number NCT02182921). Signed informed consents for the use of their clinical data were obtained from all participants before cataract surgery.

Data of 1,450 highly myopic eyes from 1,450 patients who had uneventful cataract surgery at our hospital were collected to develop and validate the models (internal dataset). Data from the Shanghai Aier Eye Hospital and the Ninth People's Hospital of Shanghai Jiaotong University were collected as an external test dataset, including another 114 highly myopic eyes from 114 patients.

The inclusion criteria were: (1) axial length (AL) >26.0 mm; (2) preoperative biometry obtained using IOLMaster 700 (version 1.80) or IOLMaster 500 (version 7.7, Carl Zeiss Meditec AG, Jena, Germany); (3) uneventful cataract surgery with credible postoperative (≥1 month) manifest refraction outcomes; and (4) best corrected distance visual acuity (BCVA) taken by a Snellen chart at 2.5 m more than 1 month after surgery. The exclusion criteria were: (1) severe corneal opacity; (2) severe maculopathy, which was defined the fundus photograph (Optos-200Tx Ultra-Widefield Retinal Imaging System, Optos, Dunfermline, United Kingdom) results reaching category 4 according to the international photographic grading system for myopic maculopathy proposed by Ohno-Matsui et al. (18), or the OCT exam (Spectralis OCT; Heidelberg Engineering, Heidelberg, Germany) revealed severe lesions such as the macular hole, choroidal neovascularization, atrophy, etc.; and (4) eyes with ocular trauma or other diseases that may influence the accuracy of manifest refraction.

The IOL models in the internal dataset included MCX 11 ASP, Rayner, 409MP, HOYA, ZCB00, SN60WF, and ZMB00, while the external dataset included MCX 11 ASP, SN60WF, and ErgomaX.

The A constants were obtained from the User Group for Laser Interference Biometry website (ocusoft.de/ulib/index.htm) for SRK/T formula, after which the constants were input into the website of BUII formula and lens factors were automatically generated.

Dataset Preparation

The project included three main parts: dataset preparation, model design, and training and evaluation.

Data from our hospital were set as the internal dataset, while 20% of the eyes were split randomly into a test dataset, and the remainders were used as the train and validation datasets. Data from the other hospitals were set as an external test dataset.

Actual postoperative refraction measured more than 1 month after cataract surgery was set as the training target, with others listed below set as features of machine learning. The four types of features were: (1) demographic information, which was the patient age; (2) biometric data, which included AL, corneal curvature (flattest and steepest K value, namely K1 and K2), steepest and flattest meridian, and anterior chamber depth (ACD, measured from epithelium to lens). We also included two additional parameters: $\frac{1}{AL}$ and $\frac{1}{(K1+K2)}$, by feature transformation during preprocessing; (3) the power of the implanted IOL model and its A constant; and (4) the predicted refraction of the implanted IOL back-calculated using the BUII formula.

Modeling

XGBoost is an algorithm in which new models are created that predict the residuals of prior models and are then added together to make the final prediction (19). Using an internal dataset, the XGBoost model was compared with another two regression models, including Random Forests (RF) (20), and linear support vector machine (SVM) regressor (21), and the one with best prediction outcomes was adopted for further analysis.

The clinical features in the training dataset were input into the three machine learning models to predict the postoperative refractions. Random search with 3-fold cross-validation was used to determine the hyperparameters of the models, which were randomly selected within a range. Through 500 repetitions, the optimal hyperparameters with the highest validation scores were chosen for our model. The hyperparameters used in our study for XGBoost were learning_rate (0,0.1], n_estimator (300,

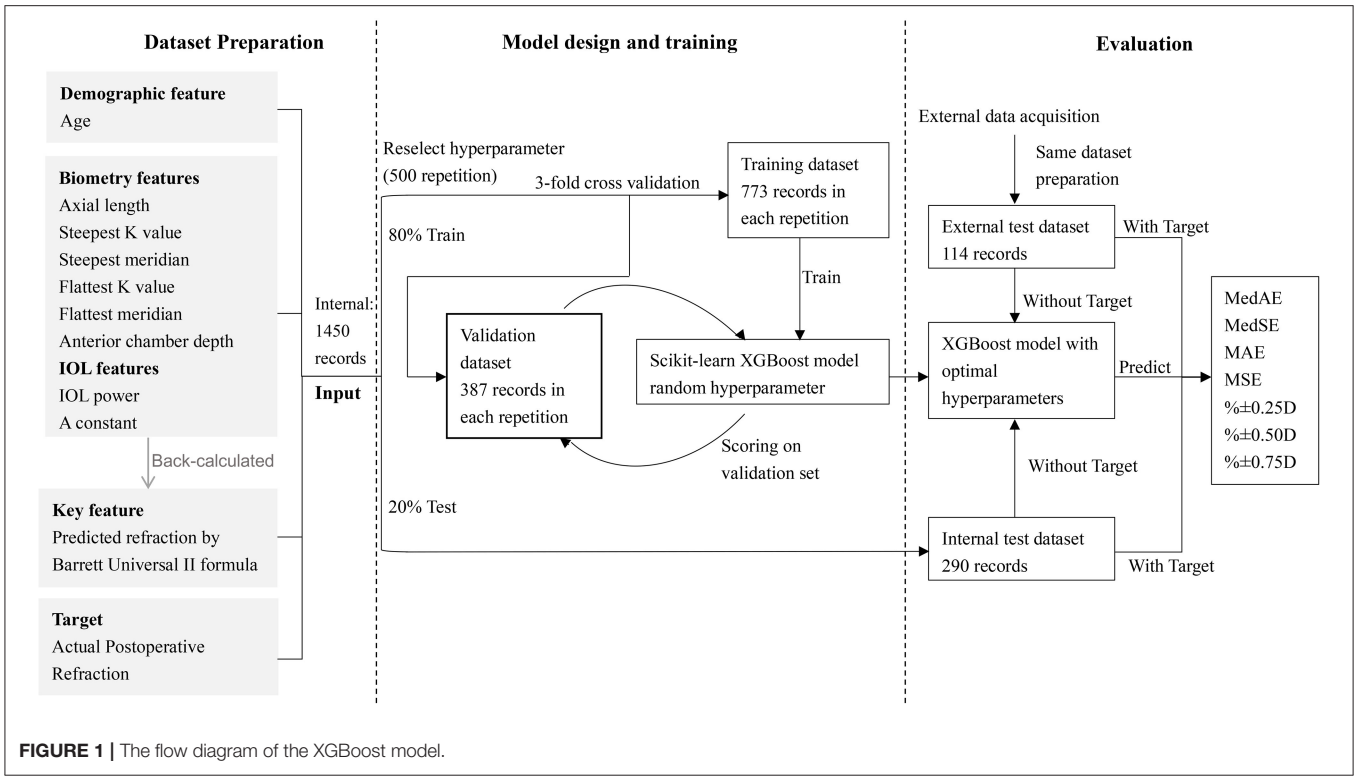

FIGURE 1 | The flow diagram of the XGBoost model.

700), max_depth (2,3), gamma (1), subsample [0.7, 0.9], and colsample_bytree [0.7, 0.9]; for RF were n_estimators [1,200], min_samples_leaf [1,1000], and max_features (1, 12); for linear SVM were epsilon [0,1] and C [0,10].

Evaluation

To evaluate the precision of the model, the trained and tuned prediction model was used to predict postoperative refraction using the internal and external test datasets. The PE was defined as the actual postoperative refraction (spherical equivalent) minus the predicted postoperative refraction (back-calculated with the actually implanted IOL power). The median absolute errors (MedAEs) (22), median squared errors (MedSEs), mean absolute errors (MAEs), mean squared errors (MSEs), and the percentages of eyes within ±0.25, ±0.50, ±0.75, and ±1.00 D of the PE were calculated and compared between the new calculator and the BUII formula. Furthermore, a comparison between the new calculator and the RBF 2.0 formula was further conducted with part of the data from the internal and external test datasets, while only cases with −2.5 to 1 D refractive targets or AL < 35 mm can be calculated with the RBF 2.0 calculator according to its user guide (23).

The flow diagram of our model was demonstrated in **Figure 1**. To validate the stability and generalizability of the model, the training dataset and internal test dataset were randomly split with a fixed proportion (80:20%) with 100 repetitions. In each repetition, a new model was established based on the training dataset and was evaluated using the same metrics and a separate test dataset.

We also conducted subgroup analysis stratified by ALs (26.0–28.0, 28.0–30.0, and ≥30.0 mm) with both test datasets. Eyes with AL ≥28.0 mm were defined as extremely myopic eyes. The accuracies of our calculator and the BUII formula were compared in each subgroup using the evaluation metrics described above.

Application

A free website for our XGBoost calculator was developed for online calculations (*zhuformula.com*, with user guide provided).

Statistical Analyses

Statistical analyses were performed with SPSS software (version 11.0, SPSS, Inc.). Continuous variables were described as the mean ± standard deviation. The student's *t*-test was used to compare the continuous variables and the χ^2 test was used to compare categorical variables. Outcome measurements with abnormal distributions were compared with the Wilcoxon signed-rank test (two groups) or the Kruskal-Wallis test (more than two groups). Linear-by-linear associations (two groups) and Kaplan-Merier test (more than two groups) were used to compare the distributions of the PE. A *P*-value of < 0.05 was considered statistically significant.

RESULTS

Demographics and Ocular Characteristics

The demographic data for the eyes in the internal and external datasets are shown in **Table 1**. There were no statistically significant between-group differences in age, sex, and laterality. However, the external dataset had longer AL, larger K1, and

TABLE 1 | Demographics of the internal and external datasets.

Parameters	Internal dataset (n = 1,450)	External dataset (n = 140)	P-value
Age (y)			
Mean ± SD	61.32 ± 9.25	62.61 ± 7.90	>0.05
Range	25–87	44–85	
Female No. (%)	794 (54.8%)	80 (57.1%)	>0.05
Eye (OD/OS)	760/690	62/52	>0.05
Axial length (mm)			
Mean ± SD	29.36 ± 2.18	29.87 ± 2.13	0.043
Range	26.01–36.46	26.05–35.99	
K1 (D)			
Mean ± SD	43.00 ± 1.97	43.64 ± 1.50	0.002
Range	32.02–48.38	39.38–46.62	
K2 (D)			
Mean ± SD	44.16 ± 2.06	44.80 ± 1.55	0.002
Range	32.96–50.15	41.31–48.64	
IOL power (D)			
Mean ± SD	9.56 ± 5.61	7.12 ± 4.70	<0.001
Range	−8.0 to 27.5	−4.0 to 17.0	

SD, standard deviation; D, diopter.
Student's t-test was used to compare the continuous variables and the χ^2 test was used to compare categorical variables between the internal and external datasets.

K2, and lower implanted IOL power. Extremely myopic eyes comprised 62.07% (180/290) of all eyes in the internal test dataset and 79.82% (91/114) in the external test dataset.

Comparisons of Accuracy

Comparisons of three regression models demonstrated that the XGBoost outperformed RF and linear SVM ($P < 0.01$, **Table 2**). We then developed our XGBoost calculator and compared its prediction results with the BUII formula in both test datasets. The Bland-Altman plots with actual postoperative refraction against the XGBoost or the BUII outputs were demonstrated in **Figure 2**, and most points were within the agreement limits. The summary of accuracy outcomes was demonstrated in **Table 3**. The mean predicted refractions in the internal test dataset were −3.09 D (range −6.88 to 0.37 D) by the XGBoost calculator, and −3.06 D (range −8.29 to 0.58 D) by the BUII; while in the external test dataset were −2.41 D (range −4.32 to 0.20 D) by the XGBoost calculator, and −2.66 D (range −4.65 to −0.15 D) by the BUII. The MedAEs and MedSEs were significantly lower with the XGBoost calculator in two test datasets (internal: MedAE: 0.25 vs. 0.42 D and MedSE: 0.06 vs. 0.17 D; external: MedAE: 0.29 vs. 0.42 D and MedSE: 0.09 vs. 0.18 D; all $P \leq 0.001$). The MAEs with our XGBoost calculator vs. the BUII were 0.33 ± 0.28 vs. 0.45 ± 0.31 D in internal test dataset, and 0.35 ± 0.24 vs. 0.43 ± 0.29 D in external test dataset. The MSEs were 0.19 ± 0.32 vs. 0.30 ± 0.36 D^2 in internal test dataset, and 0.18 ± 0.21 vs. 0.27 ± 0.29 D^2 in external test dataset. As for the 100 times random cross-validation analyses, the MAEs of our XGBoost formula were consistently lower in all rounds of modeling and calculation (**Supplementary Figure 1**).

The percentages of eyes within ±0.25, ±0.50, ±0.75, and ±1.00 D of the PE were greater with the XGBoost calculator in the internal (±0.25 D: 49.66 vs. 29.66%; ±0.50 D: 78.28 vs. 60.34%; ±0.75 D: 90.69 vs. 84.14%; ±1.00 D: 97.24 vs. 93.45%; P <0.001) and external dataset (±0.25 D: 43.86 vs. 35.96%; ±0.50 D: 72.81 vs. 58.77%; ±0.75 D: 92.98 vs. 85.09%; ±1.00 D: 99.12 vs. 97.37%; both $P < 0.05$) (**Table 3** and **Figure 3**). Furthermore, the new XGBoost calculator also outperformed the RBF 2.0 calculator in the internal and external test datasets (**Supplementary Table 1**).

Subgroup Analysis

Table 4 shows the results of the AL subgroup analysis. The MedAEs and MedSEs were significantly lower with the XGBoost calculator than the BUII formula in all subgroups in the internal dataset (all $P < 0.001$) and in the AL ≥30.0 mm subgroup in the external dataset ($P < 0.001$). The mean absolute errors (MAEs) with our XGBoost calculator vs. the BUII in three AL subgroups in internal test dataset were 0.29 ± 0.24, 0.35 ± 0.30, and 0.36 ± 0.30 D, respectively, vs. 0.42 ± 0.29, 0.48 ± 0.35, and 0.46 ± 0.29 D, respectively; while in the AL subgroups of the external test dataset were 0.35 ± 0.26, 0.35 ± 0.24, and 0.34 ± 0.24 D, respectively, vs. 0.35 ± 0.24, 0.38 ± 0.27, and 0.51 ± 0.30 D, respectively. The mean squared errors (MSEs) in the AL subgroups of the internal test dataset were 0.14 ± 0.21, 0.21 ± 0.40, and 0.22 ± 0.35 D^2, respectively, vs. 0.26 ± 0.32, 0.35 ± 0.45, and 0.30 ± 0.33 D^2, respectively; while in the AL subgroups of the external test dataset were 0.18 ± 0.25, 0.18 ± 0.21, and 0.17 ± 0.20 D^2, respectively, vs. 0.18 ± 0.22, 0.21 ± 0.22, and 0.35 ± 0.33 D^2, respectively.

DISCUSSION

Accurately predicting the IOL power for highly myopic eyes is quite difficult, especially for extremely myopic eyes. Although the BUII formula appears to be the most accurate formula currently available for highly myopic eyes (8, 12, 24), its accuracy decreases when it is applied to extremely myopic eyes (17). Moreover, despite the promising outcomes of the BUII formula in terms of the percentage of eyes within ±0.50 D of the PE (11, 12, 14, 24), the percentage of eyes within ±0.25 D of the PE remains unsatisfied (25.0–38.3%) (14, 15, 17). Therefore, there is still room for improving the BUII formula for extremely myopic eyes. In this study, we developed a new XGBoost IOL calculator that showed improved accuracy in highly myopic eyes. It performed well in a dataset in which more than two-thirds of eyes were extremely myopic, and it greatly improved the percentage of eyes within ±0.25 D of the PE relative to the BUII formula using the internal (49.66 vs. 29.66%) and external (43.86 vs. 35.96%) test datasets.

In long eyes, the PE is generally attributable to two factors, the ocular biometry and the calculation formula itself. In terms of biometry, longer AL, greater ACD, the occurrence of staphyloma (25, 26), and poor fixation stability can influence the measurement of highly myopic eyes (27). However, the use

TABLE 2 | Comparison regression models including the XGBoost, Linear Support Vector Machine, and Random Forest using the internal test dataset.

Parameters	XGBoost	Random Forest	Linear SVM	*P*-value
MedAE (D)	0.25	0.30	0.70	<0.01
MedSE (D^2)	0.06	0.09	0.49	<0.01
MAE (D) ± SD	0.33 ± 0.28	0.38 ± 0.33	0.96 ± 0.90	
MSE (D^2) ± SD	0.19 ± 0.32	0.25 ± 0.50	1.74 ± 3.14	
Eyes within PE (%)				<0.01
±0.25 D	49.66%	45.17%	20.34%	
±0.50 D	78.28%	75.17%	38.97%	
±0.75 D	90.96%	88.97%	52.76%	
±1.00 D	97.24%	94.14%	63.97%	

SVM, support vector machine; MedAE, median absolute error; MedSE, median squared error; MAE, mean absolute error; SD, standard deviation; MSE, mean squared error; D, diopter; PE, prediction error.
Kruskal-Wallis tests were used to compare the MedAE and MedSE results. Kaplan-Merier test was used to compare the percentages of eyes within ±0.25, ±0.50, ±0.75, and ±1.00 D of PE.

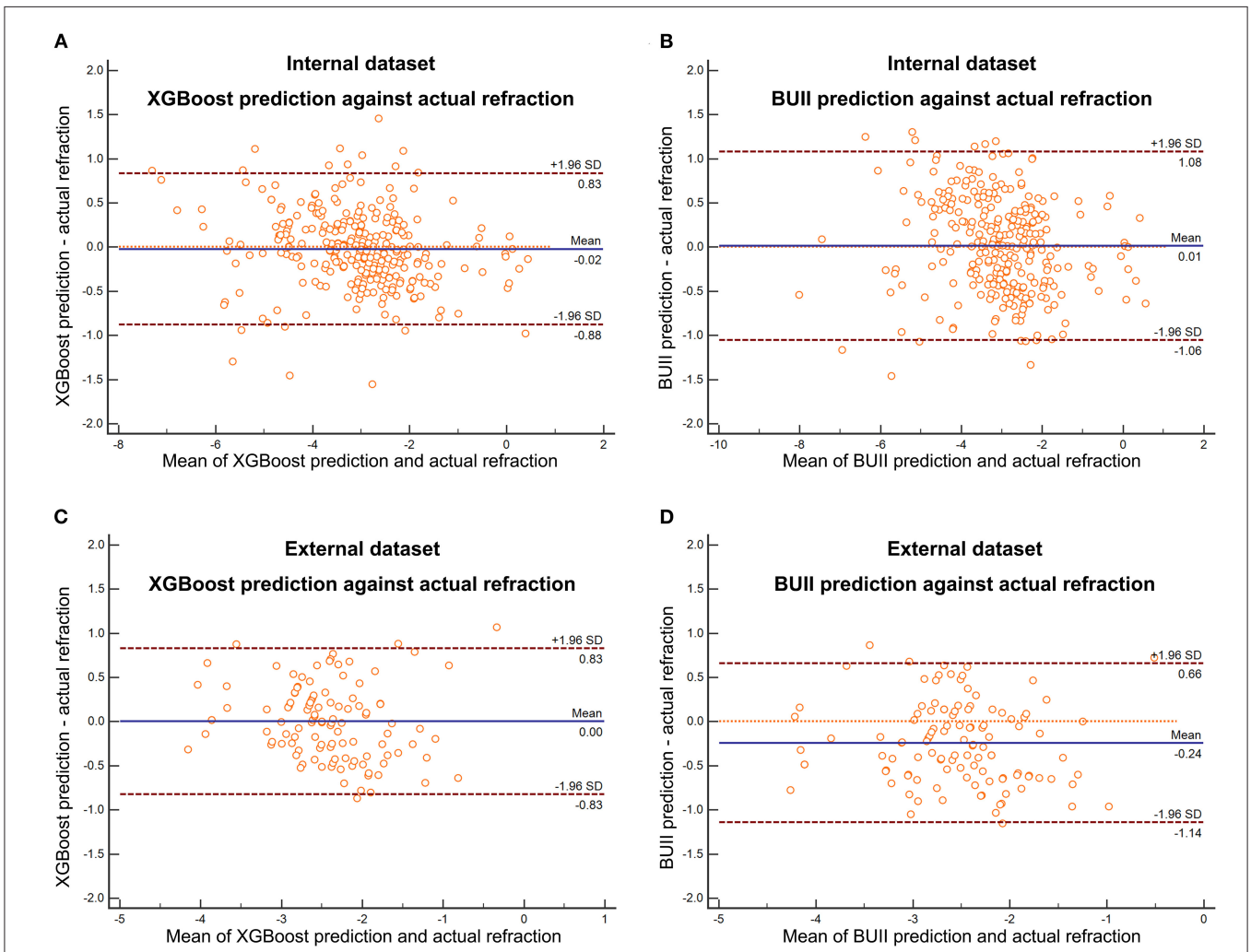

FIGURE 2 | The Bland-Altman plots with actual postoperative refraction against the XGBoost prediction in the internal **(A)** and external **(C)** test dataset or Barrett Universal II formula (BUII) prediction in the internal **(B)** and external **(D)** test dataset.

TABLE 3 | Summary of outcomes for the XGBoost calculator and the Barrett Universal II formula for the internal and external test datasets.

Parameters	Internal test dataset (n = 290)			External test dataset (n = 114)		
	XGBoost	BUII formula	*P*-value	XGBoost	BUII formula	*P*-value
Mean predicted refraction [range]	−3.09 [−6.88, 0.37]	−3.06 [−8.29, 0.58]		−2.41 [−4.32, 0.20]	−2.66 [−4.65, −0.15,]	
MedAE (D)	0.25	0.42	<0.001	0.29	0.42	0.001
MedSE (D^2)	0.06	0.17	<0.001	0.09	0.18	0.001
MAE (D) ± SD	0.33 ± 0.28	0.45 ± 0.31		0.35 ± 0.24	0.43 ± 0.29	
MSE (D^2) ± SD	0.19 ± 0.32	0.30 ± 0.36		0.18 ± 0.21	0.27 ± 0.29	
Eyes within PE (%)			<0.001			0.031
±0.25 D	49.66%	29.66%		43.86%	35.96%	
±0.50 D	78.28%	60.34%		72.81%	58.77%	
±0.75 D	90.69%	84.14%		92.98%	85.09%	
±0.10 D	97.24%	93.45%		99.12%	97.37%	

BUII, Barrett Universal II; MAE, mean absolute error; MedAE, median absolute error; SD, standard deviation; MSE, mean squared error; MedSE, median squared error; D, diopter. Wilcoxon signed-rank tests were used to compare the MedAE and MedSE results, and linear-by-linear associations were used to compare the distributions of the refractive errors.

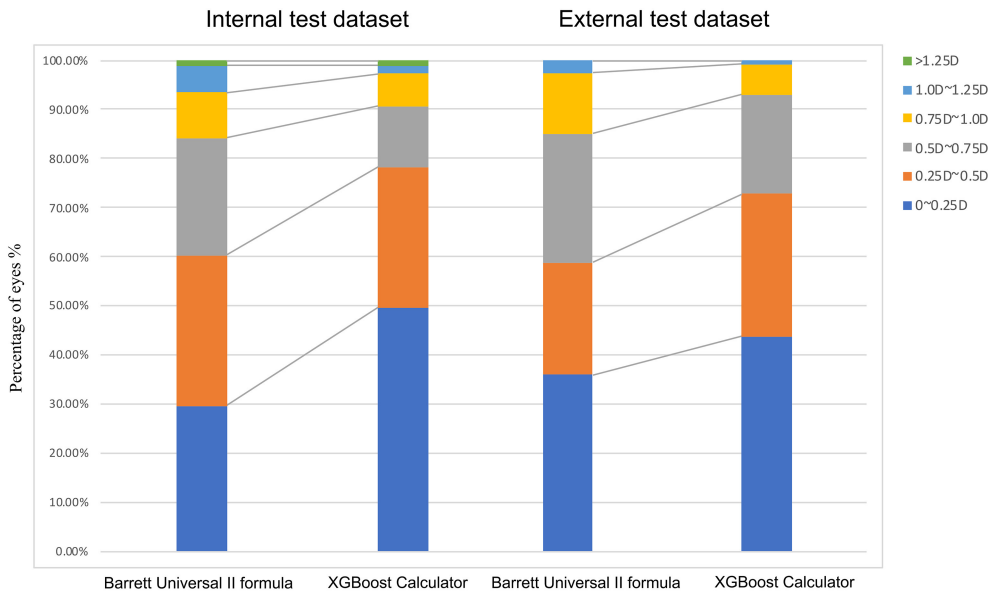

FIGURE 3 | Distribution of eyes within ±0.25 D, ±0.50 D, ±0.75 D, ±1.00 D, or ±1.25 D of the prediction errors in the internal test dataset.

of noncontact partial coherence interferometry can eliminate measurement errors, thus errors from the selected formula itself are of more concern (11, 28). Optimizing the constants of the existing formulas is one solution (29–31), while improving formulas that consider more characteristic variables for highly myopic eyes might be another.

In recent years, several new formulas that incorporate additional factors into the calculation have been developed, and efforts have been made to determine the most accurate formulas in eyes with ALs >26.0 mm (8, 11, 12, 14, 15, 17). The BUII formula seemed to show the best performance, and when used, the percentage of eyes within ±0.50 D of the PE varies from 62.7 to 89.5% (11, 12, 14, 15, 17). However, its refractive errors inevitably increase as AL increases (6). When we included more eyes with extreme myopia in our previous study, only 70% of eyes were within ±0.50 D of the PE using the BUII formula, with a corresponding value of 60.34% in the current study (17). Apart from that, the percentage of eyes within ±0.25 D of BUII formula was still unsatisfied in highly myopic eyes [25.0% (4), 34.7% (15), or 38.3% (14)]. Therefore, the BUII formula can still be improved for highly or especially extremely myopic eyes. On these grounds, we used machine learning to develop a new calculator to improve the BUII formula for long eyes.

Machine learning and data-driven approaches are becoming more important in ophthalmology (32). The RBF formula is another widely-used formula based on artificial intelligence. Although 86.6% of highly myopic eyes were within ±0.50 D of the PE using the latest version (24), their average AL of

TABLE 4 | Summary of outcomes from axial length subgroup analyses comparing the XGBoost calculator and the Barrett Universal II formula in the internal and external test datasets.

Subgroups/Parameters	Internal test dataset (n = 290)			External test dataset (n = 114)		
	XGBoost	BUII formula	*P*-value	XGBoost	BUII formula	*P*-value
AXIAL LENGTH						
26.0–28.0 mm						
Number of eyes	110			23		
MedAE (D)	0.23	0.40	<0.001	0.30	0.38	>0.05
MedSE (D^2)	0.05	0.16	<0.001	0.09	0.14	>0.05
MAE (D) ± SD	0.29 ± 0.24	0.42 ± 0.29		0.35 ± 0.26	0.35 ± 0.24	
MSE (D^2) ± SD	0.14 ± 0.21	0.26 ± 0.32		0.18 ± 0.25	0.18 ± 0.22	
28.0–30.0 mm						
Number of eyes	82			37		
MedAE (D)	0.25	0.41	<0.001	0.26	0.42	>0.05
MedSE (D^2)	0.06	0.17	<0.001	0.07	0.18	>0.05
MAE (D) ± SD	0.35 ± 0.30	0.48 ± 0.35		0.35 ± 0.24	0.38 ± 0.27	
MSE (D^2) ± SD	0.21 ± 0.40	0.35 ± 0.45		0.18 ± 0.21	0.21 ± 0.22	
≥30.0 mm						
Number of eyes	98			54		
MedAE (D)	0.35	0.44	<0.001	0.32	0.52	<0.001
MedSE (D^2)	0.12	0.20	<0.001	0.11	0.27	<0.001
MAE (D) ± SD	0.36 ± 0.30	0.46 ± 0.29		0.34 ± 0.24	0.51 ± 0.30	
MSE (D^2) ± SD	0.22 ± 0.35	0.30 ± 0.33		0.17 ± 0.20	0.35 ± 0.33	

XGBoost, new XGBoost calculator; BUII, Barrett Universal II; MedAE, median absolute error; MedSE, median squared error; MAE, mean absolute error; SD, standard deviation; MSE, mean squared error; D, diopter; PE, prediction error.
Wilcoxon signed-rank tests were used to compare the MedAE and MedSE results.

the included eyes was 27.72 mm (maximum: 32.36 mm) (24), indicating the validation of the RBF formula in extremely long eyes was still inadequate. In our study, the average AL was >29.00 mm (maximum: 36.46 mm), and more promising accuracy of the XGBoost calculator was also found over the RBF 2.0 formula. Therefore, our XGBoost calculator may be more reliable for extremely long eyes. Moreover, the RBF 2.0 formula is only used in cases where the postoperative target outcome is within −2.5 to 1 D (23). Its implementation is refined when <-2.5 D myopic refractive targets were scheduled for extremely long eyes. Compared with the RBF formula, our calculator might be more useful for IOL power prediction in highly or extremely myopic eyes.

In the present study, it is noteworthy that similar outcomes were also found using the external test dataset, which contained a greater proportion of extremely myopic eyes (79.82%), indicating the generalizability potential of our calculator. Furthermore, when the training and internal test datasets were subjected to 100 rounds of random splitting, our calculator showed high stability with more promising accuracy than the BUII formula. Using our website, surgeons need only enter the IOL power and the predicted refractions calculated with the BUII formula, together with the other clinical feature data required, to yield more accurate predictions of IOL power, and thereby assist surgeons with surgical planning for highly or extremely myopic eyes. Moreover, using the same algorithm, we are willing to further include more data of low or moderate myopic eyes to train the model, and thus further expand the scope of application for our calculator in the future.

In conclusion, we developed a new XGBoost machine learning-based calculator, which demonstrated good accuracy for IOL power prediction in highly and extremely myopic eyes.

DATA AVAILABILITY STATEMENT

The raw data supporting the conclusions of this article will be made available by the authors, without undue reservation.

ETHICS STATEMENT

The studies involving human participants were reviewed and approved by the Institutional Review Board of the Eye and Ear, Nose, and Throat (ENT) Hospital of Fudan University (Shanghai, China). The patients/participants provided their written informed consent to participate in this study.

AUTHOR CONTRIBUTIONS

LW: collected data, performed analyses, and wrote the manuscript. YS: programmed model and performed analyses. WH: collected data and performed analyses. XC and BM: collected data. YL: gained the fund and supervised the process.

XZ: revised the manuscript, gained the fund, and supervised the process. All authors contributed to the article and approved the submitted version.

FUNDING

This article was supported by research grants from the National Natural Science Foundation of the People's Republic of China (Grant Nos. 81870642, 81970780, 81470613, and 81670835), the Shanghai Shenkang Hospital Development Center Municipal Hospital Clinical Research and Cultivation Project (Grant No. SHDC120219X08), National Key R&D Program of China (Grant No. 2018YFC0116800), the Excellent Clinician-Excellent Clinical Scientist Program of the Eye and ENT Hospital of Fudan University, and Specialized Research Program for Shanghai Wise Information Technology of Medicine (Grant No. 2018ZHYL0220).

SUPPLEMENTARY MATERIAL

The Supplementary Material for this article can be found online at: https://www.frontiersin.org/articles/10.3389/fmed.2020.592663/full#supplementary-material

REFERENCES

1. Holden BA, Fricke TR, Wilson DA, Jong M, Naidoo KS, Sankaridurg P, et al. Global prevalence of myopia and high myopia and temporal trends from 2000 through 2050. *Ophthalmology.* (2016) 123:1036–42. doi: 10.1016/j.ophtha.2016.01.006
2. Holden B, Sankaridurg P, Smith E, Aller T, Jong M, He M. Myopia, an underrated global challenge to vision: where the current data takes us on myopia control. *Eye.* (2014) 28:142–6. doi: 10.1038/eye.2013.256
3. Hoffer KJ. Biometry of 7,500 cataractous eyes. *Am J Ophthalmol.* (1980) 90:360–8. doi: 10.1016/S0002-9394(14)74917-7
4. Zhu X, Li D, Du Y, He W, Lu Y. DNA hypermethylation-mediated downregulation of antioxidant genes contributes to the early onset of cataracts in highly myopic eyes. *Redox Biol.* (2018) 19:179–89. doi: 10.1016/j.redox.2018.08.012
5. Kanthan GL, Mitchell P, Rochtchina E, Cumming RG, Wang JJ. Myopia and the long-term incidence of cataract and cataract surgery: the Blue Mountains Eye Study. *Clin Exp Ophthalmol.* (2014) 42:347–53. doi: 10.1111/ceo.12206
6. Melles RB, Holladay JT, Chang WJ. Accuracy of intraocular lens calculation formulas. *Ophthalmology.* (2018) 125:169–78. doi: 10.1016/j.ophtha.2017.08.027
7. Wang L, Shirayama M, Ma XJ, Kohnen T, Koch DD. Optimizing intraocular lens power calculations in eyes with axial lengths above 25.0 mm. *J Cataract Refract Surg.* (2011) 37:2018–27. doi: 10.1016/j.jcrs.2011.05.042
8. Bang S, Edell E, Yu Q, Pratzer K, Stark W. Accuracy of intraocular lens calculations using the IOLMaster in eyes with long axial length and a comparison of various formulas. *Ophthalmology.* (2011) 118:503–6. doi: 10.1016/j.ophtha.2010.07.008
9. Wang JK, Hu CY, Chang SW. Intraocular lens power calculation using the IOLMaster and various formulas in eyes with long axial length. *J Cataract Refract Surg.* (2008) 34:262–7. doi: 10.1016/j.jcrs.2007.10.017
10. Barrett GD. An improved universal theoretical formula for intraocular lens power prediction. *J Cataract Refract Surg.* (1993) 19:713–20. doi: 10.1016/S0886-3350(13)80339-2
11. Cooke DL, Cooke TL. Comparison of 9 intraocular lens power calculation formulas. *J Cataract Refract Surg.* (2016) 42:1157–64. doi: 10.1016/j.jcrs.2016.06.029
12. Abulafia A, Barrett GD, Rotenberg M, Kleinmann G, Levy A, Reitblat O, et al. Intraocular lens power calculation for eyes with an axial length greater than 26.0 mm: comparison of formulas and methods. *J Cataract Refract Surg.* (2015) 41:548–56. doi: 10.1016/j.jcrs.2014.06.033
13. Roberts TV, Hodge C, Sutton G, Lawless M. Comparison of Hill-radial basis function, Barrett Universal and current third generation formulas for the calculation of intraocular lens power during cataract surgery. *Clin Exp Ophthalmol.* (2018) 46:240–6. doi: 10.1111/ceo.13034
14. Kane JX, Van Heerden A, Atik A, Petsoglou C. Accuracy of 3 new methods for intraocular lens power selection. *J Cataract Refract Surg.* (2017) 43:333–9. doi: 10.1016/j.jcrs.2016.12.021
15. Kane JX, Van Heerden A, Atik A, Petsoglou C. Intraocular lens power formula accuracy: comparison of 7 formulas. *J Cataract Refract Surg.* (2016) 42:1490–500. doi: 10.1016/j.jcrs.2016.07.021
16. Wang Q, Jiang W, Lin T, Zhu Y, Chen C, Lin H, et al. Accuracy of intraocular lens power calculation formulas in long eyes: a systematic review and meta-analysis. *Clin Exp Ophthalmol.* (2018) 46:738–49. doi: 10.1111/ceo.13184
17. Rong X, He W, Zhu Q, Qian D, Lu Y, Zhu X. Intraocular lens power calculation in eyes with extreme myopia: comparison of Barrett Universal II, Haigis, and Olsen formulas. *J Cataract Refract Surg.* (2019) 45:732–7. doi: 10.1016/j.jcrs.2018.12.025
18. Sugar A, Sadri E, Dawson DG, Musch DC. Refractive stabilization after temporal phacoemulsification with foldable acrylic intraocular lens implantation. *J Cataract Refract Surg.* (2001) 27:1741–5. doi: 10.1016/S0886-3350(01)00894-X
19. Chen TQ, Guestrin C, Association for Computing Machinery. XGBoost: a scalable tree boosting system. In: *Kdd'16: Proceedings of the 22nd Acm Sigkdd International Conference on Knowledge Discovery and Data Mining*. New York, NY: Association for Computing Machinery (2016).
20. Breiman L. Random forests. *Mach Learn.* (2001) 45:5–32. doi: 10.1023/A:1010933404324
21. Mark S, Alex G, Vladimir V, Vladimir V, Chris W, Jason W. Support vector regression with ANOVA decomposition kernels. In: Scholkopf B, Burghes CJC, Smola AJ, editors. *Advances in Kernel Methods: Support Vector Learning.* Cambridge, MA: MIT Press (1999). p. 285–91.
22. Hoffer KJ, Aramberri J, Haigis W, Olsen T, Savini G, Shammas HJ, et al. Protocols for studies of intraocular lens formula accuracy. *Am J Ophthalmol.* (2015) 160:403–5 e401. doi: 10.1016/j.ajo.2015.05.029
23. *Hill-RBF Calculator Instruction for Use*. Version V2.0 (2018). Available online at: https://rbfcalculator.com/docs/Hill-RBF-Calculator-Instructions.pdf (accessed October 21, 2020).
24. Wan KH, Lam TCH, Yu MCY, Chan TCY. Accuracy and precision of intraocular lens calculations using the New Hill-RBF Version 2.0 in eyes with high axial myopia. *Am J Ophthalmol.* (2019) 205:66–73. doi: 10.1016/j.ajo.2019.04.019
25. Norrby S. Sources of error in intraocular lens power calculation. *J Cataract Refract Surg.* (2008) 34:368–76. doi: 10.1016/j.jcrs.2007.10.031
26. Olsen T. Sources of error in intraocular lens power calculation. *J Cataract Refract Surg.* (1992) 18:125–9. doi: 10.1016/S0886-3350(13)80917-0
27. Zhu X, He W, Sun X, Dai J, Lu Y. Fixation stability and refractive error after cataract surgery in highly myopic eyes. *Am J Ophthalmol.* (2016) 169:89–94. doi: 10.1016/j.ajo.2016.06.022
28. Shen P, Zheng Y, Ding X, Liu B, Congdon N, Morgan I, et al. Biometric measurements in highly myopic eyes. *J Cataract Refract Surg.* (2013) 39:180–7. doi: 10.1016/j.jcrs.2012.08.064
29. Lee TH, Sung MS, Cui L, Li Y, Yoon KC. Factors affecting the accuracy of intraocular lens power calculation with lenstar. *Chonnam Med J.* (2015) 51:91–6. doi: 10.4068/cmj.2015.51.2.91
30. Aristodemou P, Knox Cartwright NE, Sparrow JM, Johnston RL. Intraocular lens formula constant optimization and partial coherence interferometry

biometry: refractive outcomes in 8108 eyes after cataract surgery. *J Cataract Refract Surg.* (2011) 37:50–62. doi: 10.1016/j.jcrs.2010.07.037

31. Petermeier K, Gekeler F, Messias A, Spitzer MS, Haigis W, Szurman P. Intraocular lens power calculation and optimized constants for highly myopic eyes. *J Cataract Refract Surg.* (2009) 35:1575–81. doi: 10.1016/j.jcrs.2009.04.028
32. Rohm M, Tresp V, Müller M, Kern C, Manakov I, Weiss M, et al. Predicting visual acuity by using machine learning in patients treated for neovascular age-related macular degeneration. *Ophthalmology.* (2018) 125:1028–36. doi: 10.1016/j.ophtha.2017.12.034

Conflict of Interest: The authors declare that the research was conducted in the absence of any commercial or financial relationships that could be construed as a potential conflict of interest.

frontiers in Medicine

ORIGINAL RESEARCH
published: 23 December 2020
doi: 10.3389/fmed.2020.615902

Morphologic Features of Myopic Choroidal Neovascularization in Pathologic Myopia on Swept-Source Optical Coherence Tomography

Jiamin Xie[1,2,3,4,5,6†], *Qiuying Chen*[1,2,3,4,5,6†], *Jiayi Yu*[1,2,3,4,5,6], *Hao Zhou*[1,2,3,4,5], *Jiangnan He*[6], *Weijun Wang*[1,2,3,4,5], *Ying Fan*[1,2,3,4,5,6*] *and Xun Xu*[1,2,3,4,5,6*]

[1] *Department of Ophthalmology, Shanghai General Hospital, Shanghai Jiao Tong University School of Medicine, Shanghai, China,* [2] *National Clinical Research Center for Eye Diseases, Shanghai, China,* [3] *Shanghai Key Laboratory of Ocular Fundus Disease, Shanghai, China,* [4] *Shanghai Engineering Center for Visual Science and Photo Medicine, Shanghai, China,* [5] *Shanghai Engineering Center for Precise Diagnosis and Treatment of Eye Diseases, Shanghai, China,* [6] *Department of Preventative Ophthalmology, Shanghai Eye Disease Prevention and Treatment Center, Shanghai Eye Hospital, Shanghai, China*

Purpose: To investigate the morphologic features and identify the risk factors of myopic choroidal neovascularization (CNV).

Methods: Eighty-eight eyes of 69 consecutive patients with myopic CNV were included in this study. About 109 eyes of 78 pathologic myopia patients without myopic CNV were randomly selected as the control group. Morphologic features and parameters including scleral thickness (ST), choroidal thickness (CT), posterior staphyloma height and the presence of scleral perforating vessels were obtained and measured by swept-source optical coherence tomography (SS-OCT). Binary logistic regression analysis was performed to identify the risk factors for myopic CNV.

Results: Patients with myopic CNV had relatively shorter axial length ($P < 0.001$) and thicker sclera ($P < 0.001$) compared to those without. After adjusting age, gender and axial length, thick sclera (OR = 1.333, $P < 0.001$ per 10-μm increase) and thin choroid (OR = 0.509, $P < 0.001$ per 10-μm increase) were associated with the presence of myopic CNV. Scleral perforating vessels were detected in the area of myopic CNV in 78.67% of the subjects.

Conclusions: A relatively thicker sclera and a thinner choroid are the biological indicators for myopic CNV on SS-OCT. Scleral perforating vessels may also play a pivotal role in the formation of myopic CNV.

Keywords: choroidal thickness, myopic choroidal neovascularization, scleral thickness, scleral perforating vessels, pathologic myopia

OPEN ACCESS

Edited by:
Xiangjia Zhu,
Fudan University, China

Reviewed by:
Peng Zhou,
Parkway Health, China
Xu Chen,
Shanghai Aier Eye Hospital, China

***Correspondence:**
Ying Fan
mdfanying@sjtu.edu.cn
Xun Xu
drxuxun@sjtu.edu.cn

†These authors have contributed equally to this work

Specialty section:
This article was submitted to Ophthalmology, a section of the journal Frontiers in Medicine

Received: *10 October 2020*
Accepted: *30 November 2020*
Published: *23 December 2020*

Citation:
Xie J, Chen Q, Yu J, Zhou H, He J, Wang W, Fan Y and Xu X (2020) Morphologic Features of Myopic Choroidal Neovascularization in Pathologic Myopia on Swept-Source Optical Coherence Tomography. Front. Med. 7:615902. doi: 10.3389/fmed.2020.615902

INTRODUCTION

Myopic choroidal neovascularization (CNV) is a common vision-threatening complication in pathologic myopia (PM) (1). The prevalence has been estimated to be 5.2 to 11.3% among individuals with PM (2). The long-term visual prognosis of myopic CNV is extremely poor without treatment. It has been reported that the visual acuity of myopic CNV deteriorated to 20/200 or worse in ∼89 and 96% of eyes in 5 years and 10 years, respectively (3). Intravitreal anti-VEGF therapy is the standard-of-care and first-line treatment for myopic CNV (4). Several studies have confirmed that early diagnosis and treatment of myopic CNV predicts a better visual outcome (5, 6). However, it is often difficult for patients with PM to notice new occurrences of myopic CNV because of the already impaired vision caused by other pathologies, which will finally lead to irreversible vision loss (4).

Optical coherence tomography (OCT) is a non-invasive imaging tool that has been used to diagnose and monitor treatment response in myopic CNV (7). Longer wavelength (1.050–1.060 nm) and deep penetrance swept-source OCT (SS-OCT) demonstrates its superiority in myopic eyes as it can provide clear visualization of the sclera and orbital fat tissue in myopes with longer axial lengths (7). In OCT image, myopic CNV presents as a highly reflective area contiguous above the RPE (type 2 CNV), usually with minimal subretinal fluid (4). Three different phases of myopic CNV have been identified based on the characteristics observed on OCT: active, scar, and atrophic phase (7).

Until recently, only few studies have described the risk factors associated with myopic CNV on OCT, and they mainly focus on choroidal morphology (8, 9). Sclera plays a pivotal role in determining eye size and the development of myopia (10). Despite its importance, the scleral morphology associated with the complications of myopia has not fully been explored yet. As such, we intend to supplement the current understanding of scleral morphology in myopic CNV.

Therefore, we aim to investigate the morphologic features and to identify the risk factors of myopic CNV on SS-OCT. Furthermore, it may help to find the high-risk groups among large-scale populations in future investigations.

METHODS

Participants

The study included 88 eyes of 69 consecutive patients with myopic CNV who had visited high myopia clinic in ophthalmological department of Shanghai General Hospital from July 2017 to July 2019. A myopic CNV was defined as a CNV that was present in eyes with PM (11). PM was defined as eyes having myopic maculopathy equal to or more severe than diffuse atrophy (12, 13). A cohort of 109 eyes of 78 PM participants were randomly selected to serve as the control group. The inclusion criteria were as follows: a SER < -6 diopters (D) or an AL $\geq$ 26 mm with PM; normal anterior chamber angles; normal optic nerve head (ONH) without glaucomatous changes; and no other ocular diseases. Exclusion criteria were as follows: previous intraocular or refractive surgery other than cataract surgery; features suggesting that the CNV may be associated with AMD, multifocal choroiditis or angioid streaks; Poor-quality images were also excluded. The diagnosis of a myopic CNV was based on the presence of a highly reflective area contiguous above the RPE (type 2 CNV), usually with minimal subretinal fluid (4, 14). Considering that myopic CNV is often bilateral (15), the fellow eye of the pre-existing myopic CNV patients were not included in the control group. This study was conducted in accordance with the Declaration of Helsinki and was approved by the ethics committee of Shanghai General Hospital. Informed consent was obtained from each patient.

Examinations

All study participants underwent a comprehensive ophthalmic examination, including measurements of slit-lamp biomicroscopy, intraocular pressure (IOP, Full Auto Tonometer TX-F; Topcon, Japan), best-corrected visual acuity (BCVA), axial length (IOL Master; Carl Zeiss, Tubingen, Germany) and assessment of the refractive error using an autorefractor instrument (model KR-8900; Topcon, Japan). The BCVA was converted into the logarithm of minimal angle resolution (logMAR). FFA was obtained by Heidelberg Spectralis HRA (Heidelberg Engineering, Heidelberg, Germany). Swept-source optical coherence tomography (SS-OCT, model DRI OCT-1 Atlantis; Topcon, Japan) was used to capture color fundus photographs and to measure the scleral thickness (ST) and choroidal thickness (CT). The OCT scanning protocols included a length of 9 mm with 12 equal radial meridian scans centered on the fovea.

Classification and Definition

According to the International Photographic Classification and Grading System, myopic maculopathy (MM) was classified based on fundus photographs into tessellated fundus (C1), diffuse chorioretinal atrophy (C2), patchy chorioretinal atrophy (C3), and macular atrophy (C4) (12). Scleral perforating vessels were defined as uniform hypo-reflective structures within the scleral stroma and macular area on SS-OCT B-scanned images (**Figures 2B,F**) (16). Dome-shaped macula (DSM) was characterized as an inward bulge of the retinal pigment epithelium of more than 50 μm in the vertical and/or horizontal direction on OCT examination (17). Myopic CNV was classified into three phases on OCT (**Figure 2**): the active phase (a hyperreflective elevation with or without exudation or hemorrhage. All features, including subretinal fluid, subretinal hyperreflective exudation and the fuzzy borders of CNV and a lack of RPE coverage indicate an active phase of a CNV), the scar phase (a hyperreflectivity in the inner surface of the CNV, with attenuation of the tissue bellow, which is also known as "Fuch's spot"), and the atrophic phase (also known as CNV-related macular atrophy with enhanced choroidal reflectivity corresponding to the area of chorioretinal atrophy, and is characterized by the formation of a hole in Bruch's membrane) (4, 7, 18). Fundus fluorescein angiography (FFA) was performed when needed. Two masked ophthalmologists (J.X. and Q.C.)

performed the classification of myopic CNV. Discrepancies were adjudicated by a senior retinal specialist (Y.F.).

Measurements

Two trained graders (J.Y. and J.H.) blinded to the study independently measured the thickness of each layer at the fovea, 1.5 mm and 3.0 mm from the macula on horizontal and vertical radial OCT scan lines. The CT was defined as the vertical distance between the outer border of the RPE and the choroidal–scleral interface. The ST was defined as the vertical distance between the choroidal–scleral interface and the outer scleral border. If the absolute difference between two measurements was $>20\,\mu m$ for the sclera or $10\,\mu m$ for the choroid, the measurements were repeated until the absolute difference was within the set limits (19). The height of the posterior staphyloma (PS) was the vertical distance from the subfoveal retinal pigment epithelium line to 3 mm nasal, temporal, superior, and inferior to the fovea (8). The relative height of the PS was expressed as either a positive or a negative number depending on the edge located anteriorly or posteriorly. The absolute height of PS is used in some specific analyses. After adjusting the magnification of the AL, the ST, CT, and PS height on the OCT B-scan were measured by the built-in software (20). The measurements from the two graders were averaged. The 1.5 mm or 3.0mm average to the fovea defined as the average measurements of 1.5 mm or 3.0 mm superior, inferior, temporal, and nasal to the fovea center. The method used to measure CT, ST, and PS height is shown in **Figure 1**.

Statistical Analysis

Statistical evaluation was performed using SPSS software (IBM SPSS Statistics 21; SPSS, Inc, Chicago, IL). Categorical variables, rank variables, and continuous variables were analyzed with the Chi-square test, Wilcoxon test and Mann-Whitey *U* test, respectively. Kruskal-Wallis test was used for comparisons of myopic CNV subtypes. Spearman's correlation was used to identify the correlations among ST/CT and AL. Binary logistic regressions were performed to evaluate the independent associations of myopic CNV occurrence, with adjustment for age, gender, and AL. Generalized estimating equations were used to account for correlation between left and right eyes of the same patient. All data were expressed as mean ± standard deviation or proportions as appropriate. A *P*-value <0.05 was considered statistically significant.

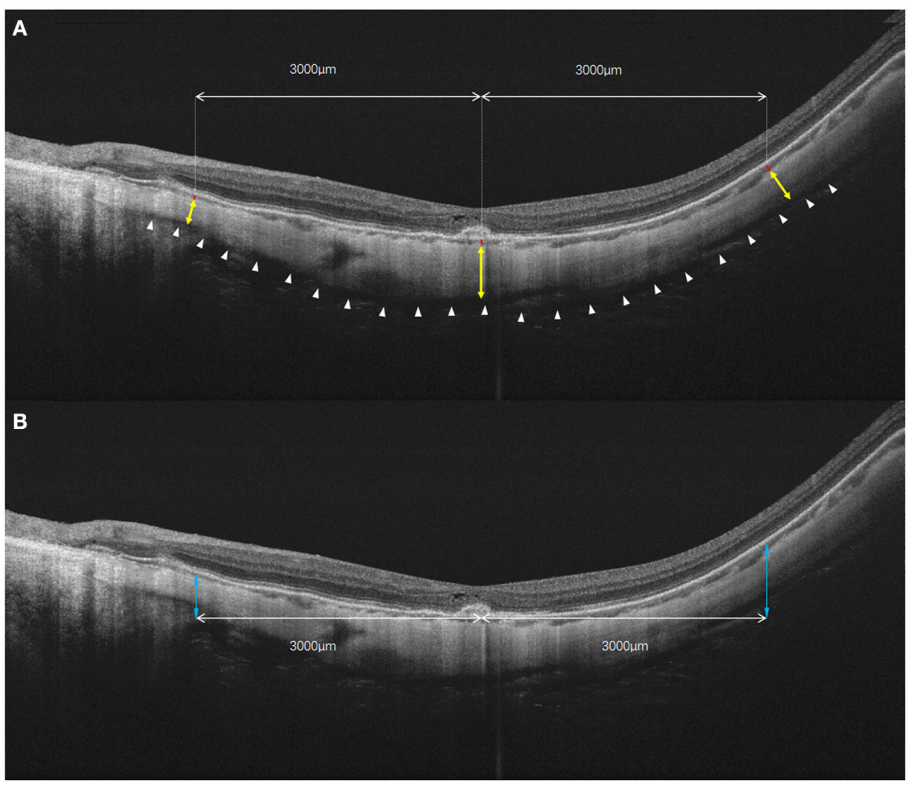

FIGURE 1 | The diagrammatic sketch for the measurements of choroidal and scleral thickness, as well as the height of posterior staphyloma. **(A)** Choroidal and scleral thickness was measured along the perpendicular axis to the curvature of the retinal pigment epithelium. Yellow double arrow: scleral thickness measured in fovea and 3 mm nasal and temporal to the fovea. Red bar: choroidal thickness measured in fovea and 3 mm nasal and temporal to the foveal. White arrowheads: outer surface of the sclera. **(B)** The height of the posterior staphyloma (double blue arrow) was measured as the vertical distance from the subfoveal retinal pigment epithelium line to the point at 3 mm from both sides of the fovea. In the vertical scan, choroidal and scleral thicknesses also were measured at 3 mm superior and inferior to the fovea.

RESULTS

The generalized estimating equation regression models revealed that there were no significant differences in ocular biometry between the two eyes; thus, it was unnecessary to adjust for associations between the two eyes.

Eighty-eight eyes of 69 patients diagnosed as myopic CNV and 109 eyes of 78 patients served as control group, were included in this study. Mean age of patients was 57.09 ± 11.93 years. Forty-one (27.9%) were men and 106 (72.1%) were women. Among eyes with myopic CNV, 41 eyes of 33 patients had received anti-VEGF treatment before the recruitment. None of them had been treated with photodynamic therapy. CNV was subfoveal in 68 (77.27%) eyes and juxtafoveal in 20 (22.73%) eyes. The mean CNV lesion size is 0.66 ± 0.77mm^2. Patient demographic data is shown in **Table 1**. Patients with myopic CNV showed less myopic refractive error (−13.36 ± 4.52 vs. −16.05 ± 3.76 D, $P < 0.0001$, after excluding pseudophakic eyes), shorter axial length (29.51 ± 1.42 vs. 30.51 ± 1.78 mm, $P < 0.0001$) and worse BCVA (0.83 ± 0.69 vs. 0.39 ± 0.26, $P < 0.0001$) than those without myopic CNV.

After exclusion of eyes with DSM ($n = 22$), 75 eyes with myopic CNV (**Figure 2**) were compared to 100 eyes without myopic CNV (**Figure 3**) on SS-OCT (**Table 2**). In eyes with myopic CNV, ST was significantly thicker at subfoveal region (290.89 ± 84.51 vs. 226.24 ± 58.38 μm, $P < 0.001$), 1.5 mm (234.76 ± 63.03 vs. 182.79 ± 44.99 μm, $P < 0.001$) and 3.0 mm (212.24 ± 51.28 vs. 172.61 ± 40.45 μm, $P < 0.001$) average to the fovea. The average ST/CT was also significantly larger in myopic CNV (12.74 ± 6.12 vs. 10.61 ± 4.70, $P = 0.046$). However, CT, average relative and absolute PS height showed no significant difference between two group.

In eyes with diffuse atrophy (C2), the ones with myopic CNV showed relatively shorter axial length ($P < 0.001$) and thicker sclera at subfoveal (312.71 ± 93.79 vs. 234.62 ± 56.18 mm, $P = 0.003$), 1.5 mm (246.81 ± 71.24 vs. 190.56 ± 44.56 mm, $P < 0.001$) and 3.0 mm (224.98 ± 52.76 vs. 179.48 ± 41.33 mm, $P < 0.001$) to the fovea. However, CT showed no significant difference between eyes with and without myopic CNV (**Table 3**). In eyes with patchy atrophy (C3), those with myopic CNV showed relatively shorter axial length ($P < 0.001$), worse BCVA ($P = 0.018$) and thicker sclera at subfoveal (254.67 ± 52.95 vs. 204.96 ± 59.52 mm, $P < 0.001$), 1.5 mm (207.03 ± 42.55 vs. 163.09 ± 40.54 mm, $P < 0.001$) and 3.0 mm (197.83 ± 41.42 vs. 155.16 ± 32.76, $P < 0.001$) average to the fovea. However, the CT of eyes with myopic CNV was significantly thicker at 1.5 mm ($P = 0.002$) and 3.0 mm ($P = 0.006$) average to the fovea (**Table 3**).

In the subgroup of myopic CNV (**Table 4**), CNV-related macular atrophy showed a worse BCVA than active and scar CNV ($P < 0.001$). Active CNV had relatively thicker CT than CNV scar and CNV-related macular atrophy group at subfoveal ($P = 0.044$) and 1.5 mm average to the fovea ($P = 0.004$), and it was relatively thicker than CNV scar at 3.0 mm average to the fovea ($P = 0.017$). ST, average relative and absolute PS height showed no significant difference between the subgroups of myopic CNV. The presence of scleral perforating vessels in the area of a CNV were found in 59 out of 75 (78.67%) eyes with myopic CNV. The rate of scleral perforating vessels found beneath or around myopic CNV showed no significant difference between the subgroups of myopic CNV ($P = 0.713$).

TABLE 1 | Comparisons of clinical characteristics between eyes with and without myopic CNV in PM.

Characteristics	Eyes with myopic CNV	Eyes without myopic CNV	*P*
Number of eyes (No. of persons)	88 (69)	109 (78)	
Age, y	58.88 ± 12.22	55.86 ±11.66	0.087
Gender, Male/Female	22/66	36/73	0.268
Eye, Right/Left	43/45	54/55	0.925
Axial length, mm	29.51 ± 1.42	30.51 ± 1.78	<0.001*
BCVA, logMAR	0.83 ± 0.69	0.39 ± 0.26	<0.001*
DSM (%)	13 (14.77%)	9(8.26%)	0.149

*CNV, choroidal neovascularization; PM, pathologic myopia; BCVA, best-corrected visual acuity; logMAR, logarithm of minimum angle of resolution; DSM, dome-shaped macula. *Significant difference.*

In all eyes without DSM, AL was inversely and significantly correlated with average ST ($r = −0.5$, $P < 0.001$) and average CT($r = −0.4$, $P < 0.001$, **Figure 4**). Similarly, AL was negatively correlated with subfoveal ST ($r = −0.5$, $P < 0.001$) and subfoveal CT ($r = −0.2$, $P = 0.007$). We then performed binary logistic regression analysis to detect risk factors of myopic CNV (**Figure 5**). Eyes with thicker sclera (OR = 1.333, $P < 0.001$ per 10-μm increase) and thinner choroid (OR = 0.509, $P = 0.010$ per 10-μm increase) were more likely to have myopic CNV. After categorizing age, axial length, average ST and CT into quartiles, we found that eyes in the third (OR = 4.818, $P = 0.006$) and fourth quartile (OR = 16.354, $P < 0.001$) of average ST were significantly more likely to have myopic CNV. On the contrary, eyes in the first quartile (OR = 3.28, $P = 0.036$) of average CT were significantly more likely to have myopic CNV. Besides, larger average ST/CT (OR = 1.134, $P = 0.002$) and shorter axial length (OR = 0.56, $P < 0.001$) increased the possibility of myopic CNV occurrence with adjustment of age, gender and average absolute PS height.

DISCUSSION

To the best of our knowledge, this is the first study to recruit all phases of myopic CNV and compare the SS-OCT features between eyes with and without myopic CNV. The results of this study showed that the patients with myopic CNV had relatively shorter axial length and thicker sclera. After adjusting age, gender and axial length, thick sclera and thin choroid were associated with the presence of myopic CNV. In addition, scleral perforating vessels were detected in the area of myopic CNV in 78.67% of the subjects. These morphologic features are particularly important for screening myopic CNV in future investigations.

Previous studies have reported that the choroid thinning and choroidal filling delay was associated with the risk of developing

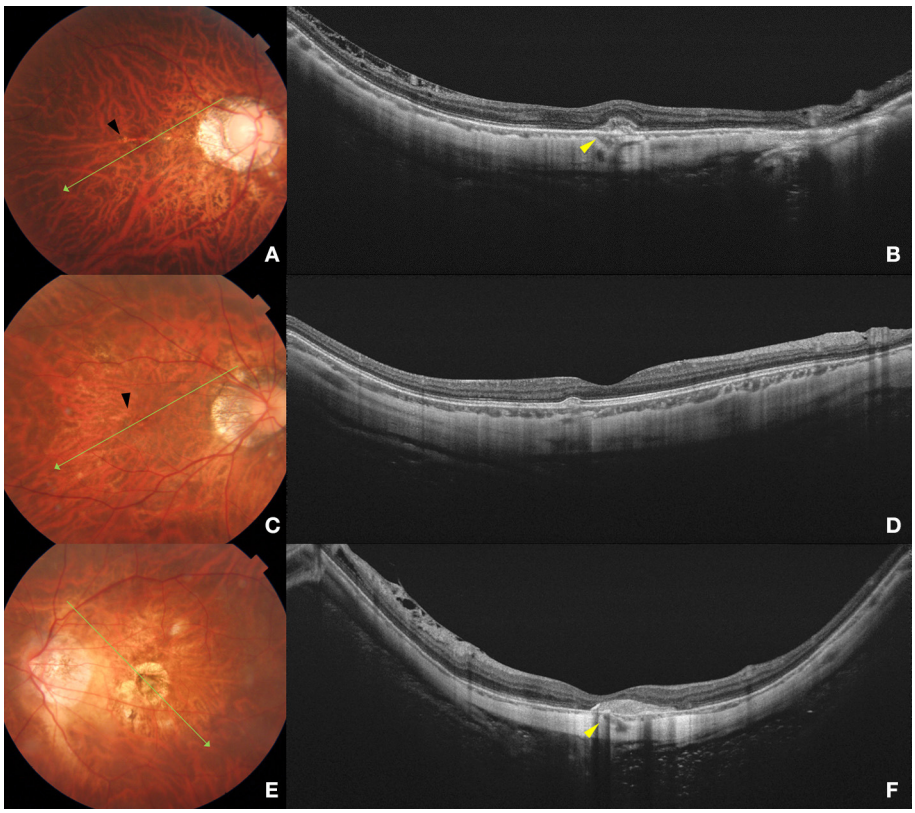

FIGURE 2 | Fundus photograph and swept-source optical coherence tomography (SS-OCT) images of different phases of myopic CNV. Left column **(A,C,E)** shows color fundus photographs. The long green arrow shows the scanned line examined by SS-OCT. Right column **(B, D, F)** shows the corresponding SS-OCT image. **(A)** A 32-year-old young male with peripapillary diffuse atrophy and an active CNV. Mild bleeding and lacquer crack (black arrow) are observed in the macular area. **(B)** B-scan SS-OCT shows a type 2 CNV with minimal subretinal hyperreflective exudation. Scleral perforating vessel (yellow arrowhead) penetrated around CNV. The subfoveal scleral thickness is 288 μm. **(C)** A 40-year-old female with peripapillary diffuse choroidal atrophy and a scar phase myopic CNV. Lacquer cracks (black arrow) are shown in the macular area. **(D)** SS-OCT shows scarred CNV as a small RPE elevation with intact ellipsoid zone and ELM. The subfoveal scleral thickness is 360 μm. **(E)** A 61-year-old female with CNV-related macular atrophy. Macular atrophy around the myopic CNV is observed in the macular area. **(F)** SS-OCT shows a scarred CNV with a scleral perforating vessel (yellow arrowhead) penetrating below the CNV lesion. The subfoveal scleral thickness is 220 μm.

myopic CNV (8, 9). However, in this study, we considered the parameters of ST and found that thicker sclera and thinner choroid may be biological indicators of CNV occurrence after adjusting age, gender and axial length. ST was reported to be significantly correlated with axial length (21), but it has rarely been discussed in the development of myopic CNV. In addition, Fang et al. (18) suggested that myopic CNV tended to develop in the eyes with an axial length of approximately 29 mm based on a long-term follow-up study. These all indicate that myopic CNV occurred during the progression of PM, but not in the late-stage of PM.

Scleral perforating vessels were reported to be associated with lacquer cracks and myopic CNV in previous studies (16, 22). In this study, approximately 80% of eyes with myopic CNV had scleral perforating vessels, this was consistent with the results of Ishida et al. (22) We tend to think that scleral perforating vessels were either concentrated forces of stretch from the sclera or the locus *minoris resistentiae* as previously reported (16) Due to the extremely thinned choroid caused by loss of large vessels, stroma and choriocapillaris, mechanical stress that is posed through scleral perforating vessels cannot be buffered and dispersed, and the force concentrated in a limited location which may cause the disruption of the RPE-BM-CC (retinal pigment epithelium-Bruch's membrane-choriocapillaris) complex, and myopic CNV may occur as an attempt to fix the mechanical break (23). Furthermore, the correlation between scleral thickness and amount of scleral perforating vessels requires sclera remodeling techniques and long-term follow-up.

The pathogenesis of myopic CNV is not fully understood but several hypotheses have been proposed, such as the mechanical theory, the heredodegenerative theory and the hemodynamic alteration in choroidal circulation (4, 23). This indicates that the presence of myopic CNV may be contributed by a combination of several factors. In this study, we described several characteristic features of myopic CNV on SS-OCT including a relatively thicker sclera and a thinner choroid with the presence of scleral perforating vessels. We especially filled the gap in the current understanding of scleral morphology in myopic CNV. Considering all the evidences above, we speculate that the unmatched decrease in scleral and choroidal thickness during the

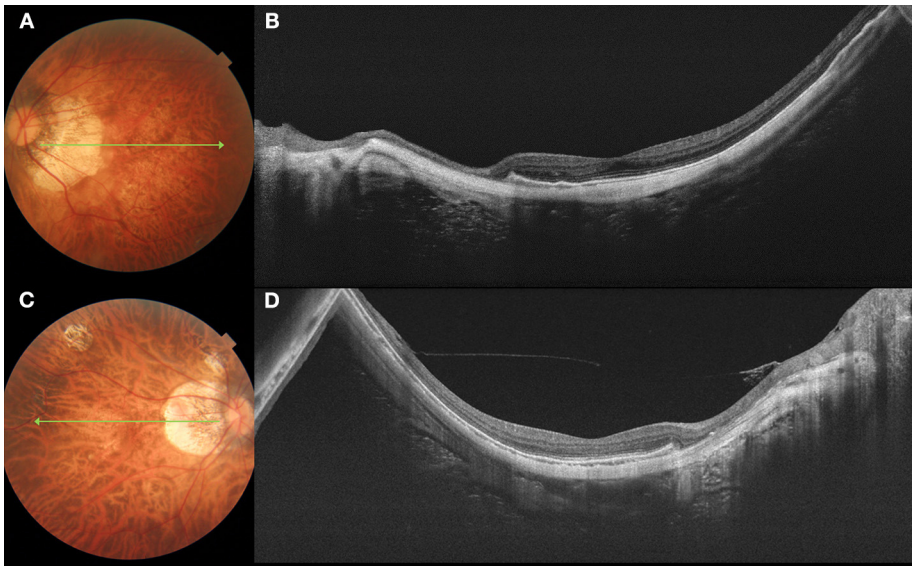

FIGURE 3 | Fundus photograph and swept-source optical coherence tomography (SS-OCT) images of pathologic myopia eyes with no myopic CNV. Left column **(A,C)** shows color fundus photographs. The long green arrow shows the scanned line examined by SS-OCT. Right column **(B,D)** shows the corresponding SS-OCT image. **(A)** A 62-year-old female with diffuse atrophy fundus. **(B)** SS-OCT shows a relative thin sclera. The subfoveal scleral thickness is 207 μm. **(C)** A 46-year-old female with patchy atrophy. **(D)** SS-OCT shows a relative thin sclera, with subfoveal scleral thickness is 135 μm.

TABLE 2 | The comparison of parameters on SS-OCT between eyes with and without myopic CNV.

	Eyes with myopic CNV ($n = 75$)	Eyes without myopic CNV ($n = 100$)	*P*	*P'*
ST, μm				
Subfoveal	290.98 ± 84.51	226.24 ± 58.38	<0.001*	<0.001*
1.5 mm average	234.76 ± 63.03	182.79 ± 44.99	<0.001*	<0.001*
3.0 mm average	212.24 ± 51.28	172.61 ± 40.45	<0.001*	<0.001*
Total average	231.00 ± 57.52	182.83 ± 41.51	<0.001*	<0.001*
CT, μm (67 eyes available in eyes with myopic CNV)				
Subfoveal	16.84 ± 9.06	17.40 ± 12.14	0.842	0.669
1.5 mm average	21.79 ± 11.16	21.57 ± 15.70	0.231	0.769
3.0 mm average	23.23 ± 110.94	22.79 ± 17.88	0.139	0.964
Total average	21.83 ± 9.69	21.63 ± 15.23	0.156	0.916
Average ST/CT	12.74 ± 6.12	10.61 ± 4.70	0.046*	0.022*
Average relative PS height, μm	425.16 ± 162.43	483.48 ± 180.846	0.107	0.195
Average absolute PS height, μm	496.07 ± 134.90	520.89 ± 154.28	0.542	0.362

SS-OCT, swept-source optical coherence tomography; CNV, choroidal neovascularization; ST, scleral thickness; CT, choroidal thickness; PS, posterior staphyloma; P', comparisons after adjusted age and gender.
**Significant difference.*

progression of pathologic myopia, with simultaneous mechanical effects caused by scleral perforating vessels may increase the risk of myopic CNV occurrence. Further studies recruiting newly onset myopic CNV patients are required to investigate whether the average ST/CT is a prognostic value to predict the occurrence of myopic CNV.

The correlation between staphyloma depth and the risk of myopic CNV is controversial. The nasal absolute staphyloma height was described to be associated with the myopic CNV occurrence in a small-scale study (8). However, we did not find any correlation between staphyloma height and myopic CNV occurrence. This is consistent with a previous study that myopic CNV usually occurs in the eyes with staphylomas of intermediary depth, and eyes with the deepest staphylomas had no myopic CNV indeed (24). These indicated that myopic CNV is a consequence of local pathological changes instead of the overall mechanical strength effect during the progressive elongation of the eyeball.

This study had several limitations. Firstly, this is a cross-sectional study, further long-term observational studies are

TABLE 3 | The comparison of characteristics and parameters on SS-OCT eyes with and without myopic CNV in C2 and C3.

	Eyes with myopic CNV		Eyes without myopic CNV		P^a	P^b	P^c	P^d
	C2	C3	C2	C3				
Number of eyes	32	26	73	27				
Age, y	59.03 ± 13.54	53.38 ± 13.25	57.33 ± 10.98	55.46 ± 10.40	0.227	0.936		
Axial length, mm	29.19 ± 1.56	29.84 ± 1.43	30.00 ± 1.59	31.76 ± 1.48	0.017*	<0.001*	0.022*	0.001*
BCVA, logMAR	0.54 ± 0.36	0.55 ± 0.28	0.40 ± 0.26	0.35 ± 0.22	0.050	0.018*	0.008*	0.025*
ST,μm								
Subfoveal	312.71 ± 93.79	254.67 ± 52.95	234.62 ± 56.18	204.96 ± 59.53	<0.001*	<0.001*	<0.001*	0.002*
1.5mm average	246.81 ± 71.24	207.03 ± 42.55	190.56 ± 44.56	163.09 ± 40.54	<0.001*	<0.001*	<0.001*	0.001*
3.0mm average	224.98 ± 52.76	197.83 ± 41.42	179.48 ± 41.33	155.16 ± 32.76	<0.001*	<0.001*	<0.001*	<0.001*
Total average	244.43 ± 63.61	208.23 ± 40.14	190.16 ± 41.55	164.22 ± 35.82	<0.001*	<0.001*	<0.001*	<0.001*
CT,μm								
Subfoveal	16.84 ± 9.61	17.22 ± 7.80	18.50 ± 12.92	14.62 ± 9.54	0.834	0.069	0.645	0.220
1.5mm average	23.83 ± 11.98	22.49 ± 9.27	24.53 ± 17.08	14.04 ± 7.52	0.582	0.002*	0.900	0.007*
3.0mm average	25.32 ± 11.74	20.83 ± 9.68	26.19 ± 19.70	14.15 ± 6.81	0.511	0.006*	0.806	0.001*
Total average	23.65 ± 10.80	21.11 ± 8.09	24.58 ± 16.72	14.13 ± 5.97	0.669	0.002*	0.894	0.005*
Average relative PS height, μm	389.56 ± 152.47	501.24 ± 178.94	434.21 ± 155.45	432.05 ± 131.17	0.058	0.570	0.056	0.528
Average absolute PS height, μm	482.82 ± 137.51	549.96 ± 136.66	483.19 ± 122.90	489.95 ± 95.71	0.326	0.442	0.169	0.300

SS-OCT, swept-source optical coherence tomography; CNV, choroidal neovascularization; BCVA, best-corrected visual acuity; logMAR, logarithm of minimum angle of resolution; ST, scleral thickness; CT, choroidal thickness; PS, posterior staphyloma; P^a, comparison between eyes with and without myopic CNV in C2; P^b, comparison between eyes with and without myopic CNV in C3; P^c, comparison between eyes with and without myopic CNV in C2 after adjusted age and gender; P^d, comparison between eyes with and without myopic CNV in C3 after adjusted age and gender.
**Significant difference.*

TABLE 4 | The comparison of parameters on SS-OCT among subgroups of myopic CNV.

	Active CNV (n = 39)	Scar/Fuch's spot (n = 20)	CNV-related macular atrophy (n = 16)	P
Age, y	59.64 ± 11.90	53.40 ± 14.93	62.13 ± 5.80	0.221
Axial length, mm	29.09 ± 1.38	30.04 ± 1.56	29.82 ± 1.24	0.060
BCVA, logMAR	0.64 ± 0.38	0.45 ± 0.27	1.55 ± 0.78	<0.001*
CNV location (subfoveal/juxtafoveal)	31/8	7/13	16/0	<0.001*
CNV size, mm^2	0.50 ± 0.55	0.28 ± 0.21	1.58 ± 0.36	0.002*
ST, μm				
Subfoveal	306.97 ± 93.04	274.75 ± 60.11	268.13 ± 76.61	0.452
1.5 mm average	246.72 ± 65.65	214.75 ± 53.46	225.86 ± 64.49	0.165
3.0 mm average	220.74 ± 51.88	203.68 ± 43.70	189.27 ± 59.40	0.102
CT, μm (8 eyes were available in CNV-related macular atrophy group)				
Subfoveal	19.23 ± 8.27	14.65 ± 9.48	12.38 ± 10.80	0.044*
1.5mm average	24.78 ± 9.33	19.16 ± 12.62	15.72 ± 12.15	0.004*
3.0mm average	25.43 ± 8.51	18.68 ± 13.10	22.59 ± 12.50	0.017*
Scleral perforating vessels (%)	76.92%	85.00%	75.00%	0.713
Average relative PS height, μm	433.52 ± 172.17	398.46 ± 162.02	453.30 ± 97.64	0.460
Average absolute PS height, μm	515.28 ± 132.38	472.06 ± 149.00	457.80 ± 90.42	0.350

SS-OCT, swept-source optical coherence tomography; CNV, myopic choroidal neovascularization; BCVA, best-corrected visual acuity; logMAR, logarithm of minimum angle of resolution; ST, scleral thickness; CT, choroidal thickness; PS, posterior staphyloma.
**Significant difference.*

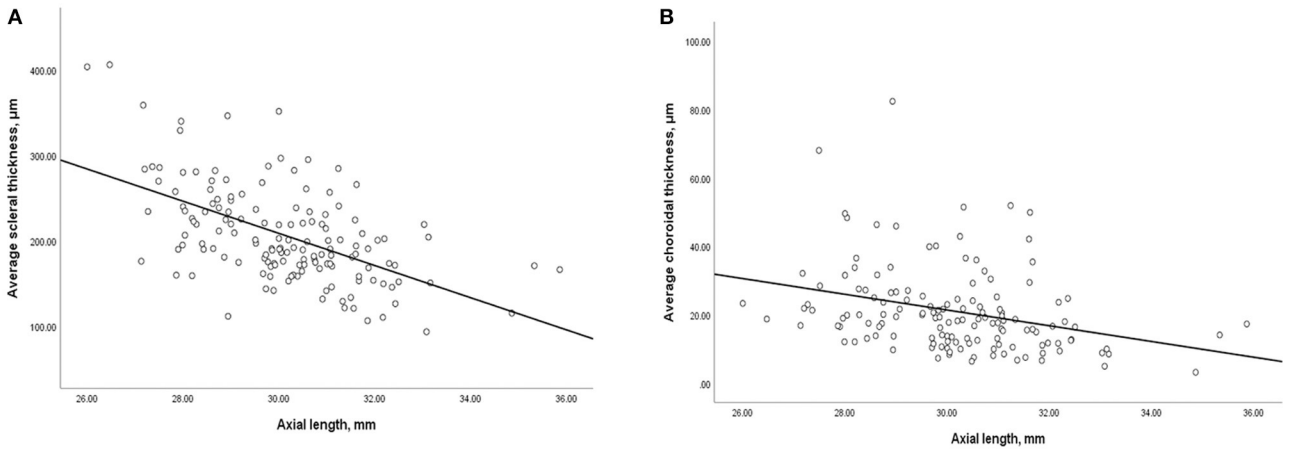

FIGURE 4 | Scatterplot showing **(A)** negative correlation between average scleral thickness and axial length, **(B)** negative correlation between average choroidal thickness and axial length.

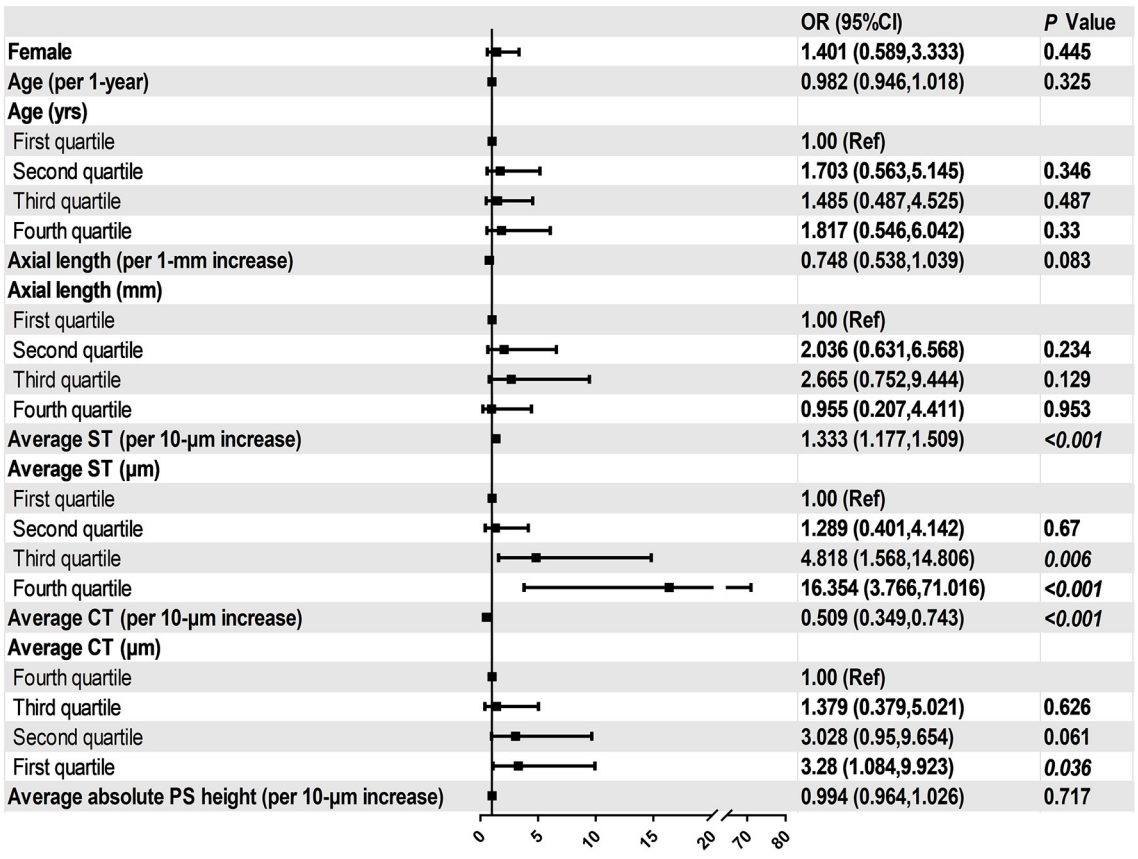

FIGURE 5 | Associations between ocular parameters and the presence of myopic CNV in the multivariate adjusted models.

required to detect whether myopic CNV develops above the scleral perforating vessels. Secondly, OCT and fundus photograph with a wide-field range of scanning may be more efficient to detect and measure PS in future analysis. Thirdly, reconstruction of choroid and scleral, as well as the corresponding myopic CNV lesions by artificial intelligence may be more comprehensive and intuitive for us to realize the morphologic features of myopic CNV. Fourthly, we did

not include eyes with lacquer cracks in myopic CNV groups. Although lacquer cracks were risk factors for CNV, the progression of lacquer cracks to CNV was uncommon (18, 25). Further longitudinal studies and new classification system may be necessary for future investigations. Finally, SS-OCT acquired only radial scan images focusing on the macula. Certain characteristic morphologies may have been missed in the para- or extra-foveal regions.

In summary, we found that relatively thicker sclera and thinner choroid were biological indicators for myopic CNV on SS-OCT after adjusting age, gender, axial length. Additionally, scleral perforating vessels may be another pivotal factor associated with the presence of myopic CNV. The specific area above the scleral perforating vessels should be given special attention for early detection of myopic CNV. SS-OCT is a useful tool to identify the high-risk groups when screening large populations. Eyes with such morphologic features presented on SS-OCT may need closer follow-ups for monitoring myopic CNV.

DATA AVAILABILITY STATEMENT

The original contributions presented in the study are included in the article/supplementary materials, further inquiries can be directed to the corresponding author/s.

ETHICS STATEMENT

This study was approved by the ethics committee of Shanghai General Hospital. Written informed consent was obtained from the individual(s) for the publication of any potentially identifiable images or data included in this article.

AUTHOR CONTRIBUTIONS

JX, YF, and XX designed this study. JX, QC, JY, HZ, and WW collected and measured data. JX and JH analyzed data. JX, QC, and YF wrote this article. All authors discussed the results and commented on the manuscript.

FUNDING

This study was supported by the National Key R&D Program of China (2016YFC0904800, 2019YFC0840607), National Science and Technology Major Project of China (2017ZX09304010), Shanghai Science and Technology Commission Research Project (Grant No. 17ZR1426900, Shanghai, China), Shanghai Municipal Science and Technology Commission (Grant No. 201640090) and National Natural Science Foundation of China (Grant No. 81703287, Beijing, China). The sponsors and funding organizations had no role in the design or conduct of this research.

REFERENCES

1. Wolf S, Balciuniene VJ, Laganovska G, Menchini U, Ohno-Matsui K, Sharma T, et al. RADIANCE: a randomized controlled study of ranibizumab in patients with choroidal neovascularization secondary to pathologic myopia. *Ophthalmology*. (2014) 121:682–92.e2. doi: 10.1016/j.ophtha.2013.10.023
2. Wong TY, Ferreira A, Hughes R, Carter G, Mitchell P. Epidemiology and disease burden of pathologic myopia and myopic choroidal neovascularization: an evidence-based systematic review. *Am J Ophthalmol.* (2014) 157:9–25.e12. doi: 10.1016/j.ajo.2013.08.010
3. Yoshida T, Ohno-Matsui K, Yasuzumi K, Kojima A, Shimada N, Futagami S, et al. Myopic choroidal neovascularization: a 10-year follow-up. *Ophthalmology.* (2003) 110:1297–305. doi: 10.1016/S0161-6420(03)00461-5
4. Ohno-Matsui K, Ikuno Y, Lai TYY, Gemmy Cheung CM. Diagnosis and treatment guideline for myopic choroidal neovascularization due to pathologic myopia. *Prog Retin Eye Res.* (2018) 63:92–106. doi: 10.1016/j.preteyeres.2017.10.005
5. Iacono P, Battaglia Parodi M, Selvi F, Parravano MC, Chiaravalloti A, Varano M, et al. Factors influencing visual acuity in patients receiving anti-vascular endothelial growth factor for myopic choroidal neovascularization. *Retina.* (2017) 37:1931–41. doi: 10.1097/IAE.0000000000001436
6. Ikuno Y, Ohno-Matsui K, Wong TY, Korobelnik J-F, Vitti R, Li T, et al. Intravitreal aflibercept injection in patients with myopic choroidal neovascularization: the MYRROR study. *Ophthalmology.* (2015) 122:1220–7. doi: 10.1016/j.ophtha.2015.01.025
7. Ruiz-Medrano J, Montero JA, Flores-Moreno I, Arias L, García-Layana A, Ruiz-Moreno JM. Myopic maculopathy: current status and proposal for a new classification and grading system (ATN). *Prog Retin Eye Res.* (2019) 69:80–115. doi: 10.1016/j.preteyeres.2018.10.005
8. Ikuno Y, Jo Y, Hamasaki T, Tano Y. Ocular risk factors for choroidal neovascularization in pathologic myopia. *Invest Ophthalmol Vis Sci.* (2010) 51:3721–5. doi: 10.1167/iovs.09-3493
9. Wakabayashi T, Ikuno Y. Choroidal filling delay in choroidal neovascularisation due to pathological myopia. *Br J Ophthalmol.* (2010) 94:611–5. doi: 10.1136/bjo.2009.163535
10. McBrien NA, Gentle A. Role of the sclera in the development and pathological complications of myopia. *Prog Retin Eye Res.* (2003) 22:307–38. doi: 10.1016/S1350-9462(02)00063-0
11. Fang Y, Du R, Nagaoka N, Yokoi T, Shinohara K, Xu X, et al. OCT-based diagnostic criteria for different stages of myopic maculopathy. *Ophthalmology.* (2019) 126:1018–32. doi: 10.1016/j.ophtha.2019.01.012
12. Ohno-Matsui K, Kawasaki R, Jonas JB, Cheung CMG, Saw S-M, Verhoeven VJM, et al. International photographic classification and grading system for myopic maculopathy. *Am J Ophthalmol.* (2015) 159:877–83.e7. doi: 10.1016/j.ajo.2015.01.022
13. Ohno-Matsui K, Lai TYY, Lai C-C, Cheung CMG. Updates of pathologic myopia. *Prog Retin Eye Res.* (2016) 52:156–87. doi: 10.1016/j.preteyeres.2015.12.001
14. Cheung CMG, Arnold JJ, Holz FG, Park KH, Lai TYY, Larsen M, et al. Myopic choroidal neovascularization: review, guidance, and consensus statement on management. *Ophthalmology.* (2017) 124:1690–711. doi: 10.1016/j.ophtha.2017.04.028
15. Ohno-Matsui K, Yoshida T, Futagami S, Yasuzumi K, Shimada N, Kojima A, et al. Patchy atrophy and lacquer cracks predispose to the development of choroidal neovascularisation in pathological myopia. *Br J Ophthalmol.* (2003) 87:570–3. doi: 10.1136/bjo.87.5.570
16. Querques G, Corvi F, Balaratnasingam C, Casalino G, Parodi MB, Introini U, et al. Lacquer cracks and perforating scleral vessels in pathologic myopia: a possible causal relationship. *Am J Ophthalmol.* (2015) 160:759–66.e2. doi: 10.1016/j.ajo.2015.07.017
17. Ellabban AA, Tsujikawa A, Matsumoto A, Yamashiro K, Oishi A, Ooto S, et al. Three-dimensional tomographic features of dome-shaped macula by swept-source optical coherence tomography. *Am J Ophthalmol.* (2013) 155:320–8.e2. doi: 10.1016/j.ajo.2012.08.007

18. Fang Y, Yokoi T, Nagaoka N, Shinohara K, Onishi Y, Ishida T, et al. Progression of myopic maculopathy during 18-year follow-up. *Ophthalmology.* (2018) 125:863–77. doi: 10.1016/j.ophtha.2017.12.005
19. Deng J, Jin J, Lv M, Jiang W, Sun S, Yao C, et al. Distribution of scleral thickness and associated factors in 810 chinese children and adolescents: a swept-source optical coherence tomography study. *Acta Ophthalmol.* (2019) 97:e410–8. doi: 10.1111/aos.13788
20. Hirasawa K, Shoji N, Yoshii Y, Haraguchi S. Comparison of Kang's and Littmann's methods of correction for ocular magnification in circumpapillary retinal nerve fiber layer measurement. *Invest Ophthalmol Vis Sci.* (2014) 55:8353–8. doi: 10.1167/iovs.14-15720
21. Jonas JB, Ohno-Matsui K, Jiang WJ, Panda-Jonas S. Bruch membrane and the mechanism of myopization: a new theory. *Retina.* (2017) 37:1428–40. doi: 10.1097/IAE.0000000000001464
22. Ishida T, Watanabe T, Yokoi T, Shinohara K, Ohno-Matsui K. Possible connection of short posterior ciliary arteries to choroidal neovascularisations in eyes with pathologic myopia. *Br J Ophthalmol.* (2019) 103:457–62. doi: 10.1136/bjophthalmol-2018-312015
23. Giuffrè C, Querques L, Carnevali A, De Vitis LA, Bandello F, Querques G. Choroidal neovascularization and coincident perforating scleral vessels in pathologic myopia. *Eur J Ophthalmol.* (2017) 27:e39–45. doi: 10.5301/ejo.5000875
24. Hsiang HW, Ohno-Matsui K, Shimada N, Hayashi K, Moriyama M, Yoshida T, et al. Clinical characteristics of posterior staphyloma in eyes with pathologic myopia. *Am J Ophthalmol.* (2008) 146:102–10. doi: 10.1016/j.ajo.2008.03.010
25. Hayashi K, Ohno-Matsui K, Shimada N, Moriyama M, Kojima A, Hayashi W, et al. Long-term pattern of progression of myopic maculopathy: a natural history study. *Ophthalmology.* (2010) 117:1595–611.e16114. doi: 10.1016/j.ophtha.2009.11.003

Conflict of Interest: The authors declare that the research was conducted in the absence of any commercial or financial relationships that could be construed as a potential conflict of interest.

frontiers in Medicine

ORIGINAL RESEARCH
published: 27 January 2021
doi: 10.3389/fmed.2021.610590

Peripheral Anterior Chamber Depth and Angle Measurements Using Pentacam After Implantation of Toric and Non-toric Implantable Collamer Lenses

Jiao Zhao[1†], *Jing Zhao*[2,3,4†], *Wen Yang*[5], *Huamao Miao*[2,3,4], *Lingling Niu*[2,3,4], *Jianmin Shang*[2,3,4], *Xiaoying Wang*[2,3,4] *and Xingtao Zhou*[2,3,4*]

[1] *Department of Ophthalmology, People's Hospital of Leshan, Leshan, China,* [2] *Eye Institute and Department of Ophthalmology, Eye, Ear, Nose and Throat Hospital, Fudan University, Shanghai, China,* [3] *National Health Center Key Laboratory of Myopia (Fudan University), Key Laboratory of Myopia, Chinese Academy of Medical Sciences, Shanghai, China,* [4] *Shanghai Research Center of Ophthalmology and Optometry, Shanghai, China,* [5] *Department of Ophthalmology, The Third People's Hospital of Chengdu, The Affiliated Hospital of Southwest Jiaotong University, Chengdu, China*

OPEN ACCESS

Edited by:
Xingchao Shentu,
Zhejiang University, China

Reviewed by:
Peng Zhou,
Parkway Health, China
Xu Chen,
Shanghai Aier Eye Hospital, China

****Correspondence:***
Xingtao Zhou
doctzhouxingtao@163.com

[†]These authors have contributed equally to this work and share first authorship

Specialty section:
This article was submitted to Ophthalmology, a section of the journal Frontiers in Medicine

Received: *26 September 2020*
Accepted: *05 January 2021*
Published: *27 January 2021*

Citation:
Zhao J, Zhao J, Yang W, Miao H, Niu L, Shang J, Wang X and Zhou X (2021) Peripheral Anterior Chamber Depth and Angle Measurements Using Pentacam After Implantation of Toric and Non-toric Implantable Collamer Lenses. Front. Med. 8:610590. doi: 10.3389/fmed.2021.610590

Purpose: To evaluate the characteristics of peripheral anterior chamber measurements by Pentacam after posterior implantable collamer lenses (ICL) and toric ICL (TICL) with central hole (V4c) implantation.

Methods: Prospective, non-randomized consecutive case series. Forty-six patients undergoing ICL implantation in one eye (Group A) and identically sized TICL in the contralateral eye (Group B) in the Refractive Surgery Center of Eye and ENT Hospital of Fudan University were prospectively included. According to ICL/TICL size, these eyes were further divided into four subgroups. Peripheral anterior chamber depth (PACD) and angle (ACA) in nasal and temporal sides were measured using Pentacam pre-operatively and 12-month post-operatively.

Results: The safety indices were 1.34 ± 0.32 and 1.25 ± 0.16 and the efficacy indices were 1.20 ± 0.24 and 1.19 ± 0.19 for ICL and TICL groups, respectively. There was no significant difference in pre-operative PACD or ACA between the two groups. Post-operative PACD and ACA were significantly lower than pre-operative values. Variations of PACD and ACA of TICL group were significantly larger than those of ICL group. The change of ACA for 13.2 mm lenses was significantly larger than that of 12.6 mm lenses. Pre-operative CACD and vault were significantly associated with post-operative PACD, while pre-operative ACA and vault were significantly associated with post-operative ACA.

Conclusions: Variations of PACD and ACA were greater in eyes after TICL (V4c) implantation compared with identically sized ICL (V4c) implantation and with larger size than smaller size lens implantation. Pre-operative anterior chamber structure and vault affect post-operative PACD and ACA.

Keywords: toric implantable collamer lens V4c, peripheral anterior chamber depth, anterior chamber angle, Pentacam, myopia, astigmatism

INTRODUCTION

Implantation of the implantable collamer lens (ICL)/ toric ICL (TICL) (V4c) with a central port is preferred over corneal refractive surgery by refractive surgeons and patients for its reversibility and excellent visual quality (1–3). ICL is positioned in the ciliary sulcus and protrudes forward to form a vault, resulting in post-operative narrowing of the anterior chamber angle (ACA) width and decreasing the central anterior chamber depth (CACD) (4).

ACA is the key anatomic parameter determining the risk for primary angle closure glaucoma (PACG) (5). Peripheral anterior synechiae and peripheral angle closure (PAC) become significant possibilities when drainage angle is ≦ grade 2 (∼20°) (6, 7). In addition to ACA, peripheral anterior chamber depth (PACD) shows good sensitivity for detecting eyes at risk for angle closure (8). Extremely shallow anterior chamber depth (ACD) or narrow ACA leads to the possibility of angle closure glaucoma (ACG) and extraction of the ICL/TICL (9, 10). For these reasons, prediction and monitoring of post-operative ACA and PACD in the long term are essential to improve the safety of ICL/TICL (V4c) implantation.

Biometric studies have demonstrated that ACD significantly correlates with PAC and PACG (11–13). The Pentacam allows for quantitative measurements of the corneal topography, corneal thickness, ACA, ACD at any point, and anterior chamber volume (ACV). Pentacam has been used to screen eyes suspected of having PAC (13, 14). In addition, White-to-white (WTW) distance and CACD measured by Pentacam are crucial parameters for sizing ICL/TICL (V4c). Nevertheless, there was only one report on ACA measurement using Pentacam after ICL/TICL (V4c) implantation (15). Furthermore, there have been no comparative specialized studies on PACD or ACA after ICL and TICL (V4c) implantation.

Therefore, in the present study, we performed a prospective, non-randomized contralateral case comparison study to explore the characteristics of PACD and ACA after implantation of ICL/TICL (V4c) with various sizes. Factors that affect post-operative PACD and ACA were also analyzed.

PATIENTS AND METHODS

Patients

This was a prospective, non-randomized consecutive case series study. Patients who underwent routine pre-operative examinations for ICL/TICL implantation and subsequent ICL (V4c) implantation in one eye (Group A) and an identically-sized TICL (V4c) implantation in the contralateral eye (Group B) between August 2018 and June 2019 were included.

TICL was selected if astigmatic diopter was beyond 0.75 D, or the percentage of astigmatic diopter to spherical diopter was higher than 10%, or the CDVA could be achieved beyond 2 lines if the astigmatic diopter was corrected by TICL. Regardless of whether TICL or ICL was selected, thorough examinations were conducted, and approval was obtained from all patients.

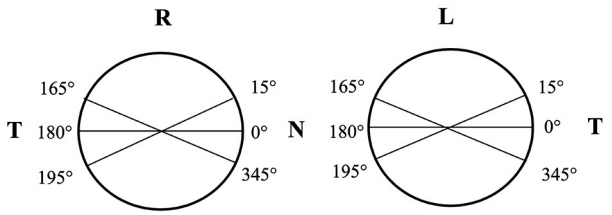

FIGURE 1 | A schematic diagram for calculation of PACD/ACA in nasal and temporal sides of right and left eyes. Arithmetical mean of PACD and ACA at 0, 15, 345° meridians was considered as the value of the nasal side (NPACD/NACA) in the right eye and temporal side (TPACD/TACA) of the left eye. The arithmetical mean of PACD and ACA at 180, 165, 195° meridians was considered as TPACD/TACA of the right eye and NPACD/NACA of the left eye.

Groups A and B were further divided into four subgroups: A_1 (12.6 mm ICL), A_2 (13.2 mm ICL), B_1 (12.6 mm TICL), and B_2 (13.2 mm TICL), based on the size of the ICL/TICL implanted.

This study was approved by the ethics committee and followed the tenets of the Declaration of Helsinki. Written informed consent was obtained from each patient after explanation of the nature and possible consequences of the study.

Examinations

Pre-operative routine ophthalmic examinations were performed as follows: (1) uncorrected distance visual acuity (UDVA), subjective refraction, corrected distance visual acuity (CDVA), intraocular pressure (IOP) measured using a tonometer (Canon Full Auto Tonometer TX-F; Canon, Tokyo, Japan), slit-lamp examination, axial length, fundus examination, endothelial cell density (ECD) (SP. 2000P; Topcon, Tokyo, Japan) were completed; and (2) horizontal sulcus-to-sulcus (STS) distance was measured using ultrasound biomicroscopy (UBM) (BME-300, MEDA, Tianjin, China). Eyes with ciliary or iris cysts were noted.

For Pentacam (OCULUS Optikgeräte GmbH, Wetzlar, Germany) examinations: PACD (defined as the ACD at 4 mm from the corneal apex) at 6 points and ACA along the 0, 15, 165, 180, 195, and 345° meridians were measured in each eye. The arithmetical means of PACD and ACA at 0, 15, and 345° meridians were considered the values of the nasal side (NPACD/NACA) in the right eye and temporal side (TPACD/TACA) of the left eye. The arithmetical means of PACD and ACA at 180, 165, and 195° meridians were considered the TPACD/TACA of the right eye and the NPACD/NACA of the left eye (**Figure 1**). WTW, central corneal thickness, flat keratometry (Kf), steep keratometry (Ks), CACD, pupil diameter (PD), and clear lens rise defined as the distance between the anterior pole of crystalline lens and the horizontal iris plane were also recorded.

ICL/TICL (V4c) Implantation

ICL/TICL sizing was based primarily on WTW and CACD measurements with Pentacam HR, as recommended by the Staar surgical calculator (http://www.staarvision.com).

All surgeries were performed by two experienced surgeons using the same technique. Binocular procedures were conducted

TABLE 1 | Pre-operative patient demographic data in group A, B and subgroups.

	Sex		Eye		Age (years)	Spherical (D)	Cylindrical (D)	SE (D)
	Male	Female	Right	Left				
Group A (ICL)	18	28	26	20	25.78 ± 4.09	−8.97 ± 2.72	−0.14 ± 0.22	−9.05 ± 2.70
Group A1 (12.6 mm)	9	15	14	10	26.58 ± 4.78	−8.92 ± 2.72	−0.17 ± 0.23	−9.02 ± 2.70
Group A2 (13.2 mm)	9	13	12	10	24.91 ± 0.96	−8.64 ± 2.50	−0.09 ± 0.18	−8.70 ± 2.48
Group B (TICL)	18	28	20	26	25.78 ± 4.09	−8.51 ± 3.08*	−1.26 ± 0.38*	−9.14 ± 3.09
Group B1 (12.6 mm)	9	15	10	14	26.58 ± 4.78	−8.34 ± 3.13	−1.14 ± 0.27	−8.91 ± 3.12
Group B2 (13.2 mm)	9	13	10	12	24.91 ± 0.96	−8.35 ± 2.64	−1.39 ± 0.48	−9.05 ± 2.68

D, Diopter; SE, Spherical equivalence.
**P < 0.05: Group A vs. Group B.*

successively, and the right eye was operated on first. Surgical procedures were as previously described (16). Eyes of Group A were implanted with ICL (V4c) in the horizontal axis while eyes of Group B were implanted with TICL (V4c) with rotation of axis within 13 degrees (4.78 ± 3.02°, range: 0–13°).

Follow-Up

The patients were followed up for 12.13 ± 4.28 months (range: 9–17 months). Follow-up examinations included assessments of UDVA, CDVA, refractive power, ECD, IOP, PACD, ACA, and vault [determined as the distance between the anterior surface of the crystalline lens and the posterior surface of ICL/TICL (V4c) on the optical axis using the Pentacam].

Statistical Analyses

All statistical analyses were performed using SPSS 23.0 software (IBM, Armonk, NY, US). The normality of all data was first checked using the Shapiro–Wilk-test. Paired *t*-tests or Wilcoxon signed-rank-tests were used to compare pre- and post-operative data and data between different groups. Pearson's correlation or Spearman's rank correlation were performed to determine the associations between age, spherical equivalence, pre-operative CACD, PACD, ACA, PD, Kf, Ks, corneal posterior radius, astigmatism axis, axial length, WTW, horizontal STS, axis rotation of TICLs, post-operative PACD, ACA, and vault. Multiple stepwise regression analysis was performed to predict post-operative PACD/ACA using significant correlation factors in Pearson's correlation or Spearman's rank correlation analysis as independent variables. $P < 0.05$ was considered statistically significant.

RESULTS

Ninety-two eyes of 46 patients who underwent ICL (V4c) implantation in one eye (Group A, 46 eyes) and an identically sized TICL (V4c) implantation in the contralateral eye (Group B, 46 eyes) were included. Pre-operative demographic data and pre-operative ocular measurements are displayed in **Tables 1**, **2**.

Safety

All surgeries were uneventful, and no complications occurred during the follow-up period. The safety indices (post-operative CDVA/pre-operative CDVA) were 1.34 ± 0.32 and 1.25 ± 0.16 in ICL and TICL groups, respectively. The LogMar CDVA values at the final follow-up were −0.09 ± 0.06 in the ICL group and −0.10 ± 0.04 in the TICL group. At the final follow-up, no patient lost lines of CDVA; 63.04 and 73.91% achieved the same CDVA as pre-operatively or increased by one line; and 36.96 and 26.09% increased by two or more lines in the ICL and TICL groups, respectively (**Figure 2A**). Safety indices were 1.39 ± 0.32, 1.29 ± 0.17, 1.25 ± 0.17, and 1.25 ± 0.16 in the 12.6 mm ICL, 13.2 mm ICL, 12.6 mm TICL, and 13.2 mm TICL groups, respectively.

No significant differences were found for IOP or ECD between ICL and TICL groups or between subgroups at pre- and post-operative time points, as well as between pre- and post-operative time points in each group ($P > 0.05$; **Tables 2**, **3**).

Efficacy and Predictability

The efficacy indices (post-operative UDVA/pre-operative CDVA) were 1.20 ± 0.24 and 1.19 ± 0.19 in the ICL and TICL groups, respectively. The LogMar UDVA values at the final follow-up were −0.05 ± 0.07 in the ICL group and −0.07 ± 0.06 in the TICL group. At the final follow-up, all eyes had post-operative LogMAR UDVAs of 0.5 or better, and 91.30 and 95.65% achieved better than LogMAR UDVAs of 0 in the ICL and TICL groups (**Figures 2B,C**).

Post-operatively, 88.23% (40 eyes) of the ICL group and 85.29% (39 eyes) of the TICL group eyes achieved within ± 0.50 D of the attempted spherical equivalence (SE). All eyes were within ± 1.00 D of the attempted SE in both groups (**Figures 2D,E**); 95.65% (44 eyes) in the TICL group had post-operative astigmatisms of ≤0.50 D (**Figure 2F**).

PACD and ACA

After surgery, NPACD decreased by 41.91 ± 9.08% and 48.55 ± 8.76% in the ICL and TICL groups, respectively, while TPACD decreased by 42.66 ± 6.35% and 50.21 ± 7.35%, respectively. NACA decreased by 39.42 ± 7.61% and 45.97 ± 7.30%, respectively, while TACA decreased by 37.66 ± 6.82% and 44.80 ± 9.69% in the ICL and TICL groups, respectively. Variations of PACD and ACA of TICL group were significantly greater than those of ICL group. Post-operative PACD and ACA in the TICL group were significantly lower than values in the

TABLE 2 | Pre-operative ocular measurements in group A, B and subgroups.

	WTW (mm)	Kf (D)	Ks (D)	Rfp (mm)	Rsp (mm)	Rmp (mm)	CCT (μm)	CACD (mm)	PD (mm)	CLR (μm)	ACV (μl)	hSTS (mm)	Axial length (mm)	IOP (mmHg)	ECD (cells/mm^2)	NPACD (mm)	TPACD (mm)	NACA (degree)	TACA (degree)
Group A (ICL)	11.62 ± 0.29	43.01 ± 1.35	43.84 ± 1.27	6.55 ± 0.19	6.20 ± 0.22	6.38 ± 0.20	519.26 ± 39.27	3.25 ± 0.21	3.34 ± 0.53	360.47 ± 131.66	205.52 ± 28.88	11.78 ± 0.51	27.16 ± 1.32	15.05 ± 2.37	2710.02 ± 263.66	1.83 ± 0.31	2.19 ± 0.29	39.89 ± 5.16	43.25 ± 5.76
Group A1 (12.6 mm ICL)	11.42 ± 0.19	43.51 ± 1.26	44.17 ± 1.18	6.46 ± 0.12	6.11 ± 0.15	6.29 ± 0.11	514.29 ± 37.58	3.13 ± 0.18	3.26 ± 0.54	378.18 ± 150.63	188.58 ± 24.49	11.52 ± 0.46	26.82 ± 1.05	14.72 ± 2.33	2702.61 ± 256.46	1.66 ± 0.28	2.01 ± 0.23	40.07 ± 5.71	41.86 ± 5.99
Group A2 (13.2 mmICL)	11.84 ± 0.21**	42.46 ± 1.25*	43.48 ± 1.29	6.65 ± 0.20*	6.29 ± 0.25*	6.48 ± 0.22*	524.68 ± 41.22	3.37 ± 0.10**	3.44 ± 0.51	341.90 ± 108.93	224.00 ± 21.10**	12.06 ± 0.41**	27.53 ± 1.50	15.40 ± 2.43	2717.77 ± 276.82	2.02 ± 0.23**	2.38 ± 0.24**	39.69 ± 4.61	42.62 ± 5.13
Group B (TICL)	11.63 ± 0.28	42.83 ± 1.32*	44.20 ± 1.41**	6.55 + 0.23	6.03 ± 0.96	6.21 ± 1.01	520.63 ± 37.61	3.24 ± 0.26	3.27 ± 0.54	366.42 ± 132.16	203.48 ± 31.76	11.80 ± 0.46	27.09 ± 1.44	15.06 ± 1.96	2741.22 ± 254.19	1.86 ± 0.36	2.22 ± 0.31	40.38 ± 5.66	42.26 ± 5.55
Group B1 (12.6 mmT ICL)	11.44 ± 0.19	43.37 ± 1.25	44.58 ± 1.34	6.44 ± 0.15	6.10 ± 0.12	5.95 ± 1.36	516.67 ± 37.71	3.12 ± 0.18	3.20 ± 0.56	380.91 ± 150.52	184.46 ± 24.49	11.57 ± 0.33	26.68 ± 1.17	14.89 ± 2.03	2729.43 ± 229.97	1.66 ± 0.28	2.11 ± 0.26	40.08 ± 6.65	44.25 ± 5.59
Group B2 (13.2 mmT ICL)	11.84 ± 0.22**	42.24 ± 1.16*	43.78 ± 1.38	6.68 ± 0.22**	5.97 ± 1.38	6.47 ± 0.22	524.95 ± 37.90	3.36 ± 0.20**	3.33 ± 0.53	351.24 ± 111.43	224.23 ± 25.31**	12.05 ± 0.46**	27.54 ± 1.60	15.25 ± 1.91	2,730 ± 254.17	2.08 ± 0.32**	2.40 ± 0.33**	40.70 ± 4.49	42.17 ± 5.88

WTW, White-to-white distance; Kf, Flat keratometry; Ks, Steep keratometry; Rfp, Corneal posterior flat radius; Rsp, Corneal posterior steep radius; Rfp, Corneal posterior mean radius; CCT, Central corneal thickness; CACD, Central anterior chamber depth; PD, Pupil diameter; CLR, Clear lens rise; ACV, Anterior chamber volume; hSTS, Horizontal sulcus-to-sulcus distance; IOP, Intraocular pressure; ECD, Endothelia cell density; NPACD, Peripheral anterior chamber depth in nasal side; TPACD, Peripheral anterior chamber depth in temporal side; NACA, Anterior chamber angle in nasal side; TACA, Anterior chamber angle in temporal side.

**P < 0.05 comparison between Group A and B, Group A1 and A2, Group B1 and B2; **P < 0.001 comparison between Group A and B, Group A1 and A2, Group B1 and B2.*

ICL group (P <0.05; **Table 3**). One exemplary case is shown in **Figure 3**.

There were statistically significant differences in pre- and post-operative PACD and ACA variations between the 12.6 and 13.2 mm ICL/TICL groups ($P < 0.05$; **Table 3**).

Pre-operative PACD, WTW, CACD, cylindrical power of TICL, astigmatism axis, axis rotation of TICLs and post-operative vault correlated significantly with post-operative PACD ($P <$ 0.05). Pre-operative ACA, PD, size of ICL/TICL, cylindrical power of TICL, astigmatism axis, axis rotation of TICLs and post-operative vault correlated significantly with post-operative ACA ($P < 0.05$; **Table 4**). Corneal posterior radius showed no significant correlation with post-operative PACD and ACA in univariate correlation analysis.

Results of the multiple stepwise regression analysis are displayed in **Table 5**. Factors significantly associated with post-operative NPACD/TPACD included pre-operative CACD and post-operative vault (NPACD adjusted $R^2 = 0.368$; TPACD adjusted $R^2 = 0.296$). Factors significantly associated with post-operative NACA/TACA included pre-operative NACA/TACA, and post-operative vault (NACA adjusted $R^2 = 0.665$; TACA adjusted $R^2 = 0.294$).

Iris and Ciliary Body Cysts

Iris and ciliary body cysts were found in 14 eyes of 8 patients (binocular cysts in 6 patients and monocular cysts in 2 eyes) using UBM examinations. There were nine eyes with a single cyst and five eyes with multiple cysts. All cysts were located in horizontal direction. Post-operative IOP, CACD, and vault were 13.47 ± 2.21 mmHg, 2.07 ± 0.12 mm, and 693.33 ± 126.59 μm, respectively. Pre- and post-operative NPACD values were 1.64 ± 0.38 mm and 0.77 ± 0.15 mm, pre- and post-operative NACA were 37.07 ± 4.66° and 19.13 ± 3.65°, while pre- and post-operative TPACD were 2.09 ± 0.22 mm and 1.11 ± 0.24 mm, TACA were 41.06 ± 6.56° and 23.45 ± 5.52°, respectively. NACA, TACA, NPACD, TPACD decreased by 48.64 ± 4.34%, 43.04 ± 9.40%, 52.93 ± 4.25%, and 46.67 ± 9.31%, respectively, compared with pre-operative values. None of the eyes had PAC or high IOP.

DISCUSSION

The present study was the first consecutive case series and contralateral eye comparison designed to investigate PACD and ACA after ICL and TICL (V4c) implantation. After 1 year of implantation, NPACD, TPACD, NACA, and TACA all decreased significantly in ICL and TICL (V4c) groups. Post-operative PACD and ACA for TICL (V4c) were significantly lower than those for ICL (V4c). Variations of these values for TICL (V4c) were significantly larger than those of ICL (V4c), although pre-operative binocular ocular measurements such as SE, WTW, and CACD remained constant. Vault for TICL (V4c) was significantly higher than that for ICL (V4c). We speculated that the higher vault might push the iris forward, resulting in more changes of anterior chamber structure after TICL (V4c) implantation. Results of correlation analysis and stepwise multivariate regression analysis validated the correlation between PACD/ACA and vault. The rotation of TICL

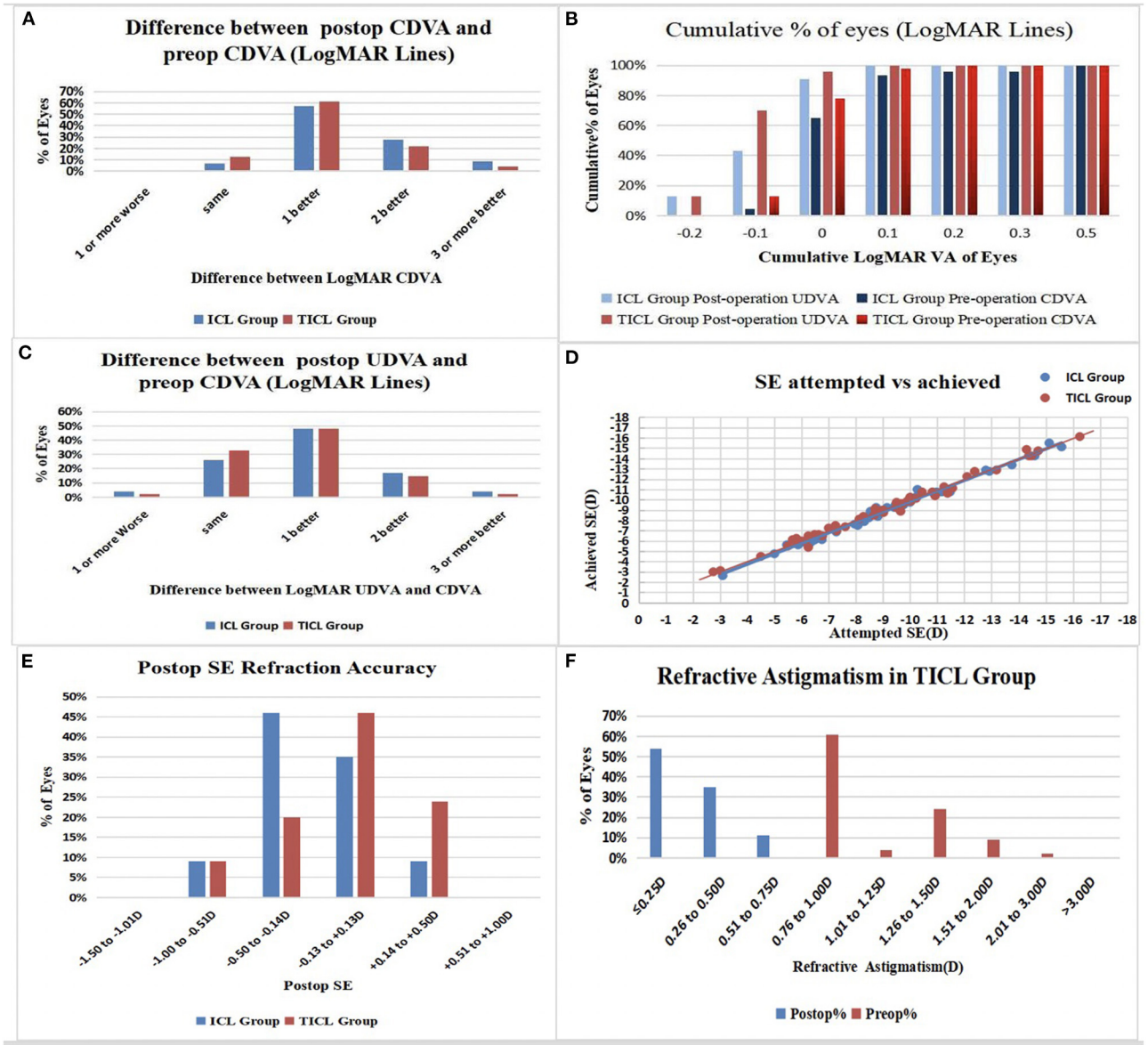

FIGURE 2 | (A) Changes of corrected distance visual acuity (CDVA): postop vs. preop CDVA; **(B)** Cumulative percentage of the eyes attaining specified cumulative levels of uncorrected distance visual acuity (UDVA); **(C)** Changes of postop UDVA vs. preop CDVA; **(D)** Attempted spherical equivalent (SE) refraction change vs. the achieved SE refraction change at the last follow-up were plotted; **(E)** Distribution of postop SE refraction; **(F)** Distribution of preop and postop astigmatism amplitude in TICL Group.

(V4c) significantly correlated with post-operative PACD/ACA in univariate correlation analysis, however no significant correlation was found in stepwise multivariate regression analysis in the present study.

Safety of ICL/TICL implantation has been a persistent concern (17–19). PACD and ACA in the ideal range are prerequisites for the safety of post-operative surgery. Zeng et al. (9) reviewed 616 myopic eyes with the previous version of ICL/TICL (V4) implantation and found eight eyes with ICL/TICL exchange for high vault leading to shallow ACD with angle closure in any quadrant or larger PD than pre-operative measurements with severe night glare. Garcia-De la Rosa et al. (20) found significant reductions in the iridocorneal angle after ICL/TICL (V4c) implantation in mesopic, photopic, and scotopic conditions. These findings suggest that it is worth investigating changes of anterior chamber structure after ICL/TICL (V4c) implantation so as to improve surgical quality and safety.

In the present study, the safety and efficacy indices were 1.34 ± 0.32 and 1.20 ± 0.24 for ICL (V4c), and the indices were 1.25 ± 0.16 and 1.19 ± 0.19 for TICL (V4c). Previously, our team reported a post-operative safety index for ICL (V4c) of 1.80 ± 0.89 and an efficacy index of 1.54 ± 1.07 (21). The present study

TABLE 3 | Post-operative ocular measurements in group A, B, A1, A2, B1, and B2.

	CACD-ICL (mm)	Vault (μm)	PD (mm)	ACV (μl)	IOP (mmHg)	ECD (cells/mm^2)	NPACD (mm)	TPACD (mm)	ΔNPACD (mm)	ΔTPACD (mm)	NACA (degree)	TACA (degree)	ΔNACA (degree)	ΔTACA (degree)
Group A (ICL)	2.45 ± 0.23	501.30 ± 161.36	3.37 ± 0.67	118.26 ± 19.60	14.60 ± 2.56	2678.37 ± 250.87	1.05 ± 0.18	1.24 ± 0.17	0.78 ± 0.25	0.94 ± 0.22	24.21 ± 4.72	26.22 ± 3.73	15.67 ± 3.49	16.00 ± 4.03
Group A1 (12.6 mm ICL)	2.39 ± 0.23	432.92 ± 182.86	3.27 ± 0.64	108.21 ± 15.78	14.31 ± 2.45	2676.78 ± 241.66	1.02 ± 0.18	1.21 ± 0.17	0.64 ± 0.17	0.79 ± 0.15	25.37 ± 5.19	27.22 ± 4.16	14.70 ± 3.68	14.64 ± 3.79
Group A2 (13.2 mmICL)	2.49 ± 0.23	575.91 ± 89.42*	3.47 ± 0.70	129.23 ± 17.58**	14.91 ± 2.70	2680.05 ± 265.85	1.08 ± 0.17	1.28 ± 0.16	0.93 ± 0.24**	1.09 ± 0.19**	22.95 ± 3.87*	25.12 ± 2.92*	16.73 ± 3.01*	17.49 ± 3.82*
Group B (TICL)	2.30 ± 0.25**	633.04 ± 211.11 **	3.38 ± 0.60	111.43 ± 19.13**	14.23 ± 3.35	2707.31 ± 249.19	0.94 ± 0.17**	1.10 ± 0.15**	0.92 ± 0.31**	1.14 ± 0.30**	21.78 ± 4.22**	23.59 ± 3.75**	18.59 ± 4.01**	23.59 ± 3.75**
Group B1 (12.6 mm TICL)	2.26 ± 0.25	544.17 ± 220.76	3.31 ± 0.65	104.50 ± 16.17	14.45 ± 2.71	2704.04 ± 231.37	0.90 ± 0.17	1.10 ± 0.14	0.75 ± 0.19	1.10 ± 0.24	22.95 ± 4.89	25.06 ± 3.83	0.75 ± 0.19	1.10 ± 0.24
Group B2 (13.2 mm TICL)	2.34 ± 0.25	730.00 ± 152.47*	3.47 ± 0.54	119.00 ± 19.56*	14.01 ± 3.92	2710.73 ± 272.27	0.98 ± 0.17	1.11 ± 0.16	1.10 ± 0.32**	1.29 ± 0.30*	20.50 ± 2.95*	21.99 ± 2.99*	1.10 ± 0.32*	1.29 ± 0.30

CACD-ICL, Central anterior chamber depth from corneal endothelium to anterior surface of ICL/TICL; PD, Pupil diameter; ACV, Anterior chamber volume; IOP, Intraocular pressure; ECD, Endothelia cell density; NPACD, Peripheral anterior chamber depth in nasal side; TPACD, Peripheral anterior chamber depth in temporal side; NACA, Anterior chamber angle in nasal side; TACA, Anterior chamber angle in temporal side.

**P < 0.05 compared between group A and B, group A1 and A2, group B1 and B2; **P < 0.001 compared between group A and B, group A1 and A2, group B1 and B2.*

FIGURE 3 | Anterior chamber image of the right eye with 13.2 mm ICL (V4c) **(A)** and left eye with 13.2 mm TICL (V4c) **(B)**. Horizontal minimal ACA was 22.2° in the right eye and 16.4° in the left eye.

further demonstrated excellent safety and efficacy of variously sized ICL/TICL (V4c). At the final follow-up, 88.23 and 85.29% of eyes for ICL (V4c) and TICL (V4c), respectively, were within ± 0.50 D of the attempted SE, while all eyes from both groups were within ± 1.00 D in the present study. Garcia-De la Rosa et al. (20) reported that, among 76 eyes implanted with ICL/TICL(V4c), 54% were within ± 0.50 D for average SE and 84% were within ± 1.00 D at 12 months post-operatively. The predictability of SE values in the present study was better than that reported by Garcia-De la Rosa et al., possibly due to the discrepancy of the maximum spherical and astigmatic diopter of eyes (−14.00 DS and −2.50 DC in the present study vs. −22.25 DS and −7.00 DC in Garcia-De la Rosa et al.'s study).

ICL (V4c) was horizontally placed in the ciliary sulcus, and axis rotation of TICL (V4c) was within 13° in the present study. PACD and ACA significantly decreased after ICL/TICL (V4c) implantation according to Pentacam HR examinations. Our results were similar to those in former reports of post-operative anterior chamber change in response to different types of phakic intraocular lens (IOL) implantation. Javaloy et al. (22) reported that peripherally shallow anterior chamber appeared to be a decisive factor for a 28.78% decrease of endothelium after iris claw phakic IOL implantation during the 5-year follow-up. In another study, Benda et al. (23) reported CACD and ACA width decreased 3 years after ICL (ICH V3) implantation compared with pre-operative measurements using Pentacam. Chung et al. (24) reported a 31.8% trabecular-iris angle (TIA) reduction detected by UBM and a 41.5% angle opening distance at 500 μm from the scleral spur (AOD_{500}) decreased at 1 month after ICL (V4) implantation, and no further reduction was observed thereafter in 2-year follow-up. Fernandez-Vigo et al. (25) found significant TIA narrowing of 34.5–42% and post-operative AOD_{500} decreasing of 50.3–58.4% at 3 months post-operatively and no further decrease in 2-year follow-up. Despite

TABLE 4 | Correlations between post-operative anterior chamber measurements and different ocular factors examined in the study group.

	Pre-operative ACA	Pre-operative PACD	CACD	WTW	ICL/TICL Size	Cylindrical power	Astigmatism axis	Axis rotation of TICL	PD	Vault
Post-NPACD	/	0.495**	0.444**	0.306*	/	0.235*	−0.233**	−0.238**	/	−0.443**
Post-NACA	0.638**	/	/	/	−0.209*	0.257*	−0.203**	−0.257**	−0.220*	−0.266*
Post-TPACD	/	0.415**	0.366**	0.264*	/	0.338*	−0.262**	−0.227**	/	−0.394*
Post-TACA	0.402**	/	/	/	−0.303*	0.306*	−0.307**	−0.288**	−0.304*	−0.273*

CACD, Central anterior chamber depth; PD, Pupil diameter; WTW, White-to-white distance; NPACD, Peripheral anterior chamber depth in nasal side; TPACD, Peripheral anterior chamber depth in temporal side; NACA, Anterior chamber angle in nasal side; TACA, Anterior chamber angle in temporal side.
**P-value of correlation coefficient < 0.05; **P-value of correlation coefficient < 0.001.*

TABLE 5 | Results of multiple stepwise regression analysis for prediction of post-operative PACD and ACA.

	Predictors	Unstandardized coefficients	Standardized coefficients	*P*-value
NPACD	Constant	−0.417		0.096
	Pre-operative CACD	0.482	0.626	0.000
	Vault	0.00	−0.373	0.005
		$R^2 = 0.397$, Adjusted $R^2 = 0.368$		
TPACD	Constant	0.139		0.608
	Pre-operative CACD	0.355	0.542	0.000
	Vault	0.00	−0.397	0.004
		$R^2 = 0.328$, Adjusted $R^2 = 0.296$		
NACA	Constant	6.743		0.608
	Pre-operative NACA	0.506	0.679	0.000
	Vault	−0.009	−0.427	0.000
		$R^2 = 0.680$, Adjusted $R^2 = 0.665$		
TACA	Constant	18.332		0.000
	Vault	−0.008	−0.471	0.001
	Pre-operative TACA	0.244	0.375	0.005
		$R^2 = 0.325$, Adjusted $R^2 = 0.294$		

NPACD, Peripheral anterior chamber depth in nasal side; CACD, Central anterior chamber depth; TPACD, Peripheral anterior chamber depth in temporal side; NACA, Anterior chamber angle in nasal side; TACA, Anterior chamber angle in temporal side.
Variables in the table body are ordered according to the strength of the contribution, which was based on the standardized partial regression coefficient.

horizontal placement of ICL, angle narrowing was similar in both horizontal and inferior quadrants. It is speculated that angle narrowing after ICL (V4c) is caused by the pushing forward of iris in the crystal optical area due to the concave optical area on the anterior surface of ICL being larger than the pupil. In the present study, percentage of PACD decreasing and ACA narrowing were similar to AOD_{500} and TIA decreasing in V4c study by Fernandez-Vigo (25). Primary angle closure becomes a significant possibility when ACA below 20° (6). Obviously, post-operative PACD and ACA in the present study decreased within the safety range. In previous UBM and anterior segment optical coherence tomography (AS-OCT) studies, AOD_{500} decreased by a larger percentage than did TIA. In the present study, post-operative PACD decreased by a larger percentage than did ACA.

In the present study, post-operative ACA for 13.2 mm lenses was significantly lower than 12.6 mm lenses, and the change of ACA for 13.2 mm lenses was larger than that of 12.6 mm lenses, suggesting a greater effect of larger-sized lenses on ACA. To our knowledge, this is the first report to compare the changes of PACD and ACA between ICL/TICL (V4c) with different sizes (12.6 vs. 13.2 mm). Zeng et al. (9) recorded outcomes after implantation of ICL/TICL (V4) of different sizes without central hole (11.5, 12.0, and 12.5 mm) and found that eyes with larger-sized phakic interocular lenses were more likely to need ICL/TICL exchange for excessively high vault, resulting in ACA closure in any quadrant. In the present study, the mean vault of 13.2 mm lenses was significantly higher than that of 12.6 mm lenses, which was within the safe range. WTW and CACD are the most important factors in determining the ICL/TICL (V4c) size using the Staar calculator software; consequentially, larger-sized lenses would be selected for eyes with larger WTW and deeper CACD. No significant difference was found in pre-operative ACA among the different subgroups, although the values of WTW, CACD, STS, and ACV in the 13.2 mm groups were significantly larger than those of the 12.6 mm ICL/TICL (V4c) groups. These findings suggest that ACA should be taken into consideration while selecting larger-sized V4c lenses.

In this study, stepwise multiple regression analysis revealed that pre-operative CACD and post-operative vault were significantly associated with post-operative PACD. Pre-operative ACA, and post-operative vault were significantly associated with post-operative ACA. Fernandez-Vigo et al. (25) identified pre-operative TIA, age, SE, CACD, axial length, and WTW as predictors of TIA at 1-month post-ICL (V4c) implantation using Fourier-domain OCT (FD-OCT). In a subsequent 2-year follow-up report, Fernandez-Vigo (26) identified pre-operative TIA, age, sex, SE, IOL size, iris thickness at the perpendicular point 500 μm to the scleral spur, and WTW affected post-operative TIA. Lee et al. (27) reported that ICL size, STS, age, and mean K readings were determinants of post-operative vault. In addition to pre-operative ocular measurements, post-operative vault was identified as an important determinant of both post-operative PACD and ACA in the present study, respectively, indicating higher vault might push ICL/TICLs more forwardly and resulting in narrower ACA or shallower PACD. In 2010, Lindland et al. (28) first reported that the vault after toric ICL

(TICL) (V4 model) implantation was higher than that of ICL (V4 model) and they presumed that addition of a cylindrical lens to the TICL optic zone may contribute to vault difference. In another study conducted by our team, we investigated the reason of ICL/TICL vault difference using multivariate parameters statistical processing and found that cylindrical power of TICL might contribute to this difference (29). We hope our conclusion will make some significance in ICL/TICL implantation surgery. Although different equipment were applied, the present study of PACD and ACA measured by Pentacam showed similar results as those of the FD-OCT study of TIA and AOD_{500} in Fernandez-Vigo's reports, suggesting that changes of anterior chamber parameters could be predicted based on pre-operative ocular measurements (25, 26).

Post-operative NPACD, TPACD, NACA, and TACA were lower than pre-operative measurements in eyes with iris and/or ciliary body cysts in the present study. Li and associates (30) found no significant differences in post-operative AOD_{500} and TIA between eyes with and without cysts. In Li's study, cysts were found predominantly in the inferior and temporal quadrants, while cysts were primarily located in the horizontal direction in the present study. Nevertheless, further research on relationships of cysts' location, size, ICL/TICL placement and PACD, and ACA change is of great importance to improve safety of ICL/TICL implantation.

The current study has some limitations. First, it utilized a relatively small sample size for few numbers of patients satisfying contralateral eye comparison design. Second, only two sizes of ICL/TICL (V4c) were analyzed, as 12.6 and 13.2 mm ICL/TICL (V4c) were selected frequently for these included patients. Future studies should be conducted with lager sample size and various lens sizes so as to make a comprehensive comparison.

In conclusion, it is possible to measure PACD and ACA using the Pentacam in ICL/TICL (V4c) implanted eyes. Pre- and post-operative variations of PACD and ACA were greater in eyes after TICL (V4c) implantation than with ICL (V4c) implantation and implantations of larger-sized lenses compared with smaller lenses. Post-operative PACD and ACA correlated with pre-operative anterior chamber structure and vault.

DATA AVAILABILITY STATEMENT

The raw data supporting the conclusions of this article will be made available by the authors, without undue reservation.

ETHICS STATEMENT

The studies involving human participants were reviewed and approved by the institutional ethics board of Eye and ENT Hospital of Fudan University (No. 2013015-1) and informed consent was taken from all the patients after a complete description of the study. The patients/participants provided their written informed consent to participate in this study.

AUTHOR CONTRIBUTIONS

The study concept and design were formulated by JiaZ, JinZ, and XZ. Data collection was done by JiaZ, JinZ, WY, HM, LN, JS, XW, and XZ. Analysis and interpretation of data was undertaken by JiaZ, JinZ, and XZ. Drafting of the manuscript was carried out by JiaZ, JinZ, and XZ. Critical revision of the manuscript was done by JiaZ, JinZ, and XZ. Supervision was done by XZ. All authors contributed to the article and approved the submitted version.

FUNDING

This work was supported in part by the National Natural Science Foundation of China (Grant No. 81770955); Joint research project of new frontier technology in municipal hospitals (SHDC12018103); the Project of Shanghai Science and Technology (Grant No. 17411950200); the National Natural Science Foundation of China for Young Scholars (Grant No. 81600762); the Project of Shanghai Science and Technology (Grant No. 19140900700) and the Shanghai Shenkang Hospital Development Center (Grant No. SHDC12016207).

ACKNOWLEDGMENTS

We would like to thank Editage (www.editage.cn) for English language editing.

REFERENCES

1. Siedlecki J, Schmelter V, Mayer WJ, Schworm B, Priglinger SG, Dirisamer M, et al. SMILE versus implantable collamer lens implantation for high myopia: a matched comparative study. *J Refract Surg*. (2020) 36:150–9. doi: 10.3928/1081597X-20200210-02
2. Sari E, Pinero D, Kubaloglu A, Evcili P, Koytak A, Kutluturk I, et al. Toric implantable collamer lens for moderate to high myopic astigmatism: 3-year follow-up. *Graefes Arch Clin Exp Ophthalmol*. (2013) 251:1413–22. doi: 10.1007/s00417-012-2172-8
3. Sanders DR, Doney K, Poco M. United States food and drug administration clinical trial of the implantable collamer lens (ICL) for moderate to high myopia: three-year follow-up. *Ophthalmology*. (2004) 111:1683–92. doi: 10.1016/j.ophtha.2004.03.026
4. Elmohamady MN, Abdelghaffar W. Anterior chamber changes after implantable collamer lens implantation in high myopia using Pentacam: a prospective study. *Ophthalmol Ther*. (2017) 6:343–9. doi: 10.1007/s40123-017-0109-3
5. Foo L-L, Nongpiur ME, Allen JC, Perera SA, Friedman DS, He M, et al. Determinants of angle width in chinese singaporeans. *Ophthalmology*. (2012) 119:278–82. doi: 10.1016/j.ophtha.2011.07.049
6. Foster PJ, Aung T, Nolan WP, Machin D, Baasanhu J, Khaw PT, et al. Defining "occludable" angles in population surveys: drainage angle width, peripheral anterior synechiae, and glaucomatous optic neuropathy in east asian people. *Br J Ophthalmol*. (2004) 88:486–90. doi: 10.1136/bjo.2003.020016
7. Shaffer RN. A suggested anatomic classification to define the pupillary block glaucomas. *Invest Ophthalmol*. (1973) 12:540–2.
8. Wong H-T, Chua JLL, Sakata LM, Wong MHY, Aung HT, Aung T. Comparison of slitlamp optical coherence tomography and scanning peripheral anterior chamber depth analyzer to evaluate angle closure in asian eyes. *Arch Ophthalmol*. (2009) 127:599–603. doi: 10.1001/archophthalmol.2009.41

9. Zeng Q-Y, Xie X-L, Chen Q. Prevention and management of collagen copolymer phakic intraocular lens exchange: causes and surgical techniques. *J Cataract Refract Surg*. (2015) 41:576–84. doi: 10.1016/j.jcrs.2014.06.036
10. Sanders DR, Vukich JA, Doney K, Gaston M. U.S. food and drug administration clinical trial of the implantable contact lens for moderate to high myopia. *Ophthalmology*. (2003) 2:255–66. doi: 10.1016/S0161-6420(02)01771-2
11. Friedman DS, Gazzard G, Foster P, Devereux J, Seah S. Ultrasonographic biomicroscopy, scheimpflug photography, and novel provocative tests in contralateral eyes of chinese patients initially seen with acute angle closure. *Arch Ophthalmol*. (2003) 121:633–42. doi: 10.1001/archopht.121.5.633
12. Wojciechowski R, Congdon N, Anninger W, Broman AT. Age, gender, biometry, refractive error, and the anterior chamber angle among alaskan eskimos. *Ophthalmology*. (2003) 110:365–75. doi: 10.1016/S0161-6420(02)01748-7
13. Kurita N, Mayama C, Tomidokoro A, Aihara M, Araie M. Potential of the pentacam in screening for primary angle closure and primary angle closure suspect. *J Glaucoma*. (2009) 18:506–12. doi: 10.1097/IJG.0b013e318193c141
14. Smith S, Singh K, Lin S, Chen P, Chen T, Francis B, et al. Evaluation of the anterior chamber angle in glaucoma: a report by the american academy of ophthalmology. *Ophthalmology*. (2013) 120:1985–97. doi: 10.1016/j.ophtha.2013.05.034
15. Eissa SA, Sadek SH, El-Deeb MWA. Anterior chamber angle evaluation following phakic posterior chamber collamer lens with CentraFLOW and its correlation with ICL vault and intraocular pressure. *J Ophthalmol*. (2016) 2016:1–7. doi: 10.1155/2016/7012826
16. Zhao J, Luo D, Sun Y, Niu L, Zhao F, Wang X, et al. Implanting a posterior chamber phakic intraocular lens in highly myopic eyes with peripheral primary iris and ciliary body cysts. *Eur J Ophthalmol*. (2019) 29:171–7. doi: 10.1177/1120672118766445
17. Jiménez-Alfaro I, Benítez del Castillo JM, García-Feijoó J, Gil de Bernabé JG, Serrano de La Iglesia JM. Safety of posterior chamber phakic intraocular lenses for the correction of high myopia. *Ophthalmology*. (2001) 108:90–9. doi: 10.1016/S0161-6420(00)00403-6
18. Higueras-Esteban A, Ortiz-Gomariz A, Gutierrez-Ortega R, Villa-Collar C, Abad-Montes J, Fernandes P, et al. Intraocular pressure after implantation of the visian implantable collamer lens with centra flow without iridotomy. *Am J Ophthalmol*. (2013) 156:800–5. doi: 10.1016/j.ajo.2013.05.018
19. Packer M. Meta-analysis and review: effectiveness, safety, and central port design of the intraocular collamer lens. *Clin Ophthalmol*. (2016) 10:1059–77. doi: 10.2147/OPTH.S111620
20. Garcia-De la Rosa G, Olivo-Payne A, Serna-Ojeda JC, Salazar-Ramos MS, Lichtinger A, Gomez-Bastar A, et al. Anterior segment optical coherence tomography angle and vault analysis after toric and non-toric implantable collamer lens V4c implantation in patients with high myopia. *Br J Ophthalmol*. (2018) 102:544–8. doi: 10.1136/bjophthalmol-2017-310518
21. Chen X, Guo L, Han T, Wu L, Wang X, Zhou X. Contralateral eye comparison of the long-term visual quality and stability between implantable collamer lens and laser refractive surgery for myopia. *Acta Ophthalmol*. (2019) 97:e471–8. doi: 10.1111/aos.13846
22. Javaloy J, Javaloy T, Borras F, Vidal MT, Mulet E, Belda JI, et al. Safety of iris claw phakic intraocular lenses: an endothelial microscopy long term study. *Invest Ophthalmol Vis Sci*. (2004) 45:337. doi: 10.1167/iovs.03-0693
23. Benda F, Filipová L, Filipec M. Correction of moderate to high hyperopia with an implantable collamer lens: medium-term results. *J Refract Surg*. (2014) 30:526–533. doi: 10.3928/1081597X-20140711-05
24. Chung T-Y, Park SC, Lee MO, Ahn K, Chung E-S. Changes in iridocorneal angle structure and trabecular pigmentation with STAAR implantable collamer lens during 2 years. *J Refract Surg*. (2009) 25:251–8. doi: 10.3928/1081597X-20090301-03
25. Fernández-Vigo J, Macarro-Merino A, Fernández-Vigo C, Fernández-Vigo J, Martnez-de-la-Casa J, Fernández-Pérez C. Effects of implantable collamer lens v4c placement on iridocorneal angle measurements by fourier-domain optical coherence tomography. *Am J Ophthalmol*. (2016) 162:43–52. doi: 10.1016/j.ajo.2015.11.010
26. Fernández-Vigo JI, Macarro-Merino A, Fernández-Vigo C, Fernández-Vigo JÁ, Pablo-Gómez-de-Liaño L, Fernández-Pérez C, et al. Impacts of implantable collamer lens v4c placement on angle measurements made by optical coherence tomography: two-year follow up. *Am J Ophthalmol*. (2017) 181:37–45. doi: 10.1016/j.ajo.2017.06.018
27. Lee D-H, Choi S-H, Chung E-S, Chung T-Y. Correlation between preoperative biometry and posterior chamber phakic visian implantable collamer lens vaulting. *Ophthalmology*. (2012) 119:272–7. doi: 10.1016/j.ophtha.2011.07.047
28. Lindland A, Heger H, Kugelberg M, Zetterström C. Vaulting of myopic and toric implantable collamer lenses during accommodation measured with visante optical coherence tomography. *Ophthalmology*. (2010) 117:1245–50. doi: 10.1016/j.ophtha.2009.10.033
29. Zhao J, Zhao J, Yang W, Li M, Hao G, Chen Z, et al. Consecutive contralateral comparison of toric and non-toric implantable collamer lenses V4c in vault after implantation for myopia and astigmatism. *Acta Ophthalmologica*. (2020) doi: 10.1111/aos.14720
30. Li Z, Xu Z, Wang Y, Liu Q, Chen B. Implantable collamer lens surgery in patients with primary iris and/or ciliary body cysts. *BMC Ophthalmol*. (2018) 18:287. doi: 10.1186/s12886-018-0935-7

Conflict of Interest: The authors declare that the research was conducted in the absence of any commercial or financial relationships that could be construed as a potential conflict of interest.

frontiers in Medicine

ORIGINAL RESEARCH
published: 11 March 2021
doi: 10.3389/fmed.2021.640269

Parameters of Capsulorrhexis and Intraocular Lens Decentration After Femtosecond and Manual Capsulotomies in High Myopic Patients With Cataracts

Yanan Zhu[1,2†], *Kexin Shi*[1,2†], *Ke Yao*[1,2], *Yuyan Wang*[1,2], *Sifan Zheng*[3], *Wen Xu*[1,2], *Peiqing Chen*[1,2], *Yibo Yu*[1,2] *and Xingchao Shentu*[1,2*]

[1] *The Eye Center, Second Affiliated Hospital of School of Medicine, Zhejiang University, Hangzhou, China,* [2] *Zhejiang Provincial Key Lab of Ophthalmology, Hangzhou, China,* [3] *GKT School of Medical Education, King's College London, London, United Kingdom*

OPEN ACCESS

Edited by:
Michele Lanza, University of Campania Luigi Vanvitelli, Italy

Reviewed by:
Lixia Luo, Sun Yat-sen University, China
Karim Mohamed-Noriega, Autonomous University of Nuevo León, Mexico
Xinyi Su, National University of Singapore, Singapore

***Correspondence:**
Xingchao Shentu
stxc@zju.edu.cn

[†]*These authors have contributed equally to this work and share first authorship*

Specialty section:
This article was submitted to Ophthalmology, a section of the journal Frontiers in Medicine

Received: *11 December 2020*
Accepted: *09 February 2021*
Published: *11 March 2021*

Citation:
Zhu Y, Shi K, Yao K, Wang Y, Zheng S, Xu W, Chen P, Yu Y and Shentu X (2021) Parameters of Capsulorrhexis and Intraocular Lens Decentration After Femtosecond and Manual Capsulotomies in High Myopic Patients With Cataracts. Front. Med. 8:640269. doi: 10.3389/fmed.2021.640269

Purpose: To compare the parameters of capsulorrhexis and intraocular lens decentration after femtosecond laser capsulotomy and manual continuous curvilinear capsulorrhexis in high myopic patients with cataracts.

Methods: This is a prospective consecutive non-randomized comparative cohort study. Selected patients with axial length > 26.0 mm were divided into femtosecond laser capsulotomy (FS) group and manual continuous curvilinear capsulorrhexis (CCC) group. Five experienced phacoemulsification surgeons conducted all surgeries. Intraoperative complications and post-operative anterior segment photography were recorded. Intraocular lens decentration, area of capsulorrhexis, circularity, and capsule overlap were measured at 1 week, 1 month, and 2 years after surgery. Between group differences of parameters were determined with independent-sample *t*-test or the Mann–Whitney *U*-test, analysis of variance test, Pearson chi-square test, and Spearman rank correlation test.

Results: The study included 142 eyes (108 patients), 68 eyes in the FS group, and 74 eyes in the CCC group. At 1 week, 1 month, and 2 years after surgery, the area of capsulorrhexis in the CCC group was significantly larger than in the FS group ($P < 0.05$), while no significant difference was noted in circularity values. The complete overlap ratio in the FS group was significantly higher than that in the CCC group ($P < 0.05$) at each measured timepoint. Significant correlations were noted between the anterior chamber depth and the area of capsulorrhexis in the CCC group ($R = 0.25$, $P = 0.04$), but did not correlate in the FS group ($P > 0.05$). In patients with an anterior chamber depth >3 mm, the capsule-intraocular lens (IOL) overlap of the CCC group was less than that of the FS group at all measured timepoints after surgery ($P < 0.05$). Meanwhile, the IOL decentration in the CCC group was significantly greater than that of the FS group in those patients at 2 years after surgery ($P < 0.05$).

Conclusion: In high myopic patients with cataracts, with anterior chamber depth more than 3 mm, femtosecond laser capsulotomy can achieve better capsulorrhexis sizing and centering. Due to more precise capsulotomy and a better capsule-IOL overlap in the FS group, femtosecond laser capsulotomy resulted in better long-term centration of the IOL.

Keywords: cataract, high myopia, intraocular lens, femtosecond laser capsulotomy, continuous curvilinear capsulorrhexis

INTRODUCTION

High myopia is typically defined as refraction >-6 D or axial length >26.0 mm (1, 2). In the past few decades, the prevalence of high myopia has markedly increased. It is estimated the incidence of high myopia will increase to ∼10% worldwide by 2050 (3). High myopia is one of the common causes of vision loss and can cause many complications, including cataracts (4). High myopic patients are likely to have an enlarged capsular bag with weak zonules and tend to develop cataracts earlier than emmetropic patients (5, 6). This increases the risk of post-operative intracapsular IOL dislocation. Cataract surgery combined with high myopia poses a greater challenge. Patients with high myopia have certain pathological changes, such as a deep anterior chamber, thin scleral wall, long axis that can lead to measurement errors, intraoperative fluctuations of anterior chamber, and/or changes of pupil size (7).

The effective position of intraocular lens is very important to the patient's visual quality after surgery. The architecture of the capsulorrheis greatly affects the position of lens, which in turn affects the subsequent refractive outcome. A perfectly circular and properly sized capsulorrhexis allows the capsular bag to completely envelop the IOL optic, providing a more predictable effective lens position and achieving optimal refractive outcome. However, if the capsulorrhexis is too large, the IOL optic can be tilted or decentered, resulting in astigmatism or compromised retinal image (8). At present, manual continuous curvilinear capsulorhexis (mainly used in conventional phacoemulsification surgery) has many uncertainties, especially in high myopia (9). In recent years, with the advent of femtosecond lasers in cataract surgery, a predictably sized, centered, and shaped anterior capsulotomy became possible (10). Earlier studies showed that femtosecond laser can achieve more regular circular capsulorrhexis (11, 12), which opens up a new opportunity for cataract surgery in patients with high myopia.

In this study, we used a large sample size in a prospective trial to compare femtosecond laser-assisted capsulotomy and manual capsulotomy in high myopic cases with cataracts with a 2-years follow-up. By measuring and comparing size and positioning parameters, the advantages of the two surgical methods were evaluated.

METHODS

Patients

This study was approved by the Institutional Review Board of the Second Affiliated Hospital of the Zhejiang University School of Medicine in Hangzhou, China. All research and data collection practices adhered to the tenets of the Declaration of Helsinki. The study was registered with the Chinese Clinical Trial Registry[1]. Written informed consent was obtained from all patients after they received a full explanation of the study.

The study consecutively recruited Chinese high myopic patients (axial length > 26.0 mm) with cataracts. All patients were given the option to choose femtosecond laser capsulotomies or continuous curvilinear capsulorrhexis. All patients had implantation of intraocular lenses. Each patient underwent a complete ophthalmologic evaluation. Patients with previous ocular surgery, trauma, active ocular disease, poorly dilated pupils, or known zonular weakness were excluded from the study. The selected patients were divided into two groups: FS and CCC. The FS group received femtosecond laser-assisted cataract surgery, and the CCC group received conventional phacoemulsification cataract surgery.

Surgical Technique

Every patient accepted the standard surgical procedure. All surgeries were performed by 5 experienced phacoemulsification surgeons (KY, WX, XS, PC, and YY). Each surgeon had performed more than 500 femtosecond laser-assisted cataract surgeries and 5,000 conventional phacoemulsification cataract surgeries. Before surgery, both groups achieved pupil dilation with an instillation of 0.5% tropicamide.

In the FS group, femtosecond laser was applied during the capsulotomy and lens fragmentation. Disposable interface contact lenses with suction rings (Softfit Patient Interface, Alcon LenSx, Inc.) were used for the corneal applanation. LenSx software (version 2.23, Alcon LenSx, Inc.) was used to create a 5.0 mm capsulotomy, and nuclear prefragmention was performed to obtain 6 pieces in a cross pattern.

In the CCC group, anterior capsules were treated conventionally [staining with trypan blue 0.06% under sodium hyaluronate 1.7% ophthalmic viscosurgical device (OVD) (Amvisc Plus, Bausch & Lomb, Inc.)]. Capsule forceps were used to complete a 5.0 mm continuous curvilinear capsulorrhexis.

In both groups, a 2.0 mm single-plane main incision and a 0.8 mm side-port corneal incision were made with a keratome. Phacoemulsification was performed using a standard stop-and-chop technique with longitudinal phacoemulsification system (Stellaris, Bausch & Lomb, Inc.). All IOLs were folded

[1]Chinese Clinical Trial Registry. *Clinical Outcomes and Complications of Femtosecond Laser-Assisted Cataract Surgery Versus Conventional Phacoemulsification Surgery*. ChiCTR-ONN-17010319. Available online at: http://www.chictr.org.cn/showproj.aspx?proj=17486 (accessed January 20, 2021).

and implanted in the capsular bag with the aid of an injection cartridge through the corneal wound. After the IOL implantation, the viscoelastic material was removed from the anterior chamber and the capsular bag by irrigation/aspiration. All incisions were left sutureless. All patients received standard regimen consisting of topical dexamethasone tobramycin 4 times a day for 2 weeks and pranoprofen for 1 month after surgery.

Patient Evaluation

Preoperatively, the medical histories of all patients were recorded. Comprehensive evaluations were also performed, including an A-scan standardized ultrasound (US) (Cinescan, Quantel Medical SA) and an IOLMaster biometry (Carl Zeiss). Anterior segment photography with a dilated pupil was captured at 1 week, 1 month, and 2 years after surgery. Photographs were imported into AutoCAD 2018 image-processing for Windows software (version 22.0, AutoDesk) to measure the IOL decentration and the following capsulotomy parameters: area of the capsulorrhexis, circularity, and the shortest and longest distance between the edge of the capsulorrhexis, and the IOL optic edge (distance min, distance max) along an elongated radius of the capsulorrhexis (**Figure 1**). Circularity is a parameter used for determining the regularity of capsulotomy shape according to the following formula: circularity $= 4\pi(\text{area}/\text{perimeter}^2)$. The quotient of the shortest and longest distance between the edge of the capsulorrhexis and the edge of the IOL optic was calculated to determine capsule-IOL overlap (capsule − IOL overlap = distance min/distance max). Circularity and overlap values of 1.0 indicate a perfect circle and an absolute regularly overlapping anterior capsule on the optic of the implanted IOL, respectively. Complete overlap is defined as when the edge of the capsulorhexis is completely within the IOL edge. If a part of capsulohexis edge outside the IOL edge, it is regarded as an incomplete overlap. AutoCAD 2018 gives a vector (determined by its length and angle to the horizontal plane) between the pupil center and center of the IOL (**Figure 2**). IOL decentration is the vector length between these 2 centers. The diameter of the implanted IOL was used as a scale to eliminate the magnification effect of the cornea. All measurements were taken by the same technician (who was masked to the patients) and conditions were kept consistent for all eyes operated.

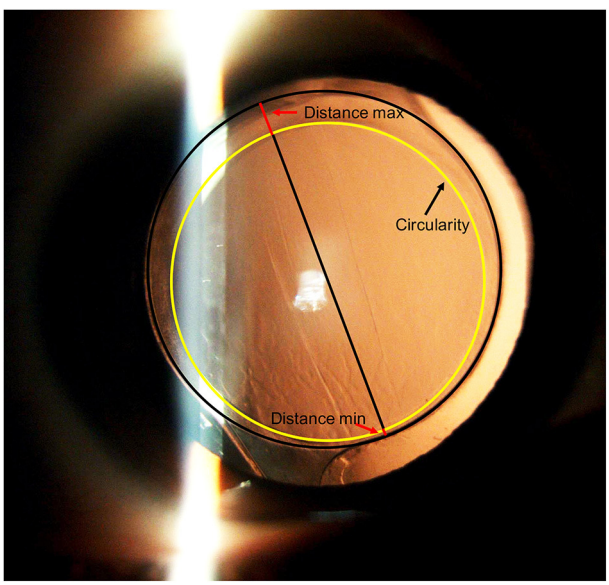

FIGURE 1 | Post-operative anterior segment photography with dilated pupil. The black circle shows the edge of the IOL, the yellow line shows the edge of the capsulorhexis. The red lines indicate the shortest and longest distance between the edge of the capsulorrhexis and the IOL optic edge along an elongated radius of the capsulorrhexis(distance min, distance max).

Statistical Analysis

The sample size was determined based on a power calculation (power 0.85; $P = 0.05$) using standard deviations obtained in our pre-study (13). At least 49 patients per group were required to be included in the analysis to achieve sufficient power in the statistical calculations.

Categorical data were defined as the number and percentage, and A Pearson chi-square analysis was used for statistical

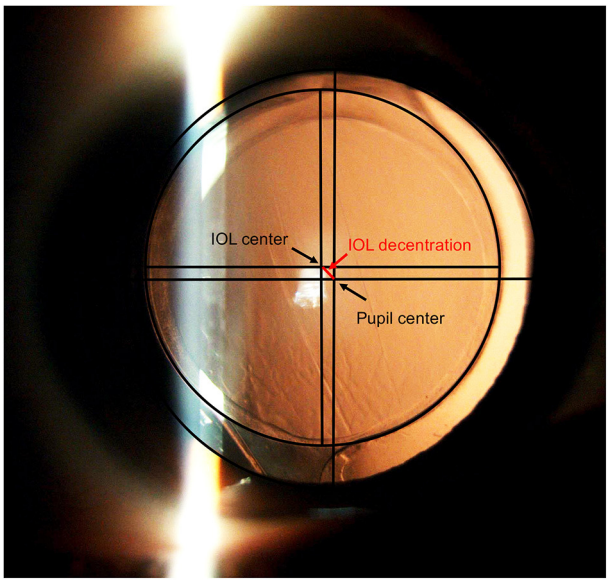

FIGURE 2 | Post-operative anterior segment photography with dilated pupil. The black circle inside shows the edge of the IOL, the black circle outside shows the edge of the pupil. The black lines indicate the horizontal and vertical diameters of the pupil and IOL. The red line between the pupil center and IOL center indicates the IOL decentration.

TABLE 1 | Demographics of patients who underwent manual continuous curvilinear capsulorrhexis or femtosecond laser capsulotomy.

Demographic	CCC group	FS group	*P*-value
Mean age (y)	64 ± 11	61 ± 13	0.26
Sex (M:F)	23:45	25:49	1.00
Axial length (mm)	29.53 ± 2.40	29.05 ± 2.17	0.21
Anterior chamber depth (mm)	2.89 ± 0.68	2.77 ± 0.69	0.30

analysis. Continuous variables were defined as means ± SD, and between-group comparative statistics were determined using the independent-sample *t*-test or the Mann–Whitney *U*-test, depending on the departure from normal distribution. The difference of capsulorrhexis parameters among multiple groups was analyzed by one-way analysis of variance test. Correlations between parameters were analyzed with Spearman rank correlation test. A $P < 0.05$ was considered statistically significant. All analyses (except when noted) were performed using IBM SPSS Statistics software (version 26.0, IBM Corp).

RESULTS

A total of 142 eyes (108 patients) attended at least 2 follow-up visits. Missing data were due to personal inconvenience, refusal to mydriasis, or temporary device failure. There were 74 eyes in the FS group and 68 eyes in the CCC group. No statistically significant differences were noted between the CCC group and FS groups in regards to age, gender distribution, axial length, or anterior chamber depth (**Table 1**). The mean age was 64 ± 11 years in the CCC group and 61 ± 13 years in the FS Group ($P = 0.26$). There were 45 women (66.2%) in the CCC group and 49 women (66.2%) in the FS group ($P = 1.00$). Axial length was 29.53 ± 2.40 mm in the CCC group and 29.05 ± 2.17 mm in the FS group ($P = 0.21$). Anterior chamber depth was 2.89 ± 0.68 mm in the CCC group and 2.77 ± 0.69 mm in the FS group, separately ($P = 0.30$). **Table 2** shows that each surgeon performed a similar number of femtosecond laser capsulotomies and manual capsulotomies. There was no significant difference of parameters in capsulotomies between the surgeons ($P > 0.05$).

Table 3 shows the parameters of the capsulotomies and IOL decentrations in the two study groups measured by AutoCAD. At 1 week, 1 month, and 2 years after surgery, the area of capsulorrhexis in the CCC group were significantly larger than those in the FS group ($P < 0.05$), while no significant difference was noted in circularity values. The complete overlap ratio in the FS group was significantly higher than that in the CCC group ($P < 0.05$) at each measured time point after surgery. However, in the cases with complete overlap, there was no significant difference in the capsule-IOL overlap between CCC group and FS group at all measured timepoints ($P > 0.05$). No significant difference was also noted in the IOL decentration between the two groups at all measured timepoints ($P > 0.05$).

Figure 3 shows no significant correlation was found between the axial length and the area of capsulotomy in either study group ($P > 0.05$). There was a statistically significant correlation between anterior chamber depth and area of capsulotomy in the CCC group ($R = 0.25$, $P = 0.04$), however no statistically significant correlation was noted between these parameters in the FS group ($P > 0.05$; **Figure 4**). Patients were subsequentoy divided into the normal anterior chamber group (anterior chamber depth <3.00 mm) and deep anterior chamber group (anterior chamber depth ≥3.00 mm), according to the results of the correlation analysis.

TABLE 2 | Statistical information about the number of operations performed by surgeons and parameter of capsulotomies after surgery.

	Number of operations		Area of capsulorrhexis (mm^2)			
Surgeon	**CCC**	**FS**	**CCC**	***P*-value**	**FS**	***P*-value**
Ke Yao	16	18	22.25 ± 1.94	0.68	21.08 ± 1.42	0.41
Wen Xu	14	16	22.11 ± 2.62		21.28 ± 1.76	
Xingchao Shentu	15	14	21.34 ± 1.44		20.79 ± 1.90	
Peiqing Chen	12	14	21.29 ± 2.45		21.36 ± 1.18	
Yibo Yu	11	12	22.27 ± 2.52		20.77 ± 1.56	

TABLE 3 | Parameters of capsulotomies and intraocular decentrations in eyes that underwent continuous curvilinear capsulorrhexis or femtosecond laser capsulotomy.

	1 week			1 month			2 years		
Parameters	**CCC**	**FS**	***P*-value**	**CCC**	**FS**	***P*-value**	**CCC**	**FS**	***P*-value**
Area of capsulorrhexis (mm^2)	21.85 ± 2.18	21.07 ± 1.54*	0.01	21.02 ± 2.16	20.19 ± 2.03*	0.04	20.86 ± 2.22	19.76 ± 2.17*	0.01
Circularity	0.99 ± 0.02	0.99 ± 0.01	0.06	0.99 ± 0.01	0.99 ± 0.01	0.13	0.99 ± 0.02	0.99 ± 0.03	0.89
Complete overlap (%)	94	100*	0.03	93	100*	0.02	90	99*	0.02
Capsule-IOL overlap	0.41 ± 0.19	0.44 ± 0.17	0.23	0.40 ± 0.19	0.45 ± 0.16	0.10	0.41 ± 0.19	0.47 ± 0.17	0.06
IOL decentration (mm)	0.12 ± 0.16	0.12 ± 0.14	0.98	0.17 ± 0.16	0.16 ± 0.16	0.73	0.23 ± 0.17	0.20 ± 0.16	0.22

$P < 0.05$ between groups at the given time point using repeated measures analysis of variance.

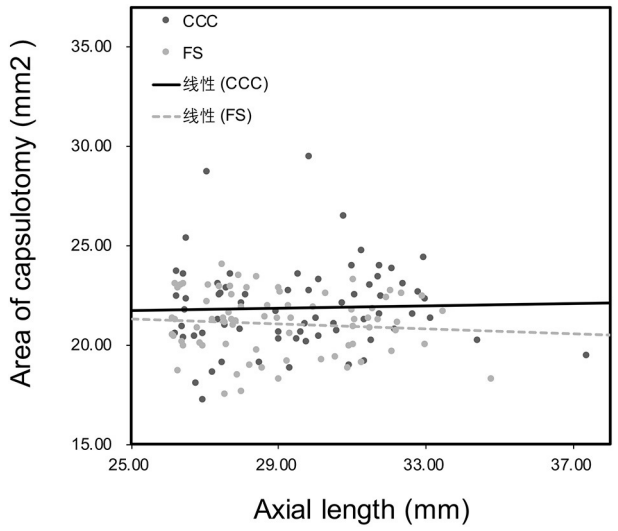

FIGURE 3 | Correlation between axial length and area of capsulotomy 1 week after surgery. No correlation was found in the manual capsulotomy group (CCC) ($R = 0.02$, $P = 0.88$) and laser capsulotomy group (FS) ($R = -0.08$, $P = 0.48$).

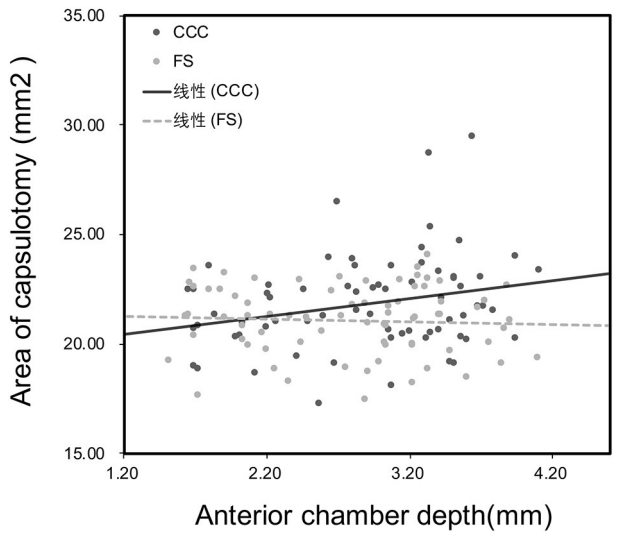

FIGURE 4 | Correlation between anterior chamber depth and area of capsulotomy 1 week after surgery. The correlation was significant in the manual capsulotomy group (CCC) ($R = 0.25$, $P = 0.04$) but not in the laser capsulotomy group (FS) ($R = -0.04$, $P = 0.75$).

There was no statistical difference in age, gender distribution, axial length or anterior chamber depth in the sub-group analysis of anterior chamber depth $\geq$3 mm or $<$ 3 mm in both the CCC group and the FS group (**Table 4**). Among patients with normal anterior chambers, the CCC group had 33 eyes and the FS group had 40 eyes. We found that in patients with normal anterior chamber, there were no significant differences in the parameters of the capsulorrhexis and the IOL decentration between the FS group and the CCC group (**Table 5**). In patients with deep anterior chamber, there were 35 eyes in the CCC group and 34 eyes in the FS group. Many statistically significant differences were noted between the two groups. As shown in **Table 6**, the area of capsulorrhexis of the CCC group was significantly larger than that of the FS group at all measured timepoints after surgery ($P < 0.05$). The complete overlap ratio in the FS group was also significantly higher than that in the CCC group ($P < 0.05$) at 1 month and 2 years after surgery. The capsule-IOL overlap of the CCC group was less than the FS group at each timepoint after surgery ($p < 0.05$) and the IOL decentration in the CCC group was significantly higher than the FS group at 2 years after surgery ($P < 0.05$).

In addition, in both the CCC and the FS group, no cases of capsular contraction syndrome was found. The area of the capsulorrhexis at 1 month and 2 years after surgery were significantly smaller than the capsular opening area at 1 week after surgery ($P < 0.05$) in both gruops. However, there was no significant difference between the value of the reduced capsulorrhexis area of the CCC group and the FS group measured at 1 week-1 month and 1 week-2 years (1.44 ± 1.31 vs. 1.75 ± 1.45 mm^2, $P = 0.53$; 1.27 ± 1.46 vs. 1.98 ± 1.84 mm^2, $P = 0.47$; respectively).

DISCUSSION

Femtosecond laser, a new technology, has been applied in cataract surgery in recent years. Previous studies had reported that femtosecond laser capsulotomy improve the centration, circularity and precision of anterior capsulorrhexis (14, 15). The size and shape of the anterior capsulorrhexis greatly affect surgical outcomes, including the position of the lens and the subsequent refractive outcomes. If the capsulorrhexis is too large, the IOL may be decentered, resulting in visual dysfunction such as refractive error and high-order aberrations increasing (16). If it is too small, the capsular bag is highly likely to contract and cause complications, such as IOL loop curling and decentration (17). High myopia is the most common risk factor for advanced intracapsular IOL dislocation (18). A previous study had also demonstrated that the frequency of IOL tilt and decentration was significantly higher in cataract eyes with high myopia than that in non-myopia cataract eyes (19). Due to the special pathological changes of high myopia, a perfectly circular and properly sized capsulorrhexis is extremely important.

Surgeons have applied femtosecond lasers to highly myopic cataracts. Previous studies indicated that femtosecond laser capsulotomy, compared with manual capsulotomy, has a more regular shape of capsulorrhexis, a higher capsule-IOL overlap, and a better IOL centration in myopic eyes (20, 21). It was also reported that the size of capsulorrhexis area and the IOL decentration in manual capsulotomy were positively correlated with the axial length, while femtosecond laser capsulotomy eliminated these errors (20). However, femtosecond laser and highly myopic cataracts were rarely reported, with a relatively small sample size and a relatively short follow-up time.Therefore, in order to further investigate the effect of femtosecond

TABLE 4 | Demographics of patients (anterior chamber depth <3.00 mm and anterior chamber depth ≥ 3.00 mm) who underwent manual continuous curvilinear capsulorrhexis or femtosecond laser capsulotomy.

	Demographic	CCC group	FS group	*P*-value
Anterior chamber depth < 3.00 mm	Mean age (y)	64 ± 12	61 ± 14	0.49
	Sex (M:F)	12:21	14:26	0.90
	Axial length (mm)	29.67 ± 2.48	28.69 ± 2.10	0.07
	Anterior chamber depth (mm)	2.32 ± 0.44	2.25 ± 0.45	0.48
Anterior chamber depth ≥3.00 mm	Mean age (y)	64 ± 9	64 ± 12	0.81
	Sex (M:F)	11:24	11:23	0.93
	Axial length (mm)	29.40 ± 2.35	29.48 ± 2.21	0.89
	Anterior chamber depth (mm)	3.43 ± 0.33	3.39 ± 0.30	0.62

TABLE 5 | Parameters of capsulotomies and intraocular decentrations in eyes that underwent continuous curvilinear capsulorrhexis or femtosecond laser capsulotomy (anterior chamber depth <3.00 mm).

	1 week			1 month			2 years		
Parameters	**CCC**	**FS**	***P*-value**	**CCC**	**FS**	***P*-value**	**CCC**	**FS**	***P*-value**
Area of capsulorrhexis (mm^2)	21.49 ± 1.85	21.00 ± 1.60	0.22	20.82 ± 2.14	20.34 ± 2.34	0.43	20.66 ± 1.89	19.85 ± 2.21	0.14
Circularity	0.99 ± 0.02	0.99 ± 0.01	0.31	0.99 ± 0.02	0.99 ± 0.01	0.14	0.99 ± 0.02	0.99 ± 0.03	0.94
Complete overlap (%)	97	100	0.27	97	100	0.27	91	98	0.22
Capsule-IOL overlap	0.43 ± 0.21	0.41 ± 0.18	0.67	0.42 ± 0.19	0.43 ± 0.16	0.85	0.42 ± 0.18	0.44 ± 0.15	0.68
IOL decentration (mm)	0.14 ± 0.18	0.11 ± 0.14	0.47	0.17 ± 0.18	0.15 ± 0.16	0.71	0.20 ± 0.19	0.20 ± 0.17	0.91

**P < 0.05 between groups at the given time point using repeated measures analysis of variance.*

TABLE 6 | Parameters of capsulotomies and intraocular decentrations in eyes that underwent continuous curvilinear capsulorrhexis or femtosecond laser capsulotomy (anterior chamber depth ≥3.00 mm).

	1 week			1 month			2 years		
Parameters	**CCC**	**FS**	***P*-value**	**CCC**	**FS**	***P*-value**	**CCC**	**FS**	***P*-value**
Area of capsulorrhexis (mm^2)	22.19 ± 2.43	21.16 ± 1.49*	0.04	21.18 ± 2.21	20.02 ± 1.63*	0.03	21.04 ± 2.50	19.64 ± 2.15*	0.03
Circularity	0.99 ± 0.01	0.99 ± 0.01	0.06	0.99 ± 0.01	0.99 ± 0.01	0.51	0.99 ± 0.01	0.99 ± 0.01	0.60
Complete Overlap (%)	91	100	0.08	89	100*	0.04	89	100*	0.04
Capsule-IOL Overlap	0.38 ± 0.17	0.48 ± 0.15*	0.01	0.37 ± 0.20	0.48 ± 0.15*	0.04	0.40 ± 0.20	0.51 ± 0.17*	0.03
IOL Decentration (mm)	0.10 ± 0.14	0.13 ± 0.14	0.38	0.17 ± 0.15	0.16 ± 0.16	0.93	0.27 ± 0.19	0.19 ± 0.15*	0.04

**P < 0.05 between groups at the given time point using repeated measures analysis of variance.*

laser application in highly myopic catarats, we conducted a prospective large-sample long-term study.

In our study, we evaluated the capsulorrhexis size, circularity, IOL decentration, and capsule-IOL overlap in high myopic patients with cataracts. In general, we found that femtosecond laser capsulotomy has better parameters of capsulorrhexis and caspule-IOL overlap, which included the capsulorrhexis area being more precise and the complete overlap ratio being superior to compared manual capsulotomy. These results are all supported by previous studies (20) and are consistent with those seen in common cataracts (22, 23). However, there is no significant difference in the circularity of the 2 types of capsulotomy in this study. Due to the advanced operation technology, the circularity of both surgical methods is extremely high (above 99%), compared with the circularity in an earlier study (20, 22) (∼85%). The circularity of the capsulorrhexis much depends on the surgeon's skill.

We attempted to find the characteristics of highly myopic cataracts. In this study, we investigated the correlation between parameters of the capsulorrxis and the axial length at first. Our results contradicted the results from Nagy et al. and no significant correlation was found between parameters of the capsulorrxis and the axial length. As the angle and depth of the capsulotomic forceps manipulation mainly depend on the anterior chamber depth, we studied the correlation between the anterior chamber depth and the capsulorrxis parameters. Our study showed a significant positive correlation between the two in the CCC group, but no correlation in the FS group. The relationship between anterior chamber depth and axial length in high myopia is controversial. Previous studies had demonstrated

that anterior chamber depth is positively correlated with axial length in myopic eyes (24). However, evidence has also emerged that the increase of axial length in patients with long eye axis was mainly due to the expansion and lengthening of vitreous cavity, rather than the change of anterior segment morphology. In eyes with long axial length, the correlation between anterior chamber depth and axial length disappeared (25). Our study has shown compared with the axial length, the depth of the anterior chamber has a greater impact on the operation of high myopic cataract surgery. We can conclude that the capsulorrhexis parameter is related to depth of the anterior chamber rather than axial length.

Our study found when the anterior chamber depth was <3 mm, the manual capsulorrhexis was significantly larger than femtosecond and more eccentric. Previous studies have also suggested statistically significant correlations between the anterior chamber depth and the pupil diameter, as well as the white-to-white corneal diameter in myopia (26, 27). Our study indicated that femtosecond laser capsulotomy has absolute advantages when the anterior chamber depth was >3 mm. This is due to the significant difference in the pupil reference and the operating angle, which causes the difficulty in manual capsulotomy. When the anterior chamber depth was <3 mm, experienced surgeons can perform capsulotomy adequately according to their experience. The long-term centration of the IOL depends on the size and location of the capsulorrhexis and the extent of the IOL coverage (22). We further found that when the anterior chamber depth was >3 mm, the FS group had better IOL centration at 2 years after surgery due to a better capsule-IOL overlap and more precise capsulorrhexis area. Because of the long-term centration of the IOL, patients can have better visual quality. Some studies had indicated that femtosecond laser surgery can provide patients with better visual quality after premium IOL implanation, such as the toric IOL and multifocal IOL (28, 29).

High myopia, small capsulorrhexis, and hydrophilic IOL are all considered risk factors for anterior capsular contraction (19, 30). In this study, although the diameter of the FS group's capsulorrhexis was smaller than the CCC group, we did not find any cases of capsular contraction syndrome. The area of the capsulorrhexis of the two groups was reduced to a certain extent after surgery, but there was no significant difference in the value of the reduced area in the two groups. Therefore, femtosecond laser does not increase the risk of capsular contraction in high myopic patients with cataracts. not only is femtosecond laser effective and comparatively safe in cataract surgery for high myopia.

Our main limitation concerns evaluating the IOL decentation. Only the value on the horizontal plane of the IOL was measured, and the changes in the anteroposterior positions of the IOL were not considered. It would be pertient to examine whether the effect of capsulotomies influences the tilting of the IOL over time. In addition, due to the additional cost of using femtosecond lasers, we must respect the wishes of patients to choose surgery. This limits the randomization of the study. A previous study also concluded that thicker lens contribute to greater IOL decentration (8). Due to the lack of equipment to measure lens thickness at the beginning of our study, this factor was not explored. Whether the percentage and magnitude of IOL decentration are different between the cases with complete or incomplete overlap should also be explored. Unforunately, the number of cases with incomplete overlap was too small for statistical comparison.

In conclusion, in high myopic patients with cataracts and anterior chamber depth >3 mm, femtosecond laser capsulotomy is the more ideal choice for surgery because it has a better IOL overlap and a better IOL positioning.

DATA AVAILABILITY STATEMENT

The raw data supporting the conclusions of this article will be made available by the authors, without undue reservation.

ETHICS STATEMENT

The studies involving human participants were reviewed and approved by Ethics Committee of Second Affiliated Hospital of Zhejiang University, College of Medicine. The patients/participants provided their written informed consent to participate in this study. Written informed consent was obtained from the individual(s) for the publication of any potentially identifiable images or data included in this article.

AUTHOR CONTRIBUTIONS

XS: study concept and design. KY, XS, WX, PC, YY, and YW: data collection. YZ, KS, and XS: analysis and interpretation of data. YZ, KS, XS, and SZ: drafting and critical revision of the manuscript. All authors contributed to the article and approved the submitted version.

FUNDING

This work was supported by the Program of National Natural Science Foundation of China (Grant Nos. 81670834 and 81970781 to XS), the Program of National Natural Science Foundation of China (Grant No. 81970779 to YZ).

REFERENCES

1. Wu PC, Huang HM, Yu HJ, Fang PC, Chen CT. Epidemiology of myopia. *Asia-Pac J Ophthalmol.* (2016) 5:386–93. doi: 10.1097/APO.0000000000000236
2. Chong EW, Mehta JS. High myopia and cataract surgery. *Curr Opin Ophthalmol.* (2016) 27:45–50. doi: 10.1097/ICU.0000000000000217
3. Holden BA, Fricke TR, Wilson DA, Jong M, Naidoo KS, Sankaridurg P, et al. Global prevalence of myopia and high myopia and temporal trends from 2000 through 2050. *Ophthalmology.* (2016) 123:1036–42. doi: 10.1016/j.ophtha.2016.01.006
4. Haarman AEG, Enthoven CA, Tideman JWL, Tedja MS, Verhoeven VJM, Klaver CCW. The complications of myopia: a review and meta-analysis. *Invest Ophthalmol Visual Sci.* (2020) 61:49. doi: 10.1167/iovs.61.4.49

5. Lam JK, Chan TC, Ng AL, Chow VW, Wong VW, Jhanji V. Outcomes of cataract operations in extreme high axial myopia. *Graefes Arch Clin Exp Ophthalmol.* (2016) 254:1811–7. doi: 10.1007/s00417-016-3414-y
6. Cetinkaya S, Acir NO, Cetinkaya YF, Dadaci Z, Yener HI, Saglam F. Phacoemulsification in eyes with cataract and high myopia. *Arq Bras Oftalmol.* (2015) 78:286–9. doi: 10.5935/0004-2749.20150076
7. Li XX, Wan XH. Research progression of surgical treatment for high myopia combined cataract. *Chin J Optomet Ophthalmol Visual Sci.* (2015) 17:441–4. doi: 10.3760/CMA.J.ISSN.1674-845X.2015.07.015
8. Chen XY, Gu XX, Wang W, Xiao W, Jin GM, Wang LH, et al. Characteristics and factors associated with intraocular lens tilt and decentration after cataract surgery. *J Cataract Refract Surg.* (2020) 46:1126–31. doi: 10.1097/j.jcrs.0000000000000219
9. Wygledowska-Promieńska D, Jaworski M, Kozieł K, Packard R. The evolution of the anterior capsulotomy. *Wideochir Inne Tech Maloinwazyjne.* (2019) 14:12–8. doi: 10.5114/wiitm.2019.81313
10. Friedman NJ, Palanker DV, Schuele G, Andersen D, Marcellino G, Seibel BS, et al. Femtosecond laser capsulotomy reply. *J Cataract Refract Surg.* (2011) 37:1189–98. doi: 10.1016/j.jcrs.2011.04.022
11. Alió JL, Abdou AA, Puente AA, Zato MA, Nagy Z. Femtosecond laser cataract surgery: updates on technologies and outcomes. *J Refract Surg.* (2014) 30:420–7. doi: 10.3928/1081597X-20140516-01
12. Ali MH, Ullah S, Javaid U, Javaid M, Jamal S, Butt NH. Comparison of characteristics of femtosecond laser-assisted anterior capsulotomy versus manual continuous curvilinear capsulorrhexis: a meta-analysis of 5-year results. *J Paki Med Assoc.* (2017) 67:1574–79.
13. Zhu YN, Chen XY, Chen PQ, Xu W, Shentu XC, Yu YB, et al. Lens capsule-related complications of femtosecond laser–assisted capsulotomy versus manual capsulorhexis for white cataracts. *Cataract Refract Surg.* (2019) 45:337–42. doi: 10.1016/j.jcrs.2018.10.037
14. Hu WF, Chen SH. Advances in capsulorhexis. *Curr Opin Ophthalmol.* (2019) 30:19–24. doi: 10.1097/ICU.0000000000000539
15. Avetisov KS, Ivanov MN, Yusef YN, Yusef SN, Aslamazova AE, Fokina ND. Morphological and clinical aspects of anterior capsulotomy in femtosecond laser-assisted cataract surgery. *Vestnik Oftalmolgii.* (2017) 1334:83–8. doi: 10.17116/oftalma2017133483-88
16. Sharma B, Abell RG, Arora T, Antony T, Vajpayee RB. Techniques of anterior capsulotomy in cataract surgery. *Ind J Ophthalmol.* (2019) 67:450–60. doi: 10.4103/ijo.IJO_1728_18
17. Li SX, Hu YP, Guo R, Shao YS, Zhao JY, Zhang JS, et al. The effects of different shapes of capsulorrhexis on postoperative refractive outcomes and the effective position of the intraocular lens in cataract surgery. *BMC Ophthalmol.* (2019) 19:59. doi: 10.1186/s12886-019-1068-3
18. Fan Q, Han XY, Zhu XJ, Cai L, Qiu XD, Lu Y, et al. Clinical characteristics of intraocular lens dislocation in Chinese Han populations. *J Ophthalmol.* (2020) 2020:8053941. doi: 10.1155/2020/8053941
19. Wang DD, Yu XY, Li ZL, Ding XX, Lian HL, Mao JY, et al. The effect of anterior capsule polishing on capsular contraction and lens stability in cataract patients with high myopia. *J Ophthalmol.* (2018) 2018:8676451. doi: 10.1155/2018/8676451
20. Nagy ZZ, Kránitz K, Takacs AI, Miháltz K, Kovács I, Knorz MC. Comparison of intraocular lens decentration parameters after femtosecond and manual capsulotomies. *J Refract Surg.* (2011) 27:564–9. doi: 10.3928/1081597X-20110607-01
21. Zheng YX, Ding XX, Wang DD, Yu XY, Zhao YE. The accuracy of postoperative diopter in cataract patients with high myopia after femtosecond laser-assisted cataract surgery. *Chin J Optomet Ophthalmol Visual Sci.* (2016) 18:650–3. doi: 10.3760/cma.j.issn.1674-845X.2016.11.003
22. Kranitz K, Takacs A, Mihaltz K, Kovács I, Knorz MC, Nagy ZZ. Femtosecond laser capsulotomy and manual continuous curvilinear capsulorrhexis parameters and their effects on intraocular lens centration. *J Refract Surg.* (2011) 27:558–63. doi: 10.3928/1081597X-20110623-03
23. Cinar E, Yuce B, Aslan F, Erbakan G, Küçükerdönmez C. Intraocular lens tilt and decentration after Nd: YAG laser posterior capsulotomy: femtosecond laser capsulorhexis versus manual capsulorhexis. *J Cataract Refract Surg.* (2019) 45:1637–44. doi: 10.1016/j.jcrs.2019.07.017
24. Chen H, Lin HT, Lin ZL, Chen JJ, Chen WR. Distribution of axial length, anterior chamber depth, and corneal curvature in an aged population in South China. *BMC Ophthalmol.* (2016) 16:47. doi: 10.1186/s12886-016-0221-5
25. Fang W, Zhang J, Yang HQ, Zhao LP. Anterior segment biometry of eyes with different axial lengths. *Int Eye Sci.* (2017) 17:1055–9. doi: 10.3980/j.issn.1672-5123.2017.6.11
26. Alfonso JF, Ferrer-Blasco T, González-Méijome JM, García-Manjarres M, Peixoto-de-Matos SC, Montés-Micó R. Pupil size, white-to-white corneal diameter, and anterior chamber depth in patients with myopia. *J Refract Surg.* (2010) 26:891–8. doi: 10.3928/1081597X-20091209-07
27. Hosny M, Alió JL, Claramonte P, Attia WH, Perez-Santonja JJ. Relationship between anterior chamber depth, refractive state, corneal diameter, and axial length. *J Refract Surg.* (2000) 16:336–40. doi: 10.1055/s-2000-7340
28. Espaillat A, Pérez O, Potvin R. Clinical outcomes using standard phacoemulsification and femtosecond laser-assisted surgery with toric intraocular lenses. *Clin Ophthalmol.* (2016) 10:555–63. doi: 10.2147/OPTH.S102083
29. Lee JA, Song WK, Kim JY, Kim MJ, Tchah H. Femtosecond laser–assisted cataract surgery versus conventional phacoemulsification: refractive and aberrometric outcomes with a diffractive multifocal intraocular lens. *J Refract Surg.* (2019) 45:21–7. doi: 10.1016/j.jcrs.2018.08.032
30. Hartman M, Rauser M, Brucks M, Chalam KV. Evaluation of anterior capsular contraction syndrome after cataract surgery with commonly used intraocular lenses. *Clin Ophthalmol.* (2018) 12:1399–403. doi: 10.2147/OPTH.S172251

Conflict of Interest: The authors declare that the research was conducted in the absence of any commercial or financial relationships that could be construed as a potential conflict of interest.

frontiers in Medicine

ORIGINAL RESEARCH
published: 26 April 2021
doi: 10.3389/fmed.2021.616249

Characteristics of Fundal Changes in Fundus Tessellation in Young Adults

Hanyi Lyu[1,2,3,4,5], *Qiuying Chen*[1,2,3,4], *Guangyi Hu*[1,2,3,4], *Ya Shi*[1,2,3,4], *Luyao Ye*[1,2,3,4], *Yao Yin*[1,2,3,4], *Ying Fan*[1,2,3,4], *Haidong Zou*[1,2,3,4], *Jiangnan He*[1,2,3,4*], *Jianfeng Zhu*[1,2,3,4*] *and Xun Xu*[1,2,3,4*]

[1] *Shanghai Eye Disease Prevention and Treatment Center, Shanghai Eye Hospital, Shanghai, China,* [2] *Shanghai General Hospital, Shanghai Jiaotong University School of Medicine, Shanghai, China,* [3] *Shanghai Jiaotong University School of Medicine, Shanghai, China,* [4] *Shanghai Engineering Center for Visual Science and Photo medicine, Shanghai Jiaotong University School of Medicine, Shanghai, China,* [5] *Ophthalmology Department of Peking University People's Hospital, Beijing, China*

Purpose: To explore the characteristics and associated factors of fundus tessellation, especially the alternation of choroidal thickness among different degrees of tessellated fundus in young adults.

Design: Cross-sectional, population-based study.

Methods: A total of 796 students were included in the study and underwent comprehensive ophthalmic examinations, including anterior segment examinations and swept-source optical coherence tomography (OCT) measurements. The degree of tessellated fundus was assessed by fundus photographs applying an early treatment of diabetic retinopathy study grid to evaluate the location of fundus tessellation and then divided into five groups. The topographic variation and factors, tilted disc ratio, parapapillary atrophy (PPA), retinal thickness (ReT), choroidal thickness (ChT), and subfoveal scleral thickness (SST) related to tessellated fundus were analyzed.

Results: Compared to normal fundus, tessellated fundus had a lower spherical equivalent (SE) ($p < 0.0001$), worse best-corrected visual acuity (BCVA)($p = 0.043$), longer axial length (AL) ($p < 0.0001$), thinner retina ($p < 0.0001$), thinner ($p < 0.0001$) choroid, and thinner sclera in center fovea ($p = 0.0035$). Among all subfields of macular and peripapillary regions, center fovea and macula-papillary region showed the most significant decrease in choroidal thickness. The proportion of fundus tessellation significantly increased with lower body weight index (BMI) ($p = 0.0067$), longer AL ($p < 0.0001$), larger PPA($p = 0.0058$), thinner choroid ($p < 0.0001$), and thinner sclera ($p < 0.0001$).

Conclusions: Eyes showed more severe myopic morphological alternation with the increasement of proportion of fundus tessellation to the center fovea, including a significant decrease in both choroid and scleral thickness. Choroidal thinning may progress most rapidly in the macula-papillary region as fundus tessellation approaches to the center fovea.

Keywords: fundus tessellation, myopia, fundal alteration, choroidal thickness, scleral thickness

OPEN ACCESS

Edited by:
Xiangtian Zhou,
Wenzhou Medical University, China

Reviewed by:
Haotian Lin,
Sun Yat-sen University, China
Pei-Chang Wu,
Kaohsiung Chang Gung Memorial Hospital, Taiwan

****Correspondence:***
Jiangnan He
hejiangnan85@126.com
Jianfeng Zhu
jfzhu1974@hotmail.com
Xun Xu
drxuxun@sjtu.edu.cn

Specialty section:
This article was submitted to Ophthalmology, a section of the journal Frontiers in Medicine

Received: *11 October 2020*
Accepted: *24 March 2021*
Published: *26 April 2021*

Citation:
Lyu H, Chen Q, Hu G, Shi Y, Ye L, Yin Y, Fan Y, Zou H, He J, Zhu J and Xu X (2021) Characteristics of Fundal Changes in Fundus Tessellation in Young Adults. Front. Med. 8:616249. doi: 10.3389/fmed.2021.616249

INTRODUCTION

The high prevalence of myopia and high myopia in young adults worldwide, especially in East and Southeast Asia, has led to a significant public health burden of visual impairment and blindness (1–8). Recently, a revised classification system for myopic maculopathy has been proposed to standardize the definition among epidemiological studies (6, 9). According to this International Photographic Classification and Grading System for myopic maculopathy (META-PM) classification, as well as previous studies, tessellated fundus has been defined as the visualization of large choroidal vessels at the posterior fundus pole, which is the first stage of pathological myopia (PM) retinopathy (category 1) (6, 9, 10). Some tessellated fundus can progress to diffuse atrophy and macular atrophy, which cause severe and irreversible impairment of visual acuity, while others could be stable at this stage for long-term (9, 11). The underlying reasons for this discrepancy remain unknown.

Fundus photographs are common in clinical practice, and can be easily accessed for clinical observation. Factors associated with fundus tessellation in elderly population have been studied using fundus photographs (12, 13), however, age-based choroidal thinning and age-related retinopathy can be interference factors for examining fundus tessellation in pathological myopia (14–17).

To investigate the characteristics associated with fundus tessellation during early stage of pathological myopia, we recruited 828 university students of all grades in Shanghai University, of which 796 students were included as participants in this study. In this cross-sectional study, we measured optical parameters, including parameters of anterior segment, axial length (AL), peripapillary atrophy (PPA), retinal thickness (ReT), choroidal thickness (ChT) and subfoveal scleral thickness (SST), and analyzed their relationships with tessellated fundus diagnosis and severity.

METHODS

Setting and Participants

This cross-sectional population-based study was approved by the ethics committee of Shanghai General Hospital, Shanghai Jiao Tong University, Shanghai, China, and followed the tenets of the Declaration of Helsinki. All participants understood the study protocol and provided signed informed consents. The study was registered at www.clinicaltrials.gov (No.NCT03446300).

The subjects were randomly selected from the students attending the Shanghai University in October 2016 (18). Age and gender were recorded and height, weight, heart rate, systolic (SBP) and diastolic (DBP) blood pressures were measured for each participant. A detailed medical history was recorded for each participant. All participants underwent comprehensive ophthalmic examinations, including refractive error assessment using an autorefractor machine (model KR-8900; Topcon, Tokyo, Japan), measurement of best-corrected visual acuity (BCVA) and intraocular pressure (IOP, Full Auto Tonometer TX-F; Topcon, Japan), slit-lamp biomicroscopy, and color fundus photograph. Central corneal thickness, lens thickness, anterior chamber depth (ACD) and AL were measured using optical low-coherence reflectometry (Aladdin; Topcon, Japan). Subjective refraction was performed by two trained optometrists for all participants. BMI is defined as the body mass divided by the square of the body height. Spherical equivalent (SE) was acquired in non-cycloplegic manner and was calculated as the sphere plus half a cylinder. BCVA was converted into the logarithm of minimal angle resolution (logMAR).

The inclusion criteria were as follows: IOP $\leq$ 21 mmHg; normal anterior chamber angles; normal optic nerve head (ONH) without glaucomatous changes, such as narrowing of neuroretina, increased cup-disc ratio and peripapillary hemorrhage. Participants with a history of ocular or systemic diseases including congenital cataract and glaucoma, hypertension and diabetes; previous intraocular or refractive surgery; and other evidence of retinopathy were excluded. Images acquired with signal strength index $\leq$60 were excluded for statistical analysis. In general, except for the fundus tessellation associated with myopia, the participants had no other ocular abnormalities. The analysis of correlation between two eyes of 30 randomly selected participants has showed that for parameters including SE, AL, PPA, SST, ChT, GCT, ReT, and the grading of fundus tessellation, correlation is significant at the 0.01 level. Only the right eye of each participant was selected for statistical analyses, for a significant correlation at 0.01 level of major parameters concerned in the study between the two eyes was detected in 30 randomly selected participants using spearman's analysis, including SE, AL, PPA, ReT, ChT, and SST.

Assessment of Fundus Tessellation, Tilted Disc (TD), and Parapapillary Atrophy Area (PPA)

The diagnostic and degree of fundus tessellation was assessed on the 45° fundus photographs centered on the macula. Retinal photographs centered on the macular and optic disc were acquired from the same SS-OCT, which was fitted with a digital, non-mydriatic retinal camera. The optic disc tilt and the PPA area were calculated from these photographs using Image J version 1.60 software (National Institutes of Health, MD, USA; http://rsb.info.nih.gov/ij/index.html) by two independent, blinded, well-trained observers (Z.H and Z.Z). Average data were used for the final analysis.

The macular area and the peripapillary area were separately analyzed using the macula photographs and the optic disc-centered photographs.

Fundus tessellations is defined by the ophthalmoscopic visualization of the large choroidal vessels. The degree of

Abbreviations: ACD, anterior chamber depth; AL, axial length; BCVA, best-corrected visual acuity; ChT, macular choroidal thickness; CI, confidence interval; TD, tilted disc; mChT, macular choroidal thickness; GCL, ganglion cell layer; mReT, macular retinal thickness; mRNFLT, macular retinal nerve fiber layer thickness; OR, odds ratio; pChT, peripapillary choroidal thickness; pGCLT, peripapillary ganglion cell layer thickness; PPA, parapapillary atrophy; pReT, peripapillary retinal thickness; pRNFLT, peripapillary retinal nerve fiber layer thickness; SE, spherical equivalent; Ref, reference; SBP, systolic blood pressure; SST, subfoveal scleral thickness.

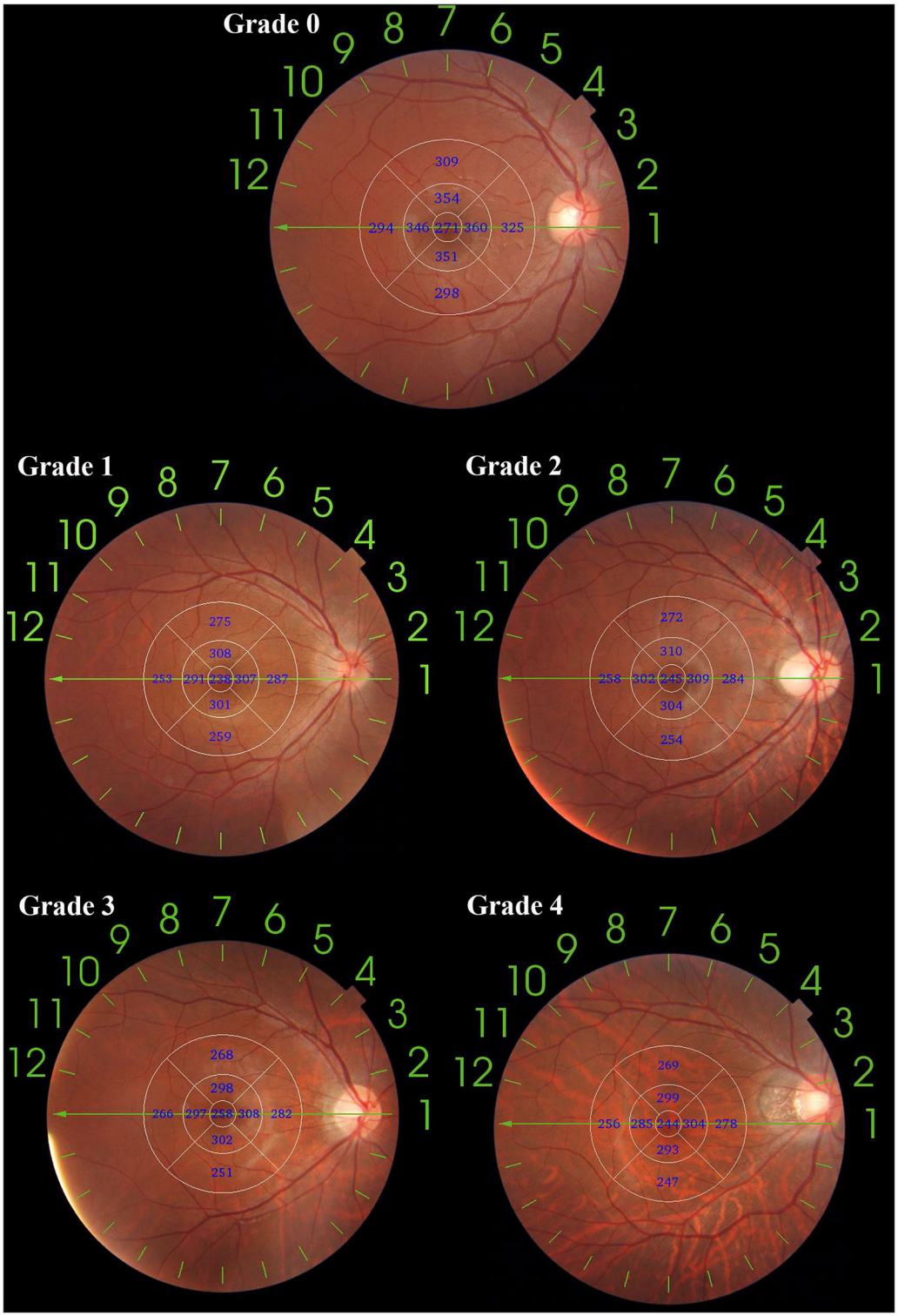

FIGURE 1 | An application of ETDRS grid on fundus tessellation grading. The diameter of center, inner and outer circle are 1, 3, and 6 mm. Eyes with no fundus tessellation were graded as Grade 0; eyes with fundus tessellation without involving the outer circle were graded as Grade 1; eyes with fundus tessellation involving the outer circle of were graded as Grade 2; eyes with fundus tessellation involving the inner circle were graded as Grade 3; eyes with fundus tessellation involving the center circle were graded as Grade 4.

tessellated fundus was assessed by fundus photographs applying an early treatment of diabetic retinopathy study (ETDRS) grid to evaluate the relative location between fundus tessellation and the fovea, where Grade 0 is defined as no large choroidal vessels visible, Grade 1 is defined as fundus tessellations visible in the posterior pole without involving ETDRS grid, Grade 2 is defined as fundus tessellations visible in the outer circle of ETDRS grid without involving the inner circle, Grade 3 is defined as fundus tessellations visible in the inner circle of ETDRS grid without involving the fovea, and Grade 4 is defined as fundus tessellations visible in the center fovea of ETDRS grid (**Figure 1**). The fundus tessellation was assessed by a trained examiner (L.H.Y), who was regularly supervised by two experienced ophthalmologists (C.Q.Y, F.Y). To assess the reproducibility of the technique, the images of 100 eyes of 100 participants were randomly selected and graded twice by a trained grader (H.G.Y) in a masked manner at an interval of 2 weeks.

The definition of TD ratio has been previously described as the tilt ratio of minimum-to-maximum disc diameter and a tilted optic disc had a tilt ratio 0.80 or less (19). The optic disc margins, defined as the inner border of the peripapillary sclera rings were lined for measurements (20). The gamma zone peripapillary atrophy was defined as the region between optic disc border and end of Bruch's membrane in previous studies (20–22). Briefly, the area of PPA area was determined as the total number of pixels in a circumferential pattern using the Image J software. Magnification by fundus camera was × 1.4, the total magnification was calculated combined with the magnification factor of Image J system. The area of PPA was converted from pixels into square millimeters. The magnification was corrected for each AL using the Littmann's formula (23).

Swept-Source Optical Coherence Tomography (SS-OCT) Imaging

The tomography thickness map of the entire macular and disc area (6 × 6 mm) was acquired from an average of four overlapped consecutive scans using SS-OCT (model DRI OCT-1 Atlantis; Topcon), which had a lateral resolution of 10 μm and a depth resolution of 8 μm. The machine had a scanning speed of 100,000 A-scans per second with a 1,050-nm-wave length light source. The scan protocol utilized the 12-line radial scan pattern with a resolution of 1,024 × 12 centered on the fovea and optic disc.

The segmentation of each layer was automatically obtained with the built-in software. ChT was defined as the distance between the Bruch membrane and the choroid-sclera interface. Manual segmentation was performed since the automatic segmentation was inaccurate or led to measurement artifacts. The tomography maps were overlapped to an early treatment diabetic retinopathy study grid (6 × 6 mm) that was focused on the macular and optic disc. The global average thickness of the choroid, retina, ganglion cell layer (GCL), and retinal nerve fiber layer (RNFL) was calculated. The circle placement was manually adjusted, if necessary. All measurements were conducted by a single technician who was experienced in taking OCT images. Images with signal strength index ≤60 were excluded for statistical analysis. The SS-OCT was performed twice for the first 30 participants to assess measurement reproducibility.

Scleral thickness was defined as the vertical distance between the choroidal–scleral interface and the outer scleral border*. The posterior scleral border was carefully identified by an experienced technician and reconfirmed by another experienced technician before measuring the lamellar structure, continuity and high reflectivity value of the retrobulbar tissue. To ensure the reproducibility of posterior scleral border, 20 OCT images were randomly selected from the database in advance and the two experienced technicians were asked to outline the posterior scleral border and measure the SST. The intraclass correlation efficient was 0.943 ($P < 0.001$), which indicates a satisfying repeatability of the method. After testing the reproducibility, measurements were performed by two skilled observers blinded to the study. The average of these measurements was calculated and included in the analysis. If the absolute difference between the two measurements were >20 μm for the sclera, 10 μm for the choroid or 20 μm for the whole fundus, the measurements were repeated until the absolute difference was within the set limits.

Statistical Analysis

The data analyses were performed by SAS 9.3 (Statistical Analysis System, version 9.3; the SAS Institute, Cary, NC, USA). Demographic and ocular characteristics were shown as counts or proportions for categorical data, and as mean ± standard deviation for continuous data. The distribution of all variables was examined for normality using the Kolmogorov-Smirnov test. The ANOVA test was performed to detect differences in demographic and ocular parameters as well as each average layer's thickness between the four groups, as appropriate. Participants' characteristics with and without accessible scleral thickness were compared using the chi-square statistic for proportions and a t-test or Mann–Whitney U test for means or medians as appropriate, using person-specific data. AL, PPA, ReT, ChT, SST were also categorically assessed (in quartiles). Logistic regression models were then performed to investigate the relationship between the proportion of fundus tessellation with ocular and systemic parameters. Parameters with $p < 0.05$ in the partial correlation analysis were included in the multivariate models.

RESULTS

Among the 828 students enrolled in the study, 11 were excluded due to diffuse chorioretinal atrophy, nine due to other retinopathy, 12 because of IOP > 21 mmHg. Subsequently, 796 students were included in the final analysis.

The general characteristics of the 796 participants and comparison among participants with or without fundus tessellation are listed in **Table 1**. There were no significant differences in age, sex, BMI, blood pressure, intraocular pressure, anterior chamber depth and lens thickness between the two groups. Eyes with fundus tessellation diagnosis had a lower SE ($p < 0.0001$), worse BCVA ($p = 0.043$), longer AL ($p < 0.0001$), thinner retina ($p < 0.0001$), thinner choroid ($p < 0.0001$), and thinner sclera in center fovea ($p = 0.0035$). Thinner ganglion

TABLE 1 | Comparison of characteristics between participants with or without fundus tessellation*.

Variable	Without fundus tessellation	With fundus tessellation	Statistic value	*p*-value
N	78	718		
Age	19.86 ± 2.20	19.82 ± 2.66	0.014	0.905[a]
Sex (male/female)	31/47	333/385	1.248	0.264[b]
BMI (kg/m^2)	21.14 ± 3.80	20.66 ± 2.85	1.836	0.176[a]
SE	−2.94 ± 2.20	−4.32 ± 2.38	23.86	< 0.0001[a]
BCVA, logMAR	0.11 ± 0.35	0.24 ± 0.57	4.101	0.043[a]
AL	24.46 ± 1.10	25.36 ± 1.08	49.174	< 0.0001[a]
PPA	0.08 ± 0.08	0.17 ± 0.11	41.754	< 0.0001[a]
Average ReT, μm	283.54 ± 11.05	276.27 ± 11.93	26.491	< 0.0001[a]
Average ChT, μm	296.02 ± 54.37	207.60 ± 50.97	208.899	< 0.0001[a]
SST, μm	518.04 ± 37.33	465.51 ± 47.37	14.515	0.0035[a]
TD- no. (%)	29(37.66)	416(58.02)	11.70	0.001[b]

BMI, body weight index; SE, spherical equivalent; BCVA, best-corrected visual acuity; AL, axial length; PPA, parapapillary atrophy; ChT, choroidal thickness; ReT, retinal thickness; SST, subfoveal sclera thickness; TD, tilted disc.

**Numbers displayed are mean ± standard deviation.*

[a]Statistical significance was tested using ANOVA test.

[b]Statistical significance was tested using Chi-square test.

TABLE 2 | Percentages of fundus tessellation in non-myopic, low myopic, and high myopic subjects.

Grading of fundus tessellation		Non-myopia *n* (%)	Low myopia *n* (%)	High myopia *n* (%)
Normal fundus	Grade 0	31 (29.25)	36 (7.45)	11 (5.31)
Tessellated fundus		75 (70.75)	447 (92.55)	196 (94.69)
	Grade 1	9 (8.49)	46 (25.14)	6 (2.90)
	Grade 2	40 (37.74)	142 (29.40)	38 (18.36)
	Grade 3	17 (16.04)	174 (36.02)	76 (36.71)
	Grade 4	9 (8.49)	85 (17.60)	76 (36.71)
Total		106 (100)	483 (100)	207 (100)

cell layer (GCL) thickness ($p < 0.0001$), and more TD existence ($p = 0.0001$).

In this study, the definition of non-myopia was AL ≤24 mm, low myopia was AL more than 24 mm but ≤26 mm, and high myopia was AL more than 26 mm. Among the 796 right eyes included in the study, 690 eyes had myopia (86.68%), and 207 eyes had high myopia (26.01%). The percentages of different grades of fundus tessellation in non-myopic, low myopic and high myopic subjects are listed in **Table 2**. The percentage of eyes with tessellated appearance from grade 1 to grade 4 in non-myopic group, low myopic group and high myopic group were 70.75, 92.55, and 94.69%.The percentage of eyes with grade 3 or grade 4 tessellated appearance in non-myopic group, low myopic group and high myopic group were 24.53, 53.62, and 73.42%.

Comparison of systematic and ophthalmologic parameters among each degree of fundus tessellation is displayed in **Table 3**. As fundus tessellation approaches to the fovea, there is a significant decrease in BMI ($p = 0.044$), SE ($p < 0.0001$), ReT ($p < 0.0001$), ChT ($p < 0.0001$), SST ($p < 0.0001$), and a significant increase in AL ($p < 0.0001$) and PPA ($p < 0.0001$).

The topographic characteristics of choroidal layer thickness in macula and peripapillary tessellation ranging from Grade 0 to Grade 4 are shown in **Table 4**. There was a significant decrease in ChT of all 9 subregion of EDTRS grid (subfoveal, inner nasal, inner superior, inner temporal, inner inferior, outer nasal, outer superior, outer temporal, outer inferior) as the proportion of fundus tessellation enlarged toward center fovea. The trend of decrease of ChT in each subregion were shown in the linear graph (**Figure 2**). The data of ChT in each subregion of each grade were then converted to a choroidal thickness map (**Figures 3**, **4**), where the value of ChT was shown in different color, with color red being the thickest to color blue the thinnest. As shown in the results of choroidal thickness map, center fovea, macular-papillary region and inferior region showed the most significant decrease in ChT as fundus tessellation enlarged.

Logistic regression analyses were used to determine the factors that were strongly associated with the increase of proportion of fundus tessellation. First, we included all the participants without considering the data of scleral thickness, the results are showed in **Table 5**. The proportion of fundus tessellation significantly increased with lower BMI($p = 0.0067$), longer AL ($p < 0.0001$), larger PPA ($p = 0.0058$), and thinner choroid ($p < 0.0001$) (**Table 4**). The data of each parameter were further divided and analyzed using interquartile range. Our results showed that for mChT, quartile 2 ($p < 0.001$; coefficient,–1.25; 95% CI, 0.19–0.43), quartile 3 ($p < 0.001$; coefficient, −2.36; 95% CI, 0.06–0.15), and quartile 4 ($p < 0.001$; coefficient, −3.49; 95% CI, 0.02–0.05) all have lower risk of enlargement of fundus tessellation toward center fovea compared with quartile 1. For AL, quartile 3 ($p = 0.0098$; Coefficient, 0.51; 95% CI, 1.13–2.44) and quartile 4 ($p = 0.0003$; Coefficient, 0.76; 95% CI, 1.41–3.24) have higher risk of enlargement of fundus tessellation compared with quartile 1. For PPA, quartile 3 ($p < 0.001$; coefficient, 1.03; 95% CI, 1.88–4.15) and quartile 4 ($p < 0.001$; coefficient, 0.84; 95% CI, 1.52–3.51) have higher risk of enlargement of fundus tessellation compared with quartile 1. While for pChT, only quartile 4 ($p < 0.001$; coefficient, −1.20; 95% CI, 0.19–0.48) showed a lower risk of enlargement of fundus tessellation compared with quartile 1.

Second, we analyzed the data of eyes where scleral thickness was measurable. Among the 796 participants, 470 scleral thickness were measurable (59.05%) with the posterior scleral border adequately visible. **Table 6** showed that for these participants, the proportion of fundus tessellation significantly increased with longer AL ($p = 0.0159$), thinner choroid ($p < 0.0001$) and thinner sclera ($p = 0.0003$).

DISCUSSION

This is the first study of a university student population-based cohort to explore factors associated with tessellated fundus

TABLE 3 | Comparisons of characteristics among eyes with different degree of fundus tessellation*.

Variable	Grade 0	Grade 1	Grade 2	Grade 3	Grade 4	*p*-value
N	78	61	220	267	170	
Age	19.86 ± 2.20	20.08 ± 2.73	19.64 ± 2.64	19.72 ± 2.44	20.12 ± 2.97	0.360[a]
Sex (male/female)	31/47	39/22	93/127	137/130	64/106	0.001[b]
BMI (kg/m^2)	21.14 ± 3.80	21.43 ± 3.69	20.54 ± 2.82	20.82 ± 2.81	20.28 ± 2.55	0.044[a]
AL, mm	24.46 ± 1.10	24.96 ± 0.91	24.95 ± 1.02	25.52 ± 1.01	25.81 ± 1.10	<0.0001[a]
SE (D)	−2.94 ± 2.20	−3.70 ± 2.14	−3.44 ± 2.16	−4.72 ± 2.29	−5.04 ± 2.47	<0.0001[a]
BCVA [logMAR (Snellen)]	0.01 ± 0.03	0.02 ± 0.04	0.02 ± 0.06	0.02 ± 0.05	0.03 ± 0.07	0.064[a]
PPA	0.08 ± 0.08	0.10 ± 0.10	0.14 ± 0.10	0.17 ± 0.10	0.22 ± 0.12	<0.0001[a]
Average ReT, μm	283.54 ± 11.05	285.16 ± 11.75	278.04 ± 11.22	274.91 ± 11.86	272.90 ± 11.12	<0.0001[a]
Average ChT, μm	296.02 ± 54.37	275.97 ± 57.35	234.02 ± 39.10	197.2– ± 35.06	165.21 ± 36.96	<0.0001[a]
SST, μm	518.04 ± 37.33	515.38 ± 34.21	478.39 ± 35.17	471.29 ± 39.46	441.70 ± 54.52	<0.0001[a]

BMI, body weight index; AL, axial length; SE, spherical equivalent; BCVA, best–corrected visual acuity; PPA, parapapillary atrophy; ChT, choroidal thickness; ReT, retinal thickness; SST, subfoveal sclera thickness.

**Numbers displayed are mean ± standard deviation.*

[a]Statistical significance was tested using ANOVA test.

[b]Statistical significance was tested using Chi–square test.

TABLE 4 | Topographical characteristics of choroidal and scleral thickness in tessellated fundus range from Grade 0 to Grade 4.

Variable	Grade 0 (*N* = 78)	Grade 1 (*N* = 61)	Grade 2 (*N* = 220)	Grade 3 (*N* = 267)	Grade 4 (*N* = 170)	Statistic value	*p*–value
Average ChT, μm	296.02±54.37	275.97±57.35	234.02±39.10	197.20±35.06	165.21±36.96	138.46	< 0.0001
Central fovea, μm	311.38±63.53	292.21±73.61	241.44±48.72	201.12±42.95	162.84±45.29	120.7	< 0.0001
Parafovea temporal, μm	317.89±68.98	298.17±63.65	258.36±50.76	219.76±45.01	181.77±45.79	98.34	< 0.0001
Perifovea temporal, μm	320.25±68.85	291.22±54.91	268.05±50.38	230.89±45.43	196.63±45.08	79.02	< 0.0001
Parafovea Superior, μm	299.57±70.52	291.04±68.03	246.57±52.07	209.65±44.35	176.28±43.70	96.34	< 0.0001
Perifovea Superior, μm	299.24±65.45	292.31±60.94	253.72±50.45	218.40±45.86	189.47±44.42	86.25	< 0.0001
Parafovea Nasal, μm	287.24±64.05	267.17±69.12	213.80±42.61	175.60±38.94	141.53±40.01	194.06	< 0.0001
Perifovea Nasal, μm	240.38±54.60	219.30±57.17	167.01±36.42	135.82±33.73	109.37±34.43	211.62	< 0.0001
Parafovea Inferior, μm	321.03±63.05	295.29±77.66	246.62±46.00	203.64±40.08	164.21±44.27	196.01	< 0.0001
Perifovea Inferior, μm	184.56±47.75	166.68±43.41	126.95±32.41	110.63±30.66	98.92±30.37	202.88	< 0.0001
SST, μm	518.04±37.33	515.38±34.21	478.39±35.17	471.29±39.46	441.70±54.52	24.73	< 0.0001

ChT, choroidal thickness; SST, subfoveal sclera thickness.

and its relative location with the fovea. In this study, we used a novel grading method to assess the severity of fundus tessellation, where the relative location between center fovea and the occurrence of fundus tessellation were taken into account. Compared with former studies which graded fundus tessellation severity by the visibility of large choroidal vessels in fundus photographs, this novel grading method has a clear standard by using ETDRS grid to determine the scope of fundus tessellation, thus can be more objective and practical in clinical practice (11, 12). The results of this study showed that the thicknesses of choroidal and scleral layers were significantly decreased, AL and PPA increased during the occurrence and enlargement of fundus tessellation toward center fovea. The thickness of retinal layer was also decreased in tessellated fundus compared to normal fundus, however, in the logistic regression analysis, the thinning of ReT was not a risk factor for the progression of fundus tessellation. In previous studies, the relationship between ReT and myopia remains controversial. Jin et al. studied the ReT in children with different refractive status and their results showed that myopic Chinese children have a thinner retina in the superior and inferior perifoveal regions than do their emmetropic and hyperopic counterparts (24). Jonas et al. studied the relationship of ReT and AL in 1,117 individuals with a mean age of 64.2 ± 9.7 years, their results showed that myopic axial globe elongation was associated with retinal thinning in the equatorial and pre-equatorial region, while foveal ReT was mostly unaffected by AL (25). Zhou et al. found that RNFL thicknesses were significantly thinner in high myopia compared to low myopia, except for the temporal quadrant (26). However, there is other study found no statistical different in the ReT between high myopia and normal population (27). Further investigation in ReT in subdivision of its location and layer are needed to reveal its relationship with fundus tessellation or other myopic retinopathy.

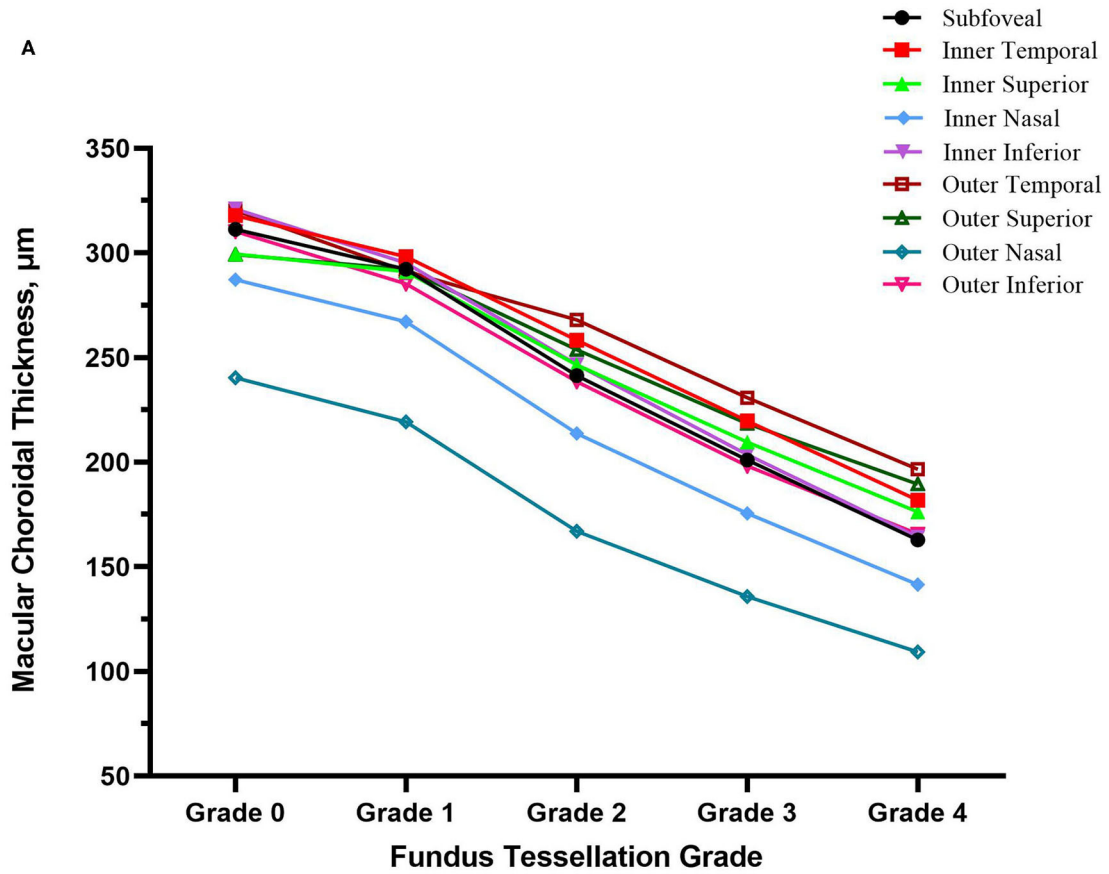

FIGURE 2 | The decrease trend of choroidal thickness in nine subregion of ETDRS grid (subfoveal, inner nasal, inner superior, inner temporal, inner inferior, outer nasal, outer superior, outer temporal, outer inferior) as fundus tessellation approaches to center fovea.

The results also showed a pattern of distribution in the decrease of ChT with higher degree of fundus tessellation, where the central fovea and the area between central fovea and optic disc showed the most significant decrease in ChT. The AL, choroidal and scleral thicknesses were independently related to macular fundus tessellation and its severity, while area of PPA and TD in addition to AL, choroidal and scleral thicknesses were independently associated with peripapillary fundus tessellation and its severity. Our results also showed that BMI could be a protective factor for the enlargement of fundus tessellation. We speculate that it can be associated with the tissular support effect and its function in preventing the deformation of the globe, yet further investigation with MRI is needed.

The results of the present study were in agreement with previous studies that reported a decrease in ChT with the progression of fundus tessellation and pathological myopia. Yan et al. (12) studied 3,468 participants with an average age of 64.4 years, and found that subfoveal ChT and AL had the strongest association with a higher degree of fundus tessellation. As compared to their data, our participants had similar ChT in grade 0 and grade 1 groups. However, the mean central foveal ChT of grade 2 and grade 3 in this study were 165 μm and 152 μm 152 μm as compared to 122 μm in grade 2 and 81 μm in grade 3 in the elderly people. might be due to age-related differences, as ChT is strongly age-related (14–17). Moreover, we noticed a pattern of ChT distribution where ChT in temporal areas was significantly thicker than that of the nasal areas, which is consistent with prior studies (12, 27, 28). The ChT in center fovea and the region between center fovea and optic disc showed the most significant decrease in ChT among all subfields of macular and peripapillary regions, which was consistent with a previous study on distribution pattern of ChT in Chinese children with myopia (29). We observed that the decrease in ChT became more significant with the progression of fundus tessellation.

Due to the limitations of technology and devices, the relationship between scleral thickness and myopia has not been extensively studied. In previous studies, Deng et al. (30) indicated that hyperopic and emmetropic children had thicker sclera than myopic children. In adults, previously reported rates of detection for the posterior scleral border with SS-OCT ranged from 53 to 84.7%, and the posterior scleral border was better seen as the AL increased (31–33). Our results showed a relevance ratio of 59.05% among university students, and indicated that eyes with fundus tessellation have a thinner SST than eyes with normal fundal appearance. Our results also showed that SST decreased significantly when fundus tessellation approaches to center fovea.

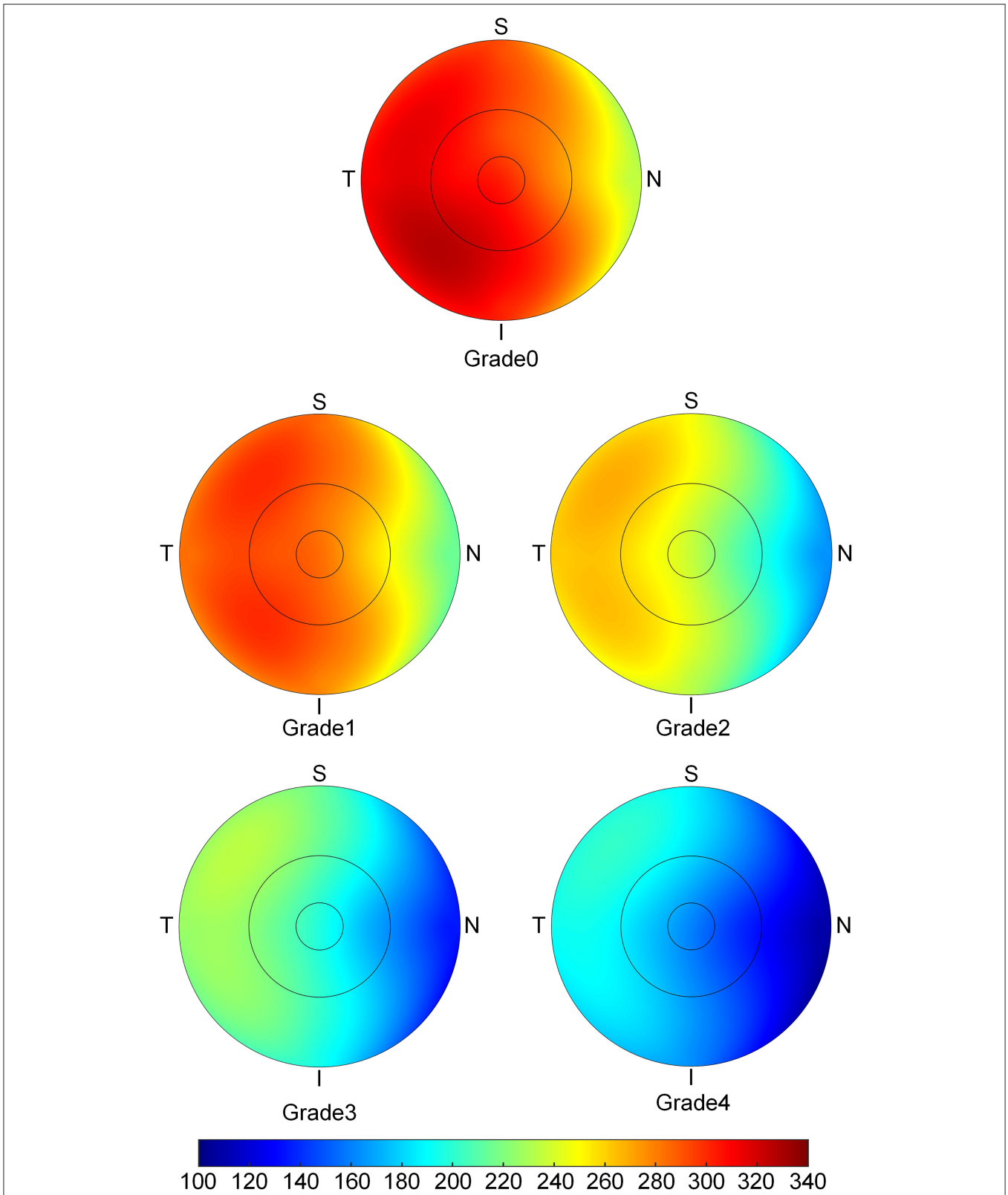

FIGURE 3 | The topographic characteristics of choroidal layer thickness in ETDRS grid centered in fovea, from Grade 0 to Grade 4. The value of choroidal thickness was shown in different color, with color red being the thickest to color blue the thinnest.

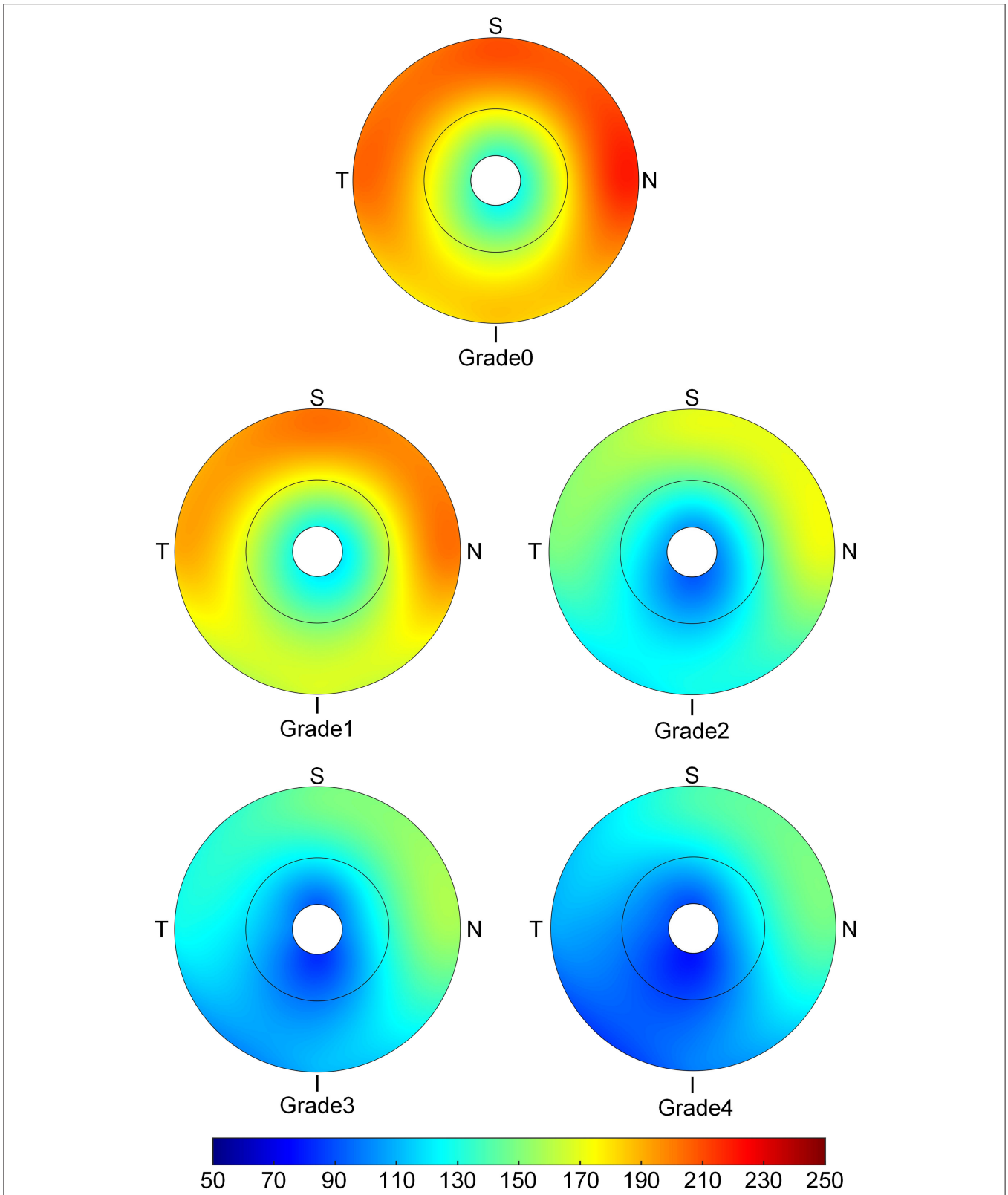

FIGURE 4 | The topographic characteristics of choroidal layer thickness in ETDRS grid centered in optic disc range from Grade 0 to Grade 4. The value of choroidal thickness was shown in different color, with color red as the thickest to color blue the thinnest.

TABLE 5 | Associations of fundus tessellation severity with ocular and systemic parameters.

Parameters	Regression coefficient		*P*-value	OR (95% CI)
Gender		−0.1629	0.2814	0.85 (0.63, 1.14)
BMI		−0.0684	0.0067	0.93 (0.89, 0.98)
	Normal weight to underweight	−0.0688	0.6910	0.93 (0.67, 1.31)
	Overweight to underweight	−0.3552	0.1188	0.70 (0.45, 1.10)
AL		0.3002	< 0.0001	1.35 (1.17, 1.55)
	Quartile 2 to Quartile 1	0.2874	0.1355	1.33 (0.91, 1.94)
	Quartile 3 to Quartile 1	0.5074	0.0098	1.66 (1.13, 2.44)
	Quartile 4 to Quartile 1	0.7603	0.0003	2.14 (1.41, 3.24)
mChT		−0.0268	< 0.0001	0.97 (0.97, 0.98)
	Quartile 2 to Quartile 1	−1.2524	< 0.0001	0.29 (0.19, 0.43)
	Quartile 3 to Quartile 1	−2.3576	< 0.0001	0.09 (0.06, 0.15)
	Quartile 4 to Quartile 1	−3.4937	< 0.0001	0.03 (0.02, 0.05)
mReT		−0.00957	0.1222	0.99 (0.98, 1.00)
	Quartile 2 to Quartile 1	0.1839	0.3512	1.20 (0.82, 1.77)
	Quartile 3 to Quartile 1	−0.2876	0.1440	0.75 (0.51, 1.10)
	Quartile 4 to Quartile 1	−0.2556	0.2117	0.77 (0.52, 1.16)
pChT		−0.00537	0.0228	0.99 (0.99, 1.00)
	Quartile 2 to Quartile 1	−0.3092	0.1352	0.73 (0.49, 1.10)
	Quartile 3 to Quartile 1	−0.1566	0.4770	0.86 (0.56, 1.32)
	Quartile 4 to Quartile 1	−1.1988	< 0.0001	0.30 (0.19, 0.48)
PPA		1.9647	0.0058	7.13 (1.76, 28.84)
	Quartile 2 to Quartile 1	0.2273	0.2393	1.26 (0.86, 1.83)
	Quartile 3 to Quartile 1	1.0275	< 0.0001	2.79 (1.88, 4.15)
	Quartile 4 to Quartile 1	0.8377	< 0.0001	2.31 (1.52, 3.51)

BMI, body weight index; AL, axial length; mChT, macular choroidal thickness; mReT, macular retinal thickness; pChT, peripapillary choroidal thickness; PPA, peripapillary atrophy.

Parapapillary gamma zone atrophy is characterized by the absence of Bruch's membrane, retinal pigment epithelium, retinal deep layers and loss of choroicapillars (20–22). PPA is well-established in primary open-angle glaucoma (POAG) and its significance in progression of glaucomatous damage and visual field loss have been confirmed. Its association with myopia is a research hotspot. Several studies found that the area of PPA was strongly associated with longer AL, myopic refraction and tilted optic disc. An increase in AL and decrease in ChT might lead to a decrease in choroidal perfusion and eventually lead to atrophy of choroicapillars (34–36). Our study found that area of parapapillary gamma zone atrophy was strongly associated with fundus tessellation and its enlargement of proportion toward center fovea.

This study investigated optical parameters and changes in thickness of retina, choroid and sclera in the occurrence and increase of fundus tessellation proportion in young adults. The distribution of the decrease in ChT may refer to the deformation of globe and staphyloma formation, which can be further studied by MRI. This study also achieved a relatively high relevance ratio of scleral thickness measurement and observed a strong association between thinner sclera and higher degree of fundus tessellation, which offers certain clues about the mechanism of formation during myopic retinopathy. In this study, we can also found fundus tessellation in non-myopic (A L$\leq$ 24) eyes, of which 75.47% are peripheral fundus tessellation (Grade0-2), while in high myopia (AL > 26), the ratio of fundus tessellation near center fovea (grade3-4) was 73.43%. This information indicate that fundus tessellation that involve center fovea could be more significative in further study of myopic retinopathy.

TABLE 6 | Associations of fundus tessellation severity with ocular and systemic parameters with scleral thickness.

Parameters	Regression coefficient	*P*-value	OR (95% CI)
Gender	0.0791	0.6931	1.08 (0.73, 1.60)
BMI	−0.0477	0.1420	0.95 (0.89, 1.02)
AL	0.3003	0.0015	1.35 (1.12, 1.62)
PPA	1.2140	0.1817	3.37 (0.57, 20.00)
mChT	−0.0306	< 0.0001	0.97 (0.96, 0.98)
mReT	−0.00945	0.2615	0.99 (0.97, 1.01)
pChT	−0.00107	0.7393	1.00 (0.99, 1.01)

BMI, body weight index; AL, axial length; mChT, macular choroidal thickness; mReT, macular retinal thickness; pChT, peripapillary choroidal thickness; PPA, peripapillary atrophy.

This study had several limitations. First, since this study exclusively included university students as participants, the results may not represent the general population of all young adults. Second, the novel grading method for tessellated fundus still has subjective element as the relative location of fundus

tessellation was determined by the examiner using ETDRS grid instead of a total objective quantitative method. Third, the SST was only measured when the posterior scleral border was clear, which means a greater loss of data in grade 0 and grade 1 tessellated fundus due to thicker choroidal and scleral layers. Due to incomplete data in eyes with unclear scleral borders, we may have underestimated the value of scleral thickness in emmetropia and low myopia participants, however, our results reveal an important tendency that SST decreased significantly with the progression of tessellated fundus.

In summary, this study suggested that BMI, AL, PPA, choroidal, and scleral thicknesses were closely correlated with fundus tessellation in Chinese young adults. Choroidal thinning may progress faster in the region between central fovea and optic disc as the fundus tessellation evolves to more severe complications of pathological myopia. The PPA and TD may play an important role in the evolvement of pathological myopia. The relative location between fundus tessellation and center fovea could be an ideal standard to assess the severity of fundus tessellation and those who has fundus tessellation involving center fovea (Grade 4) should be closely supervised as they showed the most severe myopic morphological alternations and may have more risks to progress into more severe myopic maculopathy. Tessellated fundus is the first stage of fundus changes during myopic maculopathy, whereby some patients will progress from diffuse atrophy to macular atrophy that causes severe and irreversible impairment to visual acuity, while others could remain stable at this stage forever. Thus, we will continue with follow-up visits of our participants, and further investigation of the progression of tessellated fundus and more severe impairment.

DATA AVAILABILITY STATEMENT

The raw data supporting the conclusions of this article will be made available by the authors, without undue reservation.

ETHICS STATEMENT

This cross-sectional population-based study was approved by the ethics committee of Shanghai General Hospital, Shanghai Jiao Tong University, Shanghai, China, and followed the tenets of the Declaration of Helsinki. All participants understood the study protocol and provided signed informed consents.

AUTHOR CONTRIBUTIONS

HL have made substantial contributions to the conception or design of the work and the acquisition, analysis, or interpretation of data for the work. QC have made contributions to the acquisition of data and the supervision of the analysis of the data. GH have made contributions to the acquisition of data and data processing work. YS and LY have made contributions to the revise work of this article. YY have made contributions to the acquisition of data and technical support. YF have made contributions to the supervision of the analysis of the data. HZ have made contributions to the supervision of the analysis of data and the writing. JH, JZ, and XX have made contributions to the supervision of the article writing and approved the final version to be published. All authors contributed to the article and approved the submitted version.

FUNDING

This study was funded by the by the Chinese National Nature Science Foundation (Grant no.81703287, Beijing, China), the Shanghai Three Year Public Health Action Program (Project no. GWIV-13.1, Shanghai, China), the Shanghai Science and Technology Commission Research Project (Project no.17ZR1426900, Shanghai, China), the Shanghai Municipal Planning Commission of science and Research Fund (Project no. 201640090, Shanghai, China), Shanghai Public Health System Three-Year Plan Personnel Construction Subjects (GWV-10.2-YQ40). The sponsor or funding organization had no role in the design or conduct of this research.

REFERENCES

1. Holden BA, Fricke TR, Wilson DA, Jong M, Naidoo KS, Sankaridurg P, et al. Global prevalence of myopia and high myopia and temporal trends from 2000 through 2050. *Ophthalmology.* (2016) 123:1036–42. doi: 10.1016/j.ophtha.2016.01.006
2. Morgan IG, Ohno-Matsui K, Saw SM. Myopia. *Lancet.* (2012) 379:1739–48. doi: 10.1016/S0140-6736(12)60272-4
3. Sawada A, Tomidokoro A, Araie M, Iwase A, Yamamoto T. Refractive errors in an elderly Japanese population: the Tajimi study. *Ophthalmology.* (2008) 115:363–70.e3. doi: 10.1016/j.ophtha.2007.03.075
4. Wong TY, Foster PJ, Hee J, Ng TP, Tielsch JM, Chew SJ, et al. Prevalence and risk factors for refractive errors in adult Chinese in Singapore. *Invest Ophthalmol Vis Sci.* (2000) 41:2486–94.
5. Fricke TR, Jong M, Naidoo KS, Sankaridurg P, Naduvilath TJ, Ho SM, et al. Global prevalence of visual impairment associated with myopic macular degeneration and temporal trends from 2000 through 2050: systematic review, meta-analysis and modelling. *Br J Ophthalmol.* (2018) 102:855–62. doi: 10.1136/bjophthalmol-2017-311266
6. Ohno-Matsui K, Lai TY, Lai CC, Cheung CM. Updates of pathologic myopia. *Prog Retin Eye Res.* (2016) 52:156–87. doi: 10.1016/j.preteyeres.2015.12.001
7. Delcourt C, Le Goff M, von Hanno T, Mirshahi A, Khawaja AP, Verhoeven VJM, et al. The decreasing prevalence of nonrefractive visual impairment in older europeans: a meta-analysis of published and unpublished data. *Ophthalmology.* (2018) 125:1149–59. doi: 10.1016/j.ophtha.2018.02.005
8. Morgan IG, French AN, Ashby RS, Guo X, Ding X, He M, et al. The epidemics of myopia: aetiology and prevention. *Prog Retin Eye Res.* (2018) 62:134–49. doi: 10.1016/j.preteyeres.2017.09.004
9. Ohno-Matsui K, Kawasaki R, Jonas JB, Cheung CM, Saw SM, Verhoeven VJ, et al. International photographic classification and grading system for myopic maculopathy. *Am J Ophthalmol.* (2015) 159:877–83.e7. doi: 10.1016/j.ajo.2015.01.022
10. Jonas JB, Gründler A. Optic disc morphology in "age-related atrophic glaucoma". *Graefes Arch Clin Exp Ophthalmol.* (1996) 234:744–9. doi: 10.1007/BF00189355
11. Yan YN, Wang YX, Yang Y, Xu L, Xu J, Wang Q, et al. Ten-year progression of myopic maculopathy: the beijing eye study 2001-2011. *Ophthalmology.* (2018) 125:1253–63. doi: 10.1016/j.ophtha.2018.01.035

12. Yan YN, Wang YX, Xu L, Xu J, Wei WB, Jonas JB. Fundus tessellation: prevalence and associated factors: the beijing eye study 2011. *Ophthalmology.* (2015) 122:1873–80. doi: 10.1016/j.ophtha.2015.05.031
13. Jin P, Zou H, Xu X, Chang TC, Zhu J, Deng J, et al. Longitudinal changes in choroidal and retinal thicknesses in children with myopic shift. *Retina.* (2019) 39:1091–9. doi: 10.1097/IAE.0000000000002090
14. Spaide RF. Age-related choroidal atrophy. *Am J Ophthalmol.* (2009) 147:801–10. doi: 10.1016/j.ajo.2008.12.010
15. Switzer DW Jr, Mendonça LS, Saito M, Zweifel SA, Spaide RF. Segregation of ophthalmoscopic characteristics according to choroidal thickness in patients with early age-related macular degeneration. *Retina.* (2012) 32:1265–71. doi: 10.1097/IAE.0b013e31824453ac
16. Warrow DJ, Hoang QV, Freund KB. Pachychoroid pigment epitheliopathy. *Retina.* (2013) 33:1659–72. doi: 10.1097/IAE.0b013e3182953df4
17. Yoshihara N, Yamashita T, Ohno-Matsui K, Sakamoto T. Objective analyses of tessellated fundi and significant correlation between degree of tessellation and choroidal thickness in healthy eyes. *PLoS ONE.* (2014) 9:e103586. doi: 10.1371/journal.pone.0103586
18. He J, Chen Q, Yin Y, Zhou H, Fan Y, Zhu J, et al. Association between retinal microvasculature and optic disc alterations in high myopia. *Eye (Lond).* (2019) 33:1494–503. doi: 10.1038/s41433-019-0438-7
19. Jonas JB, Jonas SB, Jonas RA, Holbach L, Dai Y, Sun X, et al. Parapapillary atrophy: histological gamma zone and delta zone. *PLoS ONE.* (2012) 7:e47237. doi: 10.1371/journal.pone.0047237
20. Dai Y, Jonas JB, Huang H, Wang M, Sun X. Microstructure of parapapillary atrophy: beta zone and gamma zone. *Invest Ophthalmol Vis Sci.* (2013) 54:2013–8. doi: 10.1167/iovs.12-11255
21. Kim M, Kim TW, Weinreb RN, Lee EJ. Differentiation of parapapillary atrophy using spectral-domain optical coherence tomography. *Ophthalmology.* (2013) 120:1790–7. doi: 10.1016/j.ophtha.2013.02.011
22. Chen Q, He J, Yin Y, Zhou H, Jiang H, Zhu J, et al. Impact of the morphologic characteristics of optic disc on choroidal thickness in young myopic patients. *Invest Ophthalmol Vis Sci.* (2019) 60:2958–67. doi: 10.1167/iovs.18-26393
23. Bennett AG, Rudnicka AR, Edgar DF. Improvements on Littmann's method of determining the size of retinal features by fundus photography. *Graefes Arch Clin Exp Ophthalmol.* (1994) 232:361–7. doi: 10.1007/BF00175988
24. Jin P, Zou H, Zhu J, Xu X, Jin J, Chang TC, et al. Choroidal and retinal thickness in children with different refractive status measured by swept-source optical coherence tomography. *Am J Ophthalmol.* (2016) 168:164–76. doi: 10.1016/j.ajo.2016.05.008
25. Jonas JB, Xu L, Wei WB, Pan Z, Yang H, Holbach L, et al. Retinal thickness and axial length. *Invest Ophthalmol Vis Sci.* (2016) 57:1791–7. doi: 10.1167/iovs.15-18529
26. Seo S, Lee CE, Jeong JH, Park KH, Kim DM, Jeoung JW. Ganglion cell-inner plexiform layer and retinal nerve fiber layer thickness according to myopia and optic disc area: a quantitative and three-dimensional analysis. *BMC Ophthalmol.* (2017) 17:22. doi: 10.1186/s12886-017-0419-1
27. Zhou Y, Song M, Zhou M, Liu Y, Wang F, Sun X. Choroidal and retinal thickness of highly myopic eyes with early stage of myopic chorioretinopathy: tessellation. *J Ophthalmol.* (2018) 2018:2181602. doi: 10.1155/2018/2181602
28. Ikuno Y, Tano Y. Retinal and choroidal biometry in highly myopic eyes with spectral-domain optical coherence tomography. *Invest Ophthalmol Vis Sci.* (2009) 50:3876–80. doi: 10.1167/iovs.08-3325
29. Bidaut-Garnier M, Schwartz C, Puyraveau M, Montard M, Delbosc B, Saleh M. Choroidal thickness measurement in children using optical coherence tomography. *Retina.* (2014) 34:768–74. doi: 10.1097/IAE.0b013e3182a487a4
30. Deng J, Jin J, Lv M, Jiang W, Sun S, Yao C, et al. Distribution of scleral thickness and associated factors in 810 Chinese children and adolescents: a swept-source optical coherence tomography study. *Acta Ophthalmol.* (2019) 97:e410–8. doi: 10.1111/aos.13788
31. Park HY, Shin HY, Park CK. Imaging the posterior segment of the eye using swept-source optical coherence tomography in myopic glaucoma eyes: comparison with enhanced-depth imaging[J]. *Am J Ophthal.* (2014) 157:550–7. doi: 10.1016/j.ajo.2013.11.008
32. Lopilly Park HY, Lee NY, Choi JA, Park CK. Measurement of scleral thickness using swept-source optical coherence tomography in patients with open-angle glaucoma and myopia[J]. *Am J Ophthal.* (2014) 157:876–84. doi: 10.1016/j.ajo.2014.01.007
33. Wong CW, Phua V, Lee SY, Wong TY, Cheung CM. Is choroidal or scleral thickness related to myopic macular degeneration? *Invest Ophthalmol Vis Sci.* (2017) 58:907–13. doi: 10.1167/iovs.16-20742
34. Hirata M, Tsujikawa A, Matsumoto A, Hangai M, Ooto S, Yamashiro K, et al. Macular choroidal thickness and volume in normal subjects measured by swept-source optical coherence tomography. *Invest Ophthalmol Vis Sci.* (2011) 52:4971–8. doi: 10.1167/iovs.11-7729
35. Guo Y, Liu LJ, Tang P, Feng Y, Lv YY, Wu M, et al. Parapapillary gamma zone and progression of myopia in school children: the beijing children eye study. *Invest Ophthalmol Vis Sci.* (2018) 59:1609–16. doi: 10.1167/iovs.17-21665
36. Jonas JB, Fang Y, Weber P, Ohno-Matsui K. Parapapillary gamma and delta zones in high myopia. *Retina.* (2018) 38:931–8. doi: 10.1097/IAE.0000000000001650

Conflict of Interest: The authors declare that the research was conducted in the absence of any commercial or financial relationships that could be construed as a potential conflict of interest.

frontiers in Medicine

ORIGINAL RESEARCH
published: 29 April 2021
doi: 10.3389/fmed.2021.657566

Imaging Features by Machine Learning for Quantification of Optic Disc Changes and Impact on Choroidal Thickness in Young Myopic Patients

Dandan Sun[1,2,3,4,5,6†], *Yuchen Du*[7†], *Qiuying Chen*[1,2,3,4,5,6†], *Luyao Ye*[1,2,3,4,5,6], *Huai Chen*[7], *Menghan Li*[1,2,3,4,5,6], *Jiangnan He*[1,2,3,4,5,6], *Jianfeng Zhu*[1,2,3,4,5,6], *Lisheng Wang*[7], *Ying Fan*[1,2,3,4,5,6*] *and Xun Xu*[1,2,3,4,5,6*]

[1] Department of Ophthalmology, Shanghai General Hospital, Shanghai Jiao Tong University School of Medicine, Shanghai, China, [2] National Clinical Research Center for Eye Diseases, Shanghai, China, [3] Shanghai Key Laboratory of Ocular Fundus Disease, Shanghai, China, [4] Shanghai Engineering Center for Visual Science and Photo Medicine, Shanghai, China, [5] Shanghai Engineering Center for Precise Diagnosis and Treatment of Eye Diseases, Shanghai, China, [6] Department of Preventative Ophthalmology, Shanghai Eye Disease Prevention and Treatment Center, Shanghai Eye Hospital, Shanghai, China, [7] Department of Automation, Institute of Image Processing and Pattern Recognition, Shanghai Jiao Tong University, Shanghai, China

OPEN ACCESS

Edited by:
Xiangjia Zhu,
Fudan University, China

Reviewed by:
Teresa Rolle,
University of Turin, Italy
Saif Aldeen AlRyalat,
The University of Jordan, Jordan

***Correspondence:**
Ying Fan
mdfanying@sjtu.edu.cn
Xun Xu
drxuxun@sjtu.edu.cn

[†]*These authors have contributed equally to this work*

Specialty section:
This article was submitted to Ophthalmology, a section of the journal Frontiers in Medicine

Received: *23 January 2021*
Accepted: *01 April 2021*
Published: *29 April 2021*

Citation:
Sun D, Du Y, Chen Q, Ye L, Chen H, Li M, He J, Zhu J, Wang L, Fan Y and Xu X (2021) Imaging Features by Machine Learning for Quantification of Optic Disc Changes and Impact on Choroidal Thickness in Young Myopic Patients. Front. Med. 8:657566. doi: 10.3389/fmed.2021.657566

Purpose: To construct quantifiable models of imaging features by machine learning describing early changes of optic disc and peripapillary region, and to explore their performance as early indicators for choroidal thickness (ChT) in young myopic patients.

Methods: Eight hundred and ninety six subjects were enrolled. Imaging features were extracted from fundus photographs. Macular ChT (mChT) and peripapillary ChT (pChT) were measured on swept-source optical coherence tomography scans. All participants were divided randomly into training (70%) and test (30%) sets. Imaging features correlated with ChT were selected by LASSO regression and combined into new indicators of optic disc (IODs) for mChT (IOD_mChT) and for pChT (IOD_pChT) by multivariate regression models in the training set. The performance of IODs was evaluated in the test set.

Results: A significant correlation between IOD_mChT and mChT ($r = 0.650$, $R^2 = 0.423$, $P < 0.001$) was found in the test set. IOD_mChT was negatively associated with axial length (AL) ($r = -0.562$, $P < 0.001$) and peripapillary atrophy (PPA) area ($r = -0.738$, $P < 0.001$) and positively associated with ovality index ($r = 0.503$, $P < 0.001$) and torsion angle ($r = 0.242$, $P < 0.001$) in the test set. Every $1 \times 10\,\mu m$ decrease in IOD_mChT was associated with an $8.87\,\mu m$ decrease in mChT. A significant correlation between IOD_pChT and pChT ($r = 0.576$, $R^2 = 0.331$, $P < 0.001$) was found in the test set. IOD_pChT was negatively associated with AL ($r = -0.478$, $P < 0.001$) and PPA area ($r = -0.651$, $P < 0.001$) and positively associated with ovality index ($r = 0.285$, $P < 0.001$) and torsion angle ($r = 0.180$, $P < 0.001$) in the test set. Every $1 \times 10\,\mu m$ decrease in IOD_pChT was associated with a $9.64\,\mu m$ decrease in pChT.

Conclusions: The study introduced a machine learning approach to acquire imaging information of early changes of optic disc and peripapillary region and constructed quantitative models significantly correlated with choroidal thickness. The objective models from fundus photographs represented a new approach that offset limitations of human annotation and could be applied in other areas of fundus diseases.

Keywords: myopia, machine learning, radiomics, optic disc, choroidal thickness

INTRODUCTION

Myopia is one of the major causes of visual impairment, of which the prevalence has been increasing worldwide in recent decades (1–3). East Asia bears a high incidence of myopic maculopathy in absolute terms (4, 5). The dramatically increasing prevalence makes it urgent to commence early control of myopia in China (6).

The progression of myopia is accompanied by various characteristic changes of optic disc and peripapillary region. With the elongation of axial length (AL), optic disc tilt and torsion appear in the beginning due to the oblique orientation of the vertical axis (7–9). With further development, characteristic features in the temporal adjacent area appear, including peripapillary atrophy (PPA), a crescent-shaped atrophic chorioretinal abnormality, and increasing disc fovea distance (10–13). In addition, the onset of chorioretinal atrophy, which leads to a gradual decrease of choroidal thickness (ChT), has become a common concern in predicting the progression of high myopia and pathological myopia. Subfoveal ChT correlated positively with visual acuity and negatively with axial elongation in mild myopia in a cohort study aged from 14 to 65 years (14). In highly myopic eyes without macular pathology, mean macular ChT (mChT) and peripapillary ChT (pChT) are important predictive factors of visual acuity (15, 16). Moreover, subfoveal ChT is an independent predictor for myopic maculopathy progression in high myopes in a recent 2-year longitudinal study (17).

Therefore, investigation of the association between optic disc changes and ChT in myopia is necessary for mining imaging indicators of optic disc (IODs) for the progression of choroid thinning and pathological myopia. However, the subtle and complex changes of optic disc and peripapillary region in the early stage of myopia are not fully explained by a few manually measured features. It is urgent to find new objective and quantifiable methods for the thorough exploration of optic disc changes and their association with ChT.

Radiomics, as a new image processing method, aims to decompose and quantify characteristics of medical imaging and construct models for disease diagnosis based on engineered hard-coded algorithms (18, 19). For eye diseases, clinical diagnosis requires a variety of imaging examinations. Color fundus photographs provide abundant information on morphology, color and texture of fundus, which brings favorable advantages for the utility of radiomics. The imaging features of optic disc and peripapillary region in patients with myopia have not been studied to construct quantifiable models for the progression of choroid thinning and pathological myopia.

The present study decided optic disc and peripapillary region as the regions of interest (ROIs) and managed to acquire imaging features from fundus photographs for the construction of IODs, and further explored their performance as early indicators for changes of ChT in young myopic patients.

MATERIALS AND METHODS

Setting and Participants

The cross-sectional study was authorized by the Ethics committee of Shanghai General Hospital, Shanghai Jiao Tong University, Shanghai, China and followed the tenets of the Declaration of Helsinki. The subjects in this study included students attending Shanghai University in October 2018. All subjects have understood the study protocol and signed informed consent forms. The protocol was consistent with those of previous studies (20, 21).

The systolic and diastolic blood pressures of all subjects were measured and calculated by the following formula to obtain the mean arterial pressure (MAP): (SBP + 2 × DBP)/3. All subjects received comprehensive ophthalmic examinations including refractive error assessment using an autorefractor instrument (model KR-8900; Topcon, Tokyo, Japan), measurement of best-corrected visual acuity (BCVA) and intraocular pressure (IOP) (Full Auto Tonometer TX-F; Topcon), slit-lamp biomicroscope, color-fundus examination, and measurement of the thickness of choroid, retina, and nerve fiber layer using swept-source optical coherence tomography (SS-OCT; model DRI OCT-1 Atlantis; Topcon). Anterior chamber depth (ACD), and AL were measured using optical low-coherence reflectometry (Lenstar; Haag-Streit AG, Koeniz, Switzerland). Subjective refraction was performed for all subjects by a trained optometrist. The spherical equivalent refraction (SER) was defined as the sphere plus half a cylinder. The BCVA was converted into the logarithm of minimal angle resolution (logMAR). The medical history of all subjects was recorded in detail. Each participant underwent all examinations on the same day.

All enrolled participants met the inclusion criteria as follows: age between 16 and 40 years; SER $<$ 0.5 diopter (D); IOP 21 mm Hg or less; normal anterior chamber angles and normal depth of the anterior chamber; with a healthy optic nerve head without glaucomatous damage; and no peripapillary retinal nerve fiber layer thickness (pRNFLT) changes on both eyes. All subjects older than 40 years were excluded, as the incidence of glaucoma is associated with age, and the lenticular changes

from aging might have an effect on the myopic refractive error. The other exclusion criteria were as follows: a history of ocular or major systemic diseases, including congenital cataract and glaucoma, hypertension, and diabetes; a history of previous intraocular or refractive surgery; a history of glaucoma among first-degree family members; and other evidence of retinal pathology. Generally, except for the optic disc and peripapillary changes associated with myopia, all participants had no other ocular abnormalities. Only the right eye of each subject was selected for statistical analysis.

SS-OCT Imaging

All subjects underwent the examination of SS-OCT by an experienced examiner from 10:00 a.m. to 3:00 p.m. to minimize the influence of diurnal variation (22, 23). The SS-OCT machine of the present study was equipped with a light source of 1,050 μm wavelength and a scanning speed of 100,000 A-scans per second, with which a depth resolution of 8 μm and a lateral resolution of 10 μm of ocular tissue was reached. Before image taking by SS-OCT scanning, spherical power diopter, cylindrical power diopter and AL, with which the SS-OCT machine calculated the scan circle size, were input to minimize the error caused by the magnification factors associated with AL. The device operator adjusted the focus settings to the specific eye model of each participant before scanning. The scan protocol used the 12-line radial scan pattern with a resolution of 1,024 × 12 centered on the fovea and optic disc. All measurements in OCT images were acquired by a single experienced technician. The SS-OCT was performed twice for the first 30 participants to assess measurement reproducibility. Images with a signal strength index of 60 or less were excluded. The borderlines of layers were identified by the built-in software, which segmented each layer automatically. Manual adjustments were performed whenever inaccurate auto segmentation of each layer led to measurement artifacts.

The average thickness of choroid, retina, and nerve fiber layer was automatically calculated using built-in software. The topographic maps were overlapped to an Early Treatment Diabetic Retinopathy Study (ETDRS) grid (6 × 6 mm) that was focused on the macula or optic disc. In this way, each scan was divided into nine regions as follows: three concentric circles including the 1-mm diameter central circle, the 3-mm diameter inner circle, and the 6-mm diameter outer circle defined the inner ring (the area between the central circle and the inner circle) and the outer ring (the area between the inner circle and the outer circle), which were further divided into four quadrants—namely, temporal, superior, nasal, and inferior. ChT was measured as the vertical distance between the Brunch's membrane and the choroidal–scleral interface. Macular retinal thickness (mReT) was measured as the vertical distance between the internal limiting membrane (ILM) and the interface between the photoreceptor outer segments and retinal pigment epithelium. pRNFLT was measured as the vertical distance between the ILM and the interface between the nerve fiber layer and the ganglion cell layer. The average thickness of all nine sectors was calculated in the macular region. While in the peripapillary area, only four regions of the outer ring were applied because no choroidal tissue was found in the central sector and the inner ring, and the topographic maps were not reliable in these regions (20, 21).

Extraction of Imaging Feature Pool on Color Fundus Photograph

Red-free and color fundus photographs centered on the optic disc were imaged by the same SS-OCT machine with a digital, non-mydriatic retinal camera. ROIs for feature extraction were delineated as follows: the margins of optic disc and PPA were carefully marked with an in-house annotation software as shown in **Figure 1A** in random order and in a masked mode, not knowing the participants' background and medical history, as described previously (7, 20). The optic disc margin was defined as the inner border of the peripapillary scleral ring. The degree of optic disc tilt was measured by the ovality index, defined as the ratio of the shortest-longest disc diameters (**Figure 1A**) (24). Torsion angle referred to the angle between the line perpendicular to the line connecting macula and the center of optic disc and the long axis of optic disc. Inferotemporal and superonasal torsion correlated with negative and positive values (**Figure 1A**) (25). PPA margin was defined as an inner crescent of chorioretinal atrophy with good visibility of the large choroidal vessels and the sclera (13). The peripapillary region was divided into eight regions as follows: optic disc margin and two Early Treatment Diabetic Retinopathy Study (ETDRS) concentric circles including the 3-mm diameter inner circle, and the 6-mm diameter outer circle defined the inner ring (the area between the optic disc margin and the inner circle) and the outer ring (the area between the inner circle and the outer circle), which were further divided into four quadrants—temporal, superior, nasal, and inferior. The imaging features were extracted from four ROIs including the optic disc (**Figure 1B**), the inner ring (**Figure 1C**), the inner temporal region (**Figure 1D**) and the outer temporal region (**Figure 1E**), separately. Vessels were excluded for imaging feature extracting.

Radiomic features describing characteristics of morphology, color and texture were acquired with the PyRadiomics package (19) implemented under Python software (Python 3.7, Python Software Foundation, Beaverton). PyRadiomics operators were input into Python in advance. Operators employed in this study were as follows: operators for morphology including 10 2D shape features; operators for color including 19 first-order statistical features; operators for texture including 24 Gray Level Cooccurrence Matrix (GLCM) features, 16 Gray Level Run Length Matrix (GLRLM) features, 16 Gray Level Size Xone Matrix (GLSM) features, 5 Neighboring Gray Tone Difference Matrix (NGTDM) features and 14 Gray Level Dependence Matrix (GLDM) features. Original photographs were transferred into three separate channels of LAB color space prior to feature extraction as the PyRadiomics package only applied to single-channel images. Operators above extracted radiomic features of designated ROIs automatically after being provided with images and corresponding masks of ROIs. The total number of pixels was converted into square millimeters or millimeters and the magnification was corrected for AL by applying Littmann's

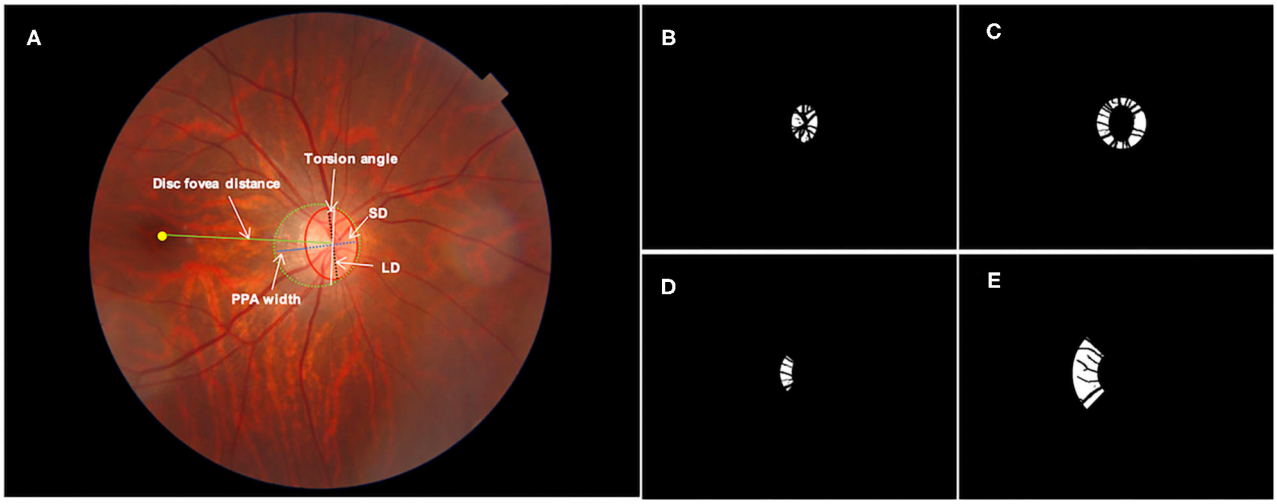

FIGURE 1 | Definition of regions of interest for imaging feature extraction: **(A)** original fundus photograph. The optic disc (red solid line), peripapillary atrophy (PPA, green dotted line) and macular fovea (yellow dot) were annotated manually. The white arrows indicate PPA width (blue solid line), disc fovea distance (green solid line), the longest diameter (LD, black dotted line) and shortest diameter (SD, blue dotted line) of the optic disc. The ovality index was defined as the ratio between the LD and SD of the optic disc. Torsion angle was measured between the LD and the vertical line (white solid line) 90° from the line connecting the fovea and the center of the optic disc. **(B)** Mask of optic disc; **(C)** mask of the inner ring; **(D)** mask of the inner temporal region and **(E)** mask of the outer temporal region. Vessels were excluded for imaging feature extracting.

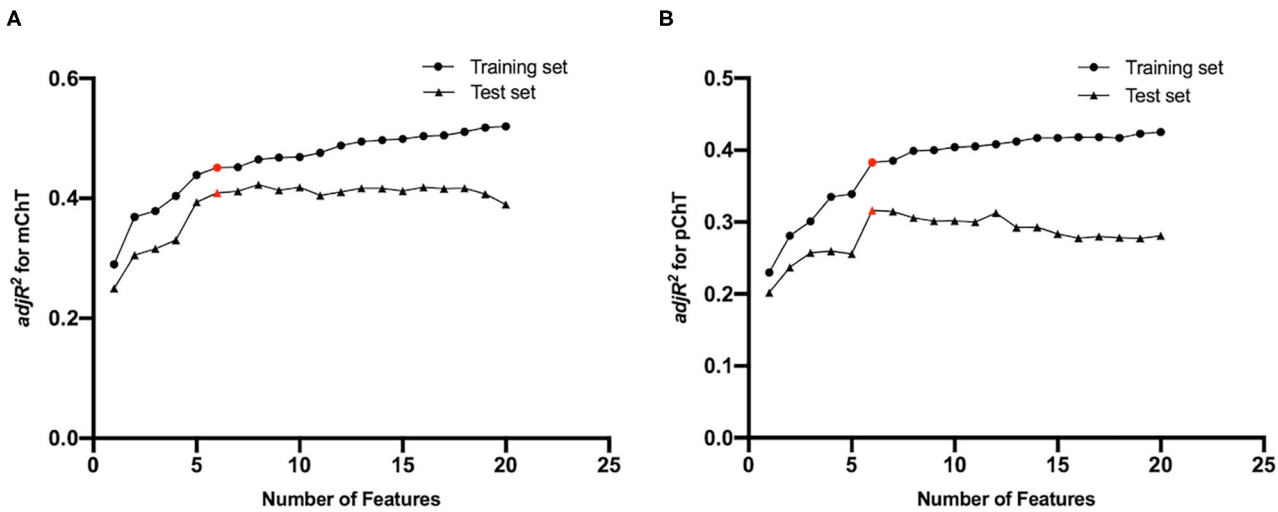

FIGURE 2 | Feature selection results by LASSO regression for **(A)** macular choroidal thickness (mChT) and **(B)** peripapillary choroidal thickness (pChT). As the number of selected features increased, adjusted coefficients of determination ($adjR^2$) in the training and test sets fluctuated. Red points represent selected feature sets.

formula (26). The package for operators above was detailed on the website (https://pyradiomics.readthedocs.io/en/latest/).

Model Construction of Imaging Indicators

All imaging features from fundus photographs were included in the final feature pool. All participants were divided into the training set (70%) and the test set (30%). LASSO regression was performed to determine the most relevant features with choroidal thickness and to exclude variables with multi-collinearity. Briefly, LASSO regression was performed in the training set. Selected features were used to constructed IODs for ChT with the multivariate regression model. Adjusted coefficients of determination ($adjR^2$) were calculated in the training and test sets separately. The models of six features were selected because $adjR^2$ was arising in both training and test sets until the number of selected features increased to six (**Figure 2**). With more features enrolled, $adjR^2$ increased slowly in the training set and decreased in the test set because of redundancy and overfitting. The IOD for mChT (IOD_mChT) were constructed with PPA width, disc fovea distance, skewness of intensity in A

channel of OT, range of intensity in L channel of IT, range of intensity in A channel of OT, range of intensity in B channel of OT. The IOD for pChT (IOD_pChT) were constructed with PPA perimeter, skewness of intensity in B channel of I, skewness of intensity in A channel of OT, range of intensity in L channel of IT, range of intensity in A channel of OT, range of intensity in B channel of OT. The definitions of imaging features were detailed on the website (https://pyradiomics.readthedocs.io/en/latest/).

Statistical Analysis

SPSS software (IBM SPSS Statistics 21; SPSS, Inc, Chicago, IL) was used for all statistical analysis. All characteristics were shown in form as means ± standard deviation for continuous data and as counts for categorical data. The distribution of all variables was examined for normality using the Kolmogorov-Smirnov test. Student's *t*-test and the χ^2 test were used to determine differences between the training and test sets.

The performance of IODs was evaluated by calculating Spearman's correlation with ChT and validated imaging features of the optic disc in the test sample. Partial correlation analysis adjusted for sex and age was performed to investigate the relationship between pChT or mChT and features of optic disc and peripapillary region. To assess the impact of optic disc changes on ChT, features with significant associations during the univariate analysis ($P < 0.05$) were included in the final multivariate regression analysis. In order to further explore the impact of IODs on ChT in people with different degrees of myopia, subjects were divided into three groups based on AL, as described previously (27, 28): AL < 24 mm, AL 24 mm to <26 mm, and AL 26 mm or more. The third group belonged to high myopia. Standardized regression coefficients and adjusted coefficients of determination ($adjR^2$) were calculated in all subjects and each group separately.

Statistical significance was set as $P < 0.05$ (two-sided).

RESULTS

General Characteristics

All participants were randomly divided into the training (70.0%) and test (30.0%) sets. The demographic and ocular characteristics of the training and test sets are shown in **Table 1**. The mean SER was −4.98 ± 3.10 D in the training set and −4.73 ± 3.05 D in the test set. The mean AL of the training and test sets were 25.52 ± 1.35 mm and 25.50 ± 1.32 mm. No significant difference was found in all ocular parameters between the training and test sets.

TABLE 1 | Demographic and ocular characteristics of the training and test sets.

	Total (*N* = 896)	Training set (N = 627)	Test set (*N* = 269)	*P*
Age, y	20.65 ± 3.04	20.80 ± 3.15	20.29 ± 2.74	0.014*
Sex, male/female	395/501	285/342	110/159	0.207
MAP, mm Hg	89.11 ± 11.11	89.38 ± 11.19	88.49 ± 10.90	0.271
IOP, mm Hg	14.00 ± 2.83	13.98 ± 2.81	14.01 ± 2.89	0.884
ACD, mm	3.60 ± 0.34	3.59 ± 0.34	3.61 ± 0.32	0.385
SER, diopter	−4.91 ± 3.08	−4.98 ± 3.10	−4.73 ± 3.05	0.266
BCVA, logMAR	0.02 ± 0.06	0.02 ± 0.05	0.03 ± 0.07	0.447
AL, mm	25.51 ± 1.34	25.52 ± 1.35	25.50 ± 1.32	0.884
PPA area, mm^2	0.68 ± 0.63	0.69 ± 0.61	0.67 ± 0.68	0.711
Ovality index	0.79 ± 0.10	0.78 ± 0.10	0.79 ± 0.09	0.226
Torsion angle, deg	4.98 ± 19.78	4.95 ± 19.87	5.06 ± 19.61	0.935
IOD_mChT, 10 μm	21.25 ± 4.21	21.19 ± 4.25	21.41 ± 4.12	0.475
IOD_pChT, 10 μm	14.34 ± 2.78	14.34 ± 2.84	14.34 ± 2.67	0.987
mChT, μm	211.00 ± 62.03	211.88 ± 63.02	208.94 ± 59.71	0.515
pChT, μm	143.33 ± 45.58	143.45 ± 45.46	143.05 ± 45.94	0.903
mReT, μm	276.01 ± 12.72	275.85 ± 13.14	276.40 ± 11.70	0.547
pRNFLT, μm	91.93 ± 10.04	91.68 ± 9.91	92.50 ± 10.33	0.268

*MAP, mean arterial pressure; IOP, intraocular pressure; ACD, anterior chamber depth; SER, spherical equivalent refraction; BCVA, best-corrected visual acuity; logMAR, logarithm of minimal angle resolution; AL, axial length; PPA, peripapillary atrophy; mChT, macular choroidal thickness; pChT, peripapillary choroidal thickness; IOD_mChT, the indicator of optic disc for mChT; IOD_pChT, the indicator of optic disc for pChT; mReT, macular retinal thickness; pRNFLT, peripapillary retinal nerve fiber layer thickness. *Significant difference.*

TABLE 2 | Correlation analysis between constructed IODs with clinical features in the test set.

	IOD_mChT, 10 μm		IOD_pChT, 10 μm	
	r	*P*	*r*	*P*
mChT, μm	0.650	< 0.001*	0.641	< 0.001*
pChT, μm	0.490	< 0.001*	0.576	< 0.001*
AL, mm	−0.562	< 0.001*	−0.478	< 0.001*
PPA area, mm^2	−0.738	< 0.001*	−0.651	< 0.001*
Ovality index	0.503	< 0.001*	0.285	< 0.001*
Torsion angle, deg	0.242	< 0.001*	0.180	0.003*

*mChT, macular choroidal thickness; pChT, peripapillary choroidal thickness; IOD_mChT, the indicator of optic disc for mChT; IOD_pChT, the indicator of optic disc for pChT; AL, axial length; PPA, peripapillary atrophy. *Significant difference.*

Performance of Imaging Indicators

To assess the performance of IODs, Spearman's correlation between IODs and clinical features associated with the progression of choroid thinning and pathological myopia was analyzed in the test set and shown in **Table 2** and Linear correlation between IODs and ChT in the test set was shown in **Figure 3.** The mean IOD_mChT of the test set was (21.41 ± 4.12) × 10 μm, whereas the average mChT of the corresponding participants was 208.94 ± 59.71 μm. A significant correlation between IOD_mChT and mChT ($r = 0.650$, $R^2 = 0.423$, $P < 0.001$) was found. Moreover, IOD_mChT was negatively associated with AL ($r = -0.562$, $P < 0.001$), and PPA area ($r = -0.738$, $P < 0.001$). IOD_mChT was positively associated with ovality index ($r = 0.503$, $P < 0.001$) and torsion angle ($r = 0.242$, $P < 0.001$). The mean IOD_pChT was (14.34 ± 2.67) × 10 μm and the mean average pChT was 143.05 ± 45.94 μm in the test set. There was also a very strong correlation between IOD_pChT and pChT ($r = 0.576$, $R^2 = 0.331$, $P < 0.001$). IOD_pChT was negatively associated with AL ($r = -0.478$, $P < 0.001$) and PPA area ($r = -0.651$, $P < 0.001$). IOD_pChT was positively associated with ovality index ($r = 0.285$, $P < 0.001$) and torsion angle ($r = 0.180$, $P = 0.003$).

The visualization of enrolled radiomic features in the models of IODs was illustrated in **Figure 4**.

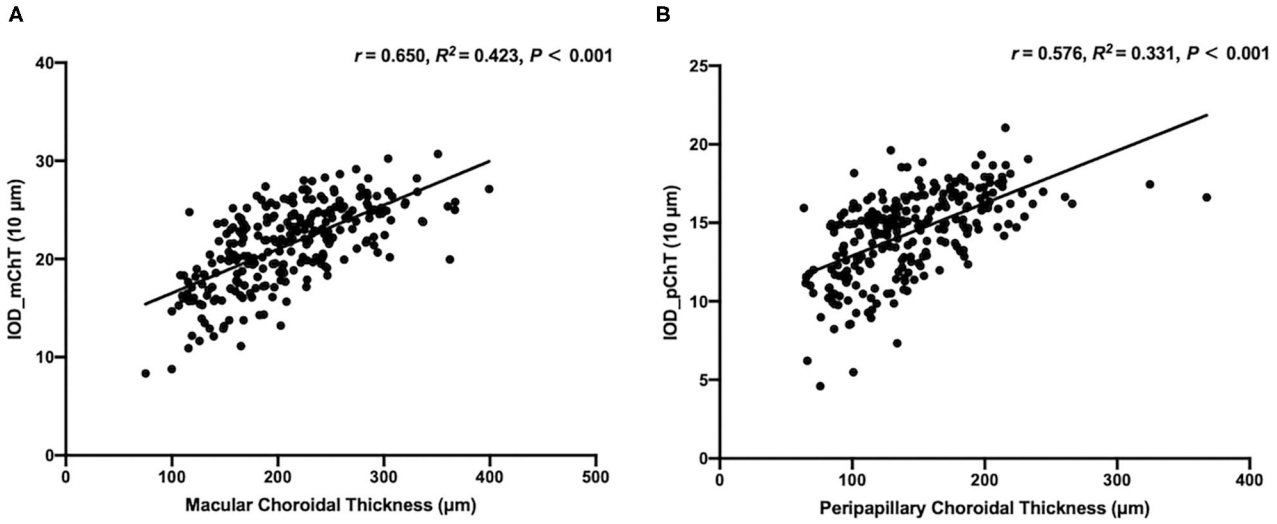

FIGURE 3 | Linear correlation between the macular choroidal thickness (mChT) and the indicator of optic disc for mChT (IOD_mChT) in the test set **(A)** and linear correlation between the peripapillary choroidal thickness (pChT) and the indicator of optic disc for pChT (IOD_pChT) in the test set **(B)**.

Correlation Between mChT and Imaging Features of Optic Disc and Peripapillary Region

Partial correlation coefficient between mChT and features of optic disc and peripapillary region after adjusting for sex and age are summarized in **Table 3**. mChT was positively associated with IOD_mChT ($r = 0.664$, $P < 0.001$), followed by SER ($r = 0.450$, $P < 0.001$), ovality index ($r = 0.332$, $P < 0.001$), and torsion angle ($r = 0.192$, $P < 0.001$). mChT was negatively associated with AL ($r = -0.497$, $P < 0.001$), PPA area ($r = -0.492$, $P < 0.001$), BCVA ($r = -0.121$, $P < 0.001$).

Multivariate regression analysis adjusted for age and sex was constructed to identify independent factors associated with mChT as shown in **Table 4**. Because the current study focused on the features of optic disc and peripapillary region, and the explanatory power of the AL was greater than that of the spherical equivalent, only variations in AL and features of optic disc were used for multivariate regression analysis. The analysis showed that sex ($P = 0.001$), AL ($P < 0.001$) and IOD_mChT ($P < 0.001$) were independently associated with mChT in all subjects. According to the model, every $1 \times 10\,\mu m$ decrease in IOD_mChT was associated with an $8.87\,\mu m$ decrease in mChT. After being stratified by myopia severity, 119 subjects belonged to the group with AL < 24 mm (13.3%), 464 subjects belonged to the group with AL 24 mm to <26 mm (51.8%), and 313 subjects belonged to the group with AL 26 mm or more (34.9%). The multivariate model showed that IOD_mChT correlated positively with mChT in all three groups (all, $P < 0.001$) while AL was only associated with mChT in the group with AL 24 mm to <26 mm ($P = 0.039$). The overall $adjR^2$ in all subjects was 0.460 and the $adjR^2$ was 0.319 for AL < 24 mm, 0.290 for AL 24 mm to <26 mm, and 0.447 for AL 26 mm or more.

Correlation Between pChT and Imaging Features of Optic Disc and Peripapillary Region

Partial correlation coefficient between pChT and morphological features of optic disc and peripapillary region after adjusting for sex and age are summarized in **Table 5**. pChT was positively associated with IOD_pChT ($r = 0.604$, $P < 0.001$), followed by SER ($r = 0.363$, $P < 0.001$), ovality index ($r = 0.124$, $P < 0.001$), torsion angle ($r = 0.124$, $P < 0.001$). pChT was negatively associated with AL ($r = -0.406$, $P < 0.001$), PPA area ($r = -0.351$, $P < 0.001$) and BCVA ($r = -0.103$, $P = 0.002$).

Multivariate regression analysis adjusted for age and sex was constructed to identify independent factors associated with pChT as shown in **Table 6**. The analysis showed that sex ($P = 0.015$), AL ($P < 0.001$), PPA area ($P = 0.044$), IOD_pChT ($P < 0.001$) were independently associated with pChT. According to the model, every $1 \times 10\,\mu m$ decrease in IOD_pChT was associated with a $9.64\,\mu m$ decrease in pChT. With stratification of myopia severity, the multivariate model showed that IOD_pChT correlated positively with pChT in all three groups (all, $P < 0.001$) while AL was only associated with pChT in the group with AL < 24 mm ($P = 0.009$). The overall $adjR^2$ for pChT yielded 0.389 while the $adjR^2$ were 0.367, 0.286, and 0.339 in the group with AL < 24 mm, 24 mm to <26 mm, and 26 mm or more, respectively.

DISCUSSION

To the best of our knowledge, this is the first study to construct objective and quantifiable models of imaging indicators describing early changes of the optic disc and peripapillary region and further assess its impact on choroidal thickness. Our results have demonstrated a positive correlation between constructed

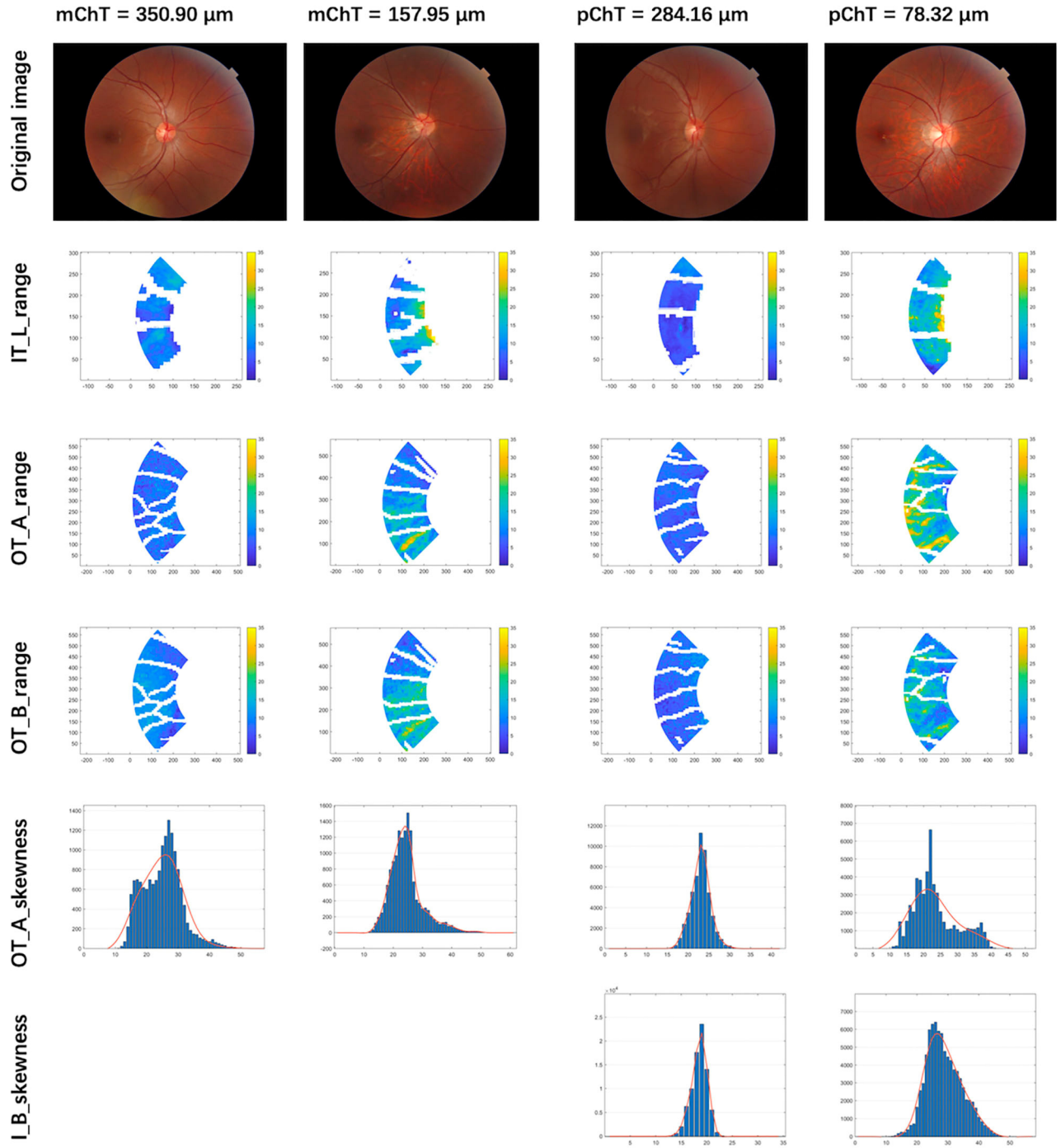

FIGURE 4 | Visualization of selected radiomic features. Column 1 and 2: patients with macular choroidal thickness (mChT) of 350.90 and 157.95 µm. Column 3 and 4: patients with peripapillary choroidal thickness (pChT) of 284.16 and 78.32 µm. Row 1: original images. Row 2: range of intensity in L channel of the inner temporal region (IT_L_range); Row 3: range of intensity in A channel of the outer temporal region (OT_A_range); Row 4: range of intensity in B channel of the outer temporal region (OT_B_range). Row 5: skewness of intensity in A channel of the outer temporal region (OT_A_skewness); Row 6: skewness of intensity in B channel of the inner ring (I_B_skewness). Higher values of range mean larger variations of intensity in the LAB channel of color. Higher values of skewness mean larger proportions of the brighter region.

IODs and ChT, even in the highly myopic group. According to features enrolled in IOD models which were visualized in **Figure 4**, thinner mChT and pChT were associated with a larger variation of color intensity and a larger proportion of brighter area in the peripapillary region, which represented changes of fundus tissue structure that could not be described objectively

but only perceived subjectively without the method of radiomics and machine learning. Moreover, the models suggested thinner mChT was associated with larger PPA, longer disc fovea distance while thinner pChT was associated with larger PPA, all of which were consistent with those of previous studies (7, 11, 29–32).

In the early stage of myopia, the optic disc and peripapillary region are undergoing complex changes that can only be perceived through the ophthalmologists' senses but indescribable and unquantifiable. Several morphological changes of the optic disc and PPA have been reported to be significantly associated with the progression of high myopia and pathological myopia (7, 11, 20, 29–31). As discussed above, choroidal thinning, which appears before visible lesions of pathological myopia, has been widely discussed as a relatively reliable indicator for future progression of high myopia and pathological myopia (14–17). All these studies highlighted the importance of early changes of the optic disc and peripapillary region as a risk indicator for choroid thinning and future progression of pathological myopia.

However, the above indicators have several obvious shortcomings. First, these clinic features were measured manually and highly depends on the ophthalmologists' subjective estimation. When measured by different ophthalmologists, different results may occur due to the lack of uniform objective standards. Second, only when changes distinguishable for human eyes appear can the features be detected and measured, and a number of early subtle changes have consequently been neglected. Thirdly, these clinical features which only described the morphology of optic disc are surely not enough to cover various changes of color, texture and so on. In that case, radiomic analysis is a powerful tool to elucidate subtle relationships between image characteristics

TABLE 3 | Partial correlation analysis between macular choroidal thickness and features of the optic disc adjusted for sex and age in all subjects.

	Total ($N = 896$)	
	r	***P***
MAP, mm Hg	0.052	0.120
IOP, mm Hg	0.072	0.032*
ACD, mm	0.039	0.239
SER, diopter	0.450	< 0.001*
BCVA, logMAR	−0.121	< 0.001*
AL, mm	−0.497	< 0.001*
PPA area, mm^2	−0.492	< 0.001*
Ovality index	0.332	< 0.001*
Torsion angle, deg	0.192	< 0.001*
IOD_mChT, 10 μm	0.664	< 0.001*

*MAP, mean arterial pressure; IOP, intraocular pressure; ACD, anterior chamber depth; SER, spherical equivalent refraction; BCVA, best-corrected visual acuity; logMAR, logarithm of minimal angle resolution; AL, axial length; PPA, peripapillary atrophy; IOD_mChT, the indicator of optic disc for macular choroidal thickness. *Significant difference.*

TABLE 5 | Partial correlation analysis between peripapillary choroidal thickness and features of the optic disc adjusted for sex and age in all subjects.

	Total ($N = 896$)	
	r	***P***
MAP, mm Hg	0.066	0.050
IOP, mm Hg	0.089	0.008*
ACD, mm	0.082	0.014*
SER, diopter	0.363	< 0.001*
BCVA, logMAR	−0.103	0.002*
AL, mm	−0.406	< 0.001*
PPA area, mm^2	−0.351	< 0.001*
Ovality index	0.124	< 0.001*
Torsion angle, deg	0.124	< 0.001*
IOD_pChT, 10 μm	0.604	< 0.001*

*MAP, mean arterial pressure; IOP, intraocular pressure; ACD, anterior chamber depth; SER, spherical equivalent refraction; BCVA, best-corrected visual acuity; logMAR, logarithm of minimal angle resolution; AL, axial length; PPA, peripapillary atrophy; IOD_pChT, the indicator of optic disc for peripapillary choroidal thickness. *Significant difference.*

TABLE 4 | Multivariate regression analysis of association with macular choroidal thickness in all subjects and groups with different degrees of myopia.

	Total ($N = 896$)			AL < 24 mm ($N = 119$)			24 mm ≤ AL < 26 mm ($N = 464$)			AL ≥ 26 mm ($N = 313$)		
	B	***β***	***P***	***B***	***β***	***P***	***B***	***β***	***P***	***B***	***β***	***P***
Age, y	−0.20	−0.01	0.697	−0.13	−0.01	0.936	0.15	0.01	0.853	−1.05	−0.06	0.167
Sex, male/female	−10.74	−0.09	0.001*	−21.84	−0.18	0.036*	−11.36	−0.10	0.020*	−7.47	−0.07	0.111
AL, mm	−7.41	−0.16	< 0.001*	−19.07	−0.15	0.093	−9.54	−0.09	0.039*	0.65	0.01	0.839
PPA area, mm^2	5.33	0.05	0.177	9.33	0.04	0.746	−0.12	0.00	0.987	6.59	0.10	0.149
Ovality index	−2.03	0.00	0.917	−54.34	−0.08	0.435	4.69	0.01	0.882	−14.03	−0.03	0.611
Torsion angle, deg	0.11	0.04	0.179	0.08	0.03	0.686	0.02	0.01	0.910	0.22	0.08	0.063
IOD_mChT, 10 μm	8.87	0.60	< 0.001*	11.61	0.57	< 0.001*	8.40	0.49	< 0.001*	8.88	0.71	< 0.001*

*AL, axial length; PPA, peripapillary atrophy; IOD_mChT, the indicator of optic disc for macular choroidal thickness. Adjusted for all variables listed. $adjR^2$ for all subjects = 0.460; $adjR^2$ for AL < 24 mm = 0.319; $adjR^2$ for AL 24 mm to < 26 mm = 0.290; $adjR^2$ for AL 26 mm or more = 0.447. *Significant difference.*

TABLE 6 | Multivariate regression analysis of association with peripapillary choroidal thickness in all subjects and groups with different degrees of myopia.

	Total ($N = 896$)			AL < 24 mm ($N = 119$)			24 mm ≤ AL < 26 mm ($N = 464$)			AL ≥ 26 mm ($N = 313$)		
	B	***β***	***P***	***B***	***β***	***P***	***B***	***β***	***P***	***B***	***β***	***P***
Age, y	−0.64	−0.04	0.113	−0.72	−0.05	0.558	−0.48	−0.03	0.420	−1.35	−0.10	0.036*
Sex, male/female	−6.17	−0.07	0.015*	−19.03	−0.20	0.016*	−5.17	−0.06	0.156	−5.12	−0.06	0.197
AL, mm	−5.30	−0.16	< 0.001*	−22.42	−0.22	0.009*	−5.38	−0.07	0.118	−1.39	−0.03	0.606
PPA area, mm^2	5.90	0.08	0.044*	29.45	0.17	0.159	0.14	0.00	0.978	5.19	0.10	0.153
Ovality index	−29.44	−0.06	0.051	28.58	0.05	0.586	−36.93	−0.08	0.119	−43.97	−0.10	0.057
Torsion angle, deg	0.04	0.02	0.493	0.32	0.16	0.040*	−0.08	−0.04	0.411	0.07	0.04	0.461
IOD_pChT, 10 μm	9.64	0.59	< 0.001*	12.25	0.56	< 0.001*	9.87	0.54	< 0.001*	8.71	0.61	< 0.001*

*AL, axial length; PPA, peripapillary atrophy; IOD_pChT, the indicator of optic disc for peripapillary choroidal thickness. Adjusted for all variables listed. adjR^2 for all subjects = 0.389; adjR^2 for AL < 24 mm = 0.367; adjR^2 for AL 24 mm to < 26 mm = 0.286; adjR^2 for AL 26 mm or more = 0.339. *Significant difference.*

and disease status through automated high-throughput feature extraction.

Recently, ophthalmological image analysis based on radiomics has achieved preliminary success in the prediction of disease prognosis and treatment effectiveness. A hybrid prediction model, composed of radiomics imaging features of OCT, demographic and visual factors in non-exudative age-related macular degeneration eyes, provided risk scores of exudation in 3 months with an area under the receiver operating characteristic curve (AUC) of 0.82 (33). For the prediction of drug effectiveness, Feng et al. (34), derived radiomic features from OCT images of patients with choroidal neovascularization and cystoid macular edema before giving anti-vascular endothelial growth factor treatment, based on which the model achieved automatic prediction of treatment effectiveness with an AUC of 0.80. In addition, a small-scale clinical trial identified two radiomics biomarkers from ultra-widefield fluorescein angiography imaging for predicting treatment durability of longer treatment intervals in diabetic macular edema with an AUC of 0.77 (35). Studies above manifested that, as a combination of medical imaging with engineering, radiomics has great potential to be a novel and powerful tool of future precision medicine in the field of ophthalmology.

Although the utility of imaging features has been frequently discussed in machine learning (36), fundus changes of myopia still lack sufficient attention. Recently, Medeiros et al. (37), constructed a model to predict RNFLT from fundus photograph as a risk indicator of glaucomatous damage. Furthermore, a retrospective cohort study validated that longitudinal changes of RNFLT predicted based on fundus photographs forecasted future conversion of glaucomatous visual field defects (38). Color fundus photograph has advantages of low cost and easy access while provides abundant information of morphology, color and texture, while imaging features by radiomics and machine learning provides an effective way to quantify these imaging characteristics. Combining these two methods makes it possible to analyze whether changes of the optic disc and peripapillary regions are related to choroidal thinning and the progression of pathological myopia with statistical methods.

In the present study, by using methods of machine learning, the imaging features of optic disc and peripapillary region were screened for features most correlated with choroidal thickness, which formed new models of risk indicators for changes of choroidal thickness. The new indicators constituted of several imaging features have several advantages. First, they were subjective and quantifiable indexes that required no manual measurements but standardized algorithms to automatically extract features from fundus photographs. Second, whether the changes were visible to the human eye, quantifiable results could be automatically acquired. Third, imaging features by machine learning covered information of color and texture in addition to morphology. All these advantages offset the shortcomings of previous clinical features.

This study had several limitations. First, although the fundus photograph provides abundant information related to morphology, color and texture of optic disc and peripapillary region, only features related to morphology and color of peripapillary region were selected by LASSO regression and enrolled in the final models. One possible reason is that indicators of other information need further designing and mining. However, it is gratifying that models constructed with only selected indicators have significantly stronger correlation than validated indicators including PPA area, ovality index and torsion angle. Second, the age of participants in the present study is limited between 16 and 40 years old, so the results may not be representative of all myopia populations. Finally, the cross-sectional study was not able to determine the causal relationships between changes of quantifiable models and ChT. Whether the changes of optic disc and peripapillary region leads to the progression of choroid thinning or pathological myopic needs further longitudinal studies.

In conclusion, the cohort study explored the possibility of finding non-invasive imaging-based risk indicators indistinguishable for human eyes from fundus photographs with the goal of predicting changes of choroidal thickness and the progression of pathological myopia from early changes of the optic disc and peripapillary region. New models of risk indicators by machine learning provided new ideas for exploring

the early changes of optic disc in myopia and its impact on choroidal thickness, which could be useful in other areas of fundus diseases.

DATA AVAILABILITY STATEMENT

The original contributions presented in the study are included in the article/supplementary material, further inquiries can be directed to the corresponding author/s.

ETHICS STATEMENT

The studies involving human participants were reviewed and approved by the ethics committee of Shanghai General Hospital. Written informed consent to participate in this study was provided by the participants' legal guardian/next of kin.

AUTHOR CONTRIBUTIONS

DS, YF, and XX designed this study. DS, YD, HC, and ML collected and measured data. DS, QC, LY, and JH analyzed data. DS, QC, and YF wrote the article. All authors discussed the results and commented on the manuscript.

FUNDING

This study was supported by the National Key R&D Program of China (2016YFC0904800, 2019YFC0840607), National Science and Technology Major Project of China (2017ZX09304010), National Natural Science Foundation of China (Grant No. 81970846, Beijing, China), and the Medical engineering cross project of Shanghai Jiao Tong University (YG2019ZDA26). The sponsors and funding organizations had no role in the design or conduct of this research.

REFERENCES

1. Bourne RR, Stevens GA, White RA, Smith JL, Flaxman SR, Price H, et al. Causes of vision loss worldwide, 1990-2010: a systematic analysis. *Lancet Glob Health.* (2013) 1:e339–49. doi: 10.1016/S2214-109X(13)70113-X
2. Fricke TR, Jong M, Naidoo KS, Sankaridurg P, Naduvilath TJ, Ho SM, et al. Global prevalence of visual impairment associated with myopic macular degeneration and temporal trends from 2000 through 2050: systematic review, meta-analysis and modelling. *Br J Ophthalmol.* (2018) 102:855–62. doi: 10.1136/bjophthalmol-2017-311266
3. Varma R, Kim JS, Burkemper BS, Wen G, Torres M, Hsu C, et al. Prevalence and causes of visual impairment and blindness in Chinese American adults: the Chinese American Eye Study. *JAMA Ophthalmol.* (2016) 134:785–93. doi: 10.1001/jamaophthalmol.2016.1261
4. Liu HH, Xu L, Wang YX, Wang S, You QS, Jonas JB. Prevalence and progression of myopic retinopathy in Chinese adults: the Beijing Eye Study. *Ophthalmology.* (2010) 117:1763–8. doi: 10.1016/j.ophtha.2010.01.020
5. Lin C, Li SM, Ohno-Matsui K, Wang BS, Fang YX, Cao K, et al. Five-year incidence and progression of myopic maculopathy in a rural Chinese adult population: the Handan Eye Study. *Ophthalmic Physiol Opt.* (2018) 38:337–45. doi: 10.1111/opo.12456
6. Jan C, Li L, Keay L, Stafford RS, Congdon N, Morgan I. Prevention of myopia, China. *Bull World Health Organ.* (2020) 98:435–37. doi: 10.2471/BLT.19.240903
7. Park HY, Lee K, Park CK. Optic disc torsion direction predicts the location of glaucomatous damage in normal-tension glaucoma patients with myopia. *Ophthalmology.* (2012) 119:1844–51. doi: 10.1016/j.ophtha.2012.03.006
8. McBrien NA, Gentle A. Role of the sclera in the development and pathological complications of myopia. *Prog Retin Eye Res.* (2003) 22:307–38. doi: 10.1016/S1350-9462(02)00063-0
9. Samarawickrama C, Mitchell P, Tong L, Gazzard G, Lim L, Wong TY, et al. Myopia-related optic disc and retinal changes in adolescent children from Singapore. *Ophthalmology.* (2011) 118:2050–7. doi: 10.1016/j.ophtha.2011.02.040
10. How AC, Tan GS, Chan YH, Wong TT, Seah SK, Foster PJ, et al. Population prevalence of tilted and torted optic discs among an adult Chinese population in Singapore: the Tanjong Pagar Study. *Arch Ophthalmol.* (2009) 127:894–9. doi: 10.1001/archophthalmol.2009.134
11. Tay E, Seah SK, Chan SP, Lim AT, Chew SJ, Foster PJ, et al. Optic disk ovality as an index of tilt and its relationship to myopia and perimetry. *Am J Ophthalmol.* (2005) 139:247–52. doi: 10.1016/j.ajo.2004.08.076
12. Xu L, Li Y, Wang S, Wang Y, Wang Y, Jonas JB. Characteristics of highly myopic eyes: the Beijing Eye Study. *Ophthalmology.* (2007) 114:121–6. doi: 10.1016/j.ophtha.2006.05.071
13. Wang YX, Panda-Jonas S, Jonas JB. Optic nerve head anatomy in myopia and glaucoma, including parapapillary zones alpha, beta, gamma and delta: histology and clinical features. *Prog Retin Eye Res.* (2020) 2020:100933. doi: 10.1016/j.preteyeres.2020.100933
14. Fledelius HC, Jacobsen N, Li XQ, Goldschmidt E. Choroidal thickness at age 66 years in the Danish high myopia study cohort 1948 compared with follow-up data on visual acuity over 40 years: a clinical update adding spectral domain optical coherence tomography. *Acta Ophthalmol.* (2018) 96:46–50. doi: 10.1111/aos.13659
15. Flores-Moreno I, Ruiz-Medrano J, Duker JS, Ruiz-Moreno JM. The relationship between retinal and choroidal thickness and visual acuity in highly myopic eyes. *Br J Ophthalmol.* (2013) 97:1010–3. doi: 10.1136/bjophthalmol-2012-302836
16. Gupta P, Cheung CY, Saw SM, Bhargava M, Tan CS, Tan M, et al. Peripapillary choroidal thickness in young Asians with high myopia. *Invest Ophthalmol Vis Sci.* (2015) 56:1475–81. doi: 10.1167/iovs.14-15742
17. Li Z, Wang W, Liu R, Wang D, Zhang J, Xiao O, et al. Choroidal thickness predicts progression of myopic maculopathy in high myopes: a 2-year longitudinal study. *Br J Ophthalmol.* (2020) 2020:316866. doi: 10.1136/bjophthalmol-2020-316866
18. Aerts HJ. The potential of radiomic-based phenotyping in precision medicine: a review. *JAMA Oncol.* (2016) 2:1636–42. doi: 10.1001/jamaoncol.2016.2631
19. van Griethuysen JJM, Fedorov A, Parmar C, Hosny A, Aucoin N, Narayan V, et al. Computational radiomics system to decode the radiographic phenotype. *Cancer Res.* (2017) 77:e104–7. doi: 10.1158/0008-5472.CAN-17-0339
20. Chen Q, He J, Yin Y, Zhou H, Jiang H, Zhu J, et al. Impact of the morphologic characteristics of optic disc on choroidal thickness in young myopic patients. *Invest Ophthalmol Vis Sci.* (2019) 60:2958–67. doi: 10.1167/iovs.18-26393
21. Hu G, Chen Q, Xu X, Lv H, Du Y, Wang L, et al. Morphological characteristics of the optic nerve head and choroidal thickness in high myopia. *Invest Ophthalmol Vis Sci.* (2020) 61:46. doi: 10.1167/iovs.61.4.46
22. Deng J, Li X, Jin J, Zhang B, Zhu J, Zou H, et al. Distribution pattern of choroidal thickness at the posterior pole in Chinese children with myopia. *Invest Ophthalmol Vis Sci.* (2018) 59:1577–86. doi: 10.1167/iovs.17-22748
23. Tan CS, Ouyang Y, Ruiz H, Sadda SR. Diurnal variation of choroidal thickness in normal, healthy subjects measured by spectral domain optical coherence tomography. *Invest Ophthalmol Vis Sci.* (2012) 53:261–6. doi: 10.1167/iovs.11-8782
24. Marsh-Tootle WL, Harb E, Hou W, Zhang Q, Anderson HA, Weise K, et al. Optic nerve tilt, crescent, ovality, and torsion in a multi-ethnic cohort of young adults with and without myopia. *Invest Ophthalmol Vis Sci.* (2017) 58:3158–71. doi: 10.1167/iovs.16-20860
25. Lee KS, Lee JR, Kook MS. Optic disc torsion presenting as unilateral glaucomatous-appearing visual field defect in young myopic Korean eyes. *Ophthalmology.* (2014) 121:1013–9. doi: 10.1016/j.ophtha.2013.11.014

26. Bennett AG, Rudnicka AR, Edgar DF. Improvements on Littmann's method of determining the size of retinal features by fundus photography. *Graefes Arch Clin Exp Ophthalmol.* (1994) 232:361–7. doi: 10.1007/BF00175988
27. Ruiz-Medrano J, Montero JA, Flores-Moreno I, Arias L, García-Layana A, Ruiz-Moreno JM. Myopic maculopathy: current status and proposal for a new classification and grading system (ATN). *Prog Retin Eye Res.* (2019) 69:80–115. doi: 10.1016/j.preteyeres.2018.10.005
28. Tideman JW, Snabel MC, Tedja MS, van Rijn GA, Wong KT, Kuijpers RW, et al. Association of axial length with risk of uncorrectable visual impairment for Europeans with myopia. *JAMA Ophthalmol.* (2016) 134:1355–63. doi: 10.1001/jamaophthalmol.2016.4009
29. Fang YX, Yokoi T, Nagaoka N, Shinohara K, Onishi Y, Ishida T, et al. Progression of myopic maculopathy during 18-year follow-up. *Ophthalmology.* (2018) 125:863–77. doi: 10.1016/j.ophtha.2017.12.005
30. Yan YN, Wang YX, Yang Y, Xu L, Xu J, Wang Q, et al. Ten-year progression of myopic maculopathy: the Beijing eye study 2001-2011. *Ophthalmology.* (2018) 125:1253–63. doi: 10.1016/j.ophtha.2018.01.035
31. Shin HY, Park HYL, Park CK. The effect of myopic optic disc tilt on measurement of spectral-domain optical coherence tomography parameters. *Br J Ophthalmol.* (2015) 99:69–74. doi: 10.1136/bjophthalmol-2014-305259
32. Sung MS, Heo H, Piao H, Guo Y, Park SW. Parapapillary atrophy and changes in the optic nerve head and posterior pole in high myopia. *Sci Rep.* (2020) 10:4607. doi: 10.1038/s41598-020-61485-2
33. Banerjee I, de Sisternes L, Hallak JA, Leng T, Osborne A, Rosenfeld PJ, et al. Prediction of age-related macular degeneration disease using a sequential deep learning approach on longitudinal SD-OCT imaging biomarkers. *Sci Rep.* (2020) 10:15434. doi: 10.1038/s41598-020-72359-y
34. Feng D, Chen X, Zhou Z, Liu H, Wang Y, Bai L, et al. A preliminary study of predicting effectiveness of anti-VEGF injection using OCT images based on deep learning. *Annu Int Conf IEEE Eng Med Biol Soc.* (2020) 2020:5428–31. doi: 10.1109/EMBC44109.2020.9176743
35. Prasanna P, Bobba V, Figueiredo N, Sevgi DD, Lu C, Braman N, et al. Radiomics-based assessment of ultra-widefield leakage patterns and vessel network architecture in the PERMEATE study: insights into treatment durability. *Br J Ophthalmol.* (2020) 2020:317182. doi: 10.1136/bjophthalmol-2020-317182
36. Tomaszewski MR, Gillies RJ. The biological meaning of radiomic features. *Radiology.* (2021) 298:505–16. doi: 10.1148/radiol.2021202553
37. Medeiros FA, Jammal AA, Thompson AC. From machine to machine: an OCT-trained deep learning algorithm for objective auantification of glaucomatous damage in fundus photographs. *Ophthalmology.* (2019) 126:513–21. doi: 10.1016/j.ophtha.2018.12.033
38. Lee T, Jammal AA, Mariottoni EB, Medeiros FA. Predicting glaucoma development with longitudinal deep learning predictions from fundus photographs. *Am J Ophthalmol.* (2021) 2:9394. doi: 10.1016/j.ajo.2020.12.031

Conflict of Interest: The authors declare that the research was conducted in the absence of any commercial or financial relationships that could be construed as a potential conflict of interest.

frontiers in Medicine

ORIGINAL RESEARCH
published: 29 April 2021
doi: 10.3389/fmed.2021.658259

Investigation of Macular Choroidal Thickness and Blood Flow Change by Optical Coherence Tomography Angiography After Posterior Scleral Reinforcement

Zheng Zhang[1,2†], *Yue Qi*[1,2*†], *Wenbin Wei*[1,2], *Zi-Bing Jin*[1,2], *Wen Wang*[1,2], *Anli Duan*[1,2] *and Wu Liu*[1,2]

[1] *Beijing Tongren Eye Center, Beijing Tongren Hospital, Capital Medical University, Beijing Ophthalmology and Visual Sciences Key Laboratory, Beijing, China,* [2] *Beijing Institute of Ophthalmology, Beijing Tongren Hospital, Capital Medical University, Beijing, China*

OPEN ACCESS

Edited by:
Xiangtian Zhou, Wenzhou Medical University, China

Reviewed by:
Chee Wai Wong, Singapore National Eye Center, Singapore
Carlo Gesualdo, University of Campania Luigi Vanvitelli, Italy

***Correspondence:**
Yue Qi
qiyue@126.com

[†] *These authors have contributed equally to this work and share the first authorship*

Specialty section:
This article was submitted to Ophthalmology, a section of the journal Frontiers in Medicine

Received: *25 January 2021*
Accepted: *18 March 2021*
Published: *29 April 2021*

Citation:
Zhang Z, Qi Y, Wei W, Jin Z-B, Wang W, Duan A and Liu W (2021) Investigation of Macular Choroidal Thickness and Blood Flow Change by Optical Coherence Tomography Angiography After Posterior Scleral Reinforcement. Front. Med. 8:658259. doi: 10.3389/fmed.2021.658259

Purpose: This work aimed to study the effect of posterior scleral reinforcement (PSR) on choroidal thickness (CT) and blood flow.

Methods: This study included 25 eyes of 24 patients with high myopia (≤-6.0 dioptres or axial length ≥ 26.0 mm) who underwent PSR surgery. All patients completed the 1-month follow-up visit. Myopic macular degeneration (MMD) was graded according to the International Meta-Analysis for Pathologic Myopia (META-PM) classification based on color fundus photographs. Swept-source optical coherence tomography angiography (SSOCTA) was performed to investigate CT, choroidal perfusion area (CPA), and choriocapillaris perfusion area (CCPA) change following PSR surgery.

Results: The distribution of MMD categories was 9 (36.0%) in category 1, 10 (40.0%) in category 2, and 6 (24.0%) in category 3 or 4. MMD severity was strongly correlated with CT (all $P < 0.01$) and CPA (all $P < 0.04$). Postoperative CT at each sector increased significantly at 1 week's follow-up, compared to preoperative measures (all $P < 0.05$). Postoperative CPA at subfoveal, superior, inferior, and nasal sectors also increased significantly 1 week after PSR surgery (all $P < 0.05$). Moreover, the increased CT, CPA, and CCPA remain after PSR surgery at 1 month's follow-up, but the difference was not statistically significant.

Conclusions: We demonstrated that the CT and choroidal blood flow increased significantly in patients with high myopia who underwent PSR surgery in a short period of time. In addition, the CT and CPA were independently associated with MMD. However, whether the transient improvement of the choroidal circulation could prevent long-term progression of high myopia warrants further study in the future.

Keywords: choroidal thickness, choroidal blood flow, swept-source optical coherence tomography angiography, posterior scleral reinforcement, myopic macular degeneration

INTRODUCTION

The rapidly increasing prevalence of myopia poses one of the most serious public health issues, especially in Asia where pathological myopia has been reported as the primary cause of blindness or low vision in 12–27% of the populations (1–3). The major alterations in pathologic myopia include excessive axial elongation of the globe and associated local ectasia of the posterior sclera, which eventually leads to characterized retinal and choroidal lesions as well as impacts on macular function (4, 5).

Laid between the retina and the sclera in the posterior eye, the highly vascular choroid is essential for maintaining the normal physiology of the eye, such as supplying oxygen and nutrients for the outer retina. There is also substantial evidence that the choroid plays an important role in controlling ocular elongation and refractive error development (6, 7). Growing evidence in the literature has demonstrated that a short-term thickening of the choroid leads to a prolonged decrease in extracellular matrix molecule synthesis and a slowing of eye growth (8–10). Therefore, controlling choroidal thinning could be a crucial approach to maintain emmetropia and reduce the incidence of severe myopic maculopathy.

As a treatment targeting the posterior pole of the eye, posterior scleral reinforcement (PSR) was first proposed by Shevelev in 1930 and later modified by Snyder and Thompson in 1972 (11). PSR has been considered an effective and safe surgical method for stabilization of the axial elongation and prevention of high myopic complications (5, 12). The mechanism by which PSR may slow down the elongation of the eyeball was presumably due to the direct mechanical force of the reinforcement band and the scleral remodeling and improvement of microcirculation within the macula (13, 14). However, whether or not PSR could change the choroidal thickness (CT) and choroidal blood flow is still under debate due to lack of satisfactory quantitative methods (5, 15).

Swept-source optical coherence tomography angiography (SSOCTA) has been introduced as a new non-invasive, quantitative approach to visualize and evaluate the choroidal microvasculature (16). In comparison with enhanced depth imaging (EDI) by spectral domain optical coherence tomography (SDOCT), swept-source optical coherence tomography (SSOCT) with a light source of 1,050 nm can provide a better-visualized full-thickness choroid and enable more accurate measurements of the choroidal structure (17).

The purpose of our study was to observe the changes of CT and the choroidal vasculature structure, as well as axial length (AL), best corrected visual acuity (BCVA), and spherical equivalent (SE), after PSR in patients with pathological myopia.

METHODS

Highly Myopic Patients Received PSR Surgery

This was a prospective, observational clinical study of consecutive patients with high myopia aged 31–68 years undergoing PSR surgery. Twenty-four patients (25 eyes) diagnosed with pathological myopia were recruited from the Beijing Tongren Eye Center from October 2019 to October 2020. The inclusion criteria were as follows: manifest SE of $\leq$-6.0 dioptres (D) with increases $\geq$-1.00 D/year, AL of $\geq$26.0 mm with annual progressive growth of $>$0.5 mm for 2 years or more, and posterior staphyloma confirmed by B-ultrasound scan (IOL Master, Carl Zeiss Inc., Jena, Germany). Exclusion criteria included the following: (1) any ocular disease that may affect measurements of the choroid, such as corneal opacities, dense cataract, central serous chorioretinopathy, polypoidal choroidal vasculopathy, choroidal neovascularization, and non-myopia-related macular scarring; (2) history of intraocular surgery and previous retinal photocoagulation or photodynamic therapy; (3) presence of other ocular diseases such as glaucoma, tumor, uveitis, and retinal vascular disease. This study was approved by the Institutional Ethics Committee of Beijing Tongren Hospital, Capital Medical University, and conducted in accordance with the tenets of the Declaration of Helsinki. All participants provided signed informed consent for their participation.

Clinical Examination

Patients were followed up at 1 week and 1 month after PSR surgery. Preoperative and postoperative examinations included logMAR BCVA, slit lamp biomicroscopic examination, AL using IOL Master (Carl Zeiss Inc., Jena, Germany), pupil-dilated funduscopy, color fundus photography (Hybrid Digital Mydriatic Retinal Camera CX-1, Canon Inc., Tokyo, Japan), and manifest refraction performed by qualified optometrists. SE was calculated using the spherical power plus half of the cylindrical power.

Grading of MMD

According to the international META-PM classification (18), the MMD severity was defined and classified into the following categories: no macular lesions was defined as META-PM category 0; tessellated fundus was defined only as META-PM category 1; diffuse chorioretinal atrophy was defined as META-PM category 2; patchy chorioretinal atrophy was defined as META-PM category 3; and macular atrophy was defined as META-PM category 4 (**Figure 1**). Two ophthalmologists, masked to patient characteristics, performed the grading of MMD severity. Discrepancies were adjudicated by a senior fundus disease specialist.

Measurement of CT, Choroidal Perfusion Area, and Choriocapillaris Perfusion Area

Optical coherence tomography angiography (OCTA) scans were obtained using the commercial VG200 SSOCTA device with a light source of 1,050 nm. Detailed information on the acquisition protocols for this device has been previously reported (16). Both optical coherence tomography (OCT) and OCTA data were obtained with a raster scan protocol of 512 $\times$ 512 B-scans, which covered an area of 3 $\times$ 3 mm centered on the fovea. The macular region was divided into foveal, temporal, superior, nasal, and inferior sectors based on the Early Treatment Diabetic Retinopathy Study (ETDRS) contour. The choroid in OCT was defined as the volume starting at the retinal pigment

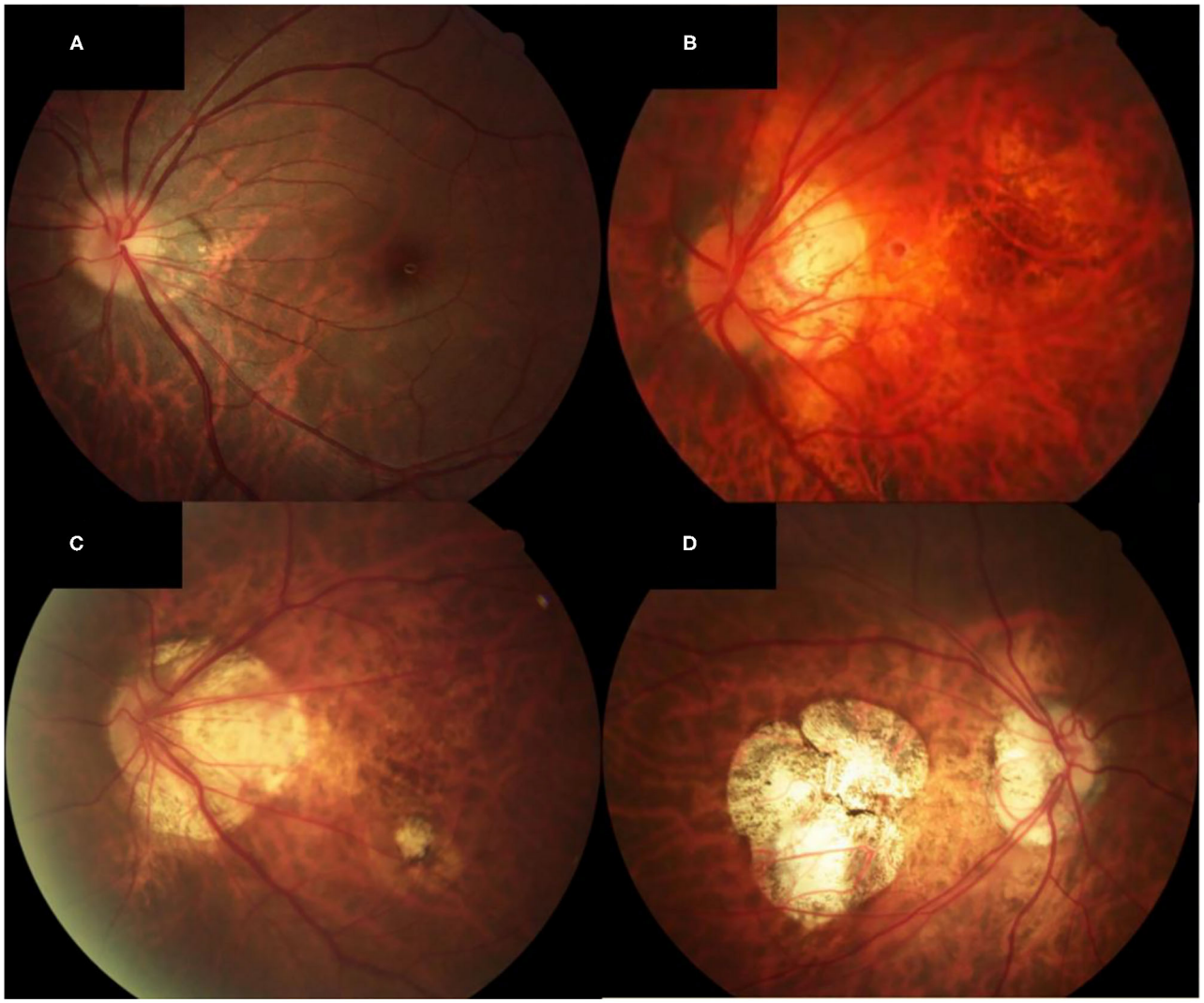

FIGURE 1 | Fundus photographs of eyes showing different MMD severity grades. **(A)** Fundus photograph of the left eye of a patient with META-PM category 1 (AL of 25.64, SE of −8.4 D, and BCVA of 0 logMAR units). Only the tessellated fundus can be seen on the fundus photograph. **(B)** Fundus photograph of the left eye of a patient with META-PM category 2 (AL of 29.36, SE of −16.5 D, and BCVA of 0.2 logMAR units). Diffuse chorioretinal atrophy is seen on the fundus photograph. **(C)** Fundus photograph of the left eye of a patient with META-PM category 3 (AL of 28.98, SE of −16.0 D, and BCVA of 0.4 logMAR units). Both diffuse and patchy chorioretinal atrophy can be seen on the fundus photograph. **(D)** Fundus photograph of the right eye of a patient with META-PM category 4 (AL of 31.04, SE of −20.0 D, and BCVA of 1.3 logMAR units). Macular atrophy is seen on the fundus photograph.

epithelium (RPE)–Bruch's membrane complex and ending at the chorioscleral junction (**Figure 2**). The choriocapillaris was defined as the volume from the basal border of the RPE–Bruch's membrane complex to approximately 20 μm beneath the RPE–Bruch's membrane complex. The CPA/CCPA was defined as the area occupied by blood vessels in a 2D retina projection image. The projection image was acquired by projecting a 3D angiography volume data of the choroidal/choriocapillaris layer onto a 2D imaging plane, which can also be called as an *en face* image. The presence of perfusion was directly indicated by an angiography signal. An algorithm was designed to separate the foreground (blood vessel) pixels from background (non-vessel tissue) pixels, by properly segmenting the image from the perspective of angiography signal strength. The perfusion area was calculated as the sum of the area of all pixels that exceed the threshold (**Figures 3**, **4**). The magnification for imaging the fundus using OCT is different in the myopic eye due to the elongation of the eye. Hence, in the present study, Bennett's formula was used to determine a scaling factor of the OCT angiograms for adjustment of the ocular magnification [scaling factor = $3.382 \times 0.013062 \times (\mathrm{AL} - 1.82)$] (19).

Surgical Procedure

The surgical techniques of PSR were basically following the modified Snyder–Thompson procedure. All PSR procedures were performed by the same surgeon (Yue Qi). Under general anesthesia, a 210° peritotomy of the conjunctiva was performed along the inferior–temporal axis of the limbus, and the inferior

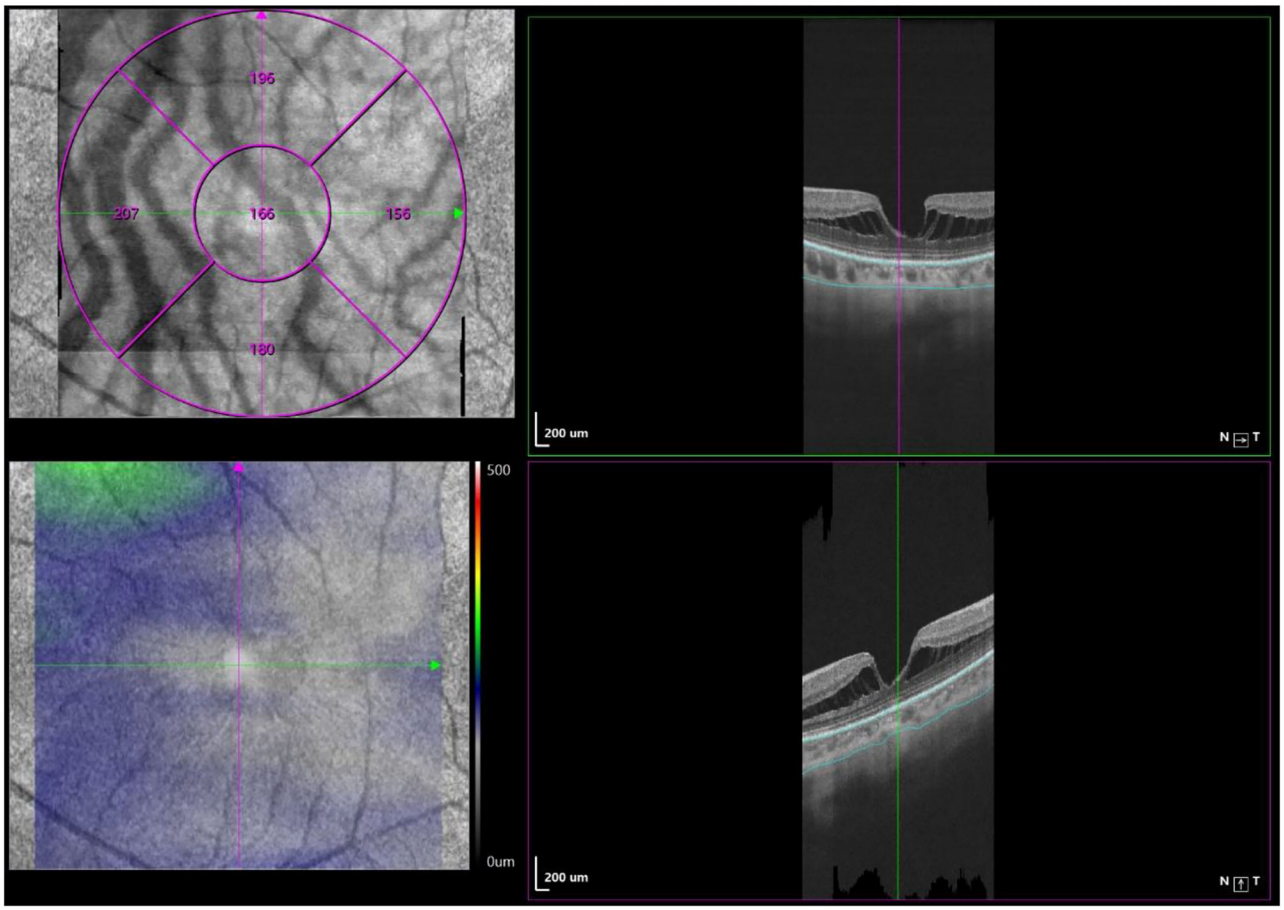

FIGURE 2 | Macular CT measurement by swept-source OCT angiography. Macular CT was separately calculated in 5 regions (fovea, tempo, superior, nasal, and inferior) based on ETDRS contour. The choroid was defined as the volume from the basal border of the RPE–Bruch's membrane complex to the chorioscleral junction.

and lateral rectus muscles were isolated and exposed. The two muscles were maneuvered by traction sutures while the eyeball was pulled toward the superior nasal side. After the inferior oblique muscle was isolated, a homologous human scleral strip with a width of 6–10 mm was sequentially inserted underneath the lateral rectus, inferior oblique, and inferior rectus muscles. The superior end of the strip was fixed at the nasal side of the scleral insertion of the superior rectus muscle, while the inferior end of the strip was anchored at the nasal side of the scleral insertion of the inferior rectus muscle. The scleral strip was stretched into a U-shape to wrap around the posterior pole and scleral staphyloma corresponding to the macular area and was flattened with the help of strabismus hooks. The relative position between the scleral strip and optic nerve was checked with a strabismus hook. The distance was kept at approximately 1 mm to ensure that the strip covered the foveal region without compressing the optic nerve (20) (**Figure 5**).

Statistical Analysis

Statistical analysis was performed using SPSS software (version 25.0; IBM, Chicago, USA). Descriptions of the quantitative data were presented as the mean ± standard deviation (SD). The independent-samples *t*-test was used for comparing continuous data between two groups. Repeated-measures analysis of variance (RMANOVA) with the *post-hoc* least significant difference (LSD) test was used to assess the differences among the eyes before PSR surgery, 1 week after PSR surgery, and 1 month after PSR surgery. Spearman correlation coefficients were calculated to analyze the correlation between AL, SE, and BCVA with MMD severity. *P*-values < 0.05 were considered significant. The software used for data visualization is RStudio.

RESULTS

Demographic and Clinical Data

Twenty-four patients with 25 eyes diagnosed with pathological myopia were recruited and completed 1 week and 1 month postoperative follow-ups. **Table 1** shows the baseline characteristics of these eyes. The mean age was 50.5 ± 11.5 years, the mean AL was 29.23 ± 1.87 mm, the mean SE was −15.3 ± 4.3 D, and the mean BCVA was 0.40 ± 0.25. Nine (36.0%) eyes had tessellated fundus only (category 1), 10 (40.0%) eyes had diffuse chorioretinal atrophy (category 2), and six (24.0%) eyes had patchy chorioretinal atrophy (category 3) or

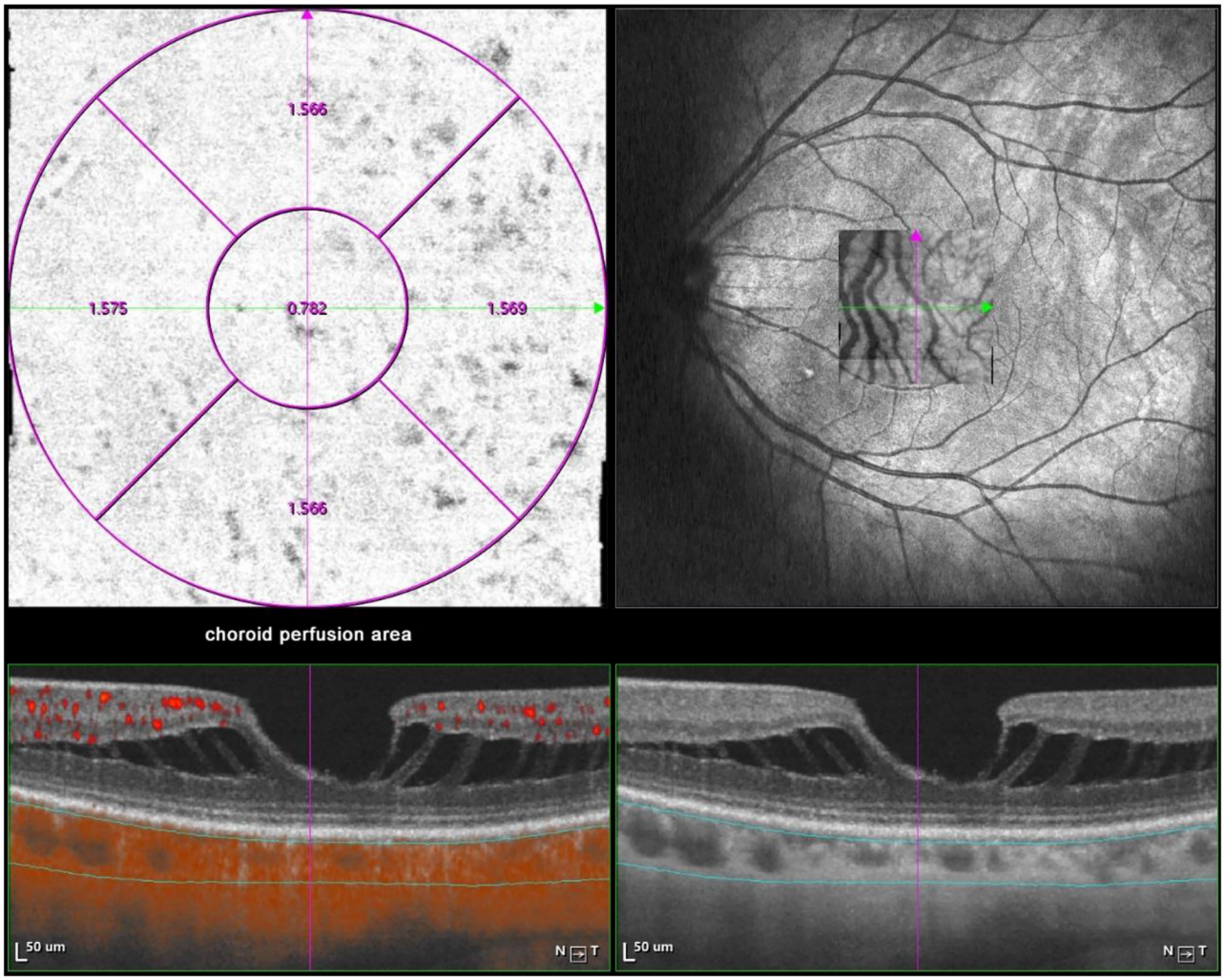

FIGURE 3 | Macular CPA measurement by SSOCTA. Macular CPA was separately calculated in five regions (foveal, temporal, superior, nasal, and inferior) based on the ETDRS contour. The CPA was defined as the area of blood flow to the whole *en face* scanning area at the choroidal layer on OCTA images.

macular atrophy (category 4). MMD severity was significantly correlated with AL (correlation coefficient $|r| = 0.72$, $P < 0.001$), SE ($r = -0.87$, $P < 0.001$), and BCVA ($r = 0.49$, $P = 0.02$). Patients with severe MMD had longer AL and more myopic refractive error compared with eyes with mild MMD (**Table 1**). The mean SE post PSR was -13.5 ± 5.9 D. The mean BCVA post PSR was 0.44 ± 0.23. No significant differences were found before and after PSR (all $P > 0.16$).

CT, CPA, and CCPA in Eyes With Different MMD Grades

Table 2 shows the CT, CPA, and CCPA in eyes with different MMD grades. The subfoveal, superior, inferior, nasal, and temporal CTs were significantly thinner in eyes with META-PM category 3 or 4 at baseline than in eyes with META-PM category 1 (all $P < 0.009$) and in eyes with META-PM category 2 (all $P < 0.027$). Nasal CT was significantly thinner in eyes with META-PM category 2 than in eyes with META-PM category 1 (83.10 ± 20.65 vs. 107.78 ± 29.48 μm, $P = 0.048$). The subfoveal, superior, inferior, and temporal CTs were thinner in eyes with META-PM category 2 than in eyes with META-PM category 1, but the difference was not statistically significant (**Figure 6** and **Table 2**). We further evaluated the correlation between MMD severity and CT (**Table 3**). CT was strongly correlated with MMD severity based on META-PM classification (all $P < 0.01$). In addition, subfoveal CT had a strong correlation with BCVA ($r = -0.49$, $P = 0.021$).

Superior and nasal CPAs were significantly lower in eyes with META-PM category 3 or 4 at baseline than in eyes with META-PM category 1 (all $P < 0.05$). The subfoveal, inferior, and temporal CPAs were lower in eyes with META-PM category 3 or 4, but the difference was not statistically significant. All superior, inferior, nasal, and temporal CCPAs were significantly lower in

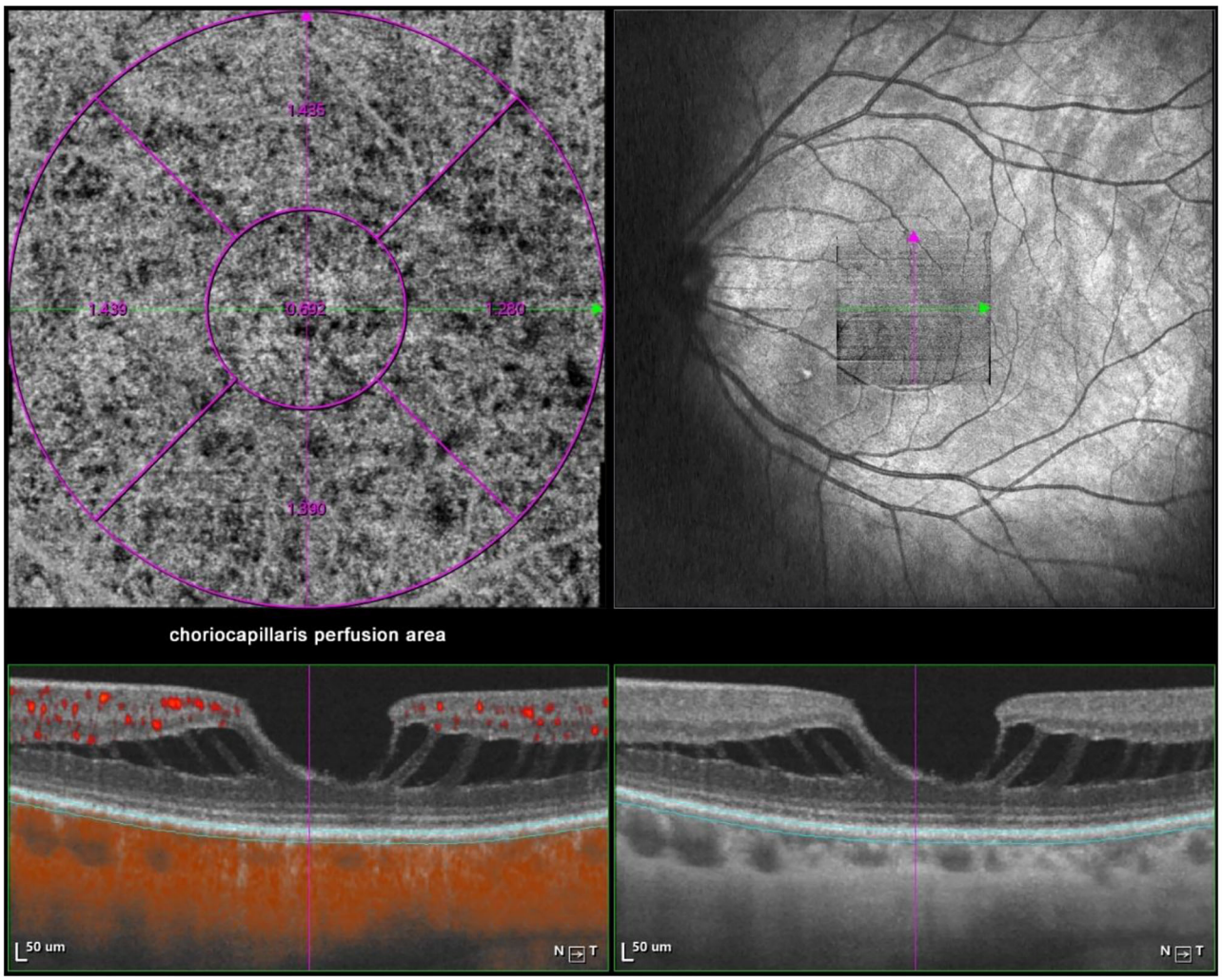

FIGURE 4 | Macular CCPA measurement by SSOCTA. Macular CCPA was separately calculated in five regions (foveal, temporal, superior, nasal, and inferior) based on the ETDRS contour. The CCPA was defined as the area of blood flow to the whole *en face* scanning area at the choriocapillaris layer on OCTA images.

eyes with META-PM category 3 or 4 at baseline than in eyes with META-PM category 1 (all $P < 0.031$). Subfoveal CCPA was lower in eyes with META-PM category 3 or 4, but the difference was not statistically significant (**Figure 6** and **Table 2**). CPA was correlated with MMD severity (all $P < 0.04$). Superior, inferior, and nasal CCPAs were correlated with MMD, but the correlation was weaker than that between CPA and MMD. In addition, CCPA had a moderate correlation with BCVA (all $P < 0.05$) (**Table 3**).

Postoperative Outcomes of CT, CPA, and CCPA

Postoperative outcomes of CT, CPA, and CCPA are presented in **Table 4**. The CT of the center subfield and parafoveal subfields increased significantly after PSR surgery at 1 week's follow-up (all $P < 0.01$). The subfoveal, superior, inferior, and nasal CPAs increased significantly after PSR surgery at 1 week's follow-up (all $P < 0.05$). The temporal CPAs were increased after PSR surgery at 1 week's follow-up, but the difference was not statistically significant. CCPA did not change significantly compared to preoperation measures. The increased CT, CPA, and CCPA remain after PSR surgery at 1 month's follow-up, but the difference was not statistically significant (all $P > 0.05$) (**Figure 7** and **Table 4**).

DISCUSSION

In this study, we demonstrated strong correlations of CT and CPA with MMD severity and significant thinning of the choroid in eyes with severe MMD compared to eyes with mild MMD. Our data support the importance of CT and choroidal blood flow in the pathogenesis of MMD. We also found that there was a transient increase in CT and CPA after PSR surgery at 1 week's follow-up. However, whether this transient improvement of the CT and choroidal blood flow could slow the elongation of the

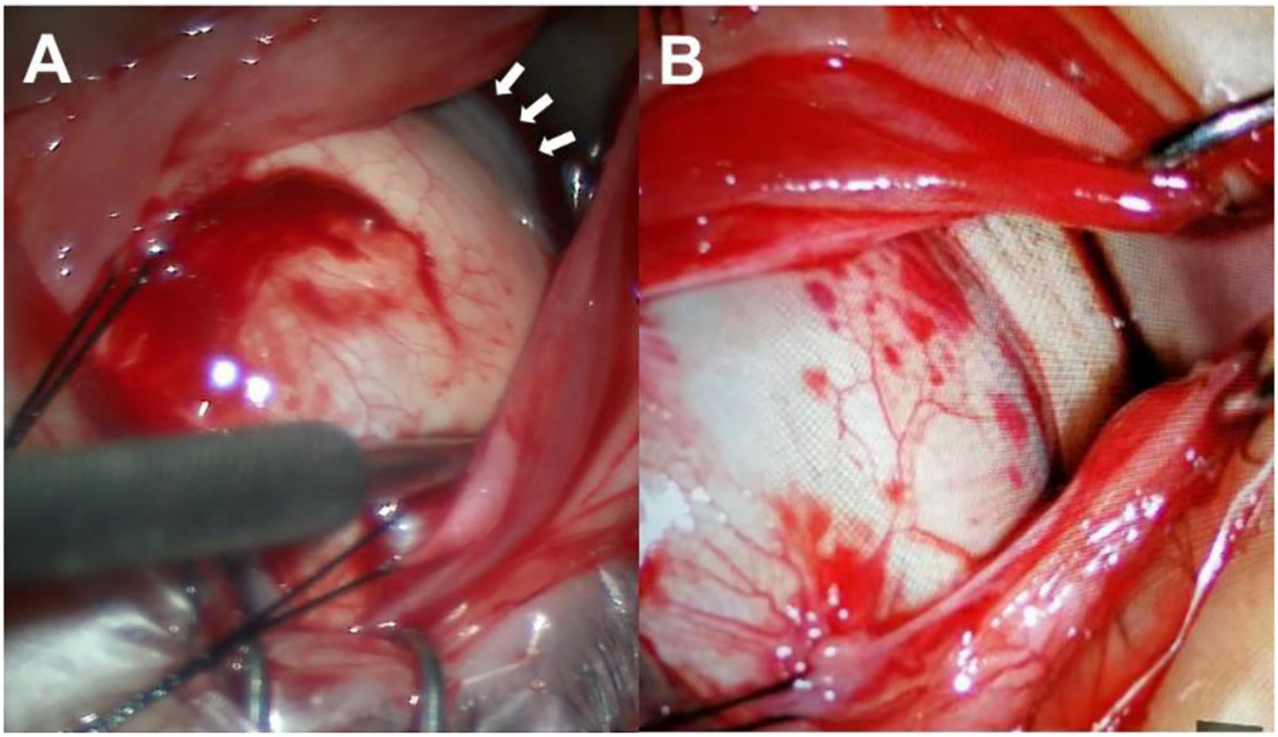

FIGURE 5 | Surgical procedures. **(A)** The inferior and lateral rectus muscles were maneuvered by traction sutures while the eyeball was pulled toward the superior nasal side to expose the scleral staphyloma (white arrows). **(B)** The scleral strip was inserted underneath the lateral rectus, inferior oblique, and inferior rectus muscles and wrapped around the posterior pole and scleral staphyloma.

TABLE 1 | Baseline characteristics of study eyes.

Baseline characteristic	Number of subjects			
	All (*n* = 24)	**META-PM category 1 (*n* = 9)**	**META-PM category 2 (*n* = 9)**	**META-PM categories 3 and 4 (*n* = 6)**
Mean age, years	50.5 ± 11.5	49.1 ± 13.4	47.7 ± 10.0	56.7 ± 10.0
Male, %	8 (33.3)	2 (22.2)	4 (44.4)	2 (33.3)
Baseline characteristic	**Number of eyes**			
	All (*n* = 25)	**META-PM category 1 (*n* = 9)**	**META-PM category 2 (*n* = 10)**	**META-PM categories 3 and 4 (*n* = 6)**
AL, mm	29.23 ± 1.87	27.60 ± 0.90	29.80 ± 1.07†	30.75 ± 2.26†
SE, D	−15.3 ± 4.3	−10.77 ± 1.96	−16.50 ± 2.79†	−20.00 ± 2.15†‡
logMAR BCVA	0.40 ± 0.25	0.30 ± 0.35	0.40 ± 0.24	0.48 ± 0.12

†*P* < 0.05 by independent-samples t-test vs. META-PM category 1.
‡*P* < 0.05 by independent-samples t-test vs. META-PM category 2.

eyeball and prevent high myopic complications still needs to be further studied.

In this study, we used the international META-PM classification to grade MMD severity. Our findings showed that MMD severity was well-correlated with anatomical and functional parameters (AL, SE, and BCVA). However, how eyes with high myopia develop the typical atrophic and degenerative changes seen in MMD, while others do not, is currently unclear. Mechanical stretching of the retina by axial elongation and choroidal ischemia are the most likely mechanisms for MMD

TABLE 2 | CT, CPA, and CCPA in eyes with different MMD severity grades.

CT/CPA/CCPA	META-PM category 1 ($n = 9$)	META-PM category 2 ($n = 10$)	META-PM categories 3 and 4 ($n = 6$)
CT, μm			
Subfoveal	101.89 ± 32.18	78.20 ± 12.73	53.50 ± 16.78†‡
Superior	113.44 ± 30.53	96.10 ± 21.39	64.67 ± 19.96†‡
Inferior	106.56 ± 25.61	90.40 ± 26.93	56.33 ± 12.16†‡
Nasal	107.78 ± 29.48	83.10 ± 20.65†	59.00 ± 15.09†‡
Temporal	111.11 ± 28.69	92.30 ± 15.53	67.17 ± 24.19†‡
CPA, mm²			
Subfoveal	0.77 ± 0.03	0.76 ± 0.03	0.71 ± 0.07
Superior	1.55 ± 0.04	1.53 ± 0.06†	1.47 ± 0.11†
Inferior	1.55 ± 0.03	1.51 ± 0.08	1.32 ± 0.31
Nasal	1.56 ± 0.03	1.52 ± 0.07	1.32 ± 0.18†‡
Temporal	1.55 ± 0.04	1.54 ± 0.04	1.40 ± 0.16
CCPA, mm²			
Subfoveal	0.66 ± 0.08	0.64 ± 0.14	0.56 ± 0.13
Superior	1.36 ± 0.16	1.24 ± 0.48	1.07 ± 0.20†
Inferior	1.34 ± 0.12	1.23 ± 0.46	1.02 ± 0.23†
Nasal	1.33 ± 0.16	1.21 ± 0.46	0.95 ± 0.29†
Temporal	1.23 ± 0.21	1.15 ± 0.47	0.93 ± 0.27†

†$P < 0.05$ by independent-samples t-test vs. META-PM category 1.
‡$P < 0.05$ by independent-samples t-test vs. META-PM category 2.

(4). Wong et al. measured posterior scleral thickness and CT with SSOCT in 62 eyes with high myopia. A thinner choroid was found to be significantly correlated with MMD severity (21). The strength of the correlation with MMD severity was stronger for CT than it was for scleral thickness, suggesting that a vascular mechanism involving choroidal ischemia may be playing a more prominent role in the pathogenesis of MMD than a mechanical mechanism related to scleral stretch. But CT is a measure of the structure of the choroid. Therefore, it may not truly demonstrate the functional aspect of choroidal blood flow. In our study, we included CPA and CCPA as biomarkers of choroidal vascularity. Our findings showed that CPA was moderately well-correlated with MMD severity. Both CPA and CCPA tend to be lower in eyes with severe MMD compared to eyes with mild MMD, although the difference was not statistically significant in some regions. Previous studies have found that more severe myopia levels were associated with longer axial elongation (22) and that eyes with severe MMD were at higher risk of MMD progression than eyes with mild MMD (23). Considering the relationship between CPA and MMD severity, these results may present a role for choroidal vascularity in the myopia development and progression.

The nutrient supply of the choroid mainly comes from the short-posterior ciliary artery. As one of the most highly vascularized tissues of the body, the choroid accounts for 65% of the blood supply within the eye; hence, it is reasonable to assume that the progression of pathological myopia is linked to the structural and functional alterations of the choroid (5, 24–26). Studies have shown that CT alterations occurred earlier than the fundus changes and that visual function abnormalities occurred in the early stage of pathologic myopia (27, 28). Nickla et al. reported that AL grew faster in eyes with thinner CT than in eyes with thicker choroids (29). Flores-Moreno et al. have reported that CT decreased by 25.9 ± 2.1 μm for each additional millimeter of AL (27). Currently, with the development of OCTA, a few available clinical studies have demonstrated that choroidal vascularity and choriocapillaris blood flow were lower in eyes with greater myopia (30–32). Furthermore, some recent experimental studies may help make a definitive conclusion regarding the relationship between choroidal vascularity and myopia development. Wu et al. (33) demonstrated that scleral hypoxia played an essential role in scleral remodeling during myopia progression. Zhou et al. (34) found that increased choroidal blood perfusion inhibited eyeball elongation and myopia development via attenuating scleral hypoxia in guinea pigs. In this study, we also found that AL is especially associated with parafoveal subfields CT and CPA.

Some studies of high myopia have also found a significant correlation between subfoveal CT and visual acuity, with a thinner choroid being correlated with poorer vision in highly myopic eyes (35–37). In accordance with these researches, in this study, we also found a significant correlation of subfoveal CT with BCVA. Moreover, we found that all center subfield and parafoveal subfield CCPAs were correlated with BCVA. Although the exact mechanism linking a thinner choroid with poor vision is not clearly revealed from the above studies, it has been proposed that the marked thinning of the choroid in eyes with high myopia may affect the function of the photoreceptor, eventually resulting in loss of vision.

PSR is believed to be a safe and reliable method for preventing axial elongation, halting further myopia development, and preserving vision acuity (5, 38). It is reasonable to speculate that PSR surgery could potentially influence the CT and choroidal blood flow as well. In the past years, various techniques had been tried to demonstrate the ocular blood flow in pathologic myopia, such as fundus fluorescein angiography (FFA), indocyanine green angiography (ICGA), color Doppler imaging (CDI). However, they are not satisfactory tools to quantitatively evaluate the microcirculation of the retina and choroid; thus, there are few studies on the microcirculation changes post PSR surgery in highly myopic eyes by far. For the past few years, OCTA was proven to be feasible in detecting choroidal and retinal microvasculature non-invasively and quantitatively. However, in a previous study, Mo et al. did not find a significant change of choriocapillary flow density after PSR, compared to untreated highly myopic eyes with matched AL and SE by RTVue XR OCT with the Angio Retina mode (20). Zhang et al. reported that choriocapillary flow density and CT did not change significantly after PSR surgery either (39). Regarding the disappointing results in previous researches, traditional SDOCT angiography (SDOCTA) may be also limited in detecting changes in choroidal blood flow.

In our present study, we evaluated the CT and choroidal vascularity by VG200 since VG200 is an SSOCTA with more

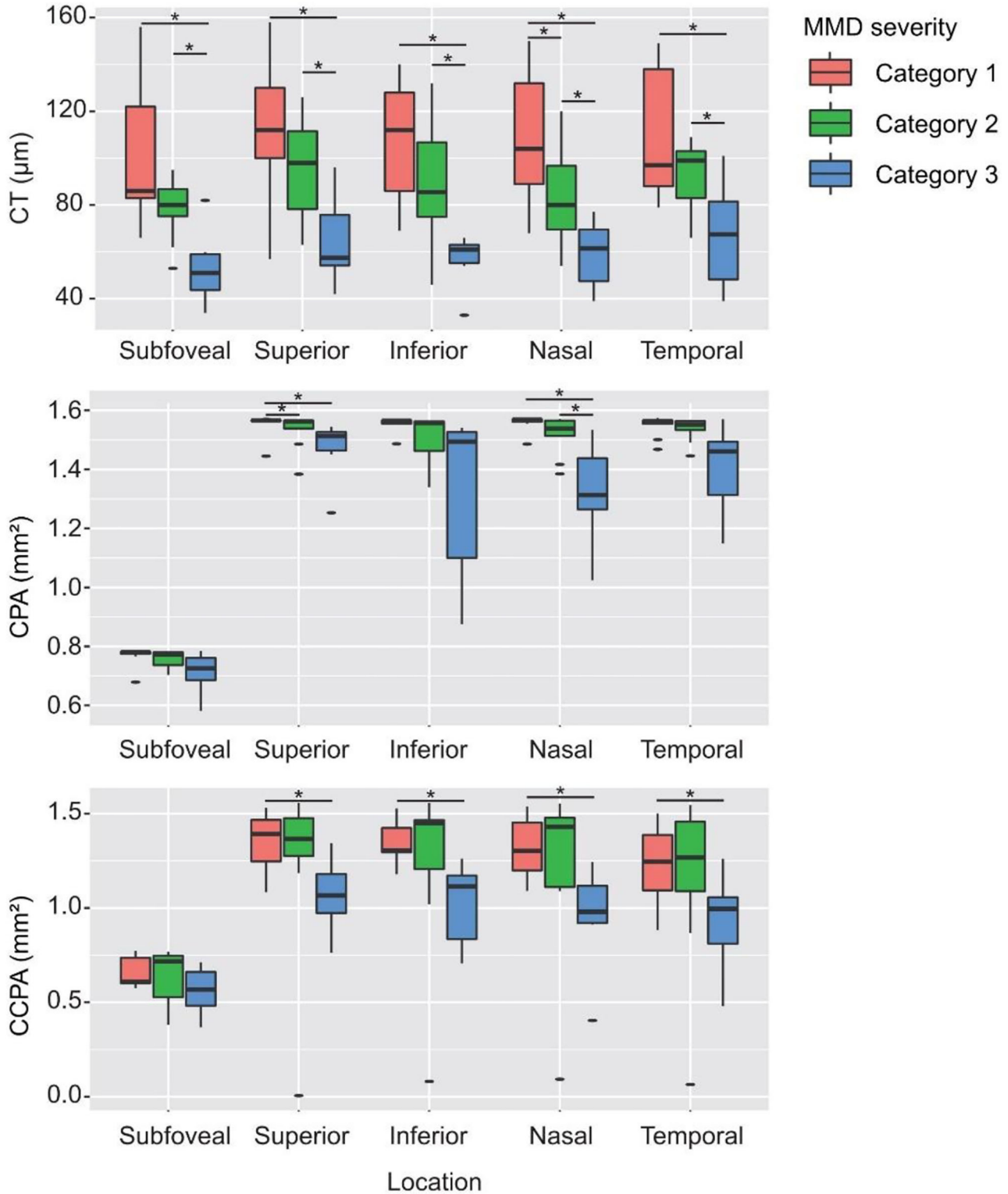

FIGURE 6 | CT, CPA, and CCPA in eyes with different MMD severity grades. *Statistically significant at $P < 0.05$ when the META-PM category 1 group or the META-PM category 2 group was compared with the META-PM category 3 group and when the META-PM category 1 group was compared with the META-PM category 2 group.

TABLE 3 | Correlation between CT, CPA, and CCPA with MMD severity, AL, SE, and BCVA.

CT/ST	MMD severity		AL		SE		BCVA	
	r	*P*-value	*r*	*P*-value	*r*	*P*-value	*r*	*P*-value
CT, μm								
Subfoveal	−0.66	<0.001†	−0.37	0.07	0.35	0.10	−0.49	0.021†
Superior	−0.62	0.001†	−0.46	0.02†	0.39	0.07	−0.21	0.35
Inferior	−0.67	<0.001†	−0.55	0.01†	0.62	0.002†	−0.26	0.25
Nasal	−0.67	<0.001†	−0.53	0.01†	0.54	0.01†	−0.19	0.40
Temporal	−0.49	0.01†	−0.41	0.04†	0.36	0.09	−0.21	0.35
CPA, mm²								
Subfoveal	−0.41	0.04†	−0.26	0.20	0.04	0.86	−0.34	0.12
Superior	−0.65	<0.001†	−0.49	0.01†	0.32	0.14	−0.40	0.07
Inferior	−0.64	0.001†	−0.63	0.001†	0.51	0.01†	−0.46	0.03†
Nasal	−0.71	<0.001†	−0.62	0.001†	0.43	0.04†	−0.42	0.05
Temporal	−0.48	0.02†	−0.41	0.04†	0.26	0.24	−0.19	0.39
CCPA, mm²								
Subfoveal	−0.27	0.20	−0.18	0.41	0.01	0.97	−0.47	0.03†
Superior	−0.41	0.04†	−0.29	0.17	0.09	0.68	−0.54	0.01†
Inferior	−0.44	0.03†	−0.26	0.22	0.21	0.34	−0.50	0.02†
Nasal	−0.47	0.02†	−0.28	0.19	0.14	0.53	−0.65	0.001†
Temporal	−0.32	0.13	−0.23	0.29	0.06	0.78	−0.43	0.05

† P < 0.05 by Spearman correlation coefficients.

TABLE 4 | Preoperative and postoperative measurements (mean ± SD) of CT, CPA, and CCPA of the center subfield and parafovea (superior, inferior, nasal, and temporal subfields).

	Baseline	1 week	1 month	*P*-value[a]
CT subfoveal (μm)	80.80 ± 28.65	107.35 ± 42.53†	89.56 ± 26.43	0.033
CT superior (μm)	94.80 ± 30.38	126.90 ± 45.20†	105.78 ± 35.57	0.019
CT inferior (μm)	88.04 ± 30.06	128.95 ± 43.30†	99.33 ± 27.21	0.001
CT nasal (μm)	86.20 ± 29.34	118.85 ± 41.64†	95.67 ± 30.76	0.008
CT temporal (μm)	93.04 ± 27.87	125.10 ± 42.00†	105.39 ± 27.10	0.007
CPA subfoveal (μm)	0.75 ± 0.05	0.77 ± 0.02†	0.77 ± 0.02	0.068
CPA superior (μm)	1.52 ± 0.07	1.56 ± 0.01†	1.55 ± 0.04	0.080
CPA inferior (μm)	1.48 ± 0.18	1.55 ± 0.03†	1.54 ± 0.04	0.087
CPA nasal (μm)	1.48 ± 0.13	1.55 ± 0.04†	1.53 ± 0.09	0.108
CPA temporal (μm)	1.51 ± 0.10	1.53 ± 0.08	1.53 ± 0.06	0.534
CCPA subfoveal (μm)	0.63 ± 0.12	0.65 ± 0.13	0.65 ± 0.12	0.771
CCPA superior (μm)	1.24 ± 0.33	1.32 ± 0.25	1.34 ± 0.20	0.466
CCPA inferior (μm)	1.22 ± 0.33	1.33 ± 0.16	1.29 ± 0.28	0.399
CCPA nasal (μm)	1.19 ± 0.35	1.26 ± 0.26	1.27 ± 0.27	0.621
CCPA temporal (μm)	1.12 ± 0.35	1.25 ± 0.26	1.19 ± 0.28	0.420

CT, choroidal thickness; CPA, choroidal perfusion area; CCPA, choriocapillaris perfusion area.
[a] RMANOVA.
† P < 0.05 by multiple comparisons (LSD post-hoc test) vs. the baseline.

accurate images for choroidal vascularity evaluation. We found that CT and subfoveal, superior, inferior, and nasal CPAs increased significantly after PSR surgery at 1 week's follow-up. But no significant differences were found at 1 month's follow-up. Therefore, it is possible that PSR can lead to a short-term increase of choroidal blood flow but cannot maintain the blood flow in pathologic myopic eyes for a long time. This is probably due to the separation of the sclera between

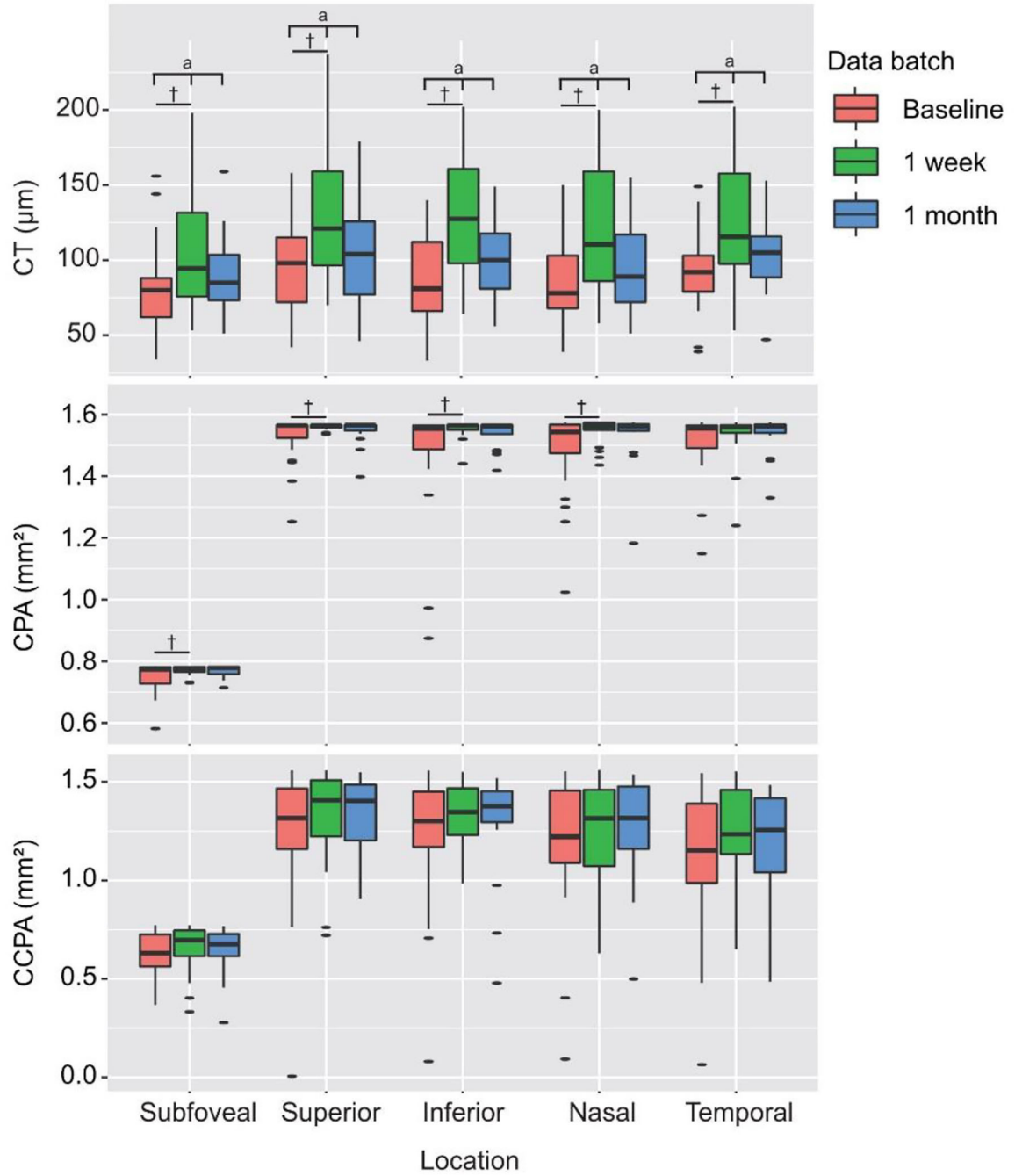

FIGURE 7 | Preoperative and postoperative measurements of CT, CPA, and CCPA of the center subfield and parafovea (superior, inferior, nasal, and temporal subfields). [a]Statistically significant at $P < 0.05$ by RMANOVA, [†]Statistically significant at $P < 0.05$ by multiple comparisons (LSD *post-hoc* test) vs. the baseline.

the posterior choroid and the reinforcement band; thus, the secondary non-specific inflammatory reaction could only mildly improve choroidal blood flow. But by the evidence that PSR could prevent eye elongation and halt thinning and atrophy of the choroid (5), there is reason to believe that deterioration of circulation was prevented. Aside from the effects of PSR surgery upon the choroid, a range of other factors known to delay ocular elongation have also been shown to lead to transient thickening of the choroid in animal research. Myopic defocus (40, 41), pharmacological agents such as muscarinic antagonists (42), and dopamine agonists (43), as well as environmental factors such as increased light exposure (44), have all been shown to lead to transient increases in CT.

Our study has several limitations. The relatively small number of eyes with different MMD severity grades limited us to further explore the changes of CT and CPA after PSR surgery in each

META-PM category group. A controlled prospective study with larger sample size was needed to further study the role of PSR in pathologic myopic choroidal flow changes with different MMD severity grades. The follow-up time is relatively short in our study. However, according to our studies, the CT and CPA were increased shortly after PSR and tended to return to preoperative status at 1 months' follow-up time. It can be inferred that the longer the follow-up time, the more difficult to detect the changes of CT and choroidal blood flow.

In conclusion, we demonstrated that CT and CPA were independently associated with MMD. The CT and choroidal blood flow increased significantly in patients with high myopia who underwent PSR surgery in a short period of time. However, whether this transient improvement of the choroidal circulation could prevent the development of high myopia is still unclear and requires further long-term investigation with larger samples.

DATA AVAILABILITY STATEMENT

The raw data supporting the conclusions of this article will be made available by the authors, without undue reservation.

ETHICS STATEMENT

The studies involving human participants were reviewed and approved by institutional ethic committee of Beijing Tongren Hospital, Capital Medical University. The patients/participants provided their written informed consent to participate in this study.

AUTHOR CONTRIBUTIONS

ZZ, YQ, WWe, and WL designed this study. ZZ and YQ collected and measured data. ZZ, YQ, Z-BJ, and WWa analyzed data. ZZ and YQ wrote this article. Z-BJ and AD revised the manuscript. All authors discussed the results and commented on the manuscript.

FUNDING

This study was supported by the Beijing Municipal Administration of Hospitals' Youth Program (QMS20200206), Beijing Municipal Administration of Hospitals Incubating Program (PX2021007), Beijing Tongren Hospital Top Talent Training Program Foundation (ZZ).

REFERENCES

1. Iwase A, Araie M, Tomidokoro A, Yamamoto T, Shimizu H, Kitazawa Y. Prevalence and causes of low vision and blindness in a Japanese adult population: the Tajimi Study. *Ophthalmology.* (2006) 113:1354–62. doi: 10.1016/j.ophtha.2006.04.022
2. Xu L, Wang Y, Li Y, Wang Y, Cui T, Li J, et al. Causes of blindness and visual impairment in urban and rural areas in Beijing: the Beijing Eye Study. *Ophthalmology.* (2006) 113:1134.e1131–11. doi: 10.1016/j.ophtha.2006.01.035
3. Yamada M, Hiratsuka Y, Roberts CB, Pezzullo ML, Yates K, Takano S, et al. Prevalence of visual impairment in the adult Japanese population by cause and severity and future projections. *Ophthalmic Epidemiol.* (2010) 17:50–7. doi: 10.3109/09286580903450346
4. Ohno-Matsui K, Lai TY, Lai CC, Cheung CM. Updates of pathologic myopia. *Prog Retin Eye Res.* (2016) 52:156–87. doi: 10.1016/j.preteyeres.2015.12.001
5. Peng C, Xu J, Ding X, Lu Y, Zhang J, Wang F, et al. Effects of posterior scleral reinforcement in pathological myopia: a 3-year follow-up study. *Graefes Arch Clin Exp Ophthalmol.* (2019) 257:607–17. doi: 10.1007/s00417-018-04212-y
6. Nickla DL, Wallman J. The multifunctional choroid. *Prog Retin Eye Res.* (2010) 29:144–68. doi: 10.1016/j.preteyeres.2009.12.002
7. Read S, Fuss J, Vincent S, Collins M, Alonso-Caneiro D. Choroidal changes in human myopia: insights from optical coherence tomography imaging. *Clin Exp Optom.* (2019) 102:270–85. doi: 10.1111/cxo.12862
8. Troilo D, Nickla DL, Wildsoet CF. Choroidal thickness changes during altered eye growth and refractive state in a primate. *Invest Ophthalmol Vis Sci.* (2000) 41:1249–58.
9. Hung LF, Wallman J, Smith EL 3rd. Vision-dependent changes in the choroidal thickness of macaque monkeys. *Invest Ophthalmol Vis Sci.* (2000) 41:1259–69.
10. Zhu X, Park TW, Winawer J, Wallman J. In a matter of minutes, the eye can know which way to grow. *Invest Ophthalmol Vis Sci.* (2005) 46:2238–41. doi: 10.1167/iovs.04-0956
11. Thompson FB. A simplified scleral reinforcement technique. *Am J Ophthalmol.* (1978) 86:782–90. doi: 10.1016/0002-9394(78)90121-6
12. Miao Z, Li L, Meng X, Guo L, Cao D, Jia Y, et al. Modified posterior scleral reinforcement as a treatment for high myopia in children and its therapeutic effect. *Biomed Res Int.* (2019) 2019:5185780. doi: 10.1155/2019/5185780
13. Yuan Y, Zong Y, Zheng Q, Qian G, Qian X, Li Y, et al. The efficacy and safety of a novel posterior scleral reinforcement device in rabbits. *Mater Sci Eng C Mater Biol Appl.* (2016) 62:233–41. doi: 10.1016/j.msec.2015.12.046
14. Zhu SQ, Zheng LY, Pan AP, Yu AY, Wang QM, Xue AQ. The efficacy and safety of posterior scleral reinforcement using genipin cross-linked sclera for macular detachment and retinoschisis in highly myopic eyes. *Br J Ophthalmol.* (2016) 100:1470–5. doi: 10.1136/bjophthalmol-2015-308087
15. Qiao L, Zhang X, Jan C, Li X, Li M, Wang H. Macular retinal thickness and flow density change by optical coherence tomography angiography after posterior scleral reinforcement. *Sci China Life Sci.* (2019) 62:930–6. doi: 10.1007/s11427-018-9484-6
16. Yang J, Wang E, Yuan M, Chen Y. Three-dimensional choroidal vascularity index in acute central serous chorioretinopathy using swept-source optical coherence tomography. *Graefes Arch Clin Exp Ophthalmol.* (2020) 258:241–7. doi: 10.1007/s00417-019-04524-7
17. Lane M, Moult EM, Novais EA, Louzada RN, Cole ED, Lee B, et al. Visualizing the choriocapillaris under drusen: comparing 1050-nm swept-source versus 840-nm spectral-domain optical coherence tomography angiography. *Invest Ophthalmol Vis Sci.* (2016) 57:585–90. doi: 10.1167/iovs.15-18915
18. Ohno-Matsui K, Kawasaki R, Jonas J, Cheung C, Saw S, Verhoeven V, et al. International photographic classification and grading system for myopic maculopathy. *Am J Ophthalmol.* (2015) 159:877–83.e877. doi: 10.1016/j.ajo.2015.01.022
19. Moghimi S, Hosseini H, Riddle J, Lee G, Bitrian E, Giaconi J, et al. Measurement of optic disc size and rim area with spectral-domain OCT and scanning laser ophthalmoscopy. *Invest Ophthalmol Vis Sci.* (2012) 53:4519–30. doi: 10.1167/iovs.11-8362
20. Mo J, Duan AL, Chan SY, Wang XF, Wei WB. Application of optical coherence tomography angiography in assessment of posterior scleral reinforcement for pathologic myopia. *Int J Ophthalmol.* (2016) 9:1761–5. doi: 10.18240/ijo.2016.12.10
21. Wong CW, Phua V, Lee SY, Wong TY, Cheung CM. Is choroidal or scleral thickness related to myopic macular degeneration? *Invest Ophthalmol Vis Sci.* (2017) 58:907–13. doi: 10.1167/iovs.16-20742
22. Ohsugi H, Ikuno Y, Shoujou T, Oshima K, Ohsugi E, Tabuchi H. Axial length changes in highly myopic eyes and influence of myopic macular complications in Japanese adults. *PLoS ONE.* (2017) 12:e0180851. doi: 10.1371/journal.pone.0180851

23. Wong YL, Sabanayagam C, Wong CW, Cheung YB, Man REK, Yeo AC, et al. Six-year changes in myopic macular degeneration in adults of the singapore epidemiology of eye diseases study. *Invest Ophthalmol Vis Sci.* (2020) 61:14. doi: 10.1167/iovs.61.4.14
24. Liu Y, Wang L, Xu Y, Pang Z, Mu G. The influence of the choroid on the onset and development of myopia: from perspectives of choroidal thickness and blood flow. *Acta Ophthalmol.* (2021). doi: 10.1111/aos.14773. [Epub ahead of print].
25. Zhou X, Ye C, Wang X, Zhou W, Reinach P, Qu J. Choroidal blood perfusion as a potential "rapid predictive index" for myopia development and progression. *Eye Vis.* (2021) 8:1. doi: 10.1186/s40662-020-00224-0
26. Gupta P, Thakku S, Saw S, Tan M, Lim E, Tan M, et al. Characterization of choroidal morphologic and vascular features in young men with high myopia using spectral-domain optical coherence tomography. *Am J Ophthalmol.* (2017) 177:27–33. doi: 10.1016/j.ajo.2017.02.001
27. Flores-Moreno I, Lugo F, Duker J, Ruiz-Moreno J. The relationship between axial length and choroidal thickness in eyes with high myopia. *Am J Ophthalmol.* (2013) 155:314–9.e311. doi: 10.1016/j.ajo.2012.07.015
28. Fledelius H, Jacobsen N, Li X, Goldschmidt E. Choroidal thickness at age 66 years in the Danish high myopia study cohort 1948 compared with follow-up data on visual acuity over 40 years: a clinical update adding spectral domain optical coherence tomography. *Acta Ophthalmol.* (2018) 96:46–50. doi: 10.1111/aos.13659
29. Nickla DL, Totonelly K. Choroidal thickness predicts ocular growth in normal chicks but not in eyes with experimentally altered growth. *Clin Exp Optom.* (2015) 98:564–70. doi: 10.1111/cxo.12317
30. Wu H, Zhang G, Shen M, Xu R, Wang P, Guan Z, et al. Assessment of choroidal vascularity and choriocapillaris blood perfusion in anisomyopic adults by SS-OCT/OCTA. *Invest Ophthalmol Vis Sci.* (2021) 62:8. doi: 10.1167/iovs.62.1.8
31. Zheng F, Chua J, Ke M, Tan B, Yu M, Hu Q, et al. Quantitative OCT angiography of the retinal microvasculature and choriocapillaris in highly myopic eyes with myopic macular degeneration. *Br J Ophthalmol.* (2021). doi: 10.1136/bjophthalmol-2020-317632. [Epub ahead of print].
32. Al-Sheikh M, Phasukkijwatana N, Dolz-Marco R, Rahimi M, Iafe N, Freund K, et al. Quantitative OCT angiography of the retinal microvasculature and the choriocapillaris in myopic eyes. *Invest Ophthalmol Vis Sci.* (2017) 58:2063–9. doi: 10.1167/iovs.16-21289
33. Wu H, Chen W, Zhao F, Zhou Q, Reinach P, Deng L, et al. Scleral hypoxia is a target for myopia control. *Proc Natl Acad Sci USA.* (2018) 115:E7091–100. doi: 10.1073/pnas.1721443115
34. Zhou X, Zhang S, Zhang G, Chen Y, Lei Y, Xiang J, et al. Increased choroidal blood perfusion can inhibit form deprivation myopia in guinea pigs. *Invest Ophthalmol Vis Sci.* (2020) 61:25. doi: 10.1167/iovs.61.13.25
35. Nishida Y, Fujiwara T, Imamura Y, Lima L, Kurosaka D, Spaide R. Choroidal thickness and visual acuity in highly myopic eyes. *Retina.* (2012) 32:1229–36. doi: 10.1097/IAE.0b013e318242b990
36. Shao L, Xu L, Wei W, Chen C, Du K, Li X, et al. Visual acuity and subfoveal choroidal thickness: the Beijing Eye Study. *Am J Ophthalmol.* (2014) 158:702–9.e701. doi: 10.1016/j.ajo.2014.05.023
37. Flores-Moreno I, Ruiz-Medrano J, Duker J, Ruiz-Moreno J. The relationship between retinal and choroidal thickness and visual acuity in highly myopic eyes. *Br J Ophthalmol.* (2013) 97:1010–3. doi: 10.1136/bjophthalmol-2012-302836
38. Shen Z, Zhang Z, Zhang L, Li Z, Chu R. Posterior scleral reinforcement combined with patching therapy for pre-school children with unilateral high myopia. *Graefes Arch Clin Exp Ophthalmol.* (2015) 253:1391–5. doi: 10.1007/s00417-015-2963-9
39. Zhang X, Qiao L, Li X, Ma N, Li M, Guan Z, et al. A preliminary study on macular retinal and choroidal thickness and blood flow change after posterior scleral reinforcement by optical coherence tomography angiography. *Chin J Ophthalmol.* (2017) 53:39–45. doi: 10.3760/cma.j.issn.0412-4081.2017.01.008
40. Wallman J, Wildsoet C, Xu A, Gottlieb M, Nickla D, Marran L, et al. Moving the retina: choroidal modulation of refractive state. *Vis Res.* (1995) 35:37–50. doi: 10.1016/0042-6989(94)E0049-Q
41. Wildsoet C, Wallman J. Choroidal and scleral mechanisms of compensation for spectacle lenses in chicks. *Vis Res.* (1995) 35:1175–94. doi: 10.1016/0042-6989(94)00233-C
42. Nickla D, Zhu X, Wallman J. Effects of muscarinic agents on chick choroids in intact eyes and eyecups: evidence for a muscarinic mechanism in choroidal thinning. *Ophthalmic Physiol Opt.* (2013) 33:245–56. doi: 10.1111/opo.12054
43. Nickla D, Totonelly K, Dhillon B. Dopaminergic agonists that result in ocular growth inhibition also elicit transient increases in choroidal thickness in chicks. *Exp Eye Res.* (2010) 91:715–20. doi: 10.1016/j.exer.2010.08.021
44. Lan W, Feldkaemper M, Schaeffel F. Bright light induces choroidal thickening in chickens. *Optom Vis Sci.* (2013) 90:1199–206. doi: 10.1097/OPX.0000000000000074

Conflict of Interest: The authors declare that the research was conducted in the absence of any commercial or financial relationships that could be construed as a potential conflict of interest.

frontiers in Medicine

ORIGINAL RESEARCH
published: 07 May 2021
doi: 10.3389/fmed.2021.657772

Optical Coherence Tomography Angiography-Based Quantitative Assessment of Morphologic Changes in Active Myopic Choroidal Neovascularization During Anti-vascular Endothelial Growth Factor Therapy

Yao Wang[1†], Zhongli Hu[2†], Tiepei Zhu[1], Zhitao Su[1], Xiaoyun Fang[1], Jijian Lin[1], Zhiqing Chen[1], Zhaoan Su[1], Panpan Ye[1], Jian Ma[1], Li Zhang[1], Jinyu Li[1], Lei Feng[1], Chuan-bin Sun[1], Zhiyong Zhang[1] and Xingchao Shentu[1*]*

[1] Eye Center of the Second Affiliated Hospital, School of Medicine, Zhejiang University, Hangzhou, China, [2] Department of Ophthalmology, Zhuji People's Hospital of Zhejiang Province, Zhuji, China

Purpose: To establish quantitative profile of the morphologic changes among patients with active myopic choroidal neovascularization (mCNV) before and after anti-vascular endothelial growth factor (VEGF) therapy using optical coherence tomography angiography (OCTA) to assess the therapeutic response.

Methods: Patients with active mCNV who received anti-VEGF injections between February 2017 to October 2020 and fit the study criteria were retrospectively reviewed. Quantitative analysis of their OCTA images were carried out to evaluate the morphologic features and vascular changes of mCNV lesions in response to anti-VEGF therapy. For further quantitative profiling, mCNV area, fractal dimension, vessel area, vessel density, vessel diameter, vessel length, vessel junction, junction density, and vessel tortuosity were obtained by means of advanced skeletonization postprocessing analyses.

Results: Thirty-one eyes of 29 consecutive patients with OCTA-positive mCNV lesions (mean spherical equivalent: −12.55 ± 3.24 diopters) were included. The 31 cases were divided into two phenotypes at baseline: organized interlacing pattern (83.87%) and disorganized vascular loops pattern (16.13%). The values of mCNV area, fractal dimension, vessel area, vessel length, vessel junction, and junction density decreased remarkably 1 month after the initial anti-VEGF injection ($p < 0.001$). Although, vessel density, vessel diameter, and vessel tortuosity increased meanwhile, only vessel diameter displayed statistical significance ($p = 0.027$). Of note, relative ratio analysis showed that vessel junction was the most sensitive biomarker in response to anti-VEGF therapy, reflecting a mean decrease of 50.36%. Sensitivity lowered successively in biomarkers of vessel length, vessel area, junction density, mCNV area, and fractal dimension. In addition, percent change of mCNV area ($r = 0.552$, $p = 0.002$), fractal

OPEN ACCESS

Edited by:
Xiangjia Zhu,
Fudan University, China

Reviewed by:
Zhaoyang Wang,
Shanghai Jiao Tong University, China
Han Zhang,
The First Affiliated Hospital of China Medical University, China
Royce Chen,
Columbia University Irving Medical Center, United States

***Correspondence:**
Yao Wang
wangyao@zju.edu.cn
Xingchao Shentu
stxc@zju.edu.cn

[†]These authors have contributed equally to this work and share first authorship

Specialty section:
This article was submitted to Ophthalmology, a section of the journal Frontiers in Medicine

Received: *24 January 2021*
Accepted: *06 April 2021*
Published: *07 May 2021*

Citation:
Wang Y, Hu Z, Zhu T, Su Z, Fang X, Lin J, Chen Z, Su Z, Ye P, Ma J, Zhang L, Li J, Feng L, Sun C-b, Zhang Z and Shentu X (2021) Optical Coherence Tomography Angiography-Based Quantitative Assessment of Morphologic Changes in Active Myopic Choroidal Neovascularization During Anti-vascular Endothelial Growth Factor Therapy. Front. Med. 8:657772. doi: 10.3389/fmed.2021.657772

dimension ($r = 0.446$, $p = 0.017$), vessel area ($r = 0.518$, $p = 0.005$), and vessel length ($r = 0.440$, $p = 0.019$) were moderately associated with that of central retinal thickness.

Conclusions: The study showed morphological as well as quantitative changes on OCTA responding to anti-VEGF treatment in mCNV patients, among which vessel junctions might be the most predictive biomarker. OCTA-based analysis, providing intuitive images and a large spectrum of quantitative data at the same time, could promote new insights into the therapeutic response assessment in mCNV patients.

Keywords: myopic choroidal neovascularization (mCNV), optical coherence tomography angiography (OCTA), skeletonization process, anti-vascular endothelial growth factor (VEGF) therapy, vessel junctions, quantitative biomarker

INTRODUCTION

It was estimated by World Health Organization that, by 2030, myopia would affect 3.36 billon people globally and present as the leading cause of vision impairment (1, 2). The number of people with high myopia projected from 399 million in 2020 (5.2% of global population) to 517 million in 2030 (6.1% of global population) (3). High myopia is defined as spherical equivalent (SE) more than −6 to −8 diopters in the context of eye elongation (ocular axial length ≥26.0–26.5 mm). Elongation of the axial length and posterior staphyloma drives the development of pathologic myopia (4). Pathologic myopia brings further irreversible vision challenges with possible complications including glaucoma, retinal detachment and myopic macular degeneration.

Myopic choroidal neovascularization (mCNV) originates in the choroid and distorts retinal anatomy and is normally classified as type 2 CNV, which is a common vision-threatening complication secondary to pathologic myopia. Approximately 5–11% of individuals with pathologic myopia will develop mCNV, especially those with patchy retinal atrophy, lacquer cracks and choroidal thinning. Development of chorioretinal atrophy around the regressed untreated-CNV lesion will lead to atrophic myopic maculopathy and poor vision prognosis (4–6). In recent years, the favorable safety and therapeutic outcomes promoted anti-vascular endothelial growth factor (VEGF) to be first-line treatment for subfoveal and juxtafoveal mCNV. Common practice includes a single intravitreal anti-VEGF injection (IVI), with a pro re nata (PRN) regimen during follow-up (4, 5).

Optical coherence tomography (OCT) has been successfully and widely used to diagnose and monitor treatment response in mCNV. Some OCT-based structural features have been recognized as traditional indicators of mCNV activity, such as retinal thickness, intraretinal fluid, and subretinal fluid (7, 8). Such biomarkers mainly reflect the secondary fluid-related consequences of CNV activity but lack direct evaluation of vascular pathology, let alone visualization of the choriocapillaries (9). Fluorescein angiography (FA), the gold standard to identify the presence and activity of mCNV, can also compromise details of neovascular network due to dye leakage (4, 10). Recently, the introduction of OCT angiography (OCTA) revolutionarily enables direct and meticulous visualization of CNV morphology through a non-invasive and dye-less approach, and enables quantitative assessment of neovascular structure and treatment response based on high-quality layered images (4). The sensitivity of OCTA to identify mCNV is 90–94% and the specificity is 93.75% (11–13). Previous literatures had reported qualitative manifestations of mCNV regression after anti-VEGF therapy in OCTA (14, 15), but only a few studies have described the quantitative changes. Among the quantitative investigators, Cheng et al. (15, 16) reported that significant decreases in mCNV area and flow area after one-month therapy of mCNV with ranibizumab or conbercept. However, OCTA parameters other than mCNV area or flow area were rarely discussed to reflect mCNV activity. As far as we are concerned, the morphological and quantitative data of OCTA had been successfully applied in patients with neovascular age-related macular degeneration (nAMD) to evaluate CNV activity, and treatment response, with thorough analysis on junction number/density, endpoint number/density, vessel length, etc., (17, 18). Therefore, it is reasonable to predict great scientific significance in an intensive quantitative investigation of mCNV with OCTA.

This study was designed to profile the quantitative changes of mCNV lesion during its most sensitive phase, namely the one dose loading phase, using OCTA and postprocessing technique, and to explore biomarkers from OCTA that could sensitively reflect the outcome of VEGF inhibition on the neovascular biology.

MATERIALS AND METHODS

This was a retrospective case series review of 31 eyes of 29 consecutive patients with mCNV who visited the Eye Center of the Second Affiliated Hospital, School of Medicine, Zhejiang University between February 2017 and October 2020. They received at least one dose injection of anti-VEGF agent (Conbercept 0.5 mg/0.05 ml or Ranibizumab 0.5 mg/0.05 ml) with at least a 6-month follow-up. This study followed the tenets of the Declaration of Helsinki and was approved by the Ethics Committee of the Second Affiliated Hospital, School of Medicine, Zhejiang University. Because of the retrospective nature of the study, patient consent for inclusion was waived.

Inclusion Criteria

The inclusion criteria were as follows: (1) myopia with spherical equivalent more than −6.0 diopters and/or the ocular axial length >26.5 mm (19, 20); (2) presence of myopic fundus changes as defined by the International Photographic Classification and Grading System for Myopic Maculopathy (2); (3) active and treatment-naïve CNV at baseline; (4) thorough ophthalmic examinations at baseline, including slit-lamp examination, dilated fundus examination with ophthalmoscope, intraocular pressure, refractive status, axial length, fundus photography, spectral-domain OCT (SD-OCT), OCTA, and FA. Activity status of mCNV at baseline was confirmed by FA and OCT. Active mCNV appeared as a dome-shaped elevation with a hyperreflective component above the retinal pigment epithelium with exudative signs including retinal thickening, intraretinal fluid and subretinal fluid on OCT imaging. FA typically revealed hyperfluorescent area in early frames indicative of filling of the neovascular complex, with late leakage into the mCNV area (4, 11). One month after anti-VEGF therapy, every patient was re-examined by OCT and OCTA. All images were reviewed for final inclusion by two independent retina specialists (YW and ZTS). Any discrepancies in the data were resolved through reassessment and discussion with a senior researcher (XYF).

Exclusion Criteria

We excluded patients with AMD, adult onset foveomacular vitelliform dystrophy, multifocal choroiditis, punctate inner choroidopathy, retinoschisis, or CNV caused by any other causes other than myopia. OCTA images with poor quality, such as projection artifacts from vessels located above the plane of the image or an overly dark image filled with extremely thick outer choroidal vessels, were excluded. Patients with history of intraocular surgery were excluded, such as pars plana vitrectomy.

Acquisition of Optical Coherence Tomography Angiography

OCTA images were obtained by a commercial SD-OCT system (RTVue-XR; Optovue, Inc., Freemont, CA). The instrument could delineate the microvascular structures of retina and choriocapillaries *via* a split spectrum amplitude-decorrelation angiography. The OCTA device with a light source centered on 840 nm and a bandwidth of 50 nm could operate with two consecutive 304 raster B-scans (each B-scan containing 304 A-scans). An A-scan rate of 70,000 scans per second with motion correction minimized artifacts arising from microsaccades and fixation changes. The OCTA software provided four *en face* images, including superficial capillary plexus, deep capillary plexus, outer retina, and choriocapillaris layers. Initially, the presence of mCNV with clear boundary was assessed on *en face* images generated by the automatically segmented choriocapillaris slab and the outer retina slab. Subsequently, the CUSTOM function in the AngioVue software (version 2018.1.0.43; Optovue, Inc.) was used for manual segmentation to acquire the entire thickness mCNV with the clearest boundary and the least perilesional artifact. The manual adjusted OCTA images were used for subsequent qualitative and quantitative analyses. Manual adjustment of segmentation changed the thickness and axial position of the OCTA slab to minimize inaccuracies in CNV contour (21).

Qualitative Evaluation of Optical Coherence Tomography Angiography Images

Two investigators independently analyzed the baseline OCTA images. On the basis of the overall appearance, mCNV lesions were classified into two phenotypes: organized interlacing pattern or disorganized vascular loops pattern, as previously reported (4, 11, 16). The morphology of the mCNV was qualitatively described based on five criteria (11, 14): (1) overall pattern, including organized interlacing and disorganized vascular loops patterns. (2) exuberant capillaries, numerous tiny capillary ramifications were typical of a recent lesion. (3) anastomoses and loops. (4) perilesional hypointense halo, local regions of choriocapillaris alteration encircling the CNV lesion. (5) feeder vessel. The well-defined organized interlacing lesions would be further classified into medusa, sea-fan or tree-in-bud patterns: medusa pattern corresponded to the lesion where vessels radiated in all directions from the center; sea-fan pattern corresponded to the lesion where vessels radiated in all directions from one side; tree-in-bud pattern corresponded to the round lesion without obvious vascular trunk (14, 16).

Quantitative Evaluation of Optical Coherence Tomography Angiography Images

To establish OCTA biomarkers for mCNV, we developed a CUSTOM MATLAB program (R2020b; MathWorks Inc., Natick, MA) to process OCTA images (**Figure 1**), as reported in previous studies (22). All OCTA images were binarized before quantitative analysis. Briefly, the boundary of mCNV area was manually outlined for further binarization. Firstly, the mCNV image was denoised using a Gaussian kernel. Then, a combined strategy with Frangi vesselness filter and local adaptive thresholding was applied to produce the final binary OCTA image. The following quantitative mCNV morphologic biomarkers were automatically calculated from both binary image and corresponding skeletonized image: mCNV area, vessel area, vessel length, vessel density, vessel diameter, and fractal dimension.

In addition, vessel junction, junction density, and vessel tortuosity were calculated using the image software (Image J, National Institutes of Health, USA), as described in published literature (23). Central retinal thickness (CRT) was automatically provided by OCT analysis, considered as a traditional OCT-based indicator of treatment response.

The OCTA metrics calculation based on skeletonized binary OCTA images were as follows:

1. mCNV area (mm^2): A lesion size biomarker that was calculated according to the manually outlined boundary of mCNV, indicating the entire size of mCNV lesion.
2. Vessel area (mm^2): A vessel size biomarker indicating the size of vessel components with flow signals in the lesion.

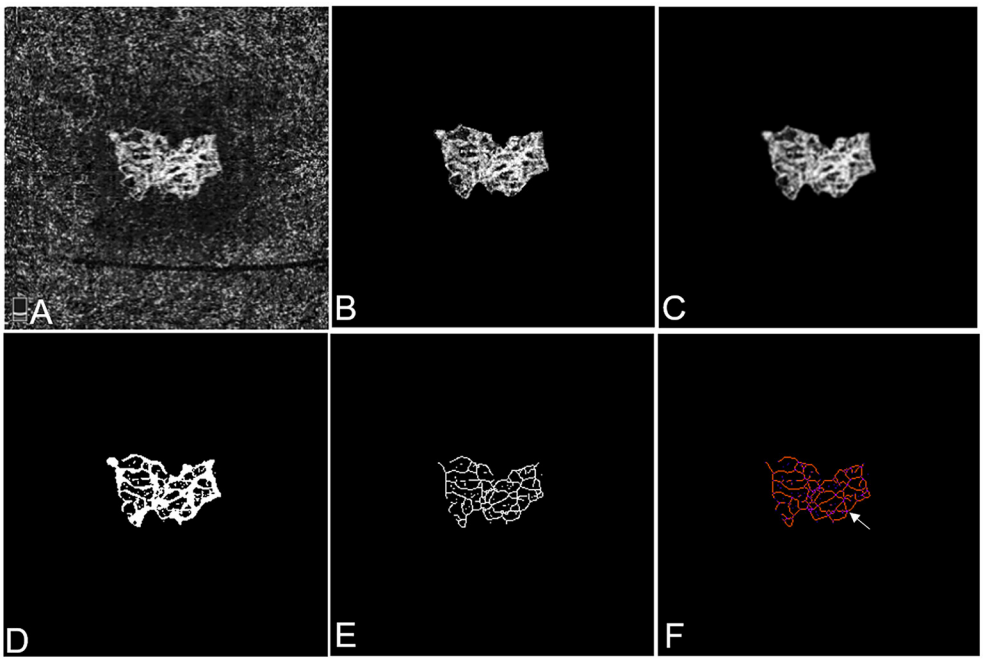

FIGURE 1 | Representative OCTA images of mCNV before and after cropping, binarisation, and skeletonisation in Patient #18, a 60-year-old female (refractive error −15.50 diopters) in the right eye. **(A)** OCTA image showing the entire thickness mCNV lesion after manual adjustment of segmentation. **(B)** The full extent of mCNV was manually delineated, and the mCNV area was measured by counting the pixels contained within the contour. **(C)** The Gaussian kernel was used to reduce the image noise and obtain a smooth image. **(D,E)** The binary OCTA image was formed by Frangi vesselness filter and local adaptive thresholding and used for calculating vessel area, fractal dimension and vessel lengths. Vessel density was calculated using vessel area and mCNV area. **(F)** Tagged Skeleton image was used to calculate the numbers of vessel junctions (white arrow). Junction density was calculated by dividing the vessel junction by the vessel length. Images **(B–E)** were acquired by MATLAB program and image **(F)** was acquired by IMAGE J software.

3. Vessel density: A vascular biomarker that was calculated as the percentage of the area occupied by vessels in the mCNV lesion.
4. Vessel length (mm): A vascular biomarker calculating the sum of Euclidean distances between the pixels of all the vessels in the CNV lesion, indicating the total neovascular length.
5. Vessel diameter (μm): A vascular biomarker that was calculated as the non-skeletonized vessel area divided by the skeletonized total vessel length, indicating the average vessel caliber of the mCNV.
6. Fractal dimension: A measure representing vessel branching complexity, which was obtained from the skeletonized binary image using the box-counting method. Higher fractal dimension values indicated more complex vessel branching pattern.
7. Vessel junction: A vascular biomarker that was defined as the points of vascular connections, indicating internal branching and anastomotic connections in vascular networks. It reflected the activity of CNV lesion.
8. Junction density (n/mm): A biomarker related to vessel branching complexity was calculated as the vessel junction number per unit vessel length. It could be interpreted as a measure of anastomotic activity in proportion to the total neovascular length, which also reflected the activity of CNV lesion.
9. Vessel tortuosity: A morphologic biomarker that quantified the microtortuosity of the CNV was calculated as the actual length of each branch divided by the imaginary straight length between two branch nodes (24). Smaller tortuosity values indicated straighter CNV vessels.

For subgroup analysis, subjects were further divided into two groups according to number of IVIs during the 6 months of follow-up, including "stable group" (one or two injections) vs. "unstable group" (more than two injections).

Statistical Analysis

Statistical analyses were performed using SPSS software (Windows version 21, SPSS Inc., Chicago, IL, USA). Descriptive statistics was expressed as mean ± standard deviation (SD). Normality tests of data distribution were assessed by Shapiro-Wilks test. Wilcoxon rank sum test was used to analysis the difference and relative ratio was used to evaluate the degree of variation between the baseline group and post-IVI group. Mann-Whitney *U*-test was used to evaluated the difference between the biomarkers in the "stable group" and "unstable group" at baseline. We used Spearman rank correlation coefficient (r, ranged from −1 to +1) (25) to evaluate the correlation between the percent change of OCTA-based biomarkers and

TABLE 1 | Demographic and morphologic characteristics of study population.

Patient characteristics ($n = 29$)	
Age, years, mean ± SD (range)	44.48 ± 12.51 (25∼67)
Sex (male/female)	12/17
Eye characteristics ($n = 31$)	
Mean SE, diopters, mean ± SD (range)	−12.55 ± 3.24 (−18.00∼-6.50)
Right eye	14
Left eye	17
Number of injections, mean ± SD	2.19 ± 0.87

SE, Spherical Equivalent.

CRT. Absolute magnitude of $r > 0.90$ was considered as "very strong correlation," 0.70–0.89 as "strong correlation," 0.40–0.69 as "moderate correlation," 0.10–0.39 as "weak correlation," and 0.00–0.09 as "negligible correlation." The significance level for all testing was set at $p < 0.05$.

RESULT

Baseline Clinical Characteristics of the Study Population

Thirty-one eyes (14 right eyes and 17 left eyes) of 29 patients (12 males and 17 females) with mCNV were included in this study. The mean age was 44.48 ± 12.51 years (ranged from 25 to 67 years old), the mean spherical equivalent was −12.55 ± 3.24 diopters (ranged from −6.50 diopters to −18.0 diopters), the mean IVI numbers were 2.19 ± 0.87 (ranged from 1 to 4). 19 and 10 eyes were classified into the stable and unstable groups, respectively. Baseline demographical and clinical characteristics are shown in **Table 1**.

Optical Coherence Tomography Angiography Characterization of Myopic Choroidal Neovascularization Morphology at Baseline

At the baseline OCTA examination in **Table 2**, the overall pattern of high-flow neovascular network could be categorized into two phenotypes: organized interlacing pattern and disorganized vascular loops pattern. In the first phenotype (26/31, 83.87%) (**Figures 2A,B**), OCTA images revealed a larger, well-circumscribed, interlacing type of neovascular membrane. This pattern comprised relatively exuberant capillary ramifications, anastomoses and loops, with a mean selected mCNV area of 0.44 ± 0.54 mm^2, a mean vessel junction number of 52.92 ± 47.84, and a mean junction density of 7.49 ± 1.69 /mm. Of note, the cases in this subgroup were further classified into medusa (12/26, 46.15%), sea-fan (3/26, 11.54%), and tree-in-bud (11/26, 42.31%) pattern.

In the second phenotype (5/31, 16.13%) (**Figures 3A,B**), OCTA images revealed a disorganized vascular loops pattern, consisting of a smaller vascular loop-like lesion, and unobvious capillary ramifications, with a mean selected mCNV area of 0.12 ± 0.09 mm^2, a mean vessel junction number of 16.67 ± 4.16 and a mean junction density of 7.11 ± 1.73 /mm. The mean values of the aforementioned three biomarkers were higher of the organized interlacing subgroup than that of the disorganized vascular loops subgroup, but the differences were not statistically significant (all $p > 0.05$).

Exuberant capillaries, anastomoses and loops, perilesional hypointense halo, and feeder vessel were identified in 26/31 (83.87%), 30/31 (96.77%), 25/31 (80.65%), and 6/31 (19.35%) cases, respectively. The 26 eyes with exuberant capillaries, and 6 eyes with visualization of feeder vessels were all included in the interlacing pattern subgroup. There were

TABLE 2 | Demographic characteristics and optical coherence tomography angiography features of patients with myopic choroidal neovascularization.

Pt No.	Age, years	Sex	Eye	SE, diopters	OP	EC	AL	HH	FV
1	58	F	L	−13.00	OI	Y	Y	N	Y
2	47	M	R	−15.50	OI	Y	Y	Y	N
3	67	F	R	−7.13	OI	Y	Y	Y	Y
4	52	F	R	−13.50	OI	Y	Y	Y	N
5	50	F	L	−12.63	OI	Y	Y	N	N
6	50	M	R	−10.88	OI	Y	Y	Y	Y
7	30	F	L	−13.50	OI	Y	Y	Y	Y
8^+	51	M	R	NA^{++}	OI	Y	Y	N	N
8^+			L	NA^{++}	DVL	N	Y	N	N
9	49	F	L	−13.25	OI	Y	Y	Y	N
10	31	F	L	−6.50	OI	Y	Y	Y	N
11^+	43	M	R	−7.75	OI	Y	Y	Y	Y
11^+			L	−9.13	OI	Y	Y	Y	N
12	25	F	L	−8.50	OI	Y	Y	Y	N
13	53	F	L	−8.50	OI	Y	Y	Y	N
14	57	F	R	−17.00	OI	Y	Y	Y	N
15	49	M	R	−14.75	OI	Y	Y	Y	N
16	37	M	L	−8.00	OI	Y	Y	Y	Y
17	35	M	L	−13.50	DVL	N	Y	Y	N
18	60	F	R	−15.50	OI	Y	Y	Y	N
19	30	F	L	−11.75	OI	Y	Y	Y	N
20	62	M	R	−11.25	OI	Y	Y	Y	N
21	28	F	L	−11.13	OI	Y	Y	Y	N
22	31	M	L	−7.00	OI	Y	Y	Y	N
23	34	F	L	−7.63	DVL	N	Y	N	N
24	58	F	L	−12.25	OI	Y	Y	Y	N
25	29	M	R	−9.88	DVL	N	N	N	N
26	35	M	R	−13.75	DVL	N	Y	Y	N
27	46	M	R	−18.00	OI	Y	Y	Y	N
28	27	F	R	−17.00	OI	Y	Y	Y	N
29	66	F	L	−10.75	OI	Y	Y	Y	N

Pt No., patient number; SE, Spherical Equivalent; OP, Overall Pattern; OI, Organized Interlacing; DVL, Disorganized Vascular Loops; EC, Exuberant Capillaries; AL, Anastomoses and Loops; HH, Hypointense Halo; FV, Feeder Vessel; F, Female; M, Male; R, Right eye; L, Left eye; N, No; Y, Yes; 8^+ and 11^+ mean that two eyes of each patient were included; NA^{++} means that we didn't obtain the diopter of eye, but axial length of right eyeball was 30.59 mm and axial length of right eyeball was 29.84 mm.

no significant differences between the two subgroups in age, sex, mean spherical equivalent, and injection number (all $p > 0.05$).

Optical Coherence Tomography Angiography Quantitative Analysis of Myopic Choroidal Neovascularization Lesion Before and After Anti-VEGF Therapy

Twenty-nine eyes were included for quantitative comparisons of the OCTA-based biomarkers associated with mCNV morphology before and after anti-VEGF therapy, as shown in **Table 3**. Two eyes with unidentifiable mCNV lesion after anti-VEGF therapy were excluded: one patient due to full disappearance of mCNV and in another due to ill-defined boundaries of the mCNV induced by projection artifacts. One month after anti-VEGF therapy, the mCNV size intuitively decreased, and the vessels of mCNV shrunk in OCTA images (**Figures 2C,D**, **3C,D**). Furthermore, the small-diameter vessels decreased or even disappeared, and the main or larger-diameter vessels were still present. The mean values of mCNV area, fractal dimension, vessel area, vessel length, vessel junction, junction density, and CRT decreased, while the mean values of vessel density, vessel diameter and vessel tortuosity increased. We found significant differences in mCNV area, fractal dimension, vessel diameter, vessel area, vessel length, vessel junction, junction density, and CRT between baseline and post-IVI group (all $p < 0.05$). Moreover, the mean values of OCTA-based biomarkers in "stable group" were lower than that in "unstable group" except vessel density and junction density, although, there were no statistical differences.

Relative ratio was calculated to indicate the percentage of biomarker change after anti-VEGF therapy (**Table 3**). The mCNV area, fractal dimension, vessel area, vessel length, vessel junction, junction density, and CRT decreased by 30.00, 12.04, 35.00, 37.07, 50.36, 32.31, and 18.74%, respectively, while vessel density, vessel diameter, and vessel tortuosity increased by 1.82, 20.44, and 7.93%, respectively.

Correlation of Optical Coherence Tomography Angiography-Based Biomarkers and Optical Coherence Tomography-Based Central Retinal Thickness

When the morphological OCTA-based biomarkers and structural therapeutic response expressed by OCT-based CRT were correlated, we found that there was statistically significant moderate correlation between the percent changes of four OCTA-based biomarkers (mCNV area, fractal dimension, vessel area and vessel length) and that of CRT ($r = 0.552$, $p = 0.002$ for mCNV area; $r = 0.446$, $p = 0.017$ for fractal dimension; $r = 0.518$, $p = 0.005$ for vessel area; $r = 0.440$, $p = 0.019$ for vessel length) (**Table 4**).

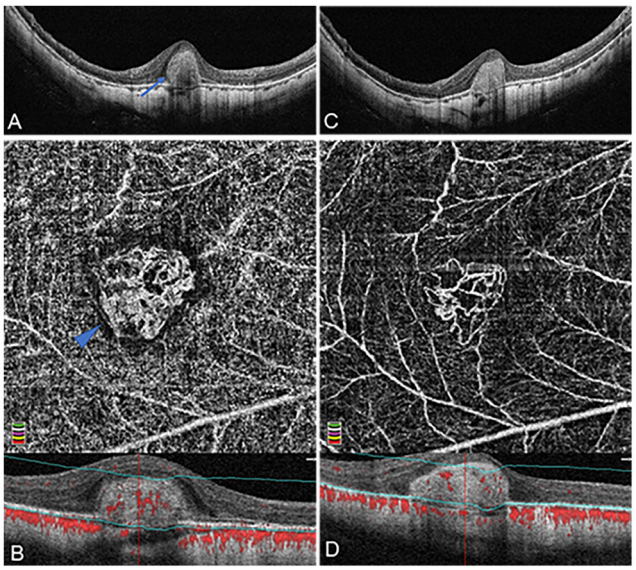

FIGURE 2 | Organized interlacing pattern of active mCNV imaged by OCT and OCTA before and after anti-VEGF injection in Patient #15, a 49-year-old man (refractive error −14.75 diopters) in the right eye. OCTA segmentation was manually adjusted to acquire a clear *en face* image visualizing the entire thickness mCNV lesion. **(A)** Spectral-domain OCT B-scan at baseline showed a typical subretinal hyper-reflective type-2 CNV (blue arrow) with discontinuous retinal pigment epithelium (RPE). **(B)** OCTA *en face* image (3 × 3 mm) at baseline depicted a larger, well-circumscribed, interlacing type of neovascular membrane. This mCNV lesion contained numerous tiny capillary ramifications, anastomoses and loops, which was bordered by a dark halo, showing a medusa shape (blue arrowhead). **(C)** One month after the first injection, OCT image revealed significant shrinkage of CNV lesion with a clearer contour. **(D)** One month after the first injection, OCTA *en face* image (3 × 3 mm) indicated a reduction of CNV size, anastomoses, and perilesional halo, a dramatic attenuation of capillaries and small caliber vessels, and a reservation of large caliber vessels. The lower parts of image **(B,D)** represented the cross-sectional structural OCT images corresponding to the upper OCTA *en face* images, respectively, displaying the boundaries (green lines) of the OCTA slabs after manual adjustment of segmentation.

DISCUSSION

High myopia is the second leading cause of CNV following nAMD and mCNV brings further irreversible visual impairment. Without treatment, more than 90% of mCNV-affected eyes are likely to experience a progressive blindness within 10 years (26, 27). Traditional structural OCT-based hallmarkers associated with fluid are widely used in nAMD patients to evaluate the treatment response and disease activity in clinical routine, but unlike the CNV in nAMD, mCNV is generally less extensive and exudative. The subjective nature also makes it difficult to reach consensus between readers. With the emerging technique of OCTA, new quantitative biomarkers for a detailed characterization of CNV morphology and objective assessment of treatment response may become available (10, 15, 28). By setting and analyzing the diverse OCTA-based biomarkers, this retrospective study aimed to quantitatively

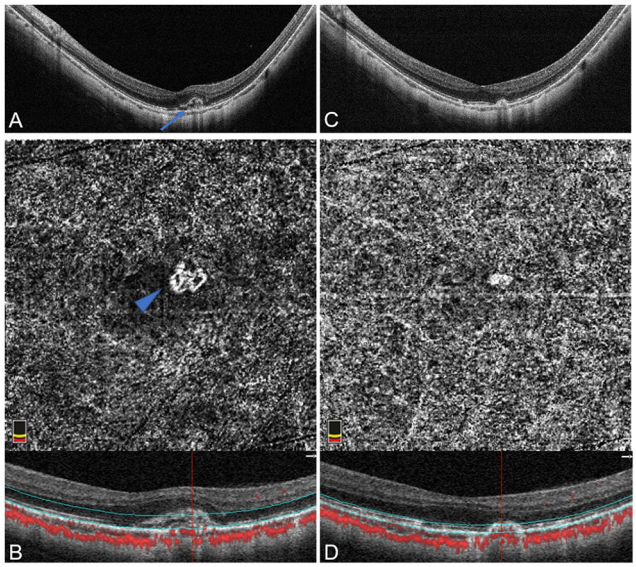

FIGURE 3 | Disorganized vascular loops pattern of active mCNV imaged by OCT and OCTA before and after anti-VEGF injection in Patient # 8, a 51-year-old man (axial length 29.84 mm) in the left eye. OCTA segmentation was manually adjusted to acquire a clear *en face* image visualizing the entire thickness mCNV lesion. **(A)** Spectral-domain OCT B-scan at baseline showed a small hyper-reflective type-2 CNV (blue arrow) beneath the neurosensory retina with fuzzy ellipsoid zone and discontinuous RPE. **(B)** OCTA *en face* image (3 × 3 mm) at baseline detected a small disorganized vascular loop-like lesion with unobvious capillary ramifications, suggesting an immature network (blue arrowhead). **(C)** One month after the first injection, OCT image revealed narrowing of mCNV lesion with a relatively clear ellipsoid zone. **(D)** One month after the first injection, OCTA *en face* image (3 × 3 mm) indicated an absence of vascular details due to the obviously attenuated mCNV lesion. The lower parts of image **(B,D)** represented the cross-sectional structural OCT images corresponding to the upper OCTA *en face* images, respectively, displaying the boundaries (green lines) of the OCTA slabs after manual adjustment of segmentation.

elucidate the mCNV biology and evaluate the therapeutic effect of IVI.

A clear and recognized classification of mCNV phenotypes on OCTA imaging has not been established. The morphology varies considerably associated with diverse factors such as stage and state of CNV lesions, as well as shape of the staphyloma. Querques et al. (28) enrolled 28 eyes with active and inactive mCNV, and defined two phenotypes of interlacing and tangled network on OCTA, which could partly reflect the activity of CNV lesion. Bruyère et al. (11) divided the active mCNV in 20 eyes (treatment-naïve and recurrent) into small disorganized vascular loops and larger organized interlacing pattern correlating with the vascular maturity, age, and treatment status. The mCNV cases included in our study were all active and treatment-naïve at baseline. We have distinguished two subtypes of mCNV similar to those reported by Bruyère et al.. At baseline, the mean mCNV area was 0.44 ± 0.54 mm^2 and the vessel area was 0.21 ± 0.20 mm^2, which were quite close to the results of Bruyère et al. The prevailing organized interlacing pattern was found to be larger and more branched than the disorganized vascular loops pattern but the differences were not statistically significant (all $p > 0.05$). Bruyère et al. hypothesized that the combination of morphology and size of the neovascular lesion, was correlated with maturity: while small, disorganized vascular loops pattern suggested an immature status, larger, highly structured interlacing pattern suggested a mature status. The above statuses might represent two sequential stages in the life cycle of mCNV development. Furthermore, mCNV completely vanished on OCTA after one anti-VEGF injection in one case of small disorganized vascular loop-like lesion in our study, which led to the speculation that the immature neovascular network would be more likely to achieve full regression.

In order to further quantitatively evaluate mCNV morphology, MATLAB, and IMAGE J were offered semiautomated analysis of several morphologic and spatial vessel biomarkers to assess the treatment response and the mCNV activity. The OCTA-based biomarkers included the mCNV area, fractal dimension, vessel area, vessel density, vessel diameter, vessel length, vessel tortuosity, vessel junction, and junction density, providing quantitative information about vessel area/density, branching pattern, and uniformity of the CNV microvasculature. The mean values of mCNV area, fractal dimension, vessel area, vessel length, vessel junction, and junction density were statistically different (all $p < 0.001$) between the baseline and post-IVI group. Compared with the baseline group, the six biomarkers decreased with a maximum change of 50.36% for vessel junction and a minimum change of 12.04% for fractal dimension, indicating significant reduction in lesion size, vascular complexity, and CNV activity after anti-VEGF therapy. Myopic CNV area and vessel area were the most frequently mentioned quantitative biomarkers in OCTA studies. Cheng et al. (15) reported that OCTA analyses revealed reduction of mCNV size, decrease of network density, and shrinkage of CNV vessels with reservation of large diameter vessels 1 month after anti-VEGF treatment. Giorno et al. (29) described that the mCNV area and vessel area reduced by almost half after anti-VEGF therapy. Those results were consistent with the changes of qualitative features and quantitative biomarkers in OCTA images of our study.

It is noteworthy that vessel junction was the most dramatically changed biomarker after anti-VEGF therapy, decreasing by 50.36%. Meanwhile, junction density decreased by 32.31%. Choi et al. (17) considered junction points to indicate internal branching and anastomotic connections in neovascular networks in nAMD. Reinhard et al. (10) suggested that the vessel junction number and/or junction density could be a measure for angiogenic vessel sprouting in nAMD; active CNV lesions would be expected to present a higher vessel junction number and/or junction density. Takeuchi et al. (30) analyzed 15 consecutive treatment-naïve eyes with typical nAMD, and found junction density was also significantly reduced after anti-VEGF therapy, suggesting that immature vessels had reduced and that the maturation of vessels proceeded despite blocking the VEGF pathway. In our study, the sprouting activity and complexity of mCNV

TABLE 3 | Quantitative biomarkers of the optical coherence tomography angiography for myopic choroidal neovascularization.

	Baseline	Post-IVI	*p*-Value	RR (%)
Quantitative biomarkers, mean (SD)				
mCNV area, mean (SD), mm^2	0.40 (0.52)	0.28 (0.41)	< 0.001	70.00
VA, mean (SD), mm^2	0.20 (0.20)	0.13 (0.14)	< 0.001	65.00
VLD, mean (SD)	0.55 (0.09)	0.56 (0.14)	0.829	102.82
FD, mean (SD)	1.08 (0.15)	0.95 (0.23)	< 0.001	87.96
VD, mean (SD), μm	31.11 (3.78)	37.47 (13.94)	0.027	120.44
VL, mean (SD), mm	6.96 (7.92)	4.38 (5.81)	< 0.001	62.93
VT, mean (SD)	1.26 (0.07)	1.36 (0.33)	0.276	107.93
VJ, mean (SD)	49.36 (47.43)	24.50 (28.25)	< 0.001	49.64
JD, mean (SD), n/mm	7.52 (1.65)	5.09 (2.26)	< 0.001	67.69
CRT, mean (SD), mm	316.75(72.72)	257.39(30.66)	< 0.001	81.26

mCNV, Myopic Choroidal Neovascularization; VA, Vessel Area; VLD, Vessel Density; VD, Vessel Diameter; VL, Vessel Length; VT, Vessel Tortuosity; VJ, Vessel Junction; JD, Junction Density; FD, Fractal Dimension; RR, relative ratio; IVI, Intravitreal anti-VEGF Injection.

lesions represented by vessel junction and junction density were significantly lower in the post-IVI group. Vessel junction number was confirmed the most sensitive indicator in response to anti-VEGF agents and could possibly be used as an indicator of disease activity and a predictive factor to assess treatment responses.

Similarly, high value of total vessel length was another biomarker assumed to characterize active CNV lesions with abundant angiogenesis (31). Vessel length decreased significantly after IVI in our study, which also verified the decline of neovascular activity and effectiveness of anti-VEGF therapy. Furthermore, Al-Sheikh et al. (32) depicted that fractal dimension was higher in active nAMD CNV than in quiescent CNV and found a reduced fractal dimension after treatment. They proposed that the pattern of the CNV lesion after treatment might be less complex due to the attenuation of small-caliber vessels that may have a less significant effect on the vessel density compared with the large mature vessels. In our mCNV patients, fractal dimension also decreased after treatment, suggesting the weakening of vessel complexity.

It was interesting to notice that vessel diameter increased remarkably by 20.44% after IVI ($p = 0.027$). A possible explanation was that IVI pruned back the newly growing vessels but could not affect the pericyte-covered larger vessels, and the higher flow in the remaining vascular network would stimulate vessels to extend. This hypothesis was supported by many researchers, who suggested that anti-VEGF injection might trigger major feeder vessels to grow larger with fewer branching points and more vascular anastomotic connections by pruning of angiogenic vascular sprouts (30, 33, 34). In addition, vessel density revealed a slight increase by 1.82% after IVI with no significant difference, as vessel area and mCNV area reduced by 35.00 and 30.00%, respectively. Vessel tortuosity, as a biomarker of vessel complexity, was rarely mentioned in CNV research, but increased retinal venular tortuosity had been recognized as an important biomarker to indicate the progression of diabetic retinopathy stages (24). Vessel tortuosity also showed a slight increasement by 7.93% in post-IVI group in ours study with inadequate statistical significance ($p = 0.276$). Further studies with a larger population will help to determine the clinical significance of OCTA-based vessel density and vessel tortuosity in mCNV patients.

Anti-VEGF is a safe and efficacious treatment option for mCNV, requiring only a limited number of injections to obtain good anatomic and functional results (35). Our patients received an average of 2.19 ± 0.87 intravitreal injections. Similarly, patients with mCNV received an average of 2.9 intravitreal injections in MYRROR study (36). It is worth noting that the biomarker values of mCNV in "stable group (≤2 injections)" were lower than those in "unstable group (>2 injections)" except vessel density and junction density at baseline. Unfortunately, there were no statistical difference for all OCTA-based biomarkers between the "stable group" and "unstable group" ($p > 0.05$). Choi et al. (17) divided 71 nAMD eyes into the stable and unstable groups, and reported the OCTA-based biomarkers (CNV area, CNV density, vessel length, and junction density), except end points, were not different between the two groups. Roberts et al. (35) divided 25 eyes with nAMD into "good responder" group and "poor responders" group, and concluded that there was no significant difference between any of the microvascular quantitative features, whose results were similar to ours.

The lesion responses to anti-VEGF therapy were expressed by percent change of newly-established OCTA-based biomarkers and that of frequently-used OCT-based CRT, and the correlation analysis between the two categories was performed. There was a moderate correlation between CRT and mCNV area, vessel area, and vessel length ($r = 0.552$, $p = 0.002$; $r = 0.518$, $p = 0.005$; $r = 0.440$, $p = 0.019$). This was expected because of the initial definitions of these biomarkers closely associated with mCNV volumes. This result further

TABLE 4 | The correlation analysis between the percent change of central retinal thickness and quantitative OCTA-based biomarkers in myopic choroidal neovascularization.

	PC (CRT)	
	r	*p*
PC (mCNV area)	0.552	0.002
PC (VA)	0.518	0.005
PC (VLD)	−0.251	0.197
PC (FD)	0.446	0.017
PC (VD)	−0.190	0.333
PC (VL)	0.440	0.019
PC (VT)	−0.152	0.467
PC (VJ)	0.357	0.062
PC (JD)	−0.090	0.649

mCNV, Myopic Choroidal Neovascularization; VA, Vessel Area; VLD, Vessel Density; VD, Vessel Diameter; VL, Vessel Length; VT, Vessel Tortuosity; VJ, Vessel Junction; JD, Junction Density; FD, Fractal Dimension; CRT, Central Retinal Thickness; PC means percent change defined as (post-IVI – baseline)/baseline.

validated the fundamental role of mCNV area and vessel area in OCTA quantitative analysis. A moderate correlation was also found between CRT and fractal dimension ($r = 0.446$, $p = 0.017$), indicating that the weakening of neovascular complexity partly accounted for the reduction of mCNV volume.

In our study, all of the biomarkers were measured in skeletonized binary OCTA images. Zhu et al. (22) used the same program to analyze the retinal vessels of diabetic retinopathy and reported that OCTA metrics obtained from skeletonized images were more effective than those from non-skeletonized images in detecting the retinal capillary. Segmentation errors were a challenging artifact for highly myopic patients, large chorioretinal atrophy areas, bad fixation, very long axial length, and deep posterior staphyloma induce inaccurate automatic layer segmentation on OCTA images. It is worth mentioning that manual segmentation in OCTA volumes increased sensitivity for CNV detection further from 53% to 92% (37). Arya et al. (21) also suggested that, automated segmentation algorithms of commercially available OCTA devices are limited in the identification and quantification of CNV lesions, and they emphasized the importance of manual adjustment of segmentation to visualize the full extent of CNV for detection and accurate area measurements. Consequently, we corrected correlation between the B-scan depth imaging and the OCTA by manually changing the boundaries of correctly contoured segmentation to obtain entire thickness mCNV.

The limitations of this study should be noted. Firstly, the follow-up period was relatively short and the number of subjects were relatively small. This may be one of the reasons why there was no statistical difference of the biomarkers between the "stable group" and "unstable group." Furthermore, this is a retrospective study and there may be a selection bias, a prospective analysis with larger number of subjects would help validate our results. Finally, measurement accuracy might be compromised by the semiautomated approach used to obtain the OCTA-based biomarkers, and the manually selected CNV area.

In conclusion, OCTA, which simultaneously provides functional (optical coherence tomography angiograms) and morphological (OCT B-scans and *en face*) information, is a promising imaging modality that facilitates physicians to characterize mCNV lesion, assess, and predict therapeutic response, and plan the follow-up treatment. We applied semiautomated postprocessing approach to obtain binarized and skeletonized OCTA images of mCNV lesion for fully quantitative analysis to elucidate the morphological changes of mCNV after anti-VEGF therapy. Vessel junction was regarded as the most sensitive indicator of the mCNV activity, and assumed to be the most helpful biomarker to predict early therapeutic response to anti-VEGF therapy. Further, studies on development of fully automated quantitative methods and establishment of recognized OCTA-based biomarkers are required to improve the clinical applicability of OCTA quantitative analysis on mCNV.

DATA AVAILABILITY STATEMENT

The raw data supporting the conclusions of this article will be made available by the authors, without undue reservation.

ETHICS STATEMENT

The study was approved by the ethics committee of the Second Affiliated Hospital, School of Medicine, Zhejiang University.

AUTHOR CONTRIBUTIONS

YW: conception, design, image interpretation, and manuscript preparation. XS: conception and design. ZH: data collection and analysis and manuscript preparation. TZ: development of the MATLAB program and image postprocessing. ZhiS: image interpretation and diagnosis. XF, JLin, ZC, ZhaS, PY, JM, LZ, JLi, LF, CS, and ZZ: patient treatment and data collection. All authors read and approved the final manuscript.

FUNDING

This work was supported by the Medical Scientific Research Foundation of Zhejiang Province, China (Grant No. 201130184) and National Natural Science Foundation of China (Grant No. 81100640).

ACKNOWLEDGMENTS

The authors wish to acknowledge the support of Eye Center of the second Affiliated Hospital, School of Medicine, Zhejiang University.

REFERENCES

1. World Health Organization. *World Report on Vision*. WHO (2019). https://www.who.int/publications-detail/world-report-on-vision (accessed October 8, 2019).
2. Ohno-Matsui K, Kawasaki R, Jonas JB, Cheung CM, Saw SM, Verhoeven VJ, et al. International photographic classification and grading system for myopic maculopathy. *Am J Ophthalmol.* (2015) 159:877–83.e7. doi: 10.1016/j.ajo.2015.01.022
3. Holden BA, Fricke TR, Wilson DA, Jong M, Naidoo KS, Sankaridurg P, et al. Global prevalence of myopia and high myopia and temporal trends from 2000 through 2050. *Ophthalmology.* (2016) 123:1036–42. doi: 10.1016/j.ophtha.2016.01.006
4. Ruiz-Medrano J, Montero JA, Flores-Moreno I, Arias L, García-Layana A, Ruiz-Moreno JM. Myopic maculopathy: Current status and proposal for a new classification and grading system (ATN). *Prog Retin Eye Res.* (2019) 69:80–115. doi: 10.1016/j.preteyeres.2018.10.005
5. Ohno-Matsui K, Ikuno Y, Lai TYY, Gemmy Cheung CM. Diagnosis and treatment guideline for myopic choroidal neovascularization due to pathologic myopia. *Prog Retin Eye Res.* (2018) 63:92–106. doi: 10.1016/j.preteyeres.2017.10.005
6. Cheung CMG, Ohno-Matsui K, Wong TY, Li T, Asmus F, Leal S. Influence of myopic macular degeneration severity on treatment outcomes with intravitreal aflibercept in the MYRROR study. *Acta Ophthalmol.* (2019) 97:e729–35. doi: 10.1111/aos.14035
7. Battaglia Parodi M, Iacono P, Bandello F. Correspondence of leakage on fluorescein angiography and optical coherence tomography parameters in diagnosis and monitoring of myopic choroidal neovascularization treated with bevacizumab. *Retina.* (2016) 36:104–9. doi: 10.1097/IAE.0000000000000684
8. Ohno-Matsui K, Lai TY, Lai CC, Cheung CM. Updates of pathologic myopia. *Prog Retin Eye Res.* (2016) 52:156–87. doi: 10.1016/j.preteyeres.2015.12.001
9. Schmidt-Erfurth U, Waldstein SM. A paradigm shift in imaging biomarkers in neovascular age-related macular degeneration. *Prog Retin Eye Res.* (2016) 50:1–24. doi: 10.1016/j.preteyeres.2015.07.007
10. Told R, Reiter GS, Mittermüller TJ, Schranz M, Reumueller A, Schlanitz FG, et al. Profiling neovascular age-related macular degeneration choroidal neovascularization lesion response to anti-vascular endothelial growth factor therapy using SSOCTA. *Acta Ophthalmol.* (2020) 99:e240–6. doi: 10.1111/aos.14554
11. Bruyère E, Miere A, Cohen SY, Martiano D, Sikorav A, Popeanga A, et al. Neovascularization secondary to high myopia imaged by optical coherence tomography angiography. *Retina.* (2017) 37:2095–101. doi: 10.1097/IAE.0000000000001456
12. Miyata M, Ooto S, Hata M, Yamashiro K, Tamura H, Akagi-Kurashige Y, et al. Detection of myopic choroidal neovascularization using optical coherence tomography angiography. *Am J Ophthalmol.* (2016) 165:108–14. doi: 10.1016/j.ajo.2016.03.009
13. Querques G, Corvi F, Querques L, Souied EH, Bandello F. Optical coherence tomography angiography of choroidal neovascularization secondary to pathologic myopia. *Dev Ophthalmol.* (2016) 56:101–6. doi: 10.1159/000442800
14. Cohen SY, Tabary S, El Ameen A, Mrejen S, Quentel G, Giocanti-Auregan A. Vascular remodeling of choroidal neovascularization in older myopic patients treated with ranibizumab. *Graefes Arch Clin Exp Ophthalmol.* (2019) 257:485–93. doi: 10.1007/s00417-018-04205-x
15. Cheng Y, Li Y, Huang X, Qu Y. Application of optical coherence tomography angiography to assess anti-vascular endothelial growth factor therapy in myopic choroidal neovascularization. *Retina.* (2019) 39:712–8. doi: 10.1097/IAE.0000000000002005
16. Cheng LN, Lin YX, Liu L, Zhang XH, Xue YQ, Zhou SD, et al. Assessment of conbercept therapy for high myopia macular neovascularization by optical coherence tomography angiography. *Sci Rep.* (2020) 10:16959. doi: 10.1038/s41598-020-74073-1
17. Choi M, Kim SW, Yun C, Oh J. OCT angiography features of neovascularization as predictive factors for frequent recurrence in age-related macular degeneration. *Am J Ophthalmol.* (2020) 213:109–19. doi: 10.1016/j.ajo.2020.01.012
18. Reiter GS, Told R, Baratsits M, Hecht A, Schlanitz FG, Sacu S, et al. Repeatability and reliability of quantitative fundus autofluorescence imaging in patients with early and intermediate age-related macular degeneration. *Acta Ophthalmol.* (2019) 97:e526–e32. doi: 10.1111/aos.13987
19. Choy BNK, You Q, Zhu MM, Lai JSM, Ng ALK, Wong IYH. Prevalence and associations of myopia in Hong Kong primary school students. *Jpn J Ophthalmol.* (2020) 64:437–49. doi: 10.1007/s10384-020-00733-4
20. Ohno-Matsui K, Jonas JB, Spaide RF. Macular bruch membrane holes in choroidal neovascularization-related myopic macular atrophy by swept-source optical coherence tomography. *Am J Ophthalmol.* (2016) 162:133–9.e1. doi: 10.1016/j.ajo.2015.11.014
21. Arya M, Rebhun CB, Cole ED, Sabrosa AS, Arcos-Villegas G, Louzada RN, et al. Visualization of choroidal neovascularization using two commercially available spectral domain optical coherence tomography angiography devices. *Retina.* (2019) 39:1682–92. doi: 10.1097/IAE.0000000000002241
22. Zhu TP, Li EH, Li JY, Dai XZ, Zhang HN, Chen BB, et al. Comparison of projection-resolved optical coherence tomography angiography-based metrics for the early detection of retinal microvascular impairments in diabetes mellitus. *Retina.* (2020) 40:1783–92. doi: 10.1097/IAE.0000000000002655
23. Schindelin J, Arganda-Carreras I, Frise E, Kaynig V, Longair M, Pietzsch T, et al. Fiji: an open-source platform for biological-image analysis. *Nat Methods.* (2012) 9:676–82. doi: 10.1038/nmeth.2019
24. Lee H, Lee M, Chung H, Kim HC. Quantification of retinal vessel tortuosity in diabetic retinopathy using optical coherence tomography angiography. *Retina.* (2018) 38:976–85. doi: 10.1097/IAE.0000000000001618
25. Schober P, Boer C, Schwarte LA. Correlation coefficients: appropriate use and interpretation. *Anesth Analg.* (2018) 126:1763–8. doi: 10.1213/ANE.0000000000002864
26. Neelam K, Cheung CM, Ohno-Matsui K, Lai TY, Wong TY. Choroidal neovascularization in pathological myopia. *Prog Retin Eye Res.* (2012) 31:495–525. doi: 10.1016/j.preteyeres.2012.04.001
27. Tan NW, Ohno-Matsui K, Koh HJ, Nagai Y, Pedros M, Freitas RL, et al. Long-term outcomes of ranibizumab treatment of myopic choroidal neovascularization in east-asian patients from the radiance study. *Retina.* (2018) 38:2228–38. doi: 10.1097/IAE.0000000000001858
28. Querques L, Giuffrè C, Corvi F, Zucchiatti I, Carnevali A, De Vitis LA, et al. Optical coherence tomography angiography of myopic choroidal neovascularisation. *Br J Ophthalmol.* (2017) 101:609–15. doi: 10.1136/bjophthalmol-2016-309162
29. Giorno P, Iacono P, Scarinci F, Di Renzo A, Varano M, Parravano M. Microvasculature changes of myopic choroidal neovascularization and the predictive value of feeder vessel disappearance after ranibizumab treatment revealed using optical coherence tomography angiography. *Ophthalmologica.* (2020) 243:263–70. doi: 10.1159/000504755
30. Takeuchi J, Kataoka K, Ito Y, Takayama K, Yasuma T, Kaneko H, et al. Optical coherence tomography angiography to quantify choroidal neovascularization in response to aflibercept. *Ophthalmologica.* (2018) 240:90–8. doi: 10.1159/000487611
31. Spaide RF. Optical coherence tomography angiography signs of vascular abnormalization with antiangiogenic therapy for choroidal neovascularization. *Am J Ophthalmol.* (2015) 160:6–16. doi: 10.1016/j.ajo.2015.04.012
32. Al-Sheikh M, Iafe NA, Phasukkijwatana N, Sadda SR, Sarraf D. Biomarkers of neovascular activity in age-related macular degeneration using optical coherence tomography angiography. *Retina.* (2018) 38:220–30. doi: 10.1097/IAE.0000000000001628
33. Pilotto E, Frizziero L, Daniele AR, Convento E, Longhin E, Guidolin F, et al. Early OCT angiography changes of type 1 CNV in exudative AMD treated with anti-VEGF. *Br J Ophthalmol.* (2019) 103:67–71. doi: 10.1136/bjophthalmol-2017-311752
34. Grunwald JE, Daniel E, Huang J, Ying GS, Maguire MG, Toth CA, et al. Risk of geographic atrophy in the comparison of age-related macular degeneration treatments trials. *Ophthalmology.* (2014) 121:150–61. doi: 10.1016/j.ophtha.2013.08.015

35. Roberts PK, Nesper PL, Gill MK, Fawzi AA. Semiautomated quantitative approach to characterize treatment response in neovascular age-related macular degeneration: a real-world study. *Retina*. (2017) 37:1492–8. doi: 10.1097/IAE.0000000000001400
36. Ikuno Y, Ohno-Matsui K, Wong TY, Korobelnik JF, Vitti R, Li T, et al. Intravitreal Aflibercept Injection in Patients with Myopic Choroidal Neovascularization: The MYRROR Study. *Ophthalmology*. (2015) 122:1220–7. doi: 10.1016/j.ophtha.2015.01.025
37. Babiuch AS, Uchida A, Figueiredo N, Hu M, Khan M, Srivastava SK, et al. Impact of optical coherence tomography angiography review strategy on detection of choroidal neovascularization. *Retina*. (2020) 40:672–8. doi: 10.1097/IAE.0000000000002443

Conflict of Interest: The authors declare that the research was conducted in the absence of any commercial or financial relationships that could be construed as a potential conflict of interest.

The handling editor is currently organizing a Research Topic with one of the authors XS.

frontiers in Medicine

ORIGINAL RESEARCH
published: 17 May 2021
doi: 10.3389/fmed.2021.619767

Assessment of the Macular Microvasculature in High Myopes With Swept Source Optical Coherence Tomographic Angiography

Chee-Wai Wong [1,2†], Saiko Matsumura [1†], Hla Myint Htoon [1,2], Shoun Tan [3], Colin S. Tan [1,2,3], Marcus Ang [1,2], Yee-Ling Wong [1,4,5], Rupesh Agrawal [1,2,3], Charumati Sabanayagam [1,2] and Seang-Mei Saw [1,2,4]*

[1] Singapore National Eye Centre, Singapore Eye Research Institute, Singapore, Singapore, [2] Duke-NUS Medical School, Singapore, Singapore, [3] National Healthcare Group Eye Institute, Tan Tock Seng Hospital, Singapore, Singapore, [4] Saw Swee Hock School of Public Health, National University of Singapore, Singapore, Singapore, [5] R&D Vision Sciences Asia, Middle East, Russia and Africa (AMERA), Essilor International, Singapore, Singapore

OPEN ACCESS

Edited by:
Xingchao Shentu,
Zhejiang University, China

Reviewed by:
Yi-Ting Hsieh,
National Taiwan University Hospital, Taiwan
Hua Zhong,
Kunming Medical University, China

***Correspondence:**
Seang-Mei Saw
ephssm@nus.edu.sg

[†]These authors share first authorship

Specialty section:
This article was submitted to Ophthalmology, a section of the journal Frontiers in Medicine

Received: 21 October 2020
Accepted: 20 April 2021
Published: 17 May 2021

Citation:
Wong C-W, Matsumura S, Htoon HM, Tan S, Tan CS, Ang M, Wong Y-L, Agrawal R, Sabanayagam C and Saw S-M (2021) Assessment of the Macular Microvasculature in High Myopes With Swept Source Optical Coherence Tomographic Angiography. Front. Med. 8:619767. doi: 10.3389/fmed.2021.619767

Background: The risk of pathologic myopia (PM) increases with worsening myopia and may be related to retinal microvasculature alterations. To evaluate this, we analyzed the macular microvasculature of myopes with swept source-optical coherence tomographic angiography (SS-OCTA) in adolescent and young adult Singaporeans.

Methods: This is a prevalent case-control study including 93 young Chinese from the Strabismus, Amblyopia and Refractive error in Singaporean children (STARS, $N = 45$) study and the Singapore Cohort Study of Risk Factors for Myopia (SCORM, $N = 48$) studies. Macular vessel density (VD) measurements were obtained from 3×3 mm SS-OCTA scans and independently assessed using ImageJ. These measurements were compared between individuals with non-high myopia [non-HM, $N = 40$; SE >-5.0 diopter (D)] and HM (SE ≤-5.0D, $N = 53$).

Results: The mean macular VD was $40.9 \pm 0.6\%$ and $38.2 \pm 0.5\%$ in the non-HM and HM, groups, respectively ($p = 0.01$ adjusted for age and gender). Mean FAZ area in the superficial layer was 0.22 ± 0.02 mm^2 in the HM group, which was smaller compared to non-HM group (0.32 ± 0.03 mm^2, $p = 0.04$). Mean deep FAZ area was similar between the two groups (0.45 ± 0.03 mm^2 and 0.48 ± 0.04 mm^2 in the HM and non-HM groups, respectively, $p = 0.70$).

Conclusions: VD was lower and superficial FAZ area was smaller, in adolescents and young adults with HM compared to non-HM. These findings require validation in prospective studies to assess their impact on the subsequent development of PM.

Keywords: high myopia, swept source OCT angiography, macular microvasculature, foveal avascular zone, macular vessel density

BACKGROUND

Pathologic myopia (PM) is a sight threatening condition seen in highly myopic eyes characterized by posterior staphyloma, chorioretinal atrophy, tractional maculopathy and choroidal neovascularization. It is a major cause of visual impairment and blindness in Asia and worldwide (1–3). The risk of PM increases with increasing degree of myopia (4, 5), but whether this increased risk is due to axial elongation or to alterations of the retinochoroidal vasculature or both is still unclear. Emerging evidence suggests the latter (6–11). Up till recently, methods of studying the vasculature have been either not sensitive enough to study the macular microvasculature (Color Doppler ultrasonography) (12, 13) or too invasive (indocyanine green angiography). Optical coherence tomographic angiography (OCTA) allows non-invasive and depth resolved imaging of the superficial and deep retinal vasculature (14, 15). These novel clinical tools may potentially help to accurately characterize the retinal vasculature in young high myopes and predict their risk of visual impairment in the future.

Several studies have studied retinal vascular changes in high myopes compared to emmetropes or non-high myopes (14–21). The vascular parameters studied include vascular branching (fractal dimensions), vessel density (VD), foveal avascular zone (FAZ) area and retinal blood flow. Most, but not all of these studies have found decreased retinal VD and vascular branching in high myopes. All of these studies were conducted using spectral domain OCTA (SD-OCTA) and were performed in hospital-based cohorts. Swept source OCTA (SS-OCTA) has higher depth penetration and lower signal drop off compared to spectral domain, and has been shown to offer some advantages in the imaging of high myopes with long axial length (AL) or deep posterior staphyloma (3). Measurement of retinal vascular parameters in high myopes using SS-OCTA may thus offer a different perspective compared to SD-OCTA. In addition, hospital-based cohorts are inherently different from population-based cohorts, in particular with respect to selection bias where cases selected into a hospital setting may have more severe disease than similar cases from the community, or where controls from a hospital setting may have other co-existing conditions which are not present in participants from the general population.

To address these gaps, we conducted this study to evaluate the macular microvasculature with SS-OCTA in adolescent and young adult Singaporeans.

METHODS

We conducted a prevalent case-control study including participants from the last follow-up visit of two independent population-based studies: The Strabismus, Amblyopia and Refractive error in Singaporean children (STARS) and the Singapore Cohort Study of Risk Factors for Myopia (SCORM) studies. We included 93 children for the current study ($N = 45$ children aged 9–14 in 2017 from STARS and $N = 48$ aged 9–14 years in 2016 from SCORM). Only Chinese participants were included and none underwent refractive surgery.

The STARS study is a population-based survey of Chinese children aged 6–72 months residing in the government apartments in Singapore (22). Overall prevalence of myopia [Spherical Equivalent (SE) ≤-0.50 diopter (D)] and high myopia (HM) (SE ≤-6.00D) at baseline were 11.0% and 0.2%, respectively (23). Forty-seven children aged 9–14 years participated in a pilot 10-year recall study in 2017. A total of 45 subjects were included after excluding subjects without OCTA imaging ($N = 2$). The mean SE was −2.80D ± 1.72 (range, +1.55D to −6.10D). The proportion of myopia was 77.8% ($N = 35$). The proportion of HM and non-HM was 11.1% ($N = 5$) and 88.9% ($N = 40$), respectively.

The SCORM study, established in 1999, is the first myopia cohort study in Asia. Children aged 7–9 years were recruited and prior publications described the methodology of the SCORM study in detail (24). Fifty-two young adults with HM (SE ≤-5.00D) aged 22–26 years were followed up in 2016. A total of 48 Chinese subjects were considered eligible after excluding non-Chinese subjects ($N = 3$) and subjects without OCTA imaging ($N = 1$). All included subjects had HM. The mean SE was −7.43D ± 1.65 (range, −5.00D to −11.38D) in the SCORM study. Written informed consent was obtained from all participants in both the STARS and SCORM studies before each examination. The tenets of the Declaration of Helsinki were observed, and the study was reviewed and approved by the Ethics Committee of the Singapore Eye Research Institute.

Eye Measurements

Cycloplegic autorefraction was performed by trained eye professionals. Cycloplegia was induced with three drops of 1% cyclopentolate 5 min apart in the STARS study, and with two drops of 1% tropicamide 5 min apart in the SCORM study. At least 30 min after the last drop, five consecutive refraction and keratometry readings were measured using an autokeratorefractometer (model RK5; Canon, Inc., Ltd., Tochigiken, Japan).

Foveal Avascular Zone and Vessel Density Measurements

Swept-source optical coherence tomography (SS-OCT; DRI OCT Triton, Topcon, Japan) was obtained after pupil dilation. Both studies followed the same imaging protocol. The swept-source OCT-A images were all processed using the angiography ratio analysis (ARA) method (25). Volumetric OCT scans were acquired over a 3 mm × 3 mm field of view and each B-scan position was repeatedly scanned four times. Segmentation for the superficial vessel plexus (SVP) was performed with an inner boundary set at 3 μm beneath the internal limiting membrane (ILM) and the outer boundary was set at 15 μm beneath the inner plexiform layer (IPL). The deep vessel plexus (DVP) was segmented with an inner boundary at 15 μm beneath the IPL and the outer boundary at 70 μm beneath the IPL.

OCT-A scans of the superficial and deep retinal vasculature were exported and independently assessed by two trained graders using ImageJ (version 1.49, National Institutes of Health, Bethesda, MD, USA). Graders were masked to patient details. After the scale was set to 320 pixels/3 mm, superficial and

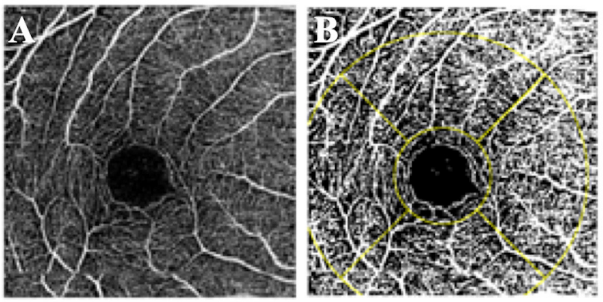

FIGURE 1 | Vessel density measurement. **(A)** OCT-A scan of the superficial retinal plexus. **(B)** Binarized image with the ETDRS grid overlaid over the fovea.

deep FAZ boundaries were manually traced by the graders as previously described (26), and the FAZ area were automatically calculated by the software. To determine VD, the image was converted to 8 bit and binarized using a pre-selected auto-thresholding method, Li Global Thresholding (**Figure 1**). Exported images from the device were first converted to 8-bit images (i.e., with 256 possible values per pixel). These were then automatically thresholded with the Li thresholding algorithm within ImageJ. The Li algorithm is an iterative technique which calculates a threshold *via* minimizing the local cross-entropy values (27). No manual input is required for this calculation. A grid comprising of the region of interest (ROI) was then demarcated around the central 1 and 3 mm Early Treatment Diabetic Retinopathy Study (ETDRS) subfields. The 3-mm zone was divided into superior, inferior, temporal, and nasal subfields. The vessel densities were obtained from each of these subfields. VD of each segment was defined as the arithmetic percentage of area occupied by retinal vessels in the thresholded image. This was automatically calculated and no additional manual input was required.

Statistical Analysis

Our main outcome measures were mean overall macular VD and mean FAZ area. SE was defined as sphere plus half negative cylinder. The participants were categorized into two groups: non-HM (SE >-5.0 D) and HM (SE ≤-5.0D). The right eye of each participant was analyzed. The differences in means were evaluated using independent *t*-tests. ANCOVA was performed, adjusted for age and gender, for the comparisons of FAZ area and VD between groups. Correlation between SE and microvascular parameters were analyzed with Pearson's correlation coefficient. Adjustments for multiple comparisons was made with Bonferroni correction. Statistical significance was set at $P = 0.05$. All statistical analyses were performed with SPSS (IBM Corp. IBM SPSS Statistics for Windows, Version 24.0. Armonk, NY: IBM Corp.).

RESULTS

Baseline Characteristics

A total of 93 participants (45 from the STARS study and 48 from the SCORM study) were included in the analysis. The participants were categorized into two groups: non-HM (SE >-5.0D, $N = 40$) and HM (SE ≤-5.0D, $N = 53$). The mean age was 22.9 ± 3.7 years (female, 43.4%) in HM group and 10.9 ± 1.6 years (female, 52.5%) in non-HM group ($p < 0.001$). The mean SE was −7.28D ± 1.64 and −2.42D ± 1.42 in HM group and non-HM group, respectively ($p < 0.001$).

Foveal Avascular Zone and Vessel Density

Mean superficial FAZ area was 0.32 ± 0.11 mm^2 and 0.22 ± 0.09 mm^2 in the non-HM and HM groups, respectively. Mean deep FAZ area was 0.45 ± 0.13 mm^2 and 0.48 ± 0.15 mm^2 in the HM and non-HM groups, respectively. In ANCOVA analysis for the difference of the FAZ area between the two groups, the superficial FAZ area was smaller, but of borderline significance, in the HM group than in the non-HM group after adjusting for age and gender ($p = 0.04$) (**Table 1**). **Table 2** shows that the difference in VD at various locations between the HM and the non-HM group. The mean overall macular VD was 40.9 ± 0.6% in non-HM group and 38.2 ± 0.5% in the HM group ($p = 0.01$ after adjusting for age and gender). There were no significant differences in the central, temporal, nasal, superior, and inferior VD after Bonferroni correction (**Table 2**). Both mean overall VD and superficial FAZ were positively correlated with more myopic SE (r = 0.56 and 0.46, respectively) (**Figure 2**).

DISCUSSION

In this study, we found decreased overall VD and smaller superficial FAZ area in high myopes compared with non-high myopes, independent of age and gender. Overall VD and superficial FAZ area correlated positively with more myopic SE. To our knowledge, this is one of the first studies utilizing SS-OCTA to measure macular VD in high myopes derived from population based cohorts.

To date, all of the OCTA studies of macular microvasculature in high myopes have been performed with SD-OCTA. One of our study objectives was to assess if the results of these studies could be validated using a SS-OCTA system. SS-OCTA is a relatively new development, with only two commercially available systems: PLEX Elite (PLEX Elite 9000, Version 1.6.0.21130; Carl Zeiss Meditec, Jena, Germany) based on optical microangiography (OMAG) and Triton (Topcon DRI OCT Triton Swept source OCT; Topcon, Tokyo, Japan) using the OCTA ratio analyses (OCTARA) algorithm. Both systems have demonstrated good reproducibility for macular VD measurements (28). Advantages of SS-OCTA imaging over SD-OCTA includes (29): (1) faster scan speeds allows for denser scans and larger scan areas compared with SD-OCT. A denser scan pattern will increase detection rate of flow signals within a given scan area. In addition, OCTA interprets flow as differences in signals between two consecutive OCT B scans separated in time, so a higher scan speed will facilitate detection flow signal in vessels where the flow rate is faster (30); (2) the longer wavelength and reduced sensitivity roll-off enhances detection of signals from the deeper retinal and choroidal layers; (3) the longer wavelength of SS-OCT is safer for the eye so a higher laser power can be used to penetrate the deeper vascular layers. In eyes with PM, SS-OCT was better than SD-OCT in

TABLE 1 | Difference of FAZ Area at different locations between high myopia and non-high myopia groups from both STARS study ($N = 45$) and SCORM study ($N = 48$).

	All participants ($N = 93$) Mean μ (SD)	High myopia ($N = 53$)Mean μ (se)	Non-high myopia ($N = 40$) Mean μ (se)	*P*
FAZ Area, mm^2				
Superficial	0.27 (0.01)	0.22 (0.02)	0.32 (0.03)	0.04
Deep	0.47 (0.2)	0.45 (0.03)	0.48 (0.04)	0.70

FAZ, Foveal avascular zone; SD, Standard deviation; se, standard error; μ, microns; mm, millimeter.
p-value: ANCOVA (adjusted for age and gender).

TABLE 2 | Difference of vessel density at different locations between high myopia and non-high myopia groups from both STARS study ($N = 43$) and SCORM study ($N = 42$).

	All participants ($N = 85$) Mean μ (SD)	High myopia ($N = 47$) Mean μ (se)	Non-high myopia ($N = 38$) Mean μ (se)	*P*	
Vessel density (%)					
Overall average	39.3 (5.6)	38.2 (0.5)	40.9 (0.6)	0.01	
	All participants ($N = 85$) Mean μ (SD)	**High myopia ($N = 47$) Mean μ (se)**	**Non-high myopia ($N = 38$) Mean μ (se)**	**Bonferroni uncorrected *P***	**Bonferroni corrected *P***
Vessel density (%)					
Central 1 mm	20.7 (5.2)	18.8 (1.2)	23.2 (1.4)	0.07	0.42
Temporal	36.4 (7.7)	33.6 (1.8)	40.0 (2.1)	0.07	0.43
Nasal	40.6 (8.6)	39.6 (2.0)	41.8 (2.4)	0.57	1.00
Superior	49.8 (8.1)	47.3 (1.7)	53.4 (2.0)	0.07	0.44
Inferior	39.3 (9.8)	39.9 (2.1)	38.5 (2.5)	0.74	1.00

SD, Standard deviation; se, standard error; μ, microns; mm, millimeter.
Uncorrected p-value: ANCOVA (adjusted for age and gender): Corrected p-value: Bonferroni correction for multiple comparisons of six measurements.

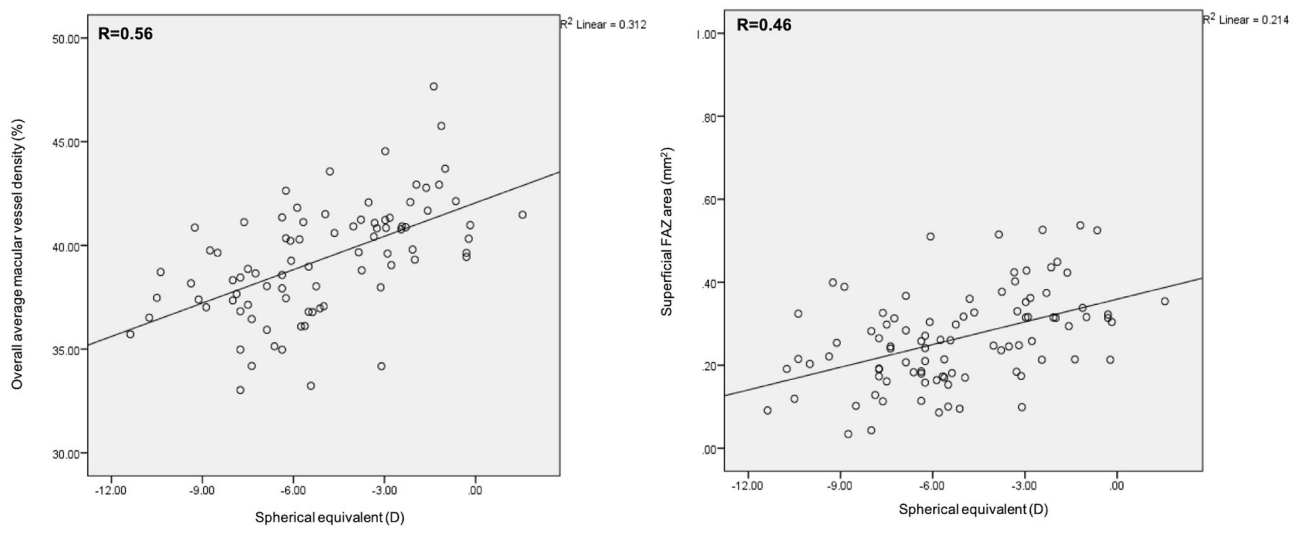

FIGURE 2 | Scatterplots of overall vessel density and superficial FAZ area with SE.

visualizing outer retinal anatomy, and revealed abnormalities not seen on SD-OCT along the posterior staphyloma walls (3). SS-OCTA was also better than SD-OCTA for visualization of the extent of choroidal neovascular complexes (31). This study was preformed because the advantages of SS-OCT, particularly in highly myopic eyes, may potentially enhance detection of retinal microvascular structures. Further studies are needed to confirm this.

Previous studies of the retinal microvasculature in high myopes using OCTA have shown inconsistent results. These

TABLE 3 | A summary of studies of the macular microvasculature in high myopes using optical coherence tomographic angiography.

Study	Sample size	Criteria	Age (years)	Refraction/axial length	Imaging modality	Retinal vascular parameter	Results
Yang et al. (14)	33 HM 47 mild myopes/EM	HM: <-6D Controls: +0.5 to −3D MMD excluded	18–40	−8.68 ± 1.87D/27.11 ± 1.27 mm	Optovue (SSADA) 3 × 3 mm	Fractal analysis of superficial, deep and whole macular vascular plexi	VD was significantly less in all layers in HM. AL was negatively correlated with vascular density
Li et al. (15)	20 HM 20 controls	HM: <-5D Controls: >-3D MMD excluded	28 ± 5	−6.31 ± 1.23D/26.44 ± 0.97 mm	Angioplex (OMAG) 3 × 3 mm, Retinal function imager	Fractal analysis and blood flow velocity	VD but not blood flow velocity was lower in HM, AL was negatively correlated with vascular density
Fan et al. (17)	28 HM 33 MM 30 Controls	HM: ≤-6D MM: ≤-3D and >-6D, Controls: <3D and >-3D MMD not excluded	36.3 ± 14.7	−11.63 ± 5.36D/29.01 ± 2.69 mm	Optovue (SSADA) 3 × 3 mm	Macular VD	Highest VD in Controls followed by MM and lowest in HM. VD associated with both AL and SE
Venkatesh et al. (20)	86 (AL range 21.77–32.28 mm)	1.75D to −20D MMD exclusion unclear	10–44	−7.17 ± 5.71D/25.95 ± 2.41 mm	Optovue (SSADA) 3 × 3 mm	Macular VD	Negative correlation between VD and AL, positive correlation with SE and visual acuity
Yang et al. (21)	81 mild myopia 117 MM 70 HM	HM: ≤-6D MM: ≤-3D and >-6D Controls: <3D and >-3D	18–32	–7.14 ± 0.94D/26.15 ± 0.93 mm	Optovue (SSADA) 3 × 3 mm	Macular VD	No difference in superficial or deep macular VD
Mo et al. (19)	45 EM 41 HM 45 PM	EM: 0.50D to −0.50D HM: ≤-6D, without MMD PM: ≤-6D and AL ≥26.5 mm with MMD	38.3 ± 13.1	HM: −6.90 ± 1.23D/25.93 ± 0.58 PM: –15.22 ± 3.79D/29.55 ± 1.73 mm	Optovue (SSADA) 3 × 3 mm	Macular VD	Compared with the EM group, VD in the macular and arcuate fiber region was 1. not decreased in the HM group. 2. decreased in the PM group AL was negatively correlated with both superficial and deep macular VD
Milani et al. (18)	42 HM 40 controls	HM: SE ≥-6D Controls: 0 ± 2D MMD excluded	51.85 ± 10.87	– 10.26 ± 3.83D	Optovue (SSADA) 3 × 3 mm	FAZ area Macular VD Outer retinal flow area	HM had lower whole superficial VD and higher flow area in the outer retina No difference in FAZ area. SE was positively correlated with superficial VD and negatively correlated with outer retina perfusion
Al Sheikh et al. (16)	50 HM 34 Controls	HM: ≤-6D and AL ≥26.5 mm MMD excluded	25–83	−8.29 ± 2.94D	Optovue (SSADA) 3 × 3 mm	Macular VD and fractal analysis	VD and fractal dimension of the retinal capillary microvasculature were significantly lower in myopic eyes

HM, high myopia; MM, moderate myopia; EM, emmetropia; PM, pathologic myopia; AL, axial length; D, diopter; SE, spherical equivalent; MMD, myopic macular degeneration; SSADA, split spectrum amplitude decorrelation angiography; OMAG, optical microangiography; FAZ, foveal avascular zone; VD, vessel density.

studies are summarized in **Table 3**. All of these studies were performed in hospital-based cohorts and were performed using 3 × 3 mm SD-OCTA scans. However, there is heterogeneity in terms of age, OCT instrument used and the methods by which VD was measured and calculated. Some studies included eyes with PM while others have excluded them. It is also unclear why high myopes were attending the eye clinic in these hospital based studies, and it is possible that some of these subjects had clinical pathology. Also, and most of these studies included more severe myopia than in our population based study (**Table 3**).

Most of these studies (14–18, 20), including ours, have found decreased macular VD in high myopes than non-high myopes or emmetropes. The most plausible explanation for a reduction in macular VD is the stretching of the macular microvasculature in axially elongated eyes, leading to reduced VD rather than a loss of perfusion. This hypothesis is supported by Li et al.'s findings of reduced macular VD but preserved blood flow velocity in high myopes (15). They also found that decreased VD was significantly correlated with refractive error but not AL. Thus, refractive error itself may represent a different mechanism, unrelated to ocular stretching, by which VD was reduced. Other studies that analyzed fractal dimensions, a measure of the branching complexity of the microvasculature, found reduced branching of the macular vasculature in high myopes (14–16). This finding is consistent with the hypothesis that retinal vessels are stretched with increasing AL.

A few studies have found the converse to be true. Venkatesh et al. described a positive correlation between the VD and flow area index in both the superficial and deep vessel plexus with increasing AL and myopic refraction (20). They postulated that thickening of the inner retinal layers and outer plexiform layers in eyes with longer AL and high myopic spherical refraction observed in their study might have resulted in the higher VD and flow area indices in both the superficial and deep vessel plexus with more severe myopia. Similar results were reported by Mo et al. whereby macular flow density did not differ between high myopes and emmetropes, but was negatively correlated with AL (19). In addition, they observed a decreased macular flow density in eyes with PM compared with HM and emmetropia. Both studies differed from ours in the inclusion of older participants and the use of SD-OCTA rather than SS-OCTA. Lastly, Yang et al. demonstrated that refractive error did not affect the macular vascular density in myopic eyes (18–32 years) without pathologic changes (21).

We found a smaller FAZ area in the superficial vessel plexus in high myopes compared to non-high myopes, although the association was small and of borderline significance. Our findings contrasted with other reports in the literature. Li et al. measured the superficial FAZ area with the Zeiss HD-OCT with Angioplex™ OCTA device (Carl Zeiss Meditec, Dublin, CA) and found no significant difference between myopes and controls (0.28 ± 0.12 mm^2 vs. 0.28 ± 0.13 mm^2, $P > 0.05$) (15). The calculated FAZ diameter in the myopia group was 0.59 ± 0.12 mm compared to the control group (0.58 ± 0.12 mm, $P > 0.05$). In another study, Milani et al. found no difference in superficial FAZ area (0.23 ± 0.1 mm^2 vs. 0.26 ± 0.1 mm^2, $P = 0.12$) in high myopes compared to controls, and no correlation of FAZ area with spherical correction (18). In their study, FAZ area was measured automatically using the AngioVue, Angioanalytics, XR Avanti device (Software V.2016.1.0.26 Optovue Inc., Fremont, CA, USA). Although both groups obtained similar findings, Li et al. corrected for ocular magnification using Bennett's formula while Milani et al. did not. Axial length can result in measurement errors on confocal scanning laser ophthalmoscopy instruments, and may explain the difference in superficial FAZ area in our study (32).

Our study was limited by the cross-sectional design and a relatively small sample size. Two studies with similar refraction methods were combined to increase power but there may be heterogeneity between studies, i.e., the age difference between the two groups. Although we have adjusted for age in our analysis, this remains an important limitation of the present study. We did not assess the relationship between retinal microvascular parameters with visual acuity or retinal layer thickness measurements as these were beyond the scope and aims of this study. The strengths of our study includes the enrolment of participants from population based cohorts and the use of SS-OCTA to assess the retinal microvasculature.

CONCLUSIONS

In conclusion, VD was lower and superficial FAZ area was smaller, in adolescents and young adults with HM compared to non-HM. Longitudinal studies in population based cohorts of high myopic individuals using different OCT-A imaging instruments may shed further light on the impact and validity of these findings on the subsequent development of PM.

DATA AVAILABILITY STATEMENT

The raw data supporting the conclusions of this article will be made available by the authors, without undue reservation.

ETHICS STATEMENT

The studies involving human participants were reviewed and approved by SingHealth Centralized Institutional Review Board. The patients/participants provided their written informed consent to participate in this study.

AUTHOR CONTRIBUTIONS

C-WW, MA, and S-MS: conceptualization. SM, HH, ST, and CT: formal analysis. S-MS: funding acquisition. HH, CT, MA, Y-LW, RA, and S-MS: methodology. C-WW, SM, HH, Y-LW, CS, and S-MS: writing—original draft. C-WW, SM, CT, MA, Y-LW, RA, CS, and S-MS: writing—review and editing. All authors contributed to the article and approved the submitted version.

FUNDING

This work was supported in part by SNEC HREF (Grant Nos. JX0071, JX0072, and JX0073).

REFERENCES

1. Wong TY, Ferreira A, Hughes R, Carter G, Mitchell P. Epidemiology and disease burden of pathologic myopia and myopic choroidal neovascularization: an evidence-based systematic review. *Am J Ophthalmol*. (2014) 157:9–25 e12. doi: 10.1016/j.ajo.2013.08.010
2. Ohno-Matsui K, Lai TY, Lai C-C, Cheung CMG. Updates of pathologic myopia. *Progress Retinal Eye Res*. (2016) 52:156–87. doi: 10.1016/j.preteyeres.2015.12.001
3. Lim LS, Cheung G, Lee SY. Comparison of spectral domain and swept-source optical coherence tomography in pathological myopia. *Eye*. (2014) 28:488–91. doi: 10.1038/eye.2013.308
4. Chen SJ, Cheng CY, Li AF, Peng KL, Chou P, Chiou SH, et al. Prevalence and associated risk factors of myopic maculopathy in elderly Chinese: the Shihpai eye study. *Investig Ophthalmol Visual Sci*. (2012) 53:4868–73. doi: 10.1167/iovs.12-9919
5. Shih YF, Ho TC, Hsiao CK, Lin LL. Visual outcomes for high myopic patients with or without myopic maculopathy: a 10 year follow up study. *Br J Ophthalmol*. (2006) 90:546–50. doi: 10.1136/bjo.2005.081992
6. Ho M, Liu DT, Chan VC, Lam DS. Choroidal thickness measurement in myopic eyes by enhanced depth optical coherence tomography. *Ophthalmology*. (2013) 120:1909–14. doi: 10.1016/j.ophtha.2013.02.005
7. Kaneko Y, Moriyama M, Hirahara S, Ogura Y, Ohno-Matsui K. Areas of non-perfusion in peripheral retina of eyes with pathologic myopia detected by ultra-widefield fluorescein angiography. *Investig Ophthalmol Visual Sci*. (2014) 55:1432–9. doi: 10.1167/iovs.13-13706
8. Shen L, You QS, Xu X, Gao F, Zhang Z, Li B, et al. Scleral and choroidal thickness in secondary high axial myopia. *Retina*. (2016) 36:1579–85. doi: 10.1097/IAE.0000000000000947
9. Summers JA. The choroid as a sclera growth regulator. *Exper Eye Res*. (2013) 114:120–7. doi: 10.1016/j.exer.2013.03.008
10. Wei WB, Xu L, Jonas JB, Shao L, Du KF, Wang S, et al. Subfoveal choroidal thickness: the Beijing eye study. *Ophthalmology*. (2013) 120:175–80. doi: 10.1016/j.ophtha.2012.07.048
11. Wong CW, Phua V, Lee SY, Wong TY, Cheung CM. Is choroidal or scleral thickness related to myopic macular degeneration? *Investig Ophthalmol Visual Sci*. (2017) 58:907–13. doi: 10.1167/iovs.16-20742
12. Akyol N, Kukner AS, Ozdemir T, Esmerligil S. Choroidal and retinal blood flow changes in degenerative myopia. *Can J Ophthalmol*. (1996) 31:113–9.
13. Benavente-Perez A, Hosking SL, Logan NS, Broadway DC. Ocular blood flow measurements in healthy human myopic eyes. *Graefe's Arch Clin Exp Ophthalmol*. (2010) 248:1587–94. doi: 10.1007/s00417-010-1407-9
14. Yang Y, Wang J, Jiang H, Yang X, Feng L, Hu L, et al. Retinal microvasculature alteration in high myopia. *Investig Ophthalmol Visual Sci*. (2016) 57:6020–30. doi: 10.1167/iovs.16-19542
15. Li M, Yang Y, Jiang H, Gregori G, Roisman L, Zheng F, et al. Retinal microvascular network and microcirculation assessments in high myopia. *Am J Ophthalmol*. (2017) 174:56–67. doi: 10.1016/j.ajo.2016.10.018
16. Al-Sheikh M, Phasukkijwatana N, Dolz-Marco R, Rahimi M, Iafe NA, Freund KB, et al. Quantitative OCT angiography of the retinal microvasculature and the choriocapillaris in myopic eyes. *Investig Ophthalmol Visual Sci*. (2017) 58:2063–9. doi: 10.1167/iovs.16-21289
17. Fan H, Chen HY, Ma HJ, Chang Z, Yin HQ, Ng DS, et al. Reduced macular vascular density in myopic eyes. *Chin Med J*. (2017) 130:445–51. doi: 10.4103/0366-6999.199844
18. Milani P, Montesano G, Rossetti L, Bergamini F, Pece A. Vessel density, retinal thickness, and choriocapillaris vascular flow in myopic eyes on OCT angiography. *Graefe's Arch Clin Exp Ophthalmol*. (2018) 256:1419–27. doi: 10.1007/s00417-018-4012-y
19. Mo J, Duan A, Chan S, Wang X, Wei W. Vascular flow density in pathological myopia: an optical coherence tomography angiography study. *BMJ Open*. (2017) 7:e013571. doi: 10.1136/bmjopen-2016-013571
20. Venkatesh R, Sinha S, Gangadharaiah D, Gadde SGK, Mohan A, Shetty R, et al. Retinal structural-vascular-functional relationship using optical coherence tomography and optical coherence tomography - angiography in myopia. *Eye Vis*. (2019) 6:8. doi: 10.1186/s40662-019-0133-6
21. Yang S, Zhou M, Lu B, Zhang P, Zhao J, Kang M, et al. Quantification of macular vascular density using optical coherence tomography angiography and its relationship with retinal thickness in myopic eyes of young adults. *J Ophthalmol*. (2017) 2017:1397179. doi: 10.1155/2017/1397179
22. Chia A, Lin X, Dirani M, Gazzard G, Ramamurthy D, Quah BL, et al. Risk factors for strabismus and amblyopia in young Singapore Chinese children. *Ophthalmic Epidemiol*. (2013) 20:138–47. doi: 10.3109/09286586.2013.767354
23. Dirani M, Chan YH, Gazzard G, Hornbeak DM, Leo SW, Selvaraj P, et al. Prevalence of refractive error in Singaporean Chinese children: the strabismus, amblyopia, and refractive error in young Singaporean Children (STARS) study. *Investig Ophthalmol Visual Sci*. (2010) 51:1348–55. doi: 10.1167/iovs.09-3587
24. Saw SM, Tong L, Chua WH, Chia KS, Koh D, Tan DT, et al. Incidence and progression of myopia in Singaporean school children. *Investig Ophthalmol Visual Sci*. (2005) 46:51–7. doi: 10.1167/iovs.04-0565
25. Stanga PE, Tsamis E, Papayannis A, Stringa F, Cole T, Jalil A. Swept-source optical coherence tomography angio (Topcon Corp, Japan): technology review. *Dev Ophthalmol*. (2016) 56:13–7. doi: 10.1159/000442771
26. Tan CS, Lim LW, Chow VS, Chay IW, Tan S, Cheong KX, et al. Optical coherence tomography angiography evaluation of the parafoveal vasculature and its relationship with ocular factors. *Investig Ophthalmol Visual Sci*. (2016) 57:OCT224–34. doi: 10.1167/iovs.15-18869
27. Li C, Peter Kwong-Shun. An iterative algorithm for minimum cross entropy thresholding. *Pattern Recog Lett*. (1998) 19:771–6. doi: 10.1016/S0167-8655(98)00057-9
28. Shoji T, Yoshikawa Y, Kanno J, Ishii H, Ibuki H, Ozaki K, et al. Reproducibility of macular vessel density calculations via imaging with two different swept-source optical coherence tomography angiography systems. *Transl Vis Sci Technol*. (2018) 7:31. doi: 10.1167/tvst.7.6.31
29. Fujimoto J, Swanson E. The development, commercialization, and impact of optical coherence tomography. *Investig Ophthalmol Visual Sci*. (2016) 57:OCT1–13. doi: 10.1167/iovs.16-19963
30. Wong CW, Teo YCK, Tsai STA, Ting SWD, Yeo YSI, Wong WKD, et al. Characterization of the choroidal vasculature in myopic maculopathy with optical coherence tomographic angiography. *Retina*. (2018) 39:1742–50. doi: 10.1097/IAE.0000000000002233
31. Novais EA, Adhi M, Moult EM, Louzada RN, Cole ED, Husvogt L, et al. Choroidal neovascularization analyzed on ultrahigh-speed swept-source optical coherence tomography angiography compared to spectral-domain optical coherence tomography angiography. *Am J Ophthalmol*. (2016) 164:80–8. doi: 10.1016/j.ajo.2016.01.011
32. Rock T, Wilhelm B, Bartz-Schmidt KU, Rock D. The influence of axial length on confocal scanning laser ophthalmoscopy and spectral-domain optical coherence tomography size measurements: a pilot study. *Graefes Arch Clin Exp Ophthalmol*. (2014) 252:589–93. doi: 10.1007/s00417-014-2578-6

Conflict of Interest: Y-LW—employee of Essilor International, Singapore.

The remaining authors declare that the research was conducted in the absence of any commercial or financial relationships that could be construed as a potential conflict of interest.

frontiers in Medicine

BRIEF RESEARCH REPORT
published: 28 May 2021
doi: 10.3389/fmed.2021.648540

Vitrectomy With Silicone Oil Tamponade and Without Internal Limiting Membrane Peeling for the Treatment of Myopic Foveoschisis With High Risk of Macular Hole Development

*Yuou Yao [1,2], Jinfeng Qu [1,2], Xuan Shi [1,2], Jie Hu [1,2], Jing Hou [1,2], Heng Miao [1,2], Yong Cheng [1,2] and Mingwei Zhao [1,2]**

[1] Beijing Key Laboratory of Diagnosis and Therapy of Retinal and Choroid Diseases, Department of Ophthalmology, Peking University People's Hospital, Beijing, China, [2] Eye Diseases and Optometry Institute, College of Optometry, Peking University Health Science Center, Beijing, China

OPEN ACCESS

Edited by:
Yi Lu,
Fudan University, China

Reviewed by:
Quan V. Hoang,
Duke-NUS Medical School, Singapore
Chunhui Jiang,
Fudan University, China

***Correspondence:**
Mingwei Zhao
dr_zhaomingwei@163.com

Specialty section:
This article was submitted to Ophthalmology, a section of the journal Frontiers in Medicine

Received: 31 December 2020
Accepted: 06 April 2021
Published: 28 May 2021

Citation:
Yao Y, Qu J, Shi X, Hu J, Hou J, Miao H, Cheng Y and Zhao M (2021) Vitrectomy With Silicone Oil Tamponade and Without Internal Limiting Membrane Peeling for the Treatment of Myopic Foveoschisis With High Risk of Macular Hole Development. Front. Med. 8:648540. doi: 10.3389/fmed.2021.648540

Purpose: To explore the efficiency and safety of the surgical procedure of pars plana vitrectomy (PPV) with silicone oil (SO) tamponade and without internal limiting membrane (ILM) peeling for myopic foveoschisis (MF) eyes with high risk of macular hole formation.

Methods: Three eyes (three patients) with MF and foveal detachment were enrolled into the study. Comprehensive preoperative ophthalmological assessments, including best corrected visual acuity (BCVA) and spectral-domain optical coherence tomography (SD-OCT) were performed on the eyes. Central foveal thickness (CFT) and thickness of continuous neurosensory retina at foveola were measured. All patients underwent PPV followed by SO tamponade and without ILM peeling. SO was removed when MF and retinal detachment were resolved. Patients were followed up postoperative at month 1, 3, 6, and 12.

Results: All the three eyes achieved complete resolution of MF and foveal reattachment with an average SO tamponade period of 11.67 ± 0.58 months. The average CFT at 6 months was 91 ± 27.5 μm, hence reduced significantly from baseline at 365.3 ± 137.85 μm ($P = 0.037$). There was no postoperative macular hole formation despite the average preoperative sensory retina thickness of 58 ± 20.07 μm. Mean BCVA was improved from logMAR 1.43 ± 0.75 to logMAR 0.8 ± 0.75 on the last follow-up. Manageable SO-related complications were reported, including SO emulsification, ocular hypertension, and cataract.

Conclusion: Vitrectomy with SO tamponade and without ILM peeling as an optional surgical protocol to treat MF is effective and safe, especially for MF eyes vulnerable to macular hole formation.

Keywords: myopic foveoschisis, vitrectomy, silicone oil tamponade, internal limiting membrane, anatomical outcome

INTRODUCTION

Myopic foveoschsis (MF) is one of the major causes of impaired vision in highly myopic eyes, which affects 9–34% patients with high myopia (1, 2). Although MF in general progresses slowly and most patients retain relatively good vision, half to two-thirds of the MF patients will develop MH or retinal detachment within 2 years (3, 4). Pars plana vitrectomy (PPV) combined with ILM peeling followed by gas tamponade is the most common surgical treatment for MF. Postoperative MH is a common complication that occurs in 5–28% of surgical cases with poor visual outcome (5–9). However, for MF eyes combined with foveal detachment (FD), which often reveal an extremely thin continuous sensory retina on an optical coherence tomography (OCT) image, ILM peeling could result in the formation of MH. Thus, we introduce PPV without ILM peeling and prolonged SO tamponade period for MF eyes with thin continuous sensory retina or FD that are vulnerable to postoperative MH formation (10).

METHODS

All methods in this study were conducted according to the Declaration of Helsinki. The ethics approval of this study was obtained from the Institutional Review Board of the Peking University People's Hospital. This study was a small prospective interventional case series, which enrolled three eyes of three consecutive MF patients with FD at the Peking University People's Hospital. All the three patients experienced progressively reduced vision or metamorphopsia, which were attributed to MF. The eyes with preoperative full-thickness MH, myopic choroidal neovascularization that could affect the central vision, and eyes with a history of other ocular fundus diseases were excluded. Before the surgical procedure, informed consent was obtained from the study subjects.

Preoperative Assessment

The following data were collected: age, sex, preoperative lens status, refractive error, axial length, and preoperative best corrected visual acuity (BCVA) (**Table 1**). Thorough fundus examination using indirect binocular ophthalmoscopy and foveal microstructures scanned using a spectral-domain OCT (SD-OCT, Optovue, Fremont, CA, US or Carl Zeiss Meditec) were performed to confirm the presence of MF. SD-OCT was performed over a retinal area of 6.0 × 6.0 mm using a radial scan. The FD and central foveal thickness (CFT) were visualized on all the lines of the radial scan images. CFT was measured at the highest foveal point of MF. Thickness of the continuous neurosensory retina at foveola was also determined based on the OCT image.

Surgical Procedure

A standard 25-gauge, three-port PPV was performed by a single experienced surgeon (MZ). Patients with apparent lens opacity underwent phacoemulsification with implantation of intraocular lens surgery at the same time. After completion of the core vitrectomy, triamcinolone acetonide (0.1–0.2 mL; 40 mg/mL) was injected to identify and help achieve complete

TABLE 1 | Demographic, ophthalmological, surgical treatment, and follow-up data of the patients.

Patient no.	Age (years)	Lens status	Refraction error (diopters)	Axial length (mm)	Surgical treatment	SO endotamponade period	SO related complications	Pre-operative BCVA (logMAR)	Post-operative BCVA (logMAR)	Follow-up period after SO removal	Total follow-up period
1	47	Pseudophakic	−10	28.01	PPV + SO tamponade	11 months	SO emulsification	1	0.7	12 months	23 months
2	60	Pakic	−14	28.15	PPV + SO tamponade	12 months	Ocular hypertention; complicated cataract	2.3	1	3 months	15 months
3	65	Phakic with lens opacity	−12	30.85	PPV + SO tamponade with phacoemulsification and IOL implanation	12 months	None	1	0.7	3 months	15 months

detachment of the posterior hyaloid from the posterior surface of the retina. The ILM was not peeled. Fluid–gas exchange was performed, followed by SO injection. Patients were instructed to maintain face-down position for 3 weeks following surgery and afterward maintain a face-down position 2 h a day until foveal reattachment.

Postoperative Assessment

Full ophthalmological examinations, including BCVA and SD-OCT, were performed at months 1, 3, 6, and 12. SO was removed until both the foveoschisis cavity and FD disappeared on all the radial SD-OCT scans. Full ophthalmological examinations and SD-OCT were performed at least 3 months following SO removal.

Anatomical and Functional Outcome Measures

Anatomical outcomes were assessed by SD-OCT morphological changes, including foveal reattachment, CFT, and resolution of foveoschisis cavity. Functional outcome was assessed by BCVA in logarithm of the minimum angle of resolution (logMAR).

Statistical Methods

Statistical analyses were carried out using the SPSS software package, V.22.0. Quantitative data were presented as mean ± SD for parametric data.

RESULTS

This study included three eyes (three patients) with symptomatic MF. Demographic, ophthalmological, surgical treatment, and the follow-up data of the patients are presented in **Table 1**. All the patients were female, with a mean age of 57.3 ± 9.29 (47–65) years. The mean preoperative BCVA was logMAR 1.43 ± 0.75 and improved to logMAR 0.8 ± 0.75 on the last follow-up visit. The average thickness of sensory retina was 58 ± 20.07 μm (37–77 μm), and the average CFT was 365.3±137.85 μm (250-518 μm). Patients 1 and 2 achieved foveola retinal reattachment at 6 months after the surgery (**Figures 1**, **2**). Patient 3 did not show up at 6 months follow-up; however, the 3 months follow-up visit postoperatively showed foveola retinal reattachment, and the 8-month visit showed foveal retinal reattachment except with the slight detachment on the temporal side of the foveola on the OCT image (**Figure 3**). In addition, the average CFT was 91 ± 27.5 μm (67–121 μm) on the 6 months visit of Patients 1 and 2 and 8-month visit of Patient 3. The CFT of 6–8 months reduced significantly compared with baseline ($P = 0.037$). The SO tamponade period was 11 months for Patient 1, and 12 months for Patients 2 and 3, with an average SO tamponade period of 11.67 ± 0.58 months, the MF and FD resolved completely. The mean follow-up period was 17.67 ± 4.62 months (15–24 months), during which two patients experienced complications during the SO tamponade period. At 6 months follow-up, SO emulsification was observed in Patient 1, which at the 11-month visit showed progression, though without ocular hypertension. Patient 2 experienced ocular hypertension at 2 weeks after SO tamponade until 4 months, which was controlled by topical anti-glaucoma medications. She also developed visually significant cataract at 12 months after SO tamponade, and received SO removal surgery combined with cataract surgery. All patients retained stable macular microstructure without retinoschisis and FD relapse at least 3 months after SO removal surgery, and Patient 1 was followed 12 months after SO removal.

DISCUSSION

There is no consensus regarding surgical indications for MF; however, many patients experience slow, progressive visual deterioration, and may exhibit a stable visual acuity for years. Moreover, spontaneous resolution of MF is rare, with various studies reporting on specific cases (11–15). From among 207 MF eyes without FD or lamellar MH, Shimada et al. (3) reported a spontaneous resolution rate of 3.7%. They also considered that eyes with extensive macular retinoschisis and posterior hyaloid are more likely to progress, rather than remain stable or exhibit a spontaneous resolution. Studies have concluded that symptomatic MF, especially FD cases, require surgical interventions to prevent the development of full-thickness macular holes (FTMH) or macular hole retinal detachment (MHRD) (5, 6). In this study, we included MF eyes with FD and progressive visual acuity deterioration.

The exact mechanisms of MF have not been elucidated; however, it is more likely to develop from complex tractional forces from adherent vitreous cortex, rigid ILM, potential retinal arterioles, pathological axial length elongation, and posterior staphyloma (16, 17). Therefore, the tractional force generated by vitreous and ILM can be relieved by PPV combined with ILM peeling to treat MF (7). When used to treat symptomatic MF patients, PPV with or without ILM peeling followed by gas tamponade has been reported to yield good anatomical and functional results. This is the most widely performed surgery (18–21).

One serious complication that is associated with vitrectomy for MF is postoperative FTMH and MHRD. Moreover, as mentioned above, MF eyes have more rigid ILM than non-myopic eyes, which is vital for MF pathogenesis. The removal of rigid ILMs in MF eyes is technically challenging, and has been correlated with postoperative FTMH (9). Epidemiologically, FTMH has been reported to occur in 5–28% of the eyes subjected to PPV with ILM peeling for MF, leading to poor visual prognosis (5–9). Since Shimada et al. (8) proposed the fovea-sparing ILM peeling technique to inhibit postoperative FTMH development, studies comparing this technique and the traditional non-fovea-sparing ILM peeling technique have reported inconsistent conclusions. Most studies reported that fovea-sparing ILM peeling inhibited intraoperative or postoperative FTMH formation, but enhanced the occurrence of postoperative contractions of the remaining ILM (0–60%) (8, 20, 21). A few studies concluded that traditional ILM peeling can achieve an FTMH formation rate that is comparable

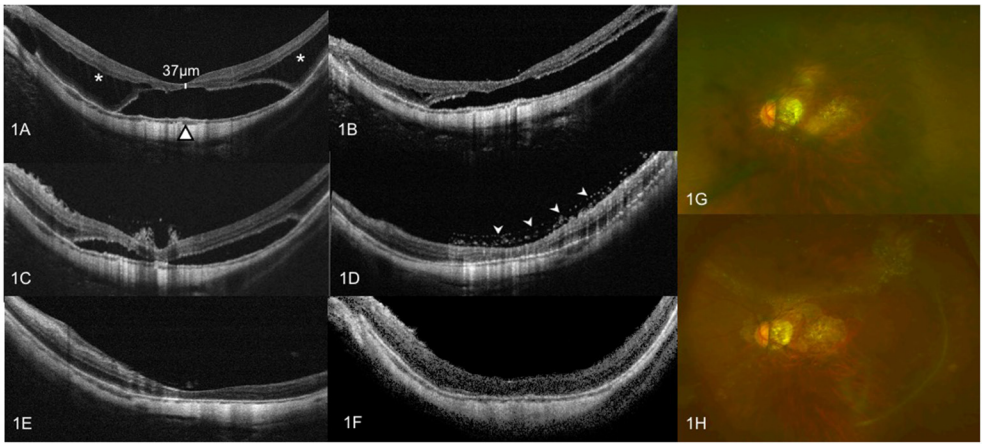

FIGURE 1 | OCT images of case 1. Left eye with a refractive error (spherical equivalent) of −10.0 diopters in a 47-year-old female: **(A)** Preoperative OCT image showing outer retinoschisis (asterisks) and FD (triangle), combined with a thickness of 37 μm of continuous neurosensory retina. **(B)** OCT image at 3 months after vitrectomy with SO tamponade showing a moderate foveoschisis and FD resolution. **(C)** OCT image at 6 months after vitrectomy with SO tamponade showing a remarkable foveoschisis and FD resolution. **(D)** OCT image at 11 months after vitrectomy with SO tamponade shows complete foveoschisis and FD resolution, with emulsified SO droplets on the surface of macular (arrow heads). **(E)** OCT image at 1 week after SO surgical removal does not show MF relapse. **(F)** OCT image at 12 months after SO surgical removal does not show MF relapse. **(G)** Preoperative color fundus image. **(H)** Color fundus image at 11 months after vitrectomy with SO tamponade showing emulsified SO droplets on the surface of retina.

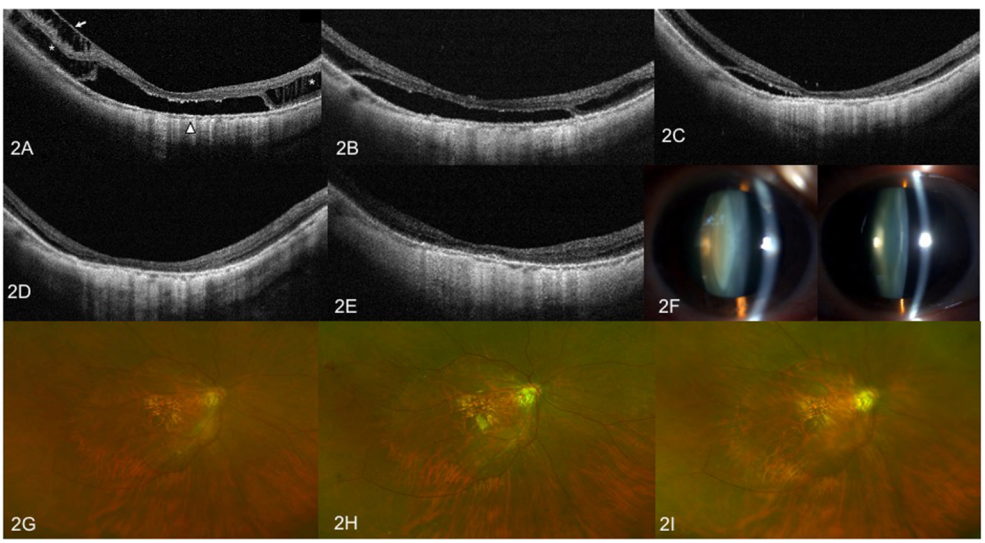

FIGURE 2 | OCT images and anterior segment photographs of case 2. Right eye with a refractive error (spherical equivalent) of −14.0 diopters in a 60-year-old female. **(A)** Preoperative OCT image showing outer retinoschisis (asterisks), inner retinoschisis (arrow), and foveal detachment (triangle). **(B)** OCT image at 3 months after vitrectomy with SO tamponade showing slight resolution of the inner retinoschisis, but no change in outer retinoschisis and FD. **(C)** OCT image at 6 months after SO tamponade showing remarkable foveoschisis and FD resolution. **(D)** OCT image at 12 months after vitrectomy with SO tamponade showing complete foveoschisis and FD resolution. **(E)** OCT image at 3 months after SO surgical resection does not show MF relapse. **(F)** Anterior segment photograph of bilateral eyes at 12 months after SO tamponade. The left image shows visually significant nuclear sclerotic cataracts of the right eye, when compared to contralateral eye. **(G)** Preoperative fundus image. **(H)** Color fundus image at 1 month after vitrectomy with SO tamponade. **(I)** Color fundus image at 3 months after SO removal surgery.

to that of fovea-sparing ILM peeling (22). Gao et al. (10) showed that defects of the inner segment/outer segment junction, including FD, increased the risk of postoperative FTMH and MHRD. MF eyes with extremely thin continuous sensory retina, which are caused by elongation of the sclera, such as the eyes in the present study, are predisposed to postoperative MH development, especially after ILM peeling. Previous studies had various inclusion criteria of MF patient enrollment, with few

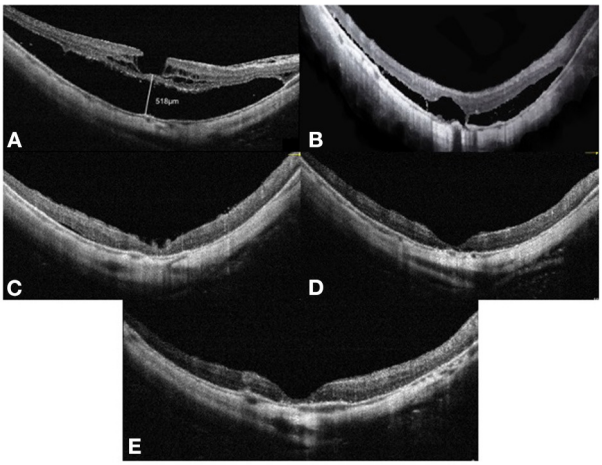

FIGURE 3 | OCT images of case 3. Right eye with a refractive error (spherical equivalent) of −12.0 diopters in a 65-year-old female: **(A)** Preoperative OCT image showing retinoschisis and foveal detachment, with a height of 518 μm. **(B)** OCT image at 3 months after vitrectomy with SO tamponade showing a moderate foveoschisis and FD resolution. **(C)** OCT image at 8 months after SO tamponade showing a remarkable foveoschisis and FD resolution. **(D)** OCT image at 12 months after vitrectomy with SO tamponade showing a complete foveoschisis and FD resolution. **(E)** OCT image at 3 months after SO surgical removal does not show MF relapse. OCT, optical coherence tomographic; FD, foveal detachment; SO, silicone oil.

including accurate thickness of the thinnest sensory retina. Wang et al. (23) have reported that foveal distortion, especially disoriented foveal Müller cell fibrils, can cause visual impairment in MF patients, indicating that the key to restoring the BCVA of MF patients might be flattening retinoschisis. It has also been suggested that ILM preservation may prevent foveola degeneration, for ILM is part of the Müller cell fibrils (24). Thus, it is reasonable to postulate that for patients who are predisposed to iatrogenic FTMH, ILM peeling should be avoided.

Vitrectomy with gas or balanced saline solution tamponade for MF without FTMH have been performed with variable high success rates (75–100%). Gas tamponade exhibited good outcomes on BCVA improvement or anatomical resolution (18, 25, 26), possibly by inducing retinal repositioning by pushing back the retina while keeping the retina surface dry. However, the SO used in vitrectomy without ILM peeling for MF without FTMH has not been scientifically evaluated. Hattori et al. (9) documented that surgeons prefer extensive and long-lasting tamponade materials for MF eyes with more severe myopic tractional maculopathy, such as MF with FD or lamellar MH.

Therefore, studies should aim at developing approaches to safely relieve the tangential traction of the rigid ILM, while tightening the force to neurosensory retina caused by elongation of the sclera without developing postoperative FTMH or MHRD. Even though SO has a smaller surface tension than gas, we found that as long as it is in vitreous cavity, it has the ability to provide a sustainable force for up to an average of 11.67 months of tamponade period. The time taken to achieve foveola reattachment after SO tamponade for three patients was around 6 months, while full retinal reattachment was achieved at around 12 months. In this study, the longer SO tamponade period led to several SO-related complications, such as emulsification, ocular hypertension, and cataract development. However, these complications can be chemotherapeutically or surgically regulated and do not necessarily leave permanent damage. Even though we enrolled high-risk FTMH formation (average 58 μm of sensory retinal thickness) MF patients, no patient in our study developed postoperative MH, thereby proving that our surgical strategy is relatively safe. All eyes achieved retinal reattachment, retinoschisis resolution, and improvement of BCVA, suggesting that the surgical protocol was effective.

The major limitation of this study is the small sample size. Furthermore, the absence of objective examination of macular functions such as multifocal electroretinogram and/or microperimetry was another limitation. Nevertheless, to the best of our knowledge, this is the first report on PPV with SO tamponade but without ILM peeling surgery to treat myopic foveal schisis eyes with a high risk for MH development. Based on our preliminary findings, this surgical technique might be easy to perform, effective for retinoschisis, and safe for preventing FTMH and MHRD, which is an optional surgical protocol for the treatment of MF. However, larger cohort studies with long-term follow-up periods are needed to confirm the effectiveness and safety of this surgical protocol.

DATA AVAILABILITY STATEMENT

The raw data supporting the conclusions of this article will be made available by the authors, without undue reservation.

ETHICS STATEMENT

The studies involving human participants were reviewed and approved by Institutional Review Board of the Peking University People's Hospital. The patients/participants provided their written informed consent to participate in this study.

AUTHOR CONTRIBUTIONS

YY and MZ designed this study and wrote this article. YY, JQ, XS, YC, JHo, and HM collected and measured data. JHu and YY analyzed data. All authors discussed the results and commented on the manuscript.

FUNDING

This work was supported by the Beijing Municipal Science and Technology Commission (Capital Characteristic Clinic Applied Research Project, Z161100000516037, Z171100002217081). The funders had no role in the study design, data collection and analysis, decision to publish or preparation of the manuscript.

REFERENCES

1. Baba T, Ohno-Matsui K, Futagami S, Yoshida T, Yasuzumi K, Kojima A, et al. Prevalence and characteristics of foveal retinal detachment without macular hole in high myopia. *Am J Ophthalmol.* (2003) 135:338–42. doi: 10.1016/s0002-9394(02)01937-2
2. Takano M, Kishi S. Foveal retinoschisis and retinal detachment in severely myopic eyes with posterior staphyloma. *Am J Ophthalmol.* (1999) 128:472–6. doi: 10.1016/s0002-9394(99)00186-5
3. Shimada N, Ohno-Matsui K, Baba T, Futagami S, Tokoro T, Mochizuki M. Natural course of macular retinoschisis in highly myopic eyes without macular hole or retinal detachment. *Am J Ophthalmol.* (2006) 142:497–500. doi: 10.1016/j.ajo.2006.03.048
4. Gaucher D, Haouchine B, Tadayoni R, Massin P, Erginay A, Benhamou N, et al. Long-term follow-up of high myopic foveoschisis: natural course and surgical outcome. *Am J Ophthalmol.* (2007) 143:455–62. doi: 10.1016/j.ajo.2006.10.053
5. Ikuno Y, Sayanagi K, Soga K, Oshima Y, Ohji M, Tano Y. Foveal anatomical status and surgical results in vitrectomy for myopic foveoschisis. *Jpn J Ophthalmol.* (2008) 52:269–76. doi: 10.1007/s10384-008-0544-8
6. Benhamou N, Massin P, Haouchine B, Erginay A, Gaudric A. Macular retinoschisis in highly myopic eyes. *Am J Ophthalmol.* (2002) 133:794–800. doi: 10.1016/s0002-9394(02)01394-6
7. Kobayashi H, Kishi S. Vitreous surgery for highly myopic eyes with foveal detachment and retinoschisis. *Ophthalmology.* (2003) 110:1702–7. doi: 10.1016/S0161-6420(03)00714-0
8. Shimada N, Sugamoto Y, Ogawa M, Takase H, Ohno-Matsui K. Fovea-sparing internal limiting membrane peeling for myopic traction maculopathy. *Am J Ophthalmol.* (2012) 154:693–701. doi: 10.1016/j.ajo.2012.04.013
9. Hattori K, Kataoka K, Takeuchi J, Ito Y, Terasaki H. predictive factors of surgical outcomes in vitrectomy for myopic traction maculopathy. *Retina.* (2018) 38(Suppl. 1):S23–30. doi: 10.1097/IAE.0000000000001927
10. Gao X, Ikuno Y, Fujimoto S, Nishida K. Risk factors for development of full-thickness macular holes after pars plana vitrectomy for myopic foveoschisis. *Am J Ophthalmol.* (2013) 155:1021–7.e1. doi: 10.1016/j.ajo.2013.01.023
11. Goldman DR, Duker JS. Spontaneous improvement of macular traction retinal detachment associated with myopic macular schisis. *Ophthalmic Surg Lasers Imaging Retina.* (2013) 44:497–8. doi: 10.3928/23258160-20130909-15
12. Chang JS, Packo KH, Flynn HW. Spontaneous anatomical and visual improvement in myopic macular retinoschisis. *Ophthalmic Surg Lasers Imaging Retina.* (2013) 44:499–501. doi: 10.3928/23258160-20130909-16
13. Lai TT, Ho TC, Yang CM. Spontaneous resolution of foveal detachment in traction maculopathy in high myopia unrelated to posterior vitreous detachment. *BMC Ophthalmol.* (2016) 16:18. doi: 10.1186/s12886-016-0195-3
14. Sayanagi K, Ikuno Y, Tano Y. Spontaneous resolution of retinoschisis and consequent development of retinal detachment in highly myopic eye. *Br J Ophthalmol.* (2006) 90:652–3. doi: 10.1136/bjo.2005.085233
15. Hoang QV, Chen CL, Garcia-Arumi J, Sherwood PR, Chang S. Radius of curvature changes in spontaneous improvement of foveoschisis in highly myopic eyes. *Br J Ophthalmol.* (2016) 100:222–6. doi: 10.1136/bjophthalmol-2015-306628
16. Bando H, Ikuno Y, Choi JS, Tano Y, Yamanaka I, Ishibashi T. Ultrastructure of internal limiting membrane in myopic foveoschisis. *Am J Ophthalmol.* (2005) 139:197–9. doi: 10.1016/j.ajo.2004.07.027
17. VanderBeek BL, Johnson MW. The diversity of traction mechanisms in myopic traction maculopathy. *Am J Ophthalmol.* (2012) 153:93–102. doi: 10.1016/j.ajo.2011.06.016
18. Zheng B, Chen Y, Chen Y, Zhao Z, Zhang Z, Zheng J, et al. Vitrectomy and internal limiting membrane peeling with perfluoropropane tamponade or balanced saline solution for myopic foveoschisis. *Retina. Apr.* (2011) 31:692–701. doi: 10.1097/IAE.0b013e3181f84fc1
19. Wang L, Wang Y, Li Y, Yan Z, Li Y, Lu L, et al. Comparison of effectiveness between complete internal limiting membrane peeling and internal limiting membrane peeling with preservation of the central fovea in combination with 25G vitrectomy for the treatment of high myopic foveoschisis. *Medicine.* (2019) 98:e14710. doi: 10.1097/MD.0000000000014710
20. Shiraki N, Wakabayashi T, Ikuno Y, Matsumura N, Sato S, Sakaguchi H, et al. Fovea-sparing versus standard internal limiting membrane peeling for myopic traction maculopathy: a study of 102 consecutive cases. *Ophthalmol Retina.* (2020) 4:1170–80. doi: 10.1016/j.oret.2020.05.016
21. Lee CL, Wu WC, Chen KJ, Chiu LY, Wu KY, Chang YC. Modified internal limiting membrane peeling technique (maculorrhexis) for myopic foveoschisis surgery. *Acta Ophthalmol.* (2017) 95:e128–31. doi: 10.1111/aos.13115
22. Al-Badawi AH, Abdelhakim M, Macky TA, Mortada HA. Efficacy of non-fovea-sparing ILM peeling for symptomatic myopic foveoschisis with and without macular hole. *Br J Ophthalmol.* (2019) 103:257–63. doi: 10.1136/bjophthalmol-2017-311775
23. Wang SW, Hung KC, Tsai CY, Chen MS, Ho TC. Myopic traction maculopathy biomarkers on optical coherence tomography angiography-An overlooked mechanism of visual acuity correction in myopic eyes. *Eye.* (2019) 33:1305–13. doi: 10.1038/s41433-019-0424-0
24. Ho TC, Yang CM, Huang JS, Yang CH, Yeh PT, Chen TC, et al. Long-term outcome of foveolar internal limiting membrane nonpeeling for myopic traction maculopathy. *Retina.* (2014) 34:1833–40. doi: 10.1097/IAE.0000000000000149
25. Yun LN, Xing YQ. Long-term outcome of highly myopic foveoschisis treated by vitrectomy with or without gas tamponade. *Int J Ophthalmol.* (2017) 10:1392–5. doi: 10.18240/ijo.2017.09.10
26. Kim KS, Lee SB, Lee WK. Vitrectomy and internal limiting membrane peeling with and without gas tamponade for myopic foveoschisis. *Am J Ophthalmol. Feb.* (2012) 153:320–6.e1. doi: 10.1016/j.ajo.2011.07.007

Conflict of Interest: The authors declare that the research was conducted in the absence of any commercial or financial relationships that could be construed as a potential conflict of interest.

frontiers in Medicine

ORIGINAL RESEARCH
published: 08 June 2021
doi: 10.3389/fmed.2021.648644

Macular Vessel Density Changes in Young Adults With High Myopia: A Longitudinal Study

Ya Shi[1,2†], Luyao Ye[1,2†], Qiuying Chen[1,2], Guangyi Hu[1,2], Yao Yin[2], Ying Fan[1], Jianfeng Zhu[2], Jiangnan He[2], Zhi Zheng[1*], Haidong Zou[1,2] and Xun Xu[1,2]*

[1] Department of Ophthalmology, Shanghai General Hospital, Shanghai Jiao Tong University, National Clinical Research Center for Eye Diseases, Shanghai Key Laboratory of Ocular Fundus Diseases, Shanghai Engineering Center for Visual Science and Photo Medicine, Shanghai Engineering Center for Precise Diagnosis and Treatment of Eye Diseases, Shanghai, China, [2] Department of Preventative Ophthalmology, Shanghai Eye Disease Prevention and Treatment Center, Shanghai Eye Hospital, Shanghai, China

OPEN ACCESS

Edited by:
Xiangjia Zhu,
Fudan University, China

Reviewed by:
Peng Zhou,
Parkway Health, China
Lan-Hsin Chuang,
Keelung Chang Gung Memorial Hospital, Taiwan

****Correspondence:***
Jiangnan He
hejiangnan85@126.com
Zhi Zheng
zzheng88@sjtu.edu.cn

[†] These authors have contributed equally to this work and share first authorship

Specialty section:
This article was submitted to Ophthalmology, a section of the journal Frontiers in Medicine

Received: *01 January 2021*
Accepted: *18 May 2021*
Published: *08 June 2021*

Citation:
Shi Y, Ye L, Chen Q, Hu G, Yin Y, Fan Y, Zhu J, He J, Zheng Z, Zou H and Xu X (2021) Macular Vessel Density Changes in Young Adults With High Myopia: A Longitudinal Study. Front. Med. 8:648644. doi: 10.3389/fmed.2021.648644

Background: To characterize the longitudinal changes of macular vessel density in young adults and its associated factors.

Methods: The right eyes of 309 participants (75 high myopic, 194 mild-to-moderate myopic, and 40 healthy) were followed up for 21 months. OCTA images were acquired at two visits using follow-up scans. Macular vessel density was calculated globally and in the nine early treatment diabetic retinopathy study (ETDRS) subfields of the macula superficial layer.

Results: The macular vessel density significantly decreased in young myopes after a 21-month follow up ($p < 0.05$), with variations among sectors. Compared with healthy eyes, HM group exhibited a faster reduction in global macular vessel density ($p = 0.0307$) as well as in sectors of inner-inferior (II), inner-temporal (IT), and outer-temporal (OT) (all $p < 0.05$). Multivariate regression analysis showed that longer baseline axial length (AL) was significantly associated with larger reduction of macular vessel density in the inner-inferior, inner-temporal and outer-temporal sectors (all $p < 0.05$).

Conclusions: Compared with emmetropes, high myopes presented greater loss of macular vessel density over time in global and in the inner-inferior, inner-temporal and outer-temporal sectors. A longer baseline AL was associated with larger changes of macular vessel density in the inner-inferior, inner-temporal and outer-temporal sectors.

Keywords: macular vessel density, high myopia, optical coherence tomography angiography, retinal thickness, longitudinal study

INTRODUCTION

Myopia has become a serious public health concern due to its significantly increasing prevalence, especially in East Asia (1–4). As a leading cause of vision loss worldwide (5), high myopia (HM) may result in retinal disorders, including lacquer crack formation, Forster-Fuchs' spots, chorioretinal atrophy, choroidal neovascularization, foveoschisis, and posterior staphyloma (6, 7). These complications are highly associated with morphological changes of retinal vessels (8, 9). Therefore, the change of retinal microvasculature in HM has been an important issue for several

decades, which may provide a critical clue for understanding the pathophysiology of HM-associated diseases. It was previously reported that in the patients with HM, reduced retinal vessel density (10) and blood flow (11) were evident in the large retinal vessels visible on fundus photographs. Moreover, decreased choroidal blood flow not only has been found to be associated with increase of axial length (AL), but also may be a possible indication for progressive myopia (12). Recently, in retinal microvasculature, studies pointed out that students with HM experienced decreased deep perifoveal vessel density and radial peripapillary capillary (13, 14). Hence, investigating the longitudinal changes in macular microvasculature and their interaction in young adults with high myopia prior to retinal damage may reveal the underlying pathophysiology of the disorder and assist to implement an effective treatment or prevention.

Optical coherence tomography angiography (OCTA), a newly developed imaging modality, has assisted scholars to quantitatively and qualitatively measure retinal and choroidal microvasculature non-invasively (15). The present study aimed to assess changes of macular vessel density using OCTA in young adults with HM, and investigate the associations between the changes of vessel density and ocular parameters through a longitudinal study.

METHODS

Study Participants

The participants in this longitudinal study, who were randomly selected from students of the Shanghai University, had been examined in October 2016 and followed up in July 2018. The study methodology of baseline examination has been previously described in detail (13). In brief, 760 participants aged 16–28 years with spherical equivalent (SE) $<$ 0.5 D, best-corrected visual acuity (BCVA) $\geq$ 20/25, intraocular pressure (IOP) $\leq$ 21 mmHg, normal anterior chamber angles, normal optic nerve head without glaucomatous changes, and no retinal nerve fiber layer abnormalities, were enrolled. The exclusion criteria were eyes with other ocular diseases (congenital cataract, glaucoma, and retinopathy), previous intraocular or refractive surgery, and any systemic diseases (hypertension and diabetes). This study was approved by the Ethics Committee of Shanghai General Hospital, Shanghai Jiao Tong University (Shanghai, China), and was conducted in accordance with the tenets of the Declaration of Helsinki. Informed consent forms were obtained from all the study subjects. The study protocol was registered at Clinical Trials.gov PRS (Registration No. NCT03446300).

Abbreviations: ACD, anterior chamber depth; AL, axial length; BCVA, best-corrected visual acuity; BMI, body mass index; CCT, central corneal thickness; DBP, diastolic blood pressure; EM, emmetropia; ETDRS, Early Treatment Diabetic Retinopathy Study; GCC, ganglion cell complex; HM, high myopia; HR, heart rate; II, inner inferior; IN, inner nasal; IOP, intraocular pressure; IS, inner superior; IT, inner temporal; logMAR, logarithm of the minimum angle of resolution; LT, lens thickness; MIM, mild myopia; MOM, moderate myopia; MOPP, mean ocular perfusion pressure; OI, outer inferior; ON, outer nasal; OS, outer superior; OT, outer temporal; RT, retinal thickness; SBP, systolic blood pressure; SD, standard deviation; SE, spherical equivalent; VD, vessel density.

Study Procedures

All participants attended two visits and underwent comprehensive eye examinations at each time, including refractive error assessment using an autorefractor machine (KR-8900; Topcon, Tokyo, Japan), measurement of IOP (TX-F; Topcon, Tokyo, Japan), slit-lamp bio-microscopy, and color fundus examination. Central corneal thickness, lens thickness, anterior chamber depth, and AL were measured using optical low-coherence reflectometry (Aladdin; Topcon, Japan). Subjective refraction was performed by a trained optometrist for all of the participants. The BCVA was converted into the logarithm of minimal angle resolution (logMAR). Additionally, systolic blood pressure (SBP), diastolic blood pressure (DBP), heart rate, height, and weight were measured. A detailed medical history was also recorded for each participant.

Swept-Source Optical Coherence Tomography Imaging

The ganglion cell complex (GCC) thicknesses and retinal thicknesses (RT) were measured using SS-OCT (DRI OCT-1 Atlantis; Topcon, Tokyo, Japan), which had a lateral resolution of 10 μm and an axial resolution of 8 μm. The tomography thickness map of the entire macular area (6 $\times$ 6 mm) was obtained from an average of four overlapped consecutive scans. The segmentation of each layer was automatically carried out using the built-in software, and manual segmentation was performed where the automatic segmentation misjudged the borderline of each layer. All measurements corrected for the magnification effects of refractive error and AL were conducted by a single technician who was expert in taking OCT images. Follow-up mode was performed to ensure the same location for follow-up scans as the baseline measurement. Images with signal strength index $\leq$60 were excluded from the statistical analysis.

OCTA Imaging

Spectral-domain OCTA imaging was performed using of a Cirrus AngioPlex device (Carl Zeiss Meditec, Inc., Dublin, CA, USA). This instrument had a center wavelength of 840 nm, a bandwidth of 90 nm, an A-scan depth of 2.0 mm in tissue (1,024 pixels), a full width at half maximum (FWHM) axial resolution of $\sim$5 lm in tissue, a lateral resolution at the retinal surface estimated at $\sim$15 lm, and a scanning rate of 68,000 A-scans per second. All scans were centered on the fovea at two visits using follow-up model after correcting for the magnification effects of refractive error and AL, and FastTrac motion correction software (Carl Zeiss Meditec, Inc., Dublin, CA, USA) was used while the images were acquired (16, 17). The OCTA scans with a signal strength index $<$40 and images with segmentation errors or residual motion artifacts were excluded.

Quantitative analysis was undertaken using Cirrus HD-OCT Review Software (version 10.0.0.14618) according to the Early Treatment Diabetic Retinopathy Study (ETDRS) grid (**Figure 1**). The diameters of the central foveal circle, inner ring, and outer ring were 1, 3, and 6 mm, respectively, and they were further divided into nine sectors (center, IS-inner superior, IN-inner nasal, II-inner inferior, IT-inner temporal, OS-outer superior, ON-outer nasal, OI-outer inferior, OT-outer temporal). The

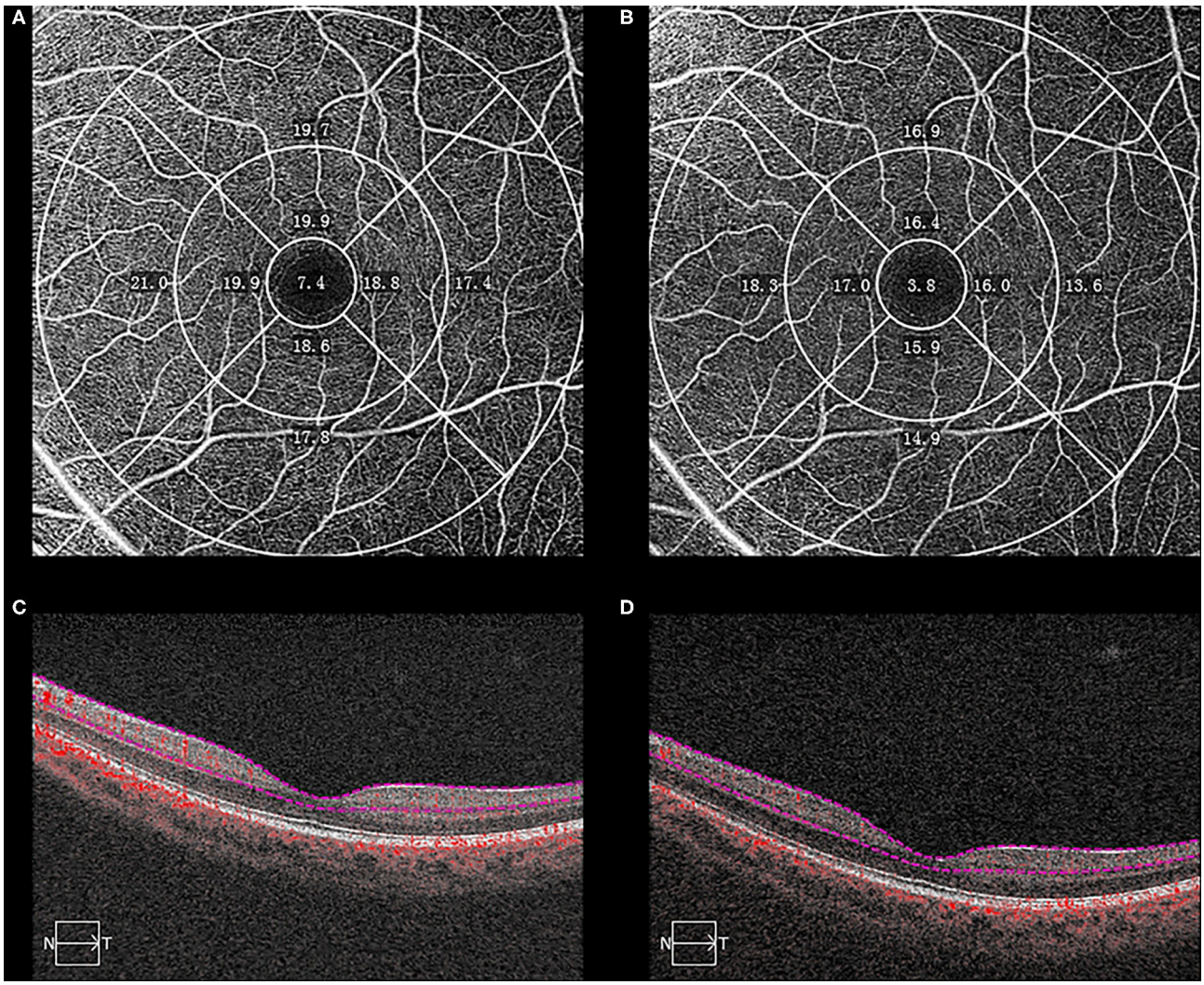

FIGURE 1 | Optical coherence tomography angiographic (OCTA) images from a 18-year-old student with myopia who was followed-up from October 2016 to July 2018. The macular vessel density (VD) decreased between baseline **(A)** and the end of follow-up **(B)** in each sector. The boundaries used for segmentation were indicated between two red lines on the cross-sectional OCTA reflectance **(C,D)**. The sectors were automatically measured according to the Early Treatment of Diabetic Retinopathy Study grid.

vessel density (VD) was defined as the total length of perfused vasculature per unit area in a region of measurement. The inner plexiform layer boundary was calculated as 70% of the distance from the internal limiting membrane to an estimated boundary of the outer plexiform layer, which was automatically detected by the software.

Statistical Analysis

In the present study, only the right eye of each participant was selected for statistical analysis. SE was calculated as the sphere plus half a cylinder. The mean arterial pressure (MAP) was calculated according to the following equation: MAP = DBP + 1/3 (SBP-DBP) (18). Mean ocular perfusion pressure (MOPP) was calculated as follows: MOPP = (2/3 × MAP – IOP) (19). The body mass index (BMI) was formulated in the following: weight (kg)/[height (m)]^2. All participants were divided into three groups by the length of ocular axis at baseline as follows: emmetropia (EM) group with an AL of 24 mm or less; mild-to-moderate myopia (MIM/MOM) group with an AL between 24 and 26 mm; and HM group with an AL of 26 mm or more.

Demographic and ocular parameters were reported as counts or proportions for categorical data, and as mean ± standard deviation for continuous data. The normal distribution of all variables was examined using the Kolmogorov-Smirnov test. Cochran-Mantel-Haenszel test, or one-way analysis of variance (ANOVA) with *post-hoc* test (Bonferroni) was performed to detect differences in demographic and ocular parameters at baseline among the three groups, as appropriate. Biometric changes between 2016 (baseline) and 2018 (follow-up) measured using OCTA and SS-OCT were compared using paired *t*-test.

TABLE 1 | Demographic and ocular characteristics of study participants.

Variables	EM ($N = 40$)	MIM/MOM ($N = 194$)	HM ($N = 75$)	*p*-value	*Post-hoc*
Age, years	19.73 ± 2.18	19.34 ± 2.27	19.25 ± 2.16	0.2336	/
Female, *n* (%)	27 (67.50)	100 (51.55)	27 (36.00)	0.0042	EM > HM
BMI, kg/m^2	20.73 ± 3.08	21.02 ± 2.73	20.77 ± 3.43	0.2375	/
SBP, mmHg	120.73 ± 17.55	120.68 ± 15.53	124.55 ± 16.24	0.2212	/
DBP, mmHg	73.70 ± 10.92	71.28 ± 10.11	73.85 ± 9.68	0.0886	/
HR, bpm	74.77 ± 10.27	74.35 ± 11.23	75.56 ± 9.85	0.6828	/
SE, D	−1.49 ± 1.69	−3.70 ± 1.95	−5.97 ± 2.38	<0.0001	EM > MIM/MOM > HM
BCVA, logMAR	0.00 ± 0.00	0.02 ± 0.06	0.03 ± 0.05	0.0004	EM < MIM/MOM, HM
IOP, mmHg	14.05 ± 3.10	13.98 ± 2.69	14.00 ± 2.80	0.9683	/
MOPP, mmHg	45.77 ± 8.54	44.54 ± 7.61	44.89 ± 12.06	0.2886	/
ACD, mm	3.60 ± 0.21	3.74 ± 0.22	3.77 ± 0.27	0.0004	EM < MIM/MOM, HM
CCT, μm	543.06 ± 35.72	539.82 ± 35.04	535.84 ± 37.34	0.5862	/
LT, mm	3.53 ± 0.22	3.49 ± 0.36	3.49 ± 0.22	0.5699	/

Data are presented as mean ± standard deviation unless otherwise indicated.
Comparison among the three groups were using the Cochran-Mantel-Haenszel test for categorical data or the one-way ANOVA test for continuous data with post-hoc test (Bonferroni). ACD, anterior chamber depth; BCVA, best-corrected visual acuity; BMI, body mass index; CCT, central corneal thickness; DBP, diastolic blood pressure; EM, emmetropia; HM, high myopia; HR, heart rate; IOP, intraocular pressure; logMAR, logarithm of minimal angle resolution; LT, lens thickness; MIM, mild myopia; MOM, moderate myopia; MOPP, mean ocular perfusion pressure; SBP, systolic blood pressure; SE, spherical equivalent.

The differences in biometric changes across different refraction groups were analyzed using one-way ANOVA test with *post-hoc* test (Bonferroni). The univariate regression analysis was used to investigate the association between changes in VD and ocular parameters. All the variables with a *p*-values <0.05 in the univariate analysis were considered for the multivariable models. After excluding variables that showed multicollinearity, multivariable regression models were constructed to explore the independent factors for the changes in VD. All statistical analyses were performed using SPSS 25.0 software (IBM, Armonk, NY, USA). A *p*-value <0.05 was considered statistically significant.

RESULTS

Seven hundred sixty participants were recruited at baseline visit, and 447 (58.82%) participants from the same cohort were followed up 21 months later. The loss to follow-up was chiefly due to school graduation. Moreover, 138 participants were further excluded at follow-up because of lacking OCTA examination ($n = 128$), poor-quality OCTA images ($n = 5$), and refractive surgery history ($n = 5$) and eventually, a total of 309 participants were involved in the final analysis. In the study, 40 participants had EM (12.95%), 194 had MIM or MOM (62.78%), and 75 had HM (24.27%). Demographic and ocular characteristics of participants at baseline are expressed in **Table 1**. There were no significant differences in age, BMI, SBP, DBP, heart rate, IOP, MOPP, central corneal thickness, and lens thickness among the three groups. However, HM group included fewer female participants ($p < 0.05$), presented significantly lower SE, worse BCVA, deeper ACD, and longer AL than EM group (all $p < 0.05$).

Table 2 and **Figure 2** demonstrates the baseline and the longitudinal changes of VD and ocular parameters over follow-up period. There was no significant difference in the baseline VD, RT and GCC among the three groups (all $p > 0.05$). The macular VD significantly decreased while AL increased in the follow-up in all the three groups (all $p < 0.05$). Of note, the HM group showed a larger reduction in VD (−1.96 ± 2.57/mm) compared with the EM group (−0.61 ± 0.97/mm) ($p = 0.0307$). There were reductions in both RT and GCC thickness after 2-year follow-up in HM and MIM/MOM groups (both $p < 0.01$), which was not seen in emmetropic eyes (both $p > 0.05$).

The changes of macular VD in all sectors of ETDRS grid were presented in **Supplementary Table 1** and **Figure 3**. The sectoral VD significantly decreased through follow-up in all the three groups (all $p < 0.05$), except for that in the outer nasal sector in EM group ($p = 0.2521$). In each group, the nasal sector minimally changed, whereas the temporal sector maximally changed in both inner ring and outer ring. In addition, the changes in the inner ring were more significant than those in the outer ring for the majority of sectors. Compared with EM group, HM group had notably higher change rate in the II sector (−3.15 ± 9.62% vs. −14.88 ± 20.11%, $p = 0.0073$), IT sector (−4.88 ± 8.43% vs. −17.22 ± 22.88%, $p = 0.0298$), and OT sector (−7.15 ± 8.40% vs. −16.20 ± 20.80%, $p = 0.0308$).

The results of the univariate regression analysis adjusted for age and gender are presented in **Supplementary Tables 2–5**. For the average macular VD, no variable was found to be correlated with the changes of VD (all $p > 0.05$). The associations of macular VD changes with other ocular parameters were further explored in selected sectors where great macular VD reduction were observed in HM group. The changes of VD significantly correlated with SE, baseline AL and the changes of AL in the II, IT, and OT sectors. BCVA and the changes of GCC thickness were negatively associated with the changes of VD in the II and IT sectors. Additionally, the changes of VD were positively correlated with baseline RT and the changes of RT in the II

TABLE 2 | Comparison of globally VD and ocular parameters between baseline and the end of follow-up period.

	EM ($N = 40$)	MIM/MOM ($N = 194$)	HM ($N = 75$)	*p*-value	*Post-hoc*
VD, mm					
Baseline	19.00 ± 0.71	18.82 ± 1.52	18.95 ± 1.36	0.5843	/
Follow-up	18.39 ± 1.01	17.99 ± 4.87	17.01 ± 2.60	0.1392	/
Changes	−0.61 ± 0.97	−0.81 ± 5.08	−1.96 ± 2.57	0.0307	EM < HM
p-value	0.0003	<0.0001	<0.0001		
AL, mm					
Baseline	23.53 ± 0.40	25.06 ± 0.54	26.59 ± 0.59	<0.0001	EM < MIM/MOM < HM
Follow-up	23.56 ± 0.41	25.15 ± 0.58	26.67 ± 0.62	<0.0001	EM < MIM/MOM < HM
Changes	0.04 ± 0.10	0.08 ± 0.18	0.08 ± 0.13	0.0384	EM < MIM/MOM, HM
p-value	0.0253	<0.0001	<0.0001		
RT, μm					
Baseline	280.08 ± 12.96	277.33 ± 11.05	273.99 ± 13.13	0.0530	/
Follow-up	278.29 ± 11.46	275.80 ± 10.74	267.13 ± 35.02	0.0052	EM, MIM/MOM > HM
Changes	−0.79 ± 2.97	−1.86 ± 3.32	−6.94 ± 32.17	0.1585	/
p-value	0.1783	<0.0001	0.0006		
GCC, μm					
Baseline	108.92 ± 4.88	109.86 ± 6.04	109.19 ± 5.89	0.6318	/
Follow-up	108.88 ± 5.00	109.32 ± 6.54	105.25 ± 16.48	0.3053	/
Changes	−0.14 ± 2.19	−0.46 ± 2.99	−3.66 ± 15.34	0.2452	/
p-value	0.7382	<0.0001	0.0031		

Data are presented as mean ± standard deviation.

Comparisons between the baseline and the follow-ups using the paired t-test. Comparison among the three groups were using the one-way ANOVA test with post-hoc test (Bonferroni). EM, emmetropia; GCC, ganglion cell complex; MIM, mild myopia, MOM, moderate myopia; HM, high myopia; RT, retinal thickness; VD, macular vessel density.

sector, whereas negatively correlated with ACD in the OT sector. Variables with a significance p-value < 0.05 were included in the stepwise multivariate models except for SE that had a stronger correlation with AL. The results of multivariable regression analysis (**Table 3** and **Figure 4**) revealed the baseline AL was independently associated with the changes of VD in II, IT, and OT sectors (all $p < 0.05$). According to the models, each 1 mm increase in baseline AL was associated with a 0.57/mm decrease in inner-inferior macular VD, a 0.73/mm decrease in inner-temporal macular VD, and a 0.44/mm decrease in outer-temporal macular VD, separately.

DISCUSSION

This prospective study, which enrolled three hundred and nine university students over 21 months, was the first longitudinal study evaluating macular microvasculature changes in young adults observed by OCTA. A significant decrease in macular VD over time was documented. In high myopes, macular VD presented larger reduction globally and in the II, IT and OT sectors. A longer baseline AL was associated with greater loss of VD in these sectors.

Earlier studies reported that age was determinant of macular VD measured by OCTA (20–22). However, these studies were generally conducted in healthy eyes. In our longitudinal study, macular microvasculature was significantly decreased in both emmetropes and myopes over a 21-month period. Jo et al. (20) reported that the majority of the sectoral peripapillary and macular VDs were significantly reduced with increase of age in healthy eyes but the VD of papillomacular bundle area was not age-dependent. The present study also demonstrated that the macular VD in the ON sector did not decrease in emmetropic students, while this sectoral VD reduced in myopic students, which indicating the effect of myopia on macular perfusion reflected in the area of papillomaular bundle area. It was revealed that the ischemic injury of the papillomacular bundle could predict poor vision in both central retinal artery occlusion and branch retinal artery occlusion (23, 24). Thus, the effects of VD loss in the papillomacular bundle area on visual impairment in myopes and its underlying mechanism still require further investigations.

Several studies used OCTA to investigate the changes of retinal microvascular in HM, and they have reported controversial findings (13, 25–28). Guo et al. (28) pointed out that HM causes a lower superficial peripapillary microvascular density, but no significant difference was found in parafoveal microvascular density among all groups. Wang et al. (26) also found a decreased vessel density in the peripapillary area, rather than in the parafoveal area of high myopic eyes. On the contrary, our previous study and a number of cross-sectional studies (13, 25, 27) have yielded a reduced parafoveal microvascular density in HM. It may lead to controversial results because the vessel density was quantified in different ways. In Guo's and Wang's studies, the vessel density was defined as the proportion of the total area occupied by vessels, while the vessel density was defined as the total length of perfused vasculature per unit area in this study. Moreover, the previous studies were all cross-sectional studies with different simple sizes. The present research prospectively

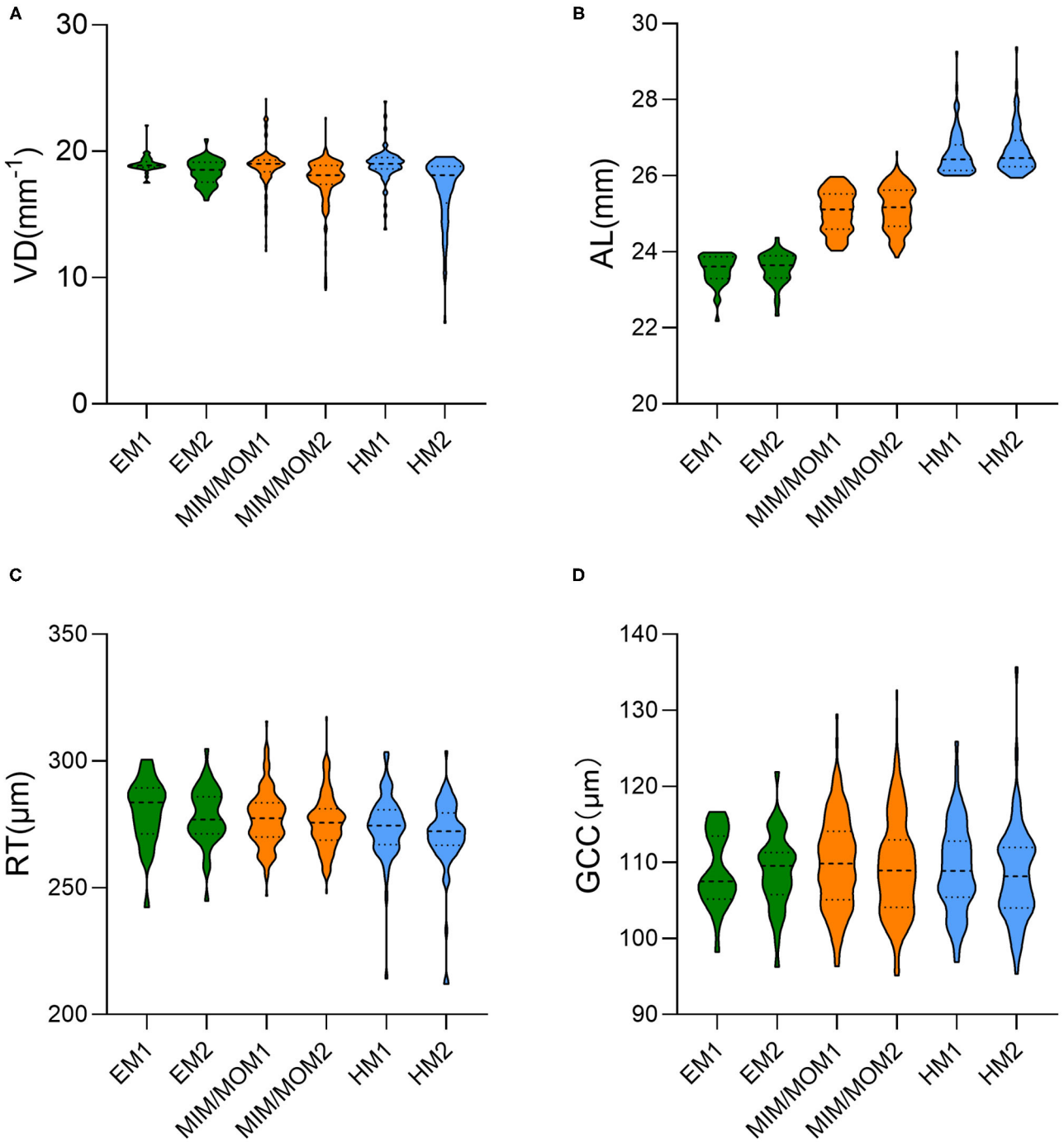

FIGURE 2 | The violin plot in distribution of **(A)** vessel density (VD), **(B)** axial length (AL), **(C)** retinal thickness (RT) and **(D)** ganglion cell complex (GCC) thickness in different groups at baseline and the end of follow-up. EM1, emmetropia at baseline; EM2, emmetropia at the end of follow-up; HM1, high myopia at baseline; HM2, high myopia at the end of follow-up; MIM/MOM1, mild-to-moderate myopia at baseline; MIM/MOM2, mild-to-moderate myopia at the end of follow-up.

evaluated the changes of macular VD and showed a significantly greater loss of VD in HM group than in EM group. However, no significant difference of global and sectoral VD changes was noted between MIM/MOM group and HM group, which was in line with Yang et al.'s findings (29). When it comes to sectoral changes of macular VD, there was no unified understanding. In the comparison with EM group, HM group presented larger longitudinal changes of macular VD in the II, IT, and OT sectors in this study, indicating these sectors might be critical focus areas in clinical practice.

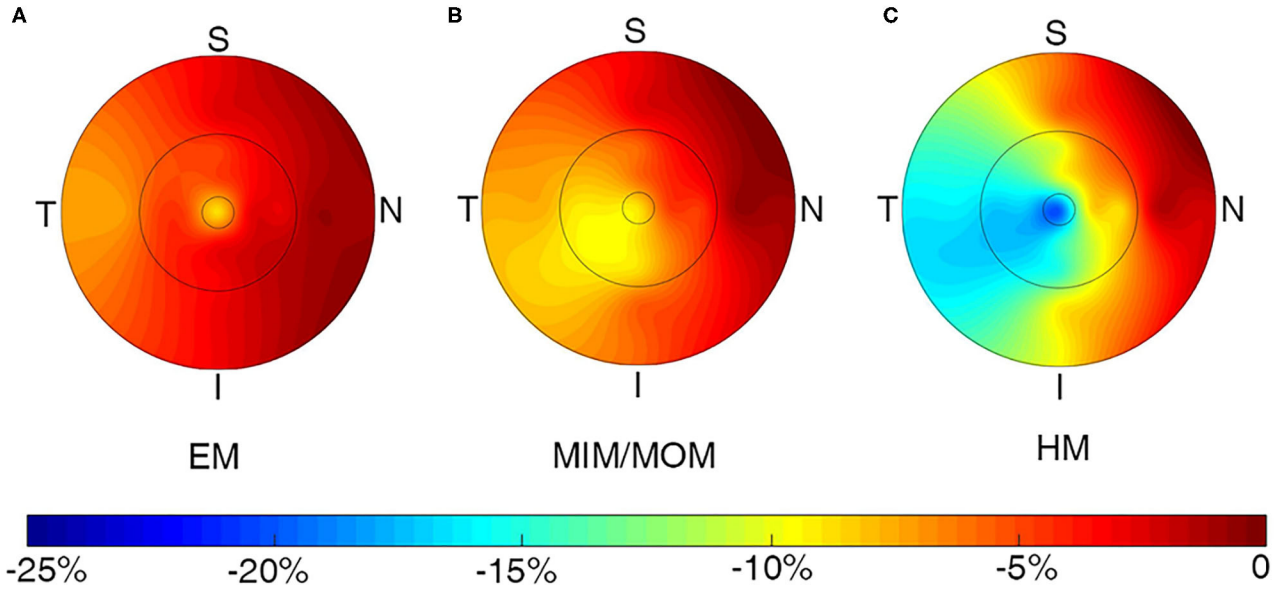

FIGURE 3 | Topographic variation of the change rate of macular vessel density in all sectors for **(A)** EM, **(B)** MIM/MOM, **(C)** HM. EM, emmetropia; HM, high myopia; MIM/MOM, mild-to-moderate myopia.

TABLE 3 | Multivariate regression analysis of association with changes of sectoral VD in all participants.

Model	Coefficient estimate	95% confidence interval	*p*-value
II			
BCVA, logMAR	3.37	−2.31 to 9.05	0.2430
Baseline AL, mm	−0.57	−1.05 to −0.08	0.0224
Changes of AL, mm	−2.59	−5.67 to 0.50	0.0995
Baseline RT, μm	0.02	−0.03 to 0.06	0.4354
Changes of RT, μm	0.02	−0.03 to 0.08	0.3874
Changes of GCC, μm	0.02	−0.10 to 0.14	0.7346
IT			
BVCA, logMAR	1.45	−4.62 to 7.51	0.6379
Baseline AL, mm	−0.73	−1.25 to −0.21	0.0057
Changes of AL, mm	−2.46	−5.76 to 0.85	0.1445
Changes of GCC, μm	0.05	−0.01 to 0.11	0.1281
OT			
ACD, mm	−1.31	−2.92 to 0.30	0.1095
Baseline AL, mm	−0.44	−0.82 to −0.05	0.0266
Changes of AL, mm	−2.10	−4.62 to 0.42	0.1022

ACD, anterior chamber depth; AL, axial length; BCVA, best-corrected visual acuity; GCC, ganglion cell complex; II, inner inferior; IT, inner temporal; logMAR, logarithm of minimal angle resolution; OT, outer temporal; RT, retinal thickness; VD, vessel density.

We previously compared the peripapillary and parafoveal vessel density with AL and retina thickness, and found a significant negative correlation between AL and vessel density (13). Li et al. (27) pointed out that microvascular density was negatively correlated with AL in myopia in both superficial and deep vascular plexuses. Ucak et al. (30) reported that the macular vessel density reduced with increase of AL and decrease of GCC thicknesses in patients with HM. The current study uncovered that the longitudinal changes of macular VD were only correlated with baseline AL in the II, IT, and OT sectors, suggesting the macular vessel loss mainly results from the elongation of eyeballs. It is suggested that with the increase of AL in myopia, the eyeball stretches, causing mechanically expanding and thinning of retina, resulting in a narrowing of the vessel diameter, which leads to the decrease of vessel density (27). Meanwhile, the macular thickness showed different rates of change in different sectors according to age and refractive status (31, 32). Since the oxygen demands of those sectors might reduce resulting from the thinning of retina, the vessels supplying blood to those regions was likely to decrease accordingly. As well as the mechanical stretch, there might be some changes in myopia-related signaling pathways, resulting in subsequent changes in vessel density. However, it is not clear which of structural changes or biochemical changes came first. Despite this, the mechanisms of sectoral changes in macular vessel density still require further study.

The capillary networks in the human retina mainly distributed in the inner five layers of the retina, of which the superficial capillary network is mainly distributed in the nerve fiber layer and the ganglion cell layer, while the deep capillaries are mainly distributed in the inner plexiform layer and the inner nuclear layer (33). There has been increasing evidence that HM has longer AL, lower peripapillary VD, and thinner peripapillary retinal nerve fiber layer thickness (26, 28, 34, 35). In addition, AL was also noted to be negatively correlated with thickness of the outer nuclear layer and photoreceptor outer segment layer (36). But the RT and GCC thickness were not related with the loss of macular VD in our multivariate regression analysis. The underlying biochemical mechanism

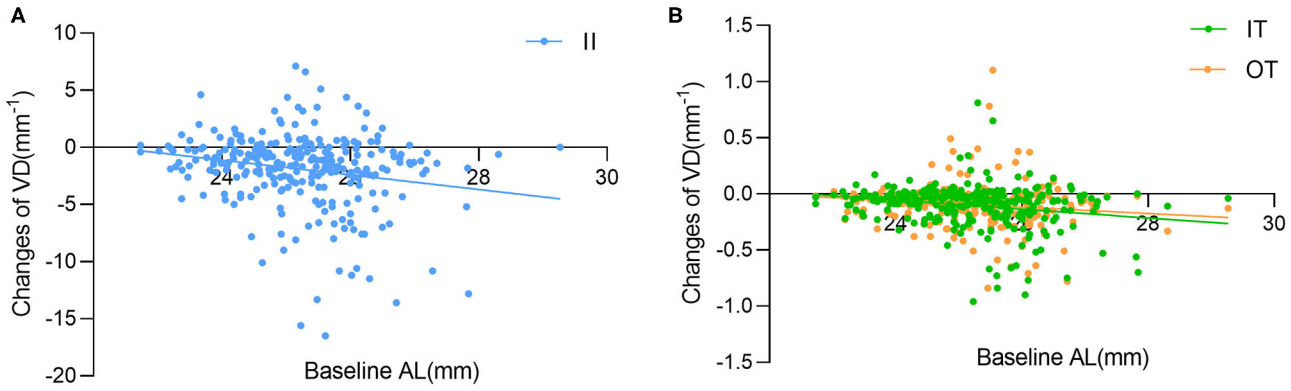

FIGURE 4 | Simple linear regression analysis between baseline AL with the changes of vessel density (VD) in the **(A)** inner inferior (II), **(B)** inner temporal (IT) and outer temporal (OT) sectors.

might give reason to changes of macular VD as well as the mechanical stretch. Dopamine, secreted by dopaminergic amacrine cell (DAC) in the inner layer of the retina, was indicated to be a key molecule in the retinal signaling pathway during myopia development, working with Melatonin and retinal ganglion cells (RGCs) (37–39). The structural changes in myopia may affect the DAC, RGCs, and outer photoreceptor cells, leading to subsequent changes in DA and melatonin synthesis and release, thereby influencing further development of myopia.

This study has several limitations. Firstly, the low follow-up rate made it not representative. Secondly, the examinations were only performed at two visits, so that we could not observe the dynamic changes during this period. Thirdly, the small sample size, especially for EM and HM groups, may significantly impact the reliability of our findings. Fourthly, OCTA deep slab images were not included in the analysis because several projection artifacts prevented qualified images.

In conclusion, the macular VD significantly decreased over time in all the sectors in young myopes, while the macular VD in the papillomacular bundle area was not age-dependent in emmetropes. A larger reduction of macular VD was observed in HM group compared with healthy eyes and correlated with longer baseline AL in the II, IT and OT sectors. Although the underlying mechanisms of physiological and pathological macular VD changes remain unknown, the reduction of macular VD might be considered as a preclinical characteristic in patients with HM. Therefore, further studies with longer follow-up periods are needed to investigate correlations between structure and function.

DATA AVAILABILITY STATEMENT

The raw data supporting the conclusions of this article will be made available by the authors, without undue reservation.

ETHICS STATEMENT

The studies involving human participants were reviewed and approved by Ethical committee of Shanghai General Hospital, Shanghai Jiao Tong University, Shanghai, China. The patients/participants provided their written informed consent to participate in this study.

AUTHOR CONTRIBUTIONS

YF, JZ, JH, and XX: study concept and design. YS, QC, GH, and YY: data collection and management. YS and LY: analysis and interpretation of data. YS: writing the manuscript. JZ, JH, ZZ, and HZ: critical revision of the manuscript. XX: supervision. All authors read and approved the final manuscript.

FUNDING

This study was funded by National Natural Science Foundation of China (Grant No. 81703287, Beijing, China), National Key R&D Program of China (Grant Nos. 2016YFC0904800, 2019YFC0840607), Shanghai Science and Technology Commission Research Project (Grant No. 17ZR1426900), National Science and Technology Major Project of China (Grant No. 2017ZX09304010), Shanghai Health Committee, Clinical Research (Project No. 2019240241), and Shanghai Shenkang Hospital Clinical Research Program (Project No. SHDC12019X18, SHDC12020127). The sponsor or funding organization had no role in the design or conduct of this research.

SUPPLEMENTARY MATERIAL

The Supplementary Material for this article can be found online at: https://www.frontiersin.org/articles/10.3389/fmed.2021.648644/full#supplementary-material

REFERENCES

1. Pan CW, Ramamurthy D, Saw SM. Worldwide prevalence and risk factors for myopia. *Ophthal Physiol Optics.* (2012) 32:3–16. doi: 10.1111/j.1475-1313.2011.00884.x
2. Dirani M, Chan YH, Gazzard G, Hornbeak DM, Leo SW, Selvaraj P, et al. Prevalence of refractive error in Singaporean Chinese children: the strabismus, amblyopia, and refractive error in young Singaporean Children (STARS) study. *Investig Ophthalmol Visual Sci.* (2010) 51:1348–55. doi: 10.1167/iovs.09-3587
3. Ding BY, Shih YF, Lin LLK, Hsiao CK, Wang IJ. Myopia among schoolchildren in East Asia and Singapore. *Survey Ophthalmol.* (2017) 62:677–97. doi: 10.1016/j.survophthal.2017.03.006
4. Lim DH, Han J, Chung TY, Kang S, Yim HW. The high prevalence of myopia in Korean children with influence of parental refractive errors: the 2008-2012 Korean National Health and Nutrition Examination Survey. *PLoS ONE.* (2018) 13:e0207690. doi: 10.1371/journal.pone.0207690
5. Holden BA, Fricke TR, Wilson DA, Jong M, Naidoo KS, Sankaridurg P, et al. Global prevalence of myopia and high myopia and temporal trends from 2000 through 2050. *Ophthalmology.* (2016) 123:1036–42. doi: 10.1016/j.ophtha.2016.01.006
6. Moriyama M, Ohno-Matsui K, Hayashi K, Shimada N, Yoshida T, Tokoro T, et al. Topographic analyses of shape of eyes with pathologic myopia by high-resolution three-dimensional magnetic resonance imaging. *Ophthalmology.* (2011) 118:1626–37. doi: 10.1016/j.ophtha.2011.01.018
7. Cho BJ, Shin JY, Yu HG. Complications of pathologic myopia. *Eye Contact Lens.* (2016) 42:9–15. doi: 10.1097/ICL.0000000000000223
8. Li H, Mitchell P, Rochtchina E, Burlutsky G, Wong TY, Wang JJ. Retinal vessel caliber and myopic retinopathy: the blue mountains eye study. *Ophthalmic Epidemiol.* (2011) 18:275–80. doi: 10.3109/09286586.2011.602508
9. Kim YM, Yoon JU, Koh HJ. The analysis of lacquer crack in the assessment of myopic choroidal neovascularization. *Eye.* (2011) 25:937–46. doi: 10.1038/eye.2011.94
10. Azemin MZ, Daud NM, Ab Hamid F, Zahari I, Sapuan AH. Influence of refractive condition on retinal vasculature complexity in younger subjects. *Sci World J.* (2014) 2014:783525. doi: 10.1155/2014/783525
11. Shimada N, Ohno-Matsui K, Harino S, Yoshida T, Yasuzumi K, Kojima A, et al. Reduction of retinal blood flow in high myopia. *Graefes Arch Clin Exp Ophthalmol.* (2004) 242:284–8. doi: 10.1007/s00417-003-0836-0
12. Meng W, Butterworth J, Malecaze F, Calvas P. Axial length of myopia: a review of current research. *Ophthalmologica.* (2011) 225:127–34. doi: 10.1159/000317072
13. He J, Chen Q, Yin Y, Zhou H, Fan Y, Zhu J, et al. Association between retinal microvasculature and optic disc alterations in high myopia. *Eye.* (2019) 33:1494–503. doi: 10.1038/s41433-019-0438-7
14. Chen Q, He J, Hua Y, Fan Y. Exploration of peripapillary vessel density in highly myopic eyes with peripapillary intrachoroidal cavitation and its relationship with ocular parameters using optical coherence tomography angiography. *Clin Exp Ophthalmol.* (2017) 45:884–93. doi: 10.1111/ceo.12986
15. Spaide RF, Fujimoto JG, Waheed NK, Sadda SR, Staurenghi G. Optical coherence tomography angiography. *Prog Retinal Eye Res.* (2018) 64:1–55. doi: 10.1016/j.preteyeres.2017.11.003
16. An L, Wang RK. In vivo volumetric imaging of vascular perfusion within human retina and choroids with optical micro-angiography. *Optics Express.* (2008) 16:11438–52. doi: 10.1364/OE.16.011438
17. Wang RK. Optical microangiography: a label free 3D imaging technology to visualize and quantify blood circulations within tissue beds *in vivo*. *IEEE J Sel Top Quantum Electron.* (2010) 16:545–54. doi: 10.1109/JSTQE.2009.2033609
18. Barbosa-Breda J, Abegao-Pinto L, Van Keer K, Jesus DA, Lemmens S, Vandewalle E, et al. Heterogeneity in arterial hypertension and ocular perfusion pressure definitions: towards a consensus on blood pressure-related parameters for glaucoma studies. *Acta Ophthalmol.* (2019) 97:e487–92. doi: 10.1111/aos.13942
19. Rishi P, Rishi E, Mathur G, Raval V. Ocular perfusion pressure and choroidal thickness in eyes with polypoidal choroidal vasculopathy, wet-age-related macular degeneration, and normals. *Eye.* (2013) 27:1038–43. doi: 10.1038/eye.2013.106
20. Jo YH, Sung KR, Shin JW. Effects of age on peripapillary and macular vessel density determined using optical coherence tomography angiography in healthy eyes. *Investig Ophthalmol Visual Sci.* (2019) 60:3492–8. doi: 10.1167/iovs.19-26848
21. Yu J, Jiang C, Wang X, Zhu L, Gu R, Xu H, et al. Macular perfusion in healthy Chinese: an optical coherence tomography angiogram study. *Investig Ophthalmol Visual Sci.* (2015) 56:3212–7. doi: 10.1167/iovs.14-16270
22. Rao HL, Pradhan ZS, Weinreb RN, Reddy HB, Riyazuddin M, Sachdeva S, et al. Determinants of peripapillary and macular vessel densities measured by optical coherence tomography angiography in normal eyes. *J Glaucoma.* (2017) 26:491–7. doi: 10.1097/IJG.0000000000000655
23. Cho KH, Ahn SJ, Jung C, Han MK, Park KH, Woo SJ. Ischemic injury of the papillomacular bundle is a predictive marker of poor vision in eyes with branch retinal artery occlusion. *Am J Ophthalmol.* (2016) 162:107–20.e2. doi: 10.1016/j.ajo.2015.11.006
24. Kim YH, Park KH, Woo SJ. Clinical manifestations and visual prognosis of cilioretinal artery sparing central retinal artery occlusion. *Korean J Ophthalmol.* (2020) 34:27–34. doi: 10.3341/kjo.2019.0099
25. Golebiewska J, Biala-Gosek K, Czeszyk A, Hautz W. Optical coherence tomography angiography of superficial retinal vessel density and foveal avascular zone in myopic children. *PLoS ONE.* (2019) 14:e0219785. doi: 10.1371/journal.pone.0219785
26. Wang X, Kong X, Jiang C, Li M, Yu J, Sun X. Is the peripapillary retinal perfusion related to myopia in healthy eyes? A prospective comparative study. *BMJ Open.* (2016) 6:e010791. doi: 10.1136/bmjopen-2015-010791
27. Li M, Yang Y, Jiang H, Gregori G, Roisman L, Zheng F, et al. Retinal microvascular network and microcirculation assessments in high myopia. *Am J Ophthalmol.* (2017) 174:56–67. doi: 10.1016/j.ajo.2016.10.018
28. Guo Y, Sung MS, Park SW. Assessment of superficial retinal microvascular density in healthy myopia. *Int Ophthalmol.* (2019) 39:1861–70. doi: 10.1007/s10792-018-1014-z
29. Yang S, Zhou M, Lu B, Zhang P, Zhao J, Kang M, et al. Quantification of macular vascular density using optical coherence tomography angiography and its relationship with retinal thickness in myopic eyes of young adults. *J Ophthalmol.* (2017) 2017:1397179. doi: 10.1155/2017/1397179
30. Ucak T, Icel E, Yilmaz H, Karakurt Y, Tasli G, Ugurlu A, et al. Alterations in optical coherence tomography angiography findings in patients with high myopia. *Eye.* (2020) 34:1129–35. doi: 10.1038/s41433-020-0824-1
31. Sung KR, Wollstein G, Bilonick RA, Townsend KA, Ishikawa H, Kagemann L, et al. Effects of age on optical coherence tomography measurements of healthy retinal nerve fiber layer, macula, and optic nerve head. *Ophthalmology.* (2009) 116:1119–24. doi: 10.1016/j.ophtha.2009.01.004
32. Jin P, Zou H, Zhu J, Xu X, Jin J, Chang TC, et al. Choroidal and retinal thickness in children with different refractive status measured by swept-source optical coherence tomography. *Am J Ophthalmol.* (2016) 168:164–76. doi: 10.1016/j.ajo.2016.05.008
33. Kur J, Newman EA, Chan-Ling T. Cellular and physiological mechanisms underlying blood flow regulation in the retina and choroid in health and disease. *Prog Retinal Eye Res.* (2012) 31:377–406. doi: 10.1016/j.preteyeres.2012.04.004
34. Yu J, Gu R, Zong Y, Xu H, Wang X, Sun X, et al. Relationship between retinal perfusion and retinal thickness in healthy subjects: an optical coherence tomography angiography study. *Investig Ophthalmol Visual Sci.* (2016) 57:Oct204-10. doi: 10.1167/iovs.15-18630
35. Li Y, Miara H, Ouyang P, Jiang B. The comparison of regional RNFL and fundus vasculature by OCTA in Chinese myopia population. *J Ophthalmol.* (2018) 2018:3490962. doi: 10.1155/2018/3490962
36. Venkatesh R, Sinha S, Gangadharaiah D, Gadde SGK, Mohan A, Shetty R, et al. Retinal structural-vascular-functional relationship using optical coherence tomography and optical coherence tomography - angiography in myopia. *Eye Vision.* (2019) 6:8. doi: 10.1186/s40662-019-0133-6
37. Stone RA, Lin T, Laties AM, Iuvone PM. Retinal dopamine and form-deprivation myopia. *Proc Natl Acad Sci USA.* (1989) 86:704–6. doi: 10.1073/pnas.86.2.704
38. Mao J, Liu S, Qin W, Li F, Wu X, Tan Q. Levodopa inhibits the development of form-deprivation myopia in guinea pigs. *Optometry Vision Sci.* (2010) 87:53–60. doi: 10.1097/OPX.0b013e3181c12b3d

39. Huang H, Wang Z, Weng SJ, Sun XH, Yang XL. Neuromodulatory role of melatonin in retinal information processing. *Prog Retinal Eye Res.* (2013) 32:64–87. doi: 10.1016/j.preteyeres.2012.07.003

Conflict of Interest: The authors declare that the research was conducted in the absence of any commercial or financial relationships that could be construed as a potential conflict of interest.

frontiers in Medicine

HYPOTHESIS AND THEORY
published: 02 July 2021
doi: 10.3389/fmed.2021.655822

Shaping Eyeballs by Scleral Collagen Cross-Linking: A Hypothesis for Myopia Treatment

Mengmeng Wang[1], Christine Carole C. Corpuz[2] and Fengju Zhang[3]*

[1] Hebei Ophthalmology Key Lab, Hebei Eye Hospital, Xingtai, China, [2] Ifugao State University Eye Center, Alfonso Lista, Philippines, [3] Beijing Tongren Eye Center, Beijing Tongren Hospital, Capital Medical University, Beijing, China

The global prevalence of myopia has brought to the attention of the different eye and vision specialists, who make way to control its progression. Evidence have shown that a proactive reshaping of the eyeball is the core point of myopia developing process, which particularly includes the weakening, thinning, and expanding of the sclera. Thus, the sclera is considered to be a prime target for therapeutic manipulation in halting progressive myopia. In the past decades, corneal collagen cross-linking has been applied in clinical practice for treating aberrant corneal remodeling diseases. In this article, we hypothesize that scleral collagen cross-linking (SXL) has a huge potential in stabilizing myopic process by shaping the eyeball and preventing the aberrant scleral remodeling. In contrast with the current methods of optometry correction, such as physiotherapy, pharmacotherapy, spectacles, contact lenses, refractive surgeries, etc., eyeball-shaping method using SXL is a fundamental intervention which aims at the pathogenesis of progressive visual loss of myopia. Compared with the current posterior scleral reinforcement, the most advantage of SXL is that there is no allotransplant into the myopic eye, which means less expenditure, lower risk, and easier to handle in operating.

Keywords: myopia, sclera remodeling, scleral collagen cross-linking, sub-tenon's injection, staphyloma

OPEN ACCESS

Edited by:
Yi Lu,
Fudan University, China

Reviewed by:
Haksu Kyung,
National Medical Center, South Korea
Jinhai Huang,
Affiliated Eye Hospital of Wenzhou Medical University, China
Adel Ebraheem,
California State University, United States

****Correspondence:***
Mengmeng Wang
wangmengmg@163.com

Specialty section:
This article was submitted to Ophthalmology, a section of the journal Frontiers in Medicine

Received: *19 January 2021*
Accepted: *08 June 2021*
Published: *02 July 2021*

Citation:
Wang M, Corpuz CCC and Zhang F (2021) Shaping Eyeballs by Scleral Collagen Cross-Linking: A Hypothesis for Myopia Treatment. Front. Med. 8:655822. doi: 10.3389/fmed.2021.655822

INTRODUCTION

Myopia is the most common cause of visual impairment worldwide (1). It was speculated that the global prevalence of myopia by 2050 will be about 4,758 million (49.8%), including 277 million (4.0% of the global population) of high myopia (2). The burden of myopia is tremendous, as adults with high myopia are more likely to develop pathologic myopia (PM) changes, such as posterior scleral staphyloma, choroidal neovascularization, retinal choroidal atrophy, streak, peripheral retinal degeneration, retinal detachment, and finally lead to blindness (3–5). Generally, myopia was believed to be a mismatch of the eye's anatomical axial length and its focal length (6) which was caused by a "multifactorial" mechanism (7, 8). Aberrant scleral remodeling is the core point during the myopic process, and has been the goal of any long-term therapy for the persistent vision loss associated with myopia (9). Collagen cross-linking, introduced by Wollensak et al. (10), is an effective approach to increase the biomechanical strength of the corneal and scleral tissue. Corneal collagen cross-linking (CXL) has been applied in clinical practice for treating aberrant corneal remodeling diseases in the past decades (11). Similarly, scleral collagen cross-linking (SXL) has a huge potential in stabilizing myopic process by shaping the eyeball and preventing the aberrant scleral remodeling, such as ocular axial elongation and staphyloma.

HYPOTHESIS

We hypothesize SXL as an eyeball-shaping method to prevent the aberrant scleral remodeling during myopic process. Such a theory has not been conceptualized yet, and has not been verified by clinical trials. We reason that the strengthening the integral sclera by SXL could slow down the process of diffuse expansion during eyeball growth; strengthening the equatorial sclera by SXL could limit the axial elongation of the progressive myopic eyeball; partially strengthening the sclera by SXL could block the local bulges which causes staphyloma. Due to its cross-linking effect only on the outer layer of the sclera, SXL is a safe method for the function of the inner tissues underneath the sclera. SXL could be artificially carried out by different cross-linking categories, doses, frequencies, sites according to the current status and prognosis of myopic eyes. For these reasons, it will prevent or halt the progression of myopia in any stage of the disease.

ABERRANT SCLERAL REMODELING OF MYOPIA

There are strong evidences from clinical and experimental studies indicating that the biochemical and biomechanical properties of the sclera play a major role in the progression of myopia (12). Thinning of the sclera and weakened biomechanical properties, particularly at the posterior pole of the eye, have long been known to be an important feature in the development of high myopia in human and mammalian models (9). It is found that myopic sclera undergoes a proactive reshaping process which includes diameter decrease and fiber gap enlargement of the collagenous fiber bundle in all parts of the myopic eye, particularly in the posterior sclera; this causes retinal fundus complications which adversely affect visual acuity (9, 12). Thus, the sclera is considered to be a prime target for therapeutic manipulation in halting progressive myopia (13). Currently, scleral reinforcement is the only available clinical option to slow down scleral bulges (such as in staphyloma), which remain controversial due to its complication risk (14). Thus, given the lack of treatment options, novel clinical solutions are becoming increasingly necessary available to halt progressive scleral remodeling and morbidity of progressive myopia.

PRINCIPLE OF SXL

Cross-linking is a natural phenomenon in the body following an enzymatic or a non-enzymatic pattern (15). Generally, the phenomenon increases in age (16) or in diabetics (17), who rarely show progressive myopia (18). On the contrary, diminished cross-linking is an important factor in the weakening process of myopic sclera (16) with a significant decrease in Young's modulus (19). It is therefore hypothesized that, instead of natural cross-linking, artificially-induced cross-linking might be used therapeutically to retard axial elongation, thereby reducing the risk of blindness.

Photochemically-induced crosslinkings, which currently include riboflavin/UV light crosslinking and riboflavin/blue light crosslinking, can create additional chemical bonds between collagen fibers by photopolymerization and increase scleral stiffness (20). This photochemically-induced cross-linking is mediated by photooxidation between riboflavin (vitamin B2) and laser light (UV light, 360–370 nm; blue light, 400–500 nm). The laser light activates riboflavin into triplet, which in turn produces reactive oxygen species (ROS) and singlet oxygen. ROS reacts with collagen fibril molecules in the corneal stroma and enhances the mechanical strength of cornea by forming new chemical bonds between amino groups of collagen fibril molecules (21). Theoretically, blue light has better penetration ability and lower damage in sclera compared to UV light considering the negative relation between wavelength and penetrating depth in tissue (22).

Chemically-induced crosslinking is another kind of artificially-induced cross-linking, which is usually applied by injecting of chemical crosslinking agents into the sub-Tenon's (sT) space and scleral surface. This kind of crosslinking could represent a simpler way to treat the posterior sclera, thus, avoiding the need for UV light exposure (23). Although there are many compounds that are suitable for industrial and commercial cross-linking purposes, only a limited number of compounds have emerged with potential for scleral stiffening *in vivo*: glyceraldehyde (24), genipin (25–27), methylglyoxal (28, 29) (also called pyruvaldehyde), formaldehyde releasers (FARs) (30), sodium hydroxymethylglycinate (SMG) (31), methylglyoxal (32). Applying the concept of the Maillard reaction (15), these crosslinking agents can be added to the ends of protein molecules and can be further transformed to advanced glycation end products, which are more stable. The resultant covalent collagen cross-links promote enhanced tissue stiffness and resistance to enzymatic degradation (33).

TECHNIQUE OF SXL

Until now, no protocol of photochemically-induced crosslinking was set up for sclera treatment, while several protocols of corneal collagen cross-linking has been suggested to be used on corneal stroma for the treatment of keratoconus, such as the Dresden protocol (34, 35), Siena University protocol (36), Athens protocol (37). Based on the experimental parameters reported in previous studies, the operating procedure of photochemically-induced SXL was generally as follows: after adequate exposure of the target scleral surface, a UV/blue light-source was set up to irradiate directly on the target scleral surface. Specific intensity and energy were performed to ensure that the exposure of UV/blue light on the cornea is below harmful levels. A syringe with a blunt needle allowed an almost continuous supply of the riboflavin photosensitizer solution during the irradiation (38).

Compared with the photochemical procedure, which requires a surgical procedure to access the posterior sclera with a UV light source, injecting into the sub-Tenon's space with chemical cross-linking agents is much simpler (27, 39). Like photochemically-induced crosslinking, no standardized protocol of chemically-induced crosslinking has been set up at present, especially in the parameters of drug concentration and dose (32). However, in

contrast to photochemically-induced crosslinking, repeated sub-Tenon's injections of crosslinking agents can be performed in different quadrants for several times in the following sequential days, months, or years. Another advantage of chemically-induced crosslinking is that, with the help of ultrasound, the chemical crosslinking agents can easily be injected via sub-Tenon's approach, to the posterior globe and even the whole sclera, and could create much larger crosslinked areas than photochemically-induced crosslinking (33, 40).

KNOWN FACTS ABOUT SXL

Photochemically-induced crosslinking has been proven to increase the mechanical strength of scleral collagen in guinea pigs (40), rabbits (41), pigs (10), primates (42), and human sclerae (43). A significant increase in the density and area of collagen fibrils and a significant decrease in the density and area of the interfibrillar spacing can be found in both the equatorial and posterior sclera with either riboflavin/UVA or riboflavin/blue light SXL for 12 months postoperatively (42–44). However, the UV/blue light irradiation with high intensities induces degenerative alterations of scleral cells mainly, in the episcleral and outer scleral layers, which is associated with extracellular matrix degradation, tissue inflammation, hemorrhage, and macrophage infiltration; and in the inner scleral layers, where treatment with high-intensity irradiation induces scleral cell activation with pronounced metabolic activity, and finally results in scleral scarring (45). Not only would the high light intensities be harmful, but also, complicated operations would bring dangerous side-effects on the ocular tissues of the crosslinked eye (46). For example, during the irradiation process, the eyes had to be stretched to expose the target scleral region. Irradiation was largely focused on the equatorial area, thereby inducing possible mechanical injury to ocular tissues. This approach made it impossible to fully expose the posterior sclera that is prone to develop staphyloma (47). Moreover, many other adverse factors were encountered in the past, such as complexity of operating riboflavin/UVA sclera collagen cross-linking, large lesions, difficulty in irradiating the posterior sclera, and difficulty in administering repetitive irradiation (48). Although a minimally invasive therapy has reported to be performed by inserting miniaturelightemitting diodes (LEDs) under the tenon's capsule to the posterior sclera without stretching the eyeball tissues (38), its drawbacks have been put forward, including limited irradiance, risk of thermal tissue damage, and poor flexibility (49).

One potential treatment modality to overcome the above adverse factors of SXL is chemically-induced crosslinking by sub-Tenon's injection of chemical crosslinking agents. This method could serve as a simple and minimally invasive approach to reach the posterior sclera without the need for any specialized UV device or UV irradiation (50). Our research team (39) has successfully used sub-Tenon's injection of 0.5% (22.1 mM) genipin to decelerate form-deprivation myopia in guinea pigs. Another previous study (33) also found that sub-Tenon's injection of 0.15 ml 0.5 M glyceraldehyde seven times during 14 days reduced the AXL elongation of rabbit eyes, with no retinal and choroidal affects under light microscopy. It was also found that glyceraldehyde could increase scleral stiffness for at least 8 months in rabbits (24). Compared with glyceraldehyde (seven fold) or methylglyoxal (30 fold), a much lower concentration of genipin is required to achieve a similar scleral stiffening effect after the sub-Tenon's injection, which means that SXL using genipin could be an alternative low-cytotoxic collagen crosslinking agents (32). Moreover, sub-Tenon's injection of FARs (30) and SMG (31) have also shown their effects in halting the progression of scleral elongation seen in myopic eyes, and would be potential cross-linking compounds. Nevertheless, it should be mentioned that the safety of chemically-induced crosslinking was not fully evaluated at present. In a previous study (51), a sub-conjunctival injection with glyceraldehyde resulted in intraocular pressure elevation and loss of retinal ganglion cell axon, which means that this type of SXL induced glaucoma in these eyes.

DISCUSSIONS AND PREDICTIONS

As scleral crosslinking remains untested on human eyes, we believe that through continuous research and development, SXL would eventually become a novel method for shaping eyeballs and retarding myopic progression. In contrast with the current methods of optometry correction (spectacle works, contact lenses, refractive surgeries, etc.), eyeball-shaping method using SXL would be a fundamental intervention which aim at the pathogenesis of progressive visual loss of myopia. SXL will be also used for preventing and treating the myopia-related complications, such as staphyloma, tractive retinal detachment and macular cleave. Compared with the current posterior scleral reinforcement (PSR) (52), the most advantage of SXL is that there is no allotransplant into the myopic eye, which means less expenditure, lower risk, and easier to handle in operating.

For photochemically-induced crosslinking, several necessary developments on light delivery system will make this SXL method much safer than the current ones. The novel light delivery will provide homogeneous light distribution on scleral spherical surface. This light-delivery system can be easily and flexibly introduced and operated deep in the eye socket to deliver light to the relatively large target region with sufficient irradiance, short procedural time and reduced invasiveness. For accuracy, this system can provide a series of irradiation area size, from several square millimeters to hundred square millimeters, without any extra light leakage to the adjacent tissues. For safety, this system can create its SXL effects on the outer and medium layers of sclera, and can be no harmful for the deeper ocular tissues.

For chemically-induced crosslinking, outstanding crosslinking agents will be selected according to their efficacy under physiologic pH and temperature, permeability, and cell toxicity (53). Mature treatment strategies will be set up and used including the drug compositions, dose, injection sites, and repetition frequency based on the illness condition. Novel drug delivery systems, such as microneedles (54), sub-tenon (episcleral) implants (55), and transscleral iontophoresis (56),

will be combined for increasing the bioavailability of crosslinking agents, improving their penetrability, reducing their systemic absorption and side effects, reducing administration frequency, and improving the comfort and compliance of patients.

Until now, the current SXL protocol has a lot of urgent questions to be answered. For example, dose-effect relationship and dose-toxicity relationship should be generalized. For photochemically-induced crosslinking, the light delivery systems should be initially optimized for less damage. For chemically-induced crosslinking, both effective and safe chemical crosslinking agents should be established using more comparative studies. Long-term observation of SXL efficacy should also be lasting for several years. Thus, there is still a long road ahead before clinical studies are conducted.

Because of their respective characteristics, both photochemically-induced crosslinking and chemically-induced crosslinking will be performed according to the myopic types and the treatment plan. Photochemically-induced crosslinking, which can be easily controlled in dosage, duration and area size of irradiation, will be applied on the symmetrical locations of sclera for axial myopia or on the partial sclera for staphyloma. For larger and homogeneous crosslinking effect, chemically-induced crosslinking can be repeatedly applied by multi-site injections around the equatorial sclera or even the whole sclera. Moreover, it should be noticed that SXL can only stabilize the situation of myopia but not improve vision. This means that SXL can only be useful on eyes while myopia is progressing but not when myopia has stabilized. Thus, we believe that a complex series of treatment, which includes not only both kinds of SXLs but also adding refractive corrections (spectacle works, contact lenses, refractive surgeries, etc.) and myopia-related complication treatments (photodynamic therapy, laser photocoagulation, anti-VEGF intravitreal injections, pars plana vitrectomy, etc.) will be applied in clinics according to the realistic conditions and treatment needs in the future.

DATA AVAILABILITY STATEMENT

The original contributions presented in the study are included in the article/supplementary material, further inquiries can be directed to the corresponding author/s.

AUTHOR CONTRIBUTIONS

MW and FZ collected the data as well as drafted and revised the manuscript. CC revised the manuscript. MW conceptualized and designed the hypothesis as well as reviewed the manuscript. All authors approved the final manuscript as submitted and agreed to be accountable for all aspects of the work.

FUNDING

This study was supported by Grants from National Natural Science Foundation of China (MW: 81700873; FZ: 81570877) and Hebei Province Science and Technology Support Program (MW: 18277754D).

REFERENCES

1. Kumar A, Chawla R, Kumawat D, Pillay G. Insight into high myopia and the macula. *Indian J Ophthalmol.* (2017) 65:85–91. doi: 10.4103/ijo.IJO_863_16
2. Holden BA, Fricke TR, Wilson DA, Jong M, Naidoo KS, SankaridurgP, et al. Global prevalence of myopia and high myopia and temporal trends from 2000 through 2050. *Ophthalmology.* (2016) 123:1036–42. doi: 10.1016/j.ophtha.2016.01.006
3. Ohno-Matsui K, Lai TYY, Lai C,Cheung CMG. Updates of pathologic myopia. *Prog Retin Eye Res.* (2016) 52:156–87. doi: 10.1016/j.preteyeres.2015.12.001
4. Chan NS, Teo K, Cheung CMG. Epidemiology and diagnosis of myopic choroidal neovascularization in asia. *Eye Contact Lens.* (2016) 42:48–55. doi: 10.1097/ICL.0000000000000201
5. Saw S, Gazzard G, Shih-Yen EC,Chua W. Myopia and associated pathological complications. *Ophthalmic Physiol Opt.* (2005) 25:381–91. doi: 10.1111/j.1475-1313.2005.00298.x
6. Stone RA, Flitcroft DI. Ocular shape and myopia. *Ann Acad Med Singap.* (2004) 33:7–15.
7. Wenbo L, Congxia B, Hui L. Genetic and environmental-genetic interaction rules for the myopia based on a family exposed to risk from a myopic environment. *Gene.* (2017) 626:305–8. doi: 10.1016/j.gene.2017.05.051
8. Hammond CJ, Snieder H, Gilbert CE, Spector TD. Genes and environment in refractive error: the twin eye study. *Invest Ophthalmol Vis Sci.* (2001) 42:1232–6.
9. McBrien NA, Gentle A. Role of the sclera in the development and pathological complications of myopia. *Prog Retin Eye Res.* (2003) 22:307–38. doi: 10.1016/S1350-9462(02)00063-0
10. Wollensak G, Spoerl E. Collagen crosslinking of human and porcine sclera. *J Cataract Refract Surg.* (2004) 30:689–95. doi: 10.1016/j.jcrs.2003.11.032
11. O'Brart DPS. Corneal collagen crosslinking for corneal ectasias: a review. *Eur J Ophthalmol.* (2017) 27:253–69. doi: 10.5301/ejo.5000916
12. Rada JAS, Shelton S, Norton TT. The sclera and myopia. *Exp Eye Res.* (2006) 82:185–200. doi: 10.1016/j.exer.2005.08.009
13. Baldivia S, Levy A, Hegde S, Aper SJA, Merkx M, Grytz R. A novel organ culture model to quantify collagen remodeling in tree shrew sclera. *PLoS ONE.* (2016) 11:e0166644. doi: 10.1371/journal.pone.0166644
14. Chen M, Dai J, Chu R, Qian Y. The efficacy and safety of modified snyder-Thompson posterior scleral reinforcement in extensive high myopia of chinese children. *Graefes Arch Clin Exp Ophthalmol.* (2013) 251:2633–8. doi: 10.1007/s00417-013-2429-x
15. Elsheikh A, Wang D, Brown M, Rama P, Campanelli M, Pye D. Assessment of corneal biomechanical properties and their variation with age. *Curr Eye Res.* (2007) 32:11–9. doi: 10.1080/02713680601077145
16. McBrien NA, Norton TT. Prevention of collagen crosslinking increases form-deprivation myopia in tree shrew. *Exp Eye Res.* (1994) 59:475–86. doi: 10.1006/exer.1994.1133
17. Sady C, Khosrof S, Nagaraj R. Advanced maillard reaction and crosslinking of corneal collagen in diabetes. *BiochemBiophys Res Commun.* (1995) 214:793–7. doi: 10.1006/bbrc.1995.2356
18. Løgstrup N, Sjølie AK, Kyvik KO, Green A. Long-term influence of insulin dependent diabetes mellitus on refraction and its components: a population based twin study. *Br J Ophthalmol.* (1997) 81:343–9. doi: 10.1136/bjo.81.5.343
19. Awetissow ES. [The role of the sclera in the pathogenesis of progressive myopia (author's transl)]. *KlinMonblAugenheilkd.* (1980) 176:777–81. doi: 10.1055/s-2008-1057552
20. Kamaev P, Friedman MD, Sherr E, Muller D. Photochemical kinetics of corneal cross-linking with riboflavin. *Invest Ophthalmol Vis Sci.* (2012) 53:2360–7. doi: 10.1167/iovs.11-9385

21. Raiskup F, Spoerl E. Corneal crosslinking with riboflavin and ultraviolet a. I. Principles. *Ocul Surf.* (2013) 11:65–74. doi: 10.1016/j.jtos.2013.01.002
22. Li Y, Zhang F, Sun M, Lai L, LvX, Liu C, et al. Safety and long-term scleral biomechanical stability of rhesus eyes after scleral cross-linking by blue light. *Curr Eye Res.* (2021) 20:1–10. doi: 10.1080/02713683.2020.1853781
23. Wollensak G, Redl B. Gel electrophoretic analysis of corneal collagen after photodynamic cross-linking treatment. *Cornea.* (2008) 27:353–6. doi: 10.1097/ICO.0b013e31815cf66a
24. Wollensak G, Iomdina E. Long-term biomechanical properties after collagen crosslinking of sclera using glyceraldehyde. *Acta Ophthalmol.* (2008) 86:887–93. doi: 10.1111/j.1755-3768.2007.01156.x
25. Avila MY, Navia JL. Effect of genipin collagen crosslinking on porcine corneas. *J Cataract Refract Surg.* (2010) 36:659–64. doi: 10.1016/j.jcrs.2009.11.003
26. Liu T, Luo X, Gu Y, Yang B, Wang Z. Correlation of discoloration and biomechanical properties in porcine sclera induced by genipin. *Int J Ophthalmol.* (2014) 7:621–5. doi: 10.3980/j.issn.2222-3959.2014.04.06
27. Liu T, Wang Z. Collagen crosslinking of porcine sclera using genipin. *Acta Ophthalmol.* (2013) 91:e253–7. doi: 10.1111/aos.12172
28. Spoerl E, Boehm AG, Pillunat LE. The influence of various substances on the biomechanical behavior of lamina cribrosa and peripapillary sclera. *Invest Ophthalmol Vis Sci.* (2005) 46:1286–90. doi: 10.1167/iovs.04-0978
29. Wong FF, Lari DR, Schultz DS, Stewart JM. Whole globe inflation testing of exogenously crosslinked sclera using genipin and methylglyoxal. *Exp Eye Res.* (2012) 103:17–21. doi: 10.1016/j.exer.2012.06.010
30. Babar N, Kim M, Cao K, Shimizu Y, Kim S, Takaoka A, et al. Cosmetic preservatives as therapeutic corneal and scleral tissue cross-linking agents. *Invest Ophthalmol Vis Sci.* (2015) 56:1274–82. doi: 10.1167/iovs.14-16035
31. Zyablitskaya M, Takaoka A, Munteanu EL, Nagasaki T, Trokel SL, Paik DC. Evaluation of therapeutic tissue crosslinking (TXL) for myopia using second harmonic generation signal microscopy in rabbit sclera. *Invest Ophthalmol Vis Sci.* (2017) 58:21–9.doi: 10.1167/iovs.16-20241
32. Campbell IC, Hannon BG, Read AT, Sherwood JM, Schwaner SA, Ethier CR. Quantification of the efficacy of collagen cross-linking agents to induce stiffening of rat sclera. *J R Soc Interface.* (2017) 14:20170014. doi: 10.1098/rsif.2017.0014
33. Lin X, Naidu RK, Dai J,Zhou X, Qu X, Zhou H. Scleral cross-Linking using glyceraldehyde for the prevention of axial elongation in the rabbit: blocked axial elongation and altered scleral microstructure. *Curr Eye Res.* (2019) 44:162–71. doi: 10.1080/02713683.2018.1522647
34. Kymionis GD, Mikropoulos DG, Portaliou DM, Voudouragkaki IC, Kozobolis VP, Konstas AGP. An overview of corneal collagen cross-linking (CXL). *Adv Ther.* (2013) 30:858–69. doi: 10.1007/s12325-013-0065-9
35. Wollensak G, Spoerl E, Seiler T. Riboflavin/ultraviolet-a-induced collagen crosslinking for the treatment of keratoconus. *Am J Ophthalmol.* (2003) 135:620–7. doi: 10.1016/S0002-9394(02)02220-1
36. Caporossi A, Mazzotta C, Baiocchi S, Bagaglia S, Caporossi O, Villano A, et al. Long-term results of riboflavin ultraviolet a corneal collagen cross-linking for keratoconus in italy: the siena eye cross study. *Am J Ophthalmol.* (2010) 149:585–93. doi: 10.1016/j.ajo.2009.10.021
37. Kanellopoulos AJ, Binder PS. Management of corneal ectasia after lASIK with combined, same-day, topography-guided partial transepithelial pRK and collagen cross-linking: the athens protocol. *J Refract Surg.* (2011) 27:323–31. doi: 10.3928/1081597X-20101105-01
38. Xiao B, Chu Y, Wang H, Han Q. Minimally invasive repetitive uVA irradiation along with riboflavin treatment increased the strength of sclera collagen cross-Linking. *J Ophthalmol.* (2017) 2017:1324012. doi: 10.1155/2017/1324012
39. Wang M, Corpuz CCC. Effects of scleral cross-linking using genipin on the process of form-deprivation myopia in the guinea pig: a randomized controlled experimental study. *BMC Ophthalmol.* (2015) 15:89. doi: 10.1186/s12886-015-0086-z
40. Chu Y, Cheng Z, Liu J, Wang Y, Guo H, Han Q. The effects of scleral collagen cross-Linking using glyceraldehyde on the progression of form-Deprived myopia in guinea pigs. *J Ophthalmol.* (2016) 2016:3526153. doi: 10.1155/2016/3526153
41. Wollensak G, Iomdina E. Long-term biomechanical properties of rabbit sclera after collagen crosslinking using riboflavin and ultraviolet a (UVA). *Acta Ophthalmol.* (2009) 87:193–8. doi: 10.1111/j.1755-3768.2008.01229.x
42. Sun M, Zhang F, Li Y, Ouyang B, Wang M, Jiao X, et al. Evaluation of the safety and long-term scleral biomechanical stability of uVA cross-linking on scleral collagen in rhesus monkeys. *J Refract Surg.* (2020) 36:696–702. doi: 10.3928/1081597X-20200807-01
43. Gawargious BA,Le A, Lesgart M, UgradarS, Demer JL. Differential regional stiffening of sclera by collagen cross-linking. *Curr Eye Res.* (2020) 45:718–25. doi: 10.1080/02713683.2019.1694157
44. Choi S, Lee S, Lee H, Cheong Y, Jung G, JinK, et al. Structural response of human corneal and scleral tissues to collagen cross-linking treatment with riboflavin and ultraviolet a light. *Lasers Med Sci.* (2013) 28:1289–96. doi: 10.1007/s10103-012-1237-6
45. Karl A, Makarov FN, Koch C, KörberN, SchuldtC, Krüger M, et al. The ultrastructure of rabbit sclera after scleral crosslinking with riboflavin and blue light of different intensities. *Graefes Arch Clin Exp Ophthalmol.* (2016) 254:1567–1577. doi: 10.1007/s00417-016-3393-z
46. Wollensak G, Iomdina E, Dittert D, Salamatina O, Stoltenburg G. Cross-linking of scleral collagen in the rabbit using riboflavin and uVA. *Acta Ophthalmol Scand.* (2005) 83:477–82. doi: 10.1111/j.1600-0420.2005.00447.x
47. Zhang X, Tao X, Zhang J, Li ZW, Xu YY, Wang YM, et al. A review of collagen cross-linking in cornea and sclera. *J Ophthalmol.* (2015) 2015:289467. doi: 10.1155/2015/289467
48. Kwok SJJ, Kim M, Lin HH, Seiler TG, Beck E, ShaoP, et al. Flexible optical waveguides for uniform periscleral cross-Linking. *Invest Ophthalmol Vis Sci.* (2017) 58:2596–602. doi: 10.1167/iovs.17-21559
49. Kwok SJJ, Forward S, Wertheimer CM, Liapis AC, Lin HH, Kim M, et al. Selective equatorial sclera crosslinking in the orbit using a metal-Coated polymer waveguide. *Invest Ophthalmol Vis Sci.* (2019) 60:2563–70. doi: 10.1167/iovs.19-26709
50. Kumar CM, McNeela BJ. Ultrasonic localization of anaesthetic fluid using sub-Tenon's cannulae of three different lengths. *Eye (Lond).* (2003) 17:1003–7. doi: 10.1038/sj.eye.6700501
51. Kimball EC, Nguyen C, Steinhart MR, Nguyen TD, Pease ME, Oglesby EN, et al. Experimental scleral cross-linking increases glaucoma damage in a mouse model. *Exp Eye Res.* (2014) 128:129–40. doi: 10.1016/j.exer.2014.08.016
52. Huang W, Duan A, Qi Y. Posterior scleral reinforcement to prevent progression of high myopia. *Asia Pac J Ophthalmol (Phila).* (2019) 8:366–70. doi: 10.1097/APO.0000000000000257
53. Takaoka A, Cao K, Oste EM, Nagasaki T, Paik DC. Topical therapeutic corneal and scleral tissue cross-linking solutions: *in vitro* formaldehyde release studies using cosmetic preservatives. *Biosci Rep.* (2019) 39:BSR20182392. doi: 10.1042/BSR20182392
54. Gupta P, Yadav KS. Applications of microneedles in delivering drugs for various ocular diseases. *Life Sci.* (2019) 237:116907. doi: 10.1016/j.lfs.2019.116907
55. Zhou C, Robert M, Kapoulea V, Lei F, Stagner AM, Jakobiec FA, et al. Sustained subconjunctival delivery of infliximab protects the cornea and retina following alkali burn to the eye. *Invest Ophthalmol Vis Sci.* (2017) 58:96–105. doi: 10.1167/iovs.16-20339
56. Perez VL, Wirostko B, Korenfeld M, From S, Raizman M. Ophthalmic drug delivery using iontophoresis: recent clinical applications. *J Ocul Pharmacol Ther.* (2020) 36:75–87. doi: 10.1089/jop.2019.0034

Conflict of Interest: The authors declare that the research was conducted in the absence of any commercial or financial relationships that could be construed as a potential conflict of interest.

frontiers in Medicine

ORIGINAL RESEARCH
published: 20 August 2021
doi: 10.3389/fmed.2021.679192

The Association in Myopic Tractional Maculopathy With Myopic Atrophy Maculopathy

*Jiaxin Tian†, Yue Qi†, Caixia Lin, Kai Cao and Ningli Wang**

Beijing Tongren Eye Center, Beijing Institute of Ophthalmology, Beijing Ophthalmology and Visual Sciences Key Laboratory, Beijing Tongren Hospital, Capital Medical University, Beijing, China

Purpose: To investigate the relationship between myopic tractional maculopathy (MTM) and myopic atrophy maculopathy (MAM).

Method: Two hundred and six eyes with definitive myopic retinoschisis were assessed in the retrospective observational case series study and the atrophic and tractional features were further evaluated. Atrophic changes were analyzed according to the atrophic component in the ATN classification and the occurrence of gamma zones and delta zones. Tractional changes were evaluated based on different retinoschisis layers, the location and range of outer retinoschisis, retinal detachment, inner lamellar macular hole (ILMH), outer lamellar MH (OLMH), full-thickness MH (FTMH), and paravascular abnormalities.

Results: Of all the eyes, 29.6, 42.7, 19.4, and 8.3% presented MAM grades with A1, A2, A3, and A4, respectively. The three layers of retinoschisis and the entire macular retinoschisis had the highest incidences in A2 (38.6%; 54.5%). The numbers of retinoschisis layers and the grades of outer retinoschisis had a weak negative correlation with MAM ($r = -0.138$, $P = 0.048$; $r = -0.139$, $P = 0.047$). All the eyes had gamma zones, and 82.52% of eyes also had delta zones. The incidence of retinal detachment and OLMH reached the peak in A2 and then decreased gradually. With MAM aggravation, the prevalence of ILMH decreased. Eyes with A1 and A2 were more likely to have OLMH, and those with A3 and A4 were more likely to have FTMH ($P = 0.028$; OR, 3.423; 95% CI, 1.144–10.236; $P = 0.004$; OR, 7.752; 95% CI, 1.951–30.803). With the MAM grades growing, the types of paravascular abnormalities increased ($r = 0.165$, $P = 0.018$).

Conclusion: Diffuse chorioretinal atrophy was the dominant MAM grade in eyes with MTM. In the study, 72.3% of eyes with MTM presented with diffuse chorioretinal atrophy and a tessellated fundus. Over 80% of eyes with MTM had both gamma zones and delta zones. Diffuse chorioretinal atrophy might be a complicated stage for MTM with the highest rate of three layers of retinoschisis, the entire macular retinoschisis, RD, and OLMH. Atrophic progression might involve the development of MH. When MTM combines with well-defined atrophy, the occurrence of FTMH should be noted.

Keywords: association, myopic tractional maculopathy, myopic atrophy maculopathy, characteristics, fundus images, optical coherence tomography

OPEN ACCESS

Edited by:
Xiangtian Zhou,
Wenzhou Medical University, China

Reviewed by:
Xingtao Zhou,
Fudan University, China
Tien Wong,
National University of Singapore, Singapore

****Correspondence:***
Ningli Wang
wningli@vip.163.com

† These authors have contributed equally to this work and share first authorship

Specialty section:
This article was submitted to Ophthalmology, a section of the journal Frontiers in Medicine

Received: *11 March 2021*
Accepted: *21 June 2021*
Published: *20 August 2021*

Citation:
Tian J, Qi Y, Lin C, Cao K and Wang N (2021) The Association in Myopic Tractional Maculopathy With Myopic Atrophy Maculopathy. Front. Med. 8:679192. doi: 10.3389/fmed.2021.679192

INTRODUCTION

As we all know, in combination with environmental changes, lifestyle, and many other factors, the prevalence of myopia is showing significant and sustained growth worldwide (1, 2). Following that, pathologic myopia and myopic macular degeneration are also increasing year by year and becoming a dominant cause of blindness (3). As an acquainted complication in highly myopic eyes, investigators first described myopic retinoschisis (MR) in 1938 (4). It was also regarded as retinal detachment (RD) without a hole in a myopic patient with posterior staphyloma in 1958 (5). In 1999, Takano and Kishi disclosed foveal retinoschisis by optical coherence tomography (OCT) in pathologic myopia patients (6). Later, Panozzo and Mercanti proposed myopic traction maculopathy (MTM), which included different stages of tractional maculopathy, like MR, RD, and macular hole (MH) (7).

Currently, investigators tend to divide myopic maculopathy into three components, myopic atrophy maculopathy (MAM), MTM, and myopic neovascular maculopathy. This classification helps us gain a comprehensive understanding of the disease and clinical management (8). As an essential part of pathologic myopia, the MAM grade reveals a general fundus condition and involves different types of myopic retinopathy. In the previous studies, people believed that MTM always occurred in the advanced stage of pathologic myopia with severe atrophic changes (9). In the study by Chen et al. there was no direct relationship between MAM and MTM based on the ATN system (10). At present, the characteristics of atrophy in MTM are not explicit. Besides, from the integrity of myopic retinopathy, both kinds of pathological changes could exist in the meanwhile. We speculate that there could be some interaction between MAM and MTM. Therefore, we made a detailed analysis of atrophic and tractional changes in eyes with definite MR to evaluate the relationship between MAM and MTM.

MATERIALS AND METHODS

Patients Enrolled and Ocular Examination

In this retrospective observational case series study, we reviewed highly myopic patients with an axial length >26.5 mm or a refractive error <-6 diopters in Beijing Tongren Hospital from October 2018 to October 2020. Eyes with definite MTM (MR and the complication stage of MTM, including RD and MH) were enrolled in the study. The exclusion criteria were as follows: vitreoretinal surgery history; combined with other ocular diseases involving fundus changes and retinoschisis, including age-related macular degeneration, diabetic retinopathy, retinal vein occlusion, glaucoma, uveitis; subjects without available fundus or OCT images, like opacities of refractive media, and images with poor quality. The study adhered to the tenets of the Declaration of Helsinki and was approved by the Ethics Committee of Beijing Tongren Hospital.

All patients underwent regular ophthalmologic examinations, including slit-lamp biomicroscopy, fundoscopy, refraction with an assessment of best-corrected visual acuity (BCVA), A-mode ultrasonography for measurement of axial length (AXL), intraocular pressure, and fundus photography (fundus camera TRC-50; Topcon, Tokyo, Japan). In addition, two kinds of spectral-domain OCT images covering a macular area were obtained. One (RTVue-XR Avanti Optovue, Inc., Fremont, CA, United States) was performed with 10 mm scans along 18 meridians centered on the fovea. The other one (Spectralis, Heidelberg Engineering Co., Heidelberg, Germany) was measured with horizontal and vertical scans in the 11.5 × 11.5 mm rectangle area. Both measuring modes could accurately reflect fundus changes.

Images Analysis

We evaluated MAM in fundus images based on the ATN system's atrophic component as follows: A0: no myopic retinal degenerative lesion; A1: tessellated fundus; A2: diffuse chorioretinal atrophy; A3: patchy chorioretinal atrophy; A4: macular atrophy (8). For parapapillary atrophy, we recorded the presence of gamma zones and delta zones according to the previous method (11).

In OCT images, we defined three layers of retinoschisis according to the previous study: inner retinoschisis (schisis between ILM and ganglion cell layer), middle retinoschisis (schisis in inner plexiform layer and/or inner nuclear layer), and outer retinoschisis (schisis in the outer plexiform layer) (12). We followed the classification proposed by Shimada et al. to assess the range and location of outer retinoschisis: S0, no macular retinoschisis; S1, extra-foveal; S2, fovea-only; S3, foveal but not entire macular area; and S4, entire macular area. If there was no outer retinoschisis, but inner retinoschisis and/or middle retinoschisis existed, we classified it into S0 (13). Besides, we recorded the occurrence of complications of MR in MTM, including RD, MH, and further divided MH into inner lamellar MH (ILMH), outer lamellar MH (OLMH), and full-thickness MH (FTMH). Paravascular abnormalities (PVAs), including paravascular microfolds, paravascular retinal cysts, and paravascular lamellar holes, were also identified (14–16).

All the images were analyzed by two ophthalmologists (J.X.T. and C.X.L.) independently. For results with disagreement, the more experienced retinal specialist (Y.Q.) was consulted to make a final decision.

Statistical Analyses

Mean values (standard deviation) and count (frequencies) were used to describe continuous and categorical data, respectively. The Kruskal-Wallis test and one-way analysis of variance (ANOVA) were performed to assess the difference among subgroups with abnormal distribution and normal distribution, respectively. Categorical data were assessed with the Chi-square test and Cramer's V coefficient. Spearman's rank correlation was used to test the relationship between different variables when at least one of them was a rank variable. After univariate analysis, multivariate logistic regression was used to assess the significance of factors in MTM. A two-sided $P < 0.05$ was considered statistically significant. All statistical analyses were performed using commercial software (SPSS version 24.0; SPSS, Inc., Chicago, IL, United States).

TABLE 1 | Demographic and ocular characteristics of patients with myopic tractional maculopathy.

Variables	Patients
Demographic characteristics	
Age (y), mean ± SD	54.02 ± 11.5
Sex, *n* (%)	
Male	53 (25.7%)
Female	153 (74.3%)
Ocular characteristics	
BCVA in logMAR unit (Snellen), mean ± SD	0.69 ± 0.54 (20/29)
Axial length (mm), mean ± SD	29.86 ± 2.05
Intraocular pressure (mmHg), mean ± SD	15.32 ± 3.59
Myopic atrophy maculopathy, *n* (%)	
Tessellated fundus (grade A1)	61 (29.6%)
Diffuse chorioretinal atrophy (grade A2)	88 (42.7%)
Patchy chorioretinal atrophy (grade A3)	40 (19.4%)
Macular atrophy (grade A4)	17 (8.3%)
Parapapillary atrophy	
Gamma zone	206 (100%)
Delta zone	170 (82.52%)
Inner retinoschisis, *n* (%)	132 (64.1%)
Middle retinoschisis, *n* (%)	83 (40.3%)
Outer retinoschisis, *n* (%)	180 (87.4%)
Number of retinoschisis layers	
One-layer retinoschisis	68 (33.0%)
Two-layer retinoschisis	72 (35.0%)
Three-layer retinoschisis	66 (32.0%)
Grade of outer retinoschisis	
S0; no outer retinoschisis	21 (10.2%)
S1; extra foveal	31 (15.0%)
S2; foveal	24 (11.7%)
S3; foveal and extra foveal	33 (16.0%)
S4; entire macular	97 (47.1%)

SD, standard deviation; BCVA, best corrected visual acuity.

RESULTS

Demographics and Ocular Characteristics of Patients

From October 2018 to October 2020, a total of 723 highly myopic patients visited the ophthalmology clinic. Among them, 128 patients with 206 eyes had defined MTM, which met the criteria, and were further enrolled in the study with detailed analyses. Clinical characteristics of the eyes are summarized in **Table 1**. The mean age was 54.02 ± 11.5 years with a range of 17–79 years. Among the patients, 15 patients (11.72%) were younger than 40 years old. The proportion of female patients was higher than that of male patients (73.4 vs. 25.7%; **Table 1**).

The results showed that as AXL rose, the grades of MAM increased ($r = 0.446$, $P < 0.001$). There was no association in AXL with the grades of outer retinoschisis and the number of retinoschisis layers ($r = -0.048$, $P = 0.507$; $r = 0.019$, $P = 0.798$). Besides, no significant difference in AXL between different grades of outer retinoschisis or different numbers of retinoschisis layers was detected (Chi-square value = 6.587, $P = 0.159$; $F = 0.103$, $P = 0.902$).

The Association in MTM With Atrophic Changes

Of all the eyes, 61 (29.6%), 88 (42.7%), 40 (19.4%), and 17 (8.3%) had MAM grades of A1, A2, A3, and A4 (**Figure 1** and **Table 1**). No eye belonged to A0. For number of retinoschisis layers, the incidence of three-layer retinoschisis was close in the MAM grades A1 (34.4%) and A2 (38.6%), peaked at A2, and then decreased. With the increasing MAM grades, the rate trend of entire macular retinoschisis was similar to that of three-layer retinoschisis, which was highest at A2 (54.5%), followed by A1 (50.8%). At A2, the incidence gradually declined (**Figure 2** and **Table 2**). Both the number of retinoschisis layers and grades of outer retinoschisis presented a weakly negative association with the severity of MAM ($r = -0.138$, $P = 0.048$; $r = -0.139$, $P = 0.047$; **Figure 2**).

Here, we took gamma zones and delta zones to evaluate parapapillary atrophic changes in MTM. All the eyes had gamma zones, and 170 (82.5%) eyes showed delta zones simultaneously. The incidence of delta zones in the eyes with MTM was 73.8, 84.1, 90.0, and 88.2%, from the MAM grade A1–A4, respectively. There was no significant difference in the incidence of delta zones between different grades of outer retinoschisis or different numbers of retinoschisis layers ($P = 0.764$; $P = 0.619$).

The Association in Complications of MR With MAM

In the study, the prevalence of ILMH, OLMH, and FTMH in the highly myopic eyes was 17.5, 16.5, and 5.3%, respectively (**Table 2**). The prevalence of ILMH went down as the severity of MAM increased. The incidence of OLMH and FTMH showed an opposite trend with the grade of MAM. The OLMH rate reached its peak at A2 and then decreased gradually. On the contrary, the incidence of FTMH reached its minimum at A2 and then increased (**Figure 3A**). The result showed that the OLMH rate weakly correlated with the grade of MAM (Cramer's V coefficient = 0.217; $P = 0.007$). The prevalence of OLMH in MR eyes with A1 and A2 was significantly higher than that in MR eyes with A3 and A4 (20.1 vs. 7.0%, $P = 0.023$). Besides, FTMH also presented a weak correlation with MAM (Cramer's V coefficient = 0.249; $P = 0.010$). The MR eyes with MAM grades A3 and A4 had a higher rate of FTMH than those with MAM grades A1 and A2 (14.0 vs. 2.0%, $P = 0.002$).

Given that myopic maculopathy might be affected by age, gender, and AXL, we conducted univariate analyses to test the association of these factors with the occurrence of OLMH and FTMH (**Table 3**). According to the result, we selected age ($P < 0.10$) and the severity of MAM as covariates to perform multivariable regression analysis for OLMH and FTMH. Compared with the MR eyes with A3 and A4, the results showed that A1 and A2 were more likely to have OLMH ($P = 0.028$; OR, 3.423; 95% CI, 1.144–10.236, **Table 4**). On the contrary, compared with A1 and A2, A3, and A4 were inclined to have FTMH ($P = 0.004$; OR, 7.752; 95% CI, 1.951–30.803; **Table 4**).

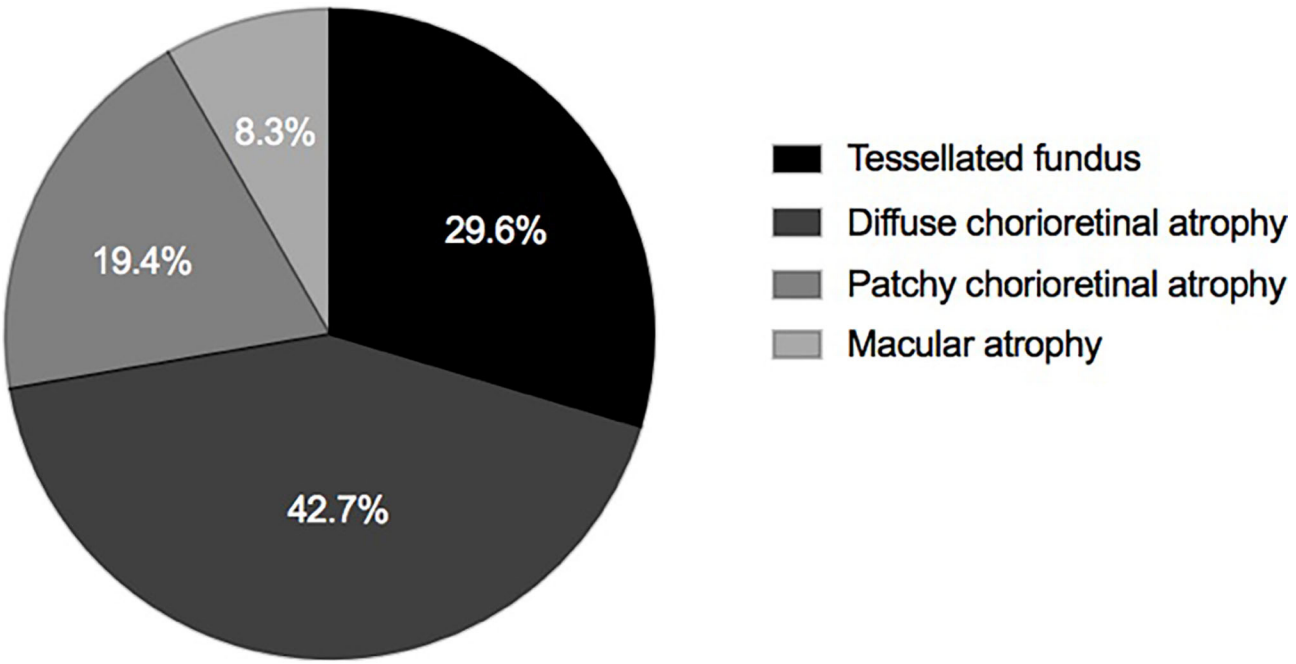

FIGURE 1 | Distributions of myopic atrophy maculopathy in eyes with definite myopic tractional maculopathy.

Sixty-two of the eyes (30.1%) presented with RD. As the severity of MAM increased, the trend of RD rate was similar to that of OLMH. Overall, 79% of RD belonged to MAM grades A1 and A2.

The Association in PVAs With MAM

For different kinds of PVAs, paravascular retinal cysts had the highest incidence (67.0%), followed by paravascular microfolds (51.5%) and then paravascular lamellar holes (16.0%). The incidence of retinal cysts and microfolds had a weak correlation with MAM (Cramer's V = 0.198, $P = 0.044$; Cramer's V = 0.225, $P = 0.016$; **Table 2**). The eyes with MAM grades A2 and A3 were more likely to have retinal cysts and microfolds than those with MAM grades A1 and A4 (74.2 vs. 55.1%, $P = 0.005$; 58.6 vs. 39.7%, $P = 0.009$). However, the rate trends of these two kinds of PVAs were still slightly different, with the increase of MAM grades. The incidence of retinal cysts was highest in A2 and then decreased with the severity of MAM rising. While the rate of paravascular microfolds reached the highest in A3 and then went down. The prevalence of paravascular lamellar holes showed an upward trend from A1 to A4 (**Figure 3B**). In addition, the varieties of PVAs had a positive correlation with the grade of MAM ($r = 0.165$, $P = 0.018$) and AXL ($r = 0.179$, $P = 0.013$).

DISCUSSION

As far as we know, this is the first time the atrophic features in eyes with definite MTM have been elaborately described. Diffuse chorioretinal atrophy occupied the most significant MAM grades in eyes with MTM, followed by tessellated fundus. These two kinds of MAM grades accounted for the vast majority in eyes with MTM (72.3%). More extensive and multi-layered forms of retinoschisis might be likely to occur in less severe MAM. More than 80% of eyes with MTM had both gamma zones and delta zones. In addition, we found that atrophic changes might be involved in the development of MH. The eyes with tessellated fundus and diffuse chorioretinal atrophy were more likely to have OLMH, and those with well-defined atrophy were more likely to present with FTMH. With MAM aggravation and AXL growth, the types of PVAs increased. To more comprehensively assess the relationship between tractional and atrophic features, we chose multiple perspectives to reflect the characteristics of MTM, like the range and location of outer retinoschisis, different layers of retinoschisis, various complications, and PVAs rather than the tractional component in the ATN classification (8).

Previous studies have shown that being female was a risk factor for myopic maculopathy (10, 17). Here, the percentage of female patients was higher than male patients. To reflect the characteristics of MTM as much as possible, we did not limit the age of the subjects to 50 years or older. While the mean age in our study was also nearly to that of previous studies (4, 13). Moreover, around 10% of patients with MTM were younger than 40 years old.

From the integrity of ocular changes in pathologic myopia, atrophic lesions involve both macular and parapapillary zones. In the study, we briefly analyzed parapapillary atrophy in MTM and found that more than 80% of eyes with MTM had both gamma zones and delta zones. Moreover, even in MR eyes with tessellated fundus, 73.8% of them had both kinds of parapapillary atrophies, representing severe parapapillary atrophy. Besides, a delta zone

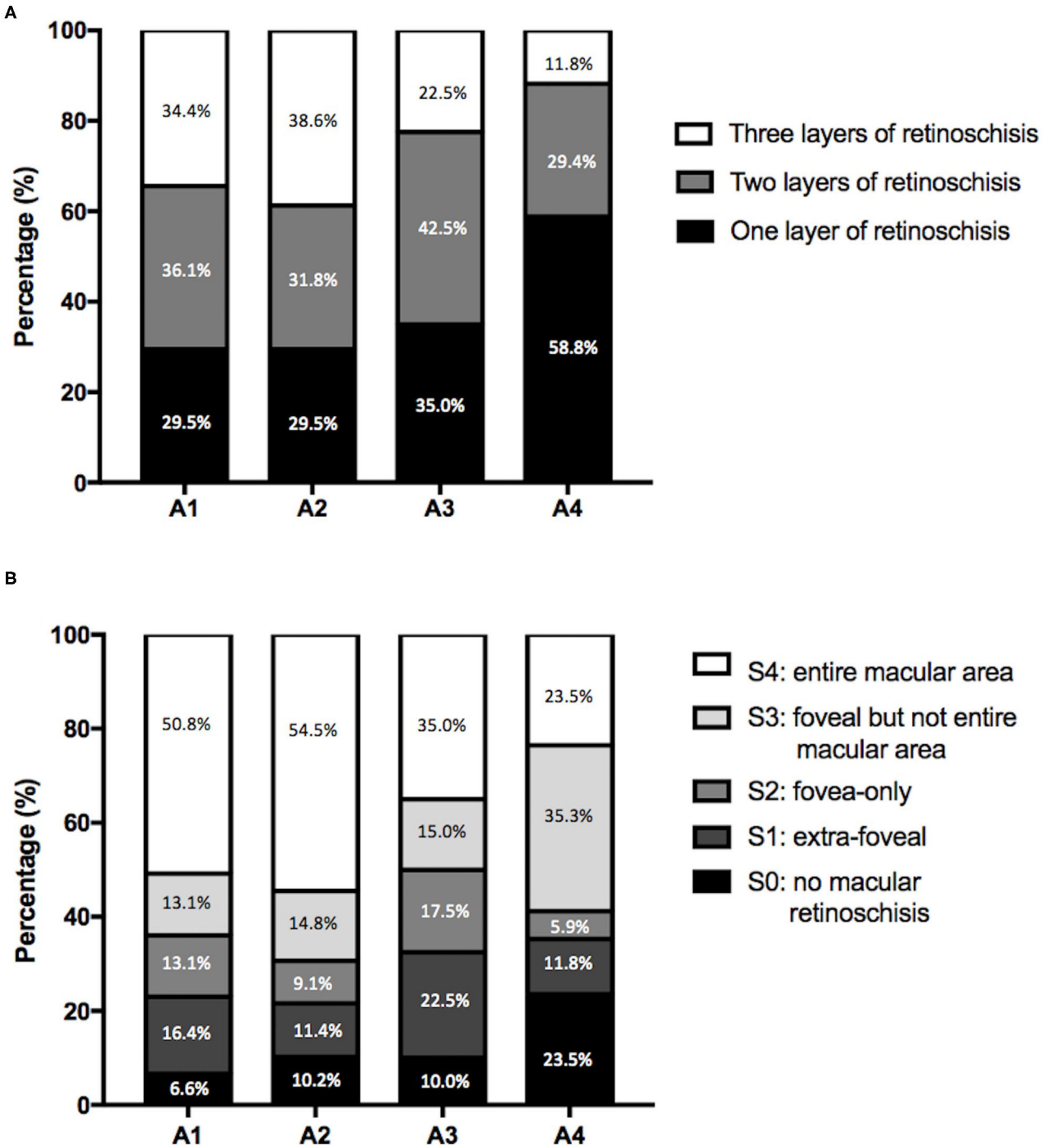

FIGURE 2 | Features of myopic retinoschisis in different myopic atrophy maculopathy (MAM) grades. **(A)** Distributions of numbers of retinoschisis layers in different MAM grades. **(B)** Distributions of the range and location of outer retinoschisis in different MAM grades. A1, tessellated fundus; A2, diffuse chorioretinal atrophy; A3, patchy chorioretinal atrophy; A4, macular atrophy.

is from the elongated and thinned peripapillary scleral flange, which implies significant remodeling of the ocular shape (11). Therefore, the high prevalence of delta zones may also suggest the effect of the sclera shape in MTM development.

In 2003, Baba et al. assessed 134 eyes with high myopia and found out of 7 eyes with foveal detachment or retinoschisis all had well-defined chorioretinal atrophy. So they believed retinoschisis always developed in eyes with severe MAM (9). In the study

TABLE 2 | Characteristics of myopic tractional maculopathy in different grades of myopic atrophy maculopathy.

	Grades of myopic atrophy maculopathy				*P*
	A1, *n* (%)	**A2, *n* (%)**	**A3, *n* (%)**	**A4, *n* (%)**	
Number of retinoschisis layers					
One-layer retinoschisis	18 (29.5%)	26 (29.5%)	14 (35%)	10 (58.8%)	0.137
Two-layer retinoschisis	22 (36.1%)	28 (31.8%)	17 (42.5%)	5 (29.4%)	
Three-layer retinoschisis	21 (34.4%)	34 (38.6%)	9 (22.5%)	2 (11.8%)	
Grade of outer retinoschisis					
S0; no outer retinoschisis	4 (6.6%)	9 (10.2%)	4 (10.0%)	4 (23.5%)	0.189
S1; extra foveal	10 (16.4%)	10 (11.4%)	9 (22.5%)	2 (11.8%)	
S2; foveal	8 (13.1%)	8 (9.1%)	7 (17.5%)	1 (5.9%)	
S3; foveal and extra foveal	8 (13.1%)	13 (14.8%)	6 (15.0%)	6 (35.3%)	
S4; entire macular	31 (50.8%)	48 (54.5%)	14 (35.0%)	4 (23.5%)	
Complications of myopic retinoschisis					
Retinal detachments	15 (24.6%)	34 (38.6%)	10 (25.0%)	3 (17.6%)	0.128
Inner lamellar macular holes	12 (19.7%)	17 (19.3%)	6 (15.0%)	1 (5.9%)	0.457
Outer lamellar macular holes	8 (13.1%)	22 (25.0%)	4 (10.0%)	0 (0.0%)	0.007
Full thickness macular holes	2 (3.3%)	1 (1.1%)	5 (12.5%)	3 (17.6%)	0.010
Paravascular abnormalities					
Paravascular microfolds	23 (37.7%)	47 (53.4%)	28 (70.0%)	8 (47.1%)	0.016
Paravascular retinal cysts	34 (55.7%)	66 (75.0%)	29 (72.5%)	9 (52.9%)	0.044
Paravascular lamellar holes	7 (11.5%)	15 (17.0%)	7 (17.5%)	4 (23.5%)	0.619

P, Chi-square test.
A1, tessellated fundus; A2, diffuse chorioretinal atrophy; A3, patchy chorioretinal atrophy; A4, macular atrophy (8).

by Chen et al. the severity of MTM was not in keeping with MAM based on the ATN classification (10). Later, Takahashi et al. further demonstrated that a shorter AXL might be a risk factor for MR (12). Here, we found that above 70% of eyes with MTM had diffuse chorioretinal atrophy and a tessellated fundus. Besides, the severity of MR presented a weak negative correlation with grades of MAM, which were in indirect agreement with previous studies (12).

Further deliberating the distributions of layers and grades of MR and the complication rates in different stages of MAM, we found that all the incidences of three layers of retinoschisis, entire macular retinoschisis, RD, and OLMH reached the highest in the MAM grade A2 (**Figures 2**, **3**). Besides, the eyes with a tessellated fundus and diffuse chorioretinal atrophy were more likely to have OLMH, and those with more advanced stages of MAM were more likely to present with FTMH. Some studies laid out detailed descriptions about the natural course from retinoschisis to the complication stage and referred to the significance of vitreous traction and premacular structure (18–20). Parolini et al. believed the natural evolution of MR depended on two forces, the perpendicular force to the retina which induced retinoschisis and FD, and the tangential force to the retina which induced MH (21).

Based on our results and the view proposed by Parolini et al. we guess the atrophic process might involve developing complications and propose a hypothesis on the mechanics-related progression of MAM and MTM. A schematic diagram is shown in **Figure 4**. In the progression of pathological myopia, the force on the macula can be mainly divided into a perpendicular force and a tangential force. The tangential force, which promotes atrophic changes, is mainly induced by AXL elongation. With the growth of AXL, the tangential force increases, and atrophy maculopathy aggravates. The perpendicular force, which induces traction maculopathy, is mainly composed of the inward pulling force of the vitreous and the backward pulling force generated during posterior sclera extension. In the early stage of pathologic myopia, the macular is mainly affected by the perpendicular force, which gradually increases under two opposite tractions and reaches the highest at A2. After A2, the vitreous might be liquefied and reduce the force that pulls the macular inward. Thus, the summation of perpendicular force falls. In the meantime, the tangential force gradually increasing becomes the dominant factor causing retinopathy. As a complicated stage, MAM grade A2 endures the incremental perpendicular force and tangential force simultaneously. That can explain why severe MR, RD, and OLMH have the highest incidences in A2. After that, the augmented tangential force further causes lamellar MH to develop into FTMH (**Figure 5**).

Recent studies have proved that PVAs represented traction on the retina and were a risk factor for retinoschisis (12, 15, 22, 23). However, on the sequence of different kinds of PVAs, people have different views. Shimada et al. believed paravascular cysts were the first (15). But Kamal-Salah et al. found more paravascular microfolds than paravascular cysts and proposed that paravascular microfolds were earlier (22). From the view of MAM progression, our study showed that

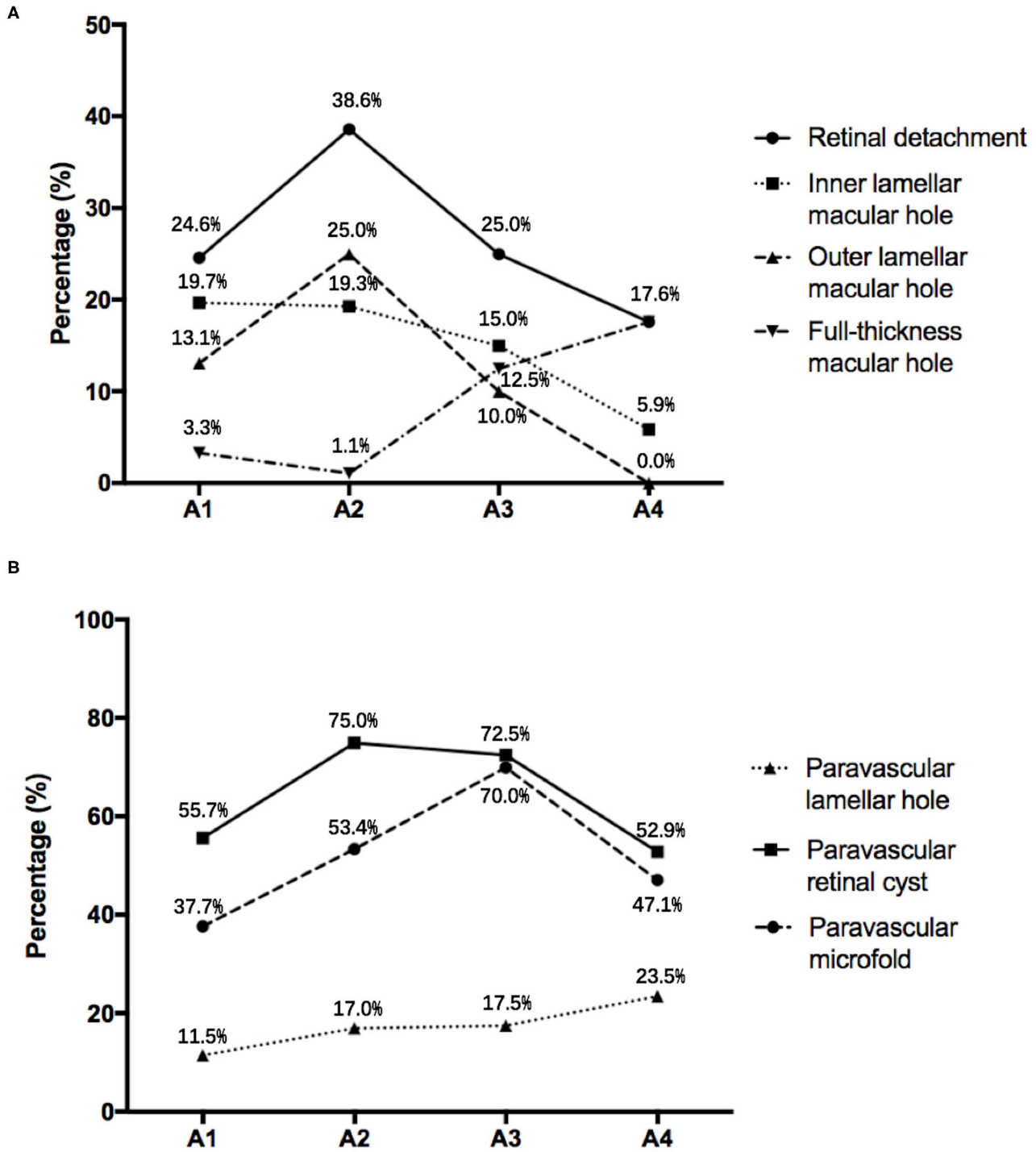

FIGURE 3 | (A) The incidence of complications of myopic retinoschisis in different myopic atrophy maculopathy (MAM) grades. **(B)** The incidence of paravascular abnormalities in different stages of MAM. A1, tessellated fundus; A2, diffuse chorioretinal atrophy; A3, patchy chorioretinal atrophy; A4, macular atrophy.

more paravascular retinal cysts became apparent in an early stage than paravascular microfolds. Paravascular microfolds could represent the inward force and form paravascular cysts. However, retinoschisis itself can also lead to cysts near vessels. Therefore, we speculated that paravascular retinal cysts appear before microfolds. Paravascular lamellar holes might come

from the breakage of paravascular cysts (15, 24). Li et al. believed that paravascular lamellar holes were the advanced stage of PVAs because all the eyes with paravascular lamellar holes had paravascular microfolds and cysts simultaneously (23). In our study, the incidence of paravascular lamellar holes was the least and presented an upward trend with MAM aggravation. Therefore, we also believe the paravascular lamellar hole was the last to appear, keeping with the previous study (23).

TABLE 3 | Univariate analysis of systemic and ocular characteristics for outer lamellar macular holes and full-thickness macular holes.

	Odds ratio (95% confidence interval)	*P*
Outer lamellar macular hole		
Age (y)	1.006 (0.973–1.040)	0.717
Gender (female)	1.152 (0.486–2.728)	0.748
Axial length (mm)	1.029 (0.859–1.232)	0.757
Full-thickness macular hole		
Age (y)	1.053 (0.992–1.117)	0.087
Gender (female)	3.636 (0.454–29.107)	0.224
Axial length (mm)	1.210 (0.906–1.616)	0.197

TABLE 4 | Multivariable analysis for outer lamellar macular holes and full-thickness macular holes.

	Odds ratio (95% confidence interval)	*P*
Model for outer lamellar macular holes		
Age (y)	1.010 (0.977–1.043)	0.557
Myopic atrophy maculopathy (A1 + A2)	3.423 (1.144–10.236)	0.028
Model for full-thickness macular hole		
Age (y)	1.057 (0.988–1.131)	0.109
Myopic atrophy maculopathy (A3 + A4)	7.752 (1.951–30.803)	0.004

A1, tessellated fundus; A2, diffuse chorioretinal atrophy; A3, patchy chorioretinal atrophy; A4, macular atrophy (8).

In our study, the incidence of paravascular lamellar holes was the least and presented an upward trend with MAM aggravation. Therefore, we also believe the paravascular lamellar hole was the last to appear, keeping with the previous study (23).

Limitations in the study need to be noted. As a cross-sectional study, it is hard to directly reflect the relationship between the progression of the two types of myopic maculopathy. The order in which different kinds of PVAs occur was inferred from the current analysis and needs further verification. To obtain more analyzable data about MTM, we conducted the study based on hospital recruitment. Therefore, some patients with good vision and early stages of MR might be missing. A large, longitudinal population study can provide more sound evidence for the correlation between MAM on MTM. Based on the study, we made a preliminary assumption on the mechanics-related changes of pathologic myopia and the interaction between MAM and MTM. The hypothesis still has many deficiencies and needs to be proved from many aspects.

In conclusion, this is the first study to demonstrate the features of atrophic changes in eyes with definite MTM. Combining MAM and MTM for a comprehensive analysis leads to a deeper understanding of the characteristics of MTM as well as the mechanism of pathologic myopia. For eyes with MTM, diffuse chorioretinal atrophy was the dominant MAM grade, followed by a tessellated fundus. Over 70% of the eyes presented with these two grades of MAM. In clinical management, even if a highly myopic patient presents with an early stage of MAM, an OCT scan is necessary for excluding MTM, especially when delta zones co-exist. Given that the three layers of retinoschisis,

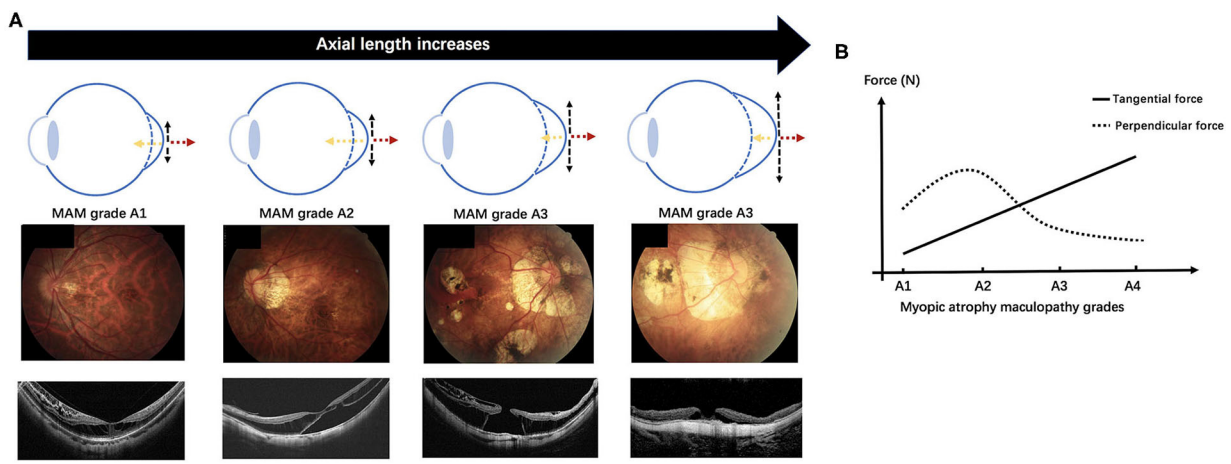

FIGURE 4 | We proposed a hypothesis on the mechanics-related changes of pathologic myopia based on the study. In the early stage of pathologic myopia, the macular is mainly affected by the perpendicular force, which gradually increases under the inward pulling force of the vitreous and the backward pulling force of posterior sclera extension, and reaches the highest at the myopic atrophy maculopathy (MAM) grade A2. After A2, the vitreous might be liquefied and reduce the inward force. The summation of perpendicular force falls and the tangential force gradually increases becoming the dominant factor causing retinopathy. **(A)** A schematic diagram demonstrates the change of the perpendicular force and the tangential force acting on the macular with the axial length growth (the top row). Fundus images with increasing MAM grades (the middle row) and optical coherence tomography images which show the corresponding myopic tractional maculopathy (the bottom row). **(B)** The variation trend of the perpendicular force and the tangential force with MAM grades increasing in the hypothesis. Myopic atrophy maculopathy, MAM; A1, tessellated fundus; A2, diffuse chorioretinal atrophy; A3, patchy chorioretinal atrophy; A4, macular atrophy. Black dotted arrow, the tangential force; yellow dotted arrow, the inward pulling force of the vitreous; red dotted arrow, the backward pulling force of the posterior sclera extension.

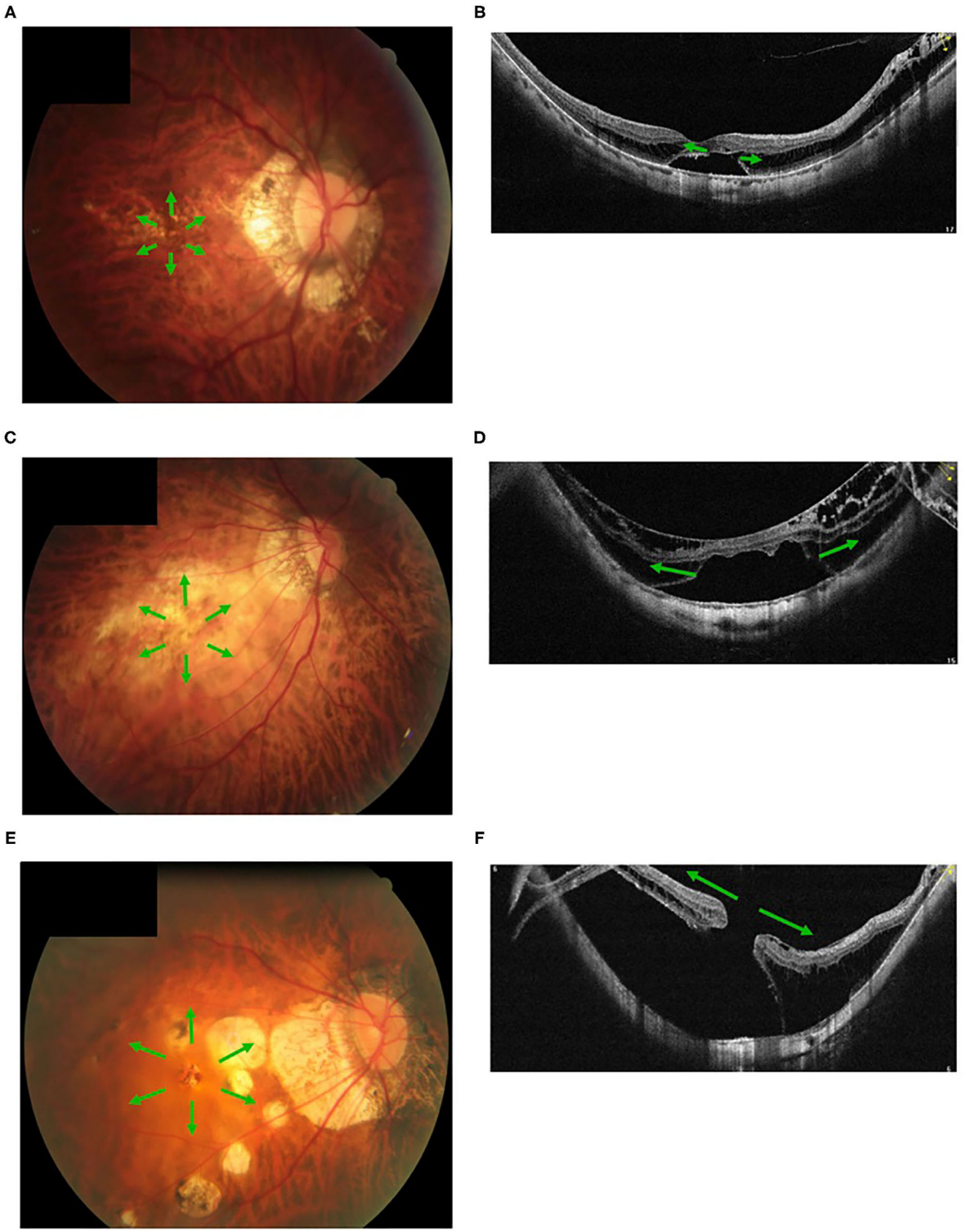

FIGURE 5 | Fundus images with different myopic atrophy maculopathy grades and corresponding myopic tractional maculopathy in optical coherence tomography. A patient with mild diffuse chorioretinal atrophy **(A)** presented with a small outer lamellar macular hole and foveal detachment **(B)**. A patient with more serious diffuse chorioretinal atrophy **(C)** presented with a large outer lamellar macular hole and foveal detachment **(D)**. A patient with patchy chorioretinal atrophy **(E)** presented with a full-thickness macular hole and retinal detachment **(F)**. Green arrow, the tangential traction on the macular might facilitate a lamellar macular hole into a full-thickness macular hole.

entire macular retinoschisis, RD, and OLMH have the highest incidence in MAM grade A2, diffuse chorioretinal atrophy might be a complicated stage for MTM. Besides, the progression of MAM might involve the development of MH. When MTM combines with well-defined atrophy, FTMH should be noted. According to the study, we proposed a preliminary hypothesis on the mechanics-related changes of pathologic myopia and the interaction between MAM and MTM. Here, we found weakly negative correlations in grades of MAM with the range and layers of MR. The relationship still needs to be demonstrated in the future.

DATA AVAILABILITY STATEMENT

The original contributions presented in the study are included in the article/supplementary material, further inquiries can be directed to the corresponding authors.

ETHICS STATEMENT

The studies involving human participants were reviewed and approved by Ethics Committee of Beijing Tongren Hospital. Written informed consent from the participants' legal guardian/next of kin was not required to participate in this study in accordance with the national legislation and the institutional requirements.

AUTHOR CONTRIBUTIONS

JT, YQ, and NW: study concept and design and manuscript revision. JT, CL, and YQ: performed study. JT and YQ: drafted manuscript. JT and KC: statistical analysis. NW: administrative, technical, material support, or study supervision. All authors participated in and provided help for the study.

FUNDING

The work was supported by Beihang University-CMU, Advanced Innovation Center for Big Data-Based Precision Medicine.

ACKNOWLEDGMENTS

The authors thank support and help from Beijing Tongren Hospital, Capital Medical University.

REFERENCES

1. Morgan I, French A, Ashby R, Guo X, Ding X, He M, et al. The epidemics of myopia: aetiology and prevention. *Prog Retin Eye Res*. (2018) 62:134–49. doi: 10.1016/j.preteyeres.2017.09.004
2. Holden B, Fricke T, Wilson D, Jong M, Naidoo K, Sankaridurg P, et al. Global prevalence of Myopia and high myopia and temporal trends from 2000 through 2050. *Ophthalmology*. (2016) 123:1036–42. doi: 10.1016/j.ophtha.2016.01.006
3. Fricke T, Jong M, Naidoo K, Sankaridurg P, Naduvilath T, Ho S, et al. Global prevalence of visual impairment associated with myopic macular degeneration and temporal trends from 2000 through 2050: systematic review, meta-analysis and modelling. *Br J Ophthalmol*. (2018) 102:855–62. doi: 10.1136/bjophthalmol-2017-311266
4. Benhamou N, Massin P, Haouchine B, Erginay A, Gaudric A. Macular retinoschisis in highly myopic eyes. *Am J Ophthalmol*. (2002) 133:794–800. doi: 10.1016/S0002-9394(02)01394-6
5. Phillips C. Retinal detachment at the posterior pole. *Br J Ophthalmol*. (1958) 42:749–53. doi: 10.1136/bjo.42.12.749
6. Takano M, Kishi S. Foveal retinoschisis and retinal detachment in severely myopic eyes with posterior staphyloma. *Am J Ophthalmol*. (1999) 128:472–6. doi: 10.1016/S0002-9394(99)00186-5
7. Panozzo G, Mercanti A. Optical coherence tomography findings in myopic traction maculopathy. *Arch Ophthalmol*. (2004) 122:1455–60. doi: 10.1001/archopht.122.10.1455
8. Ruiz-Medrano J, Montero J, Flores-Moreno I, Arias L, García-Layana A, Ruiz-Moreno J. Myopic maculopathy: current status and proposal for a new classification and grading system (ATN). *Prog Retin Eye Res*. (2019) 69:80–115. doi: 10.1016/j.preteyeres.2018.10.005
9. Baba T, Ohno-Matsui K, Futagami S, Yoshida T, Yasuzumi K, Kojima A, et al. Prevalence and characteristics of foveal retinal detachment without macular hole in high myopia. *Am J Ophthalmol*. (2003) 135:338–42. doi: 10.1016/S0002-9394(02)01937-2
10. Chen Q, He J, Hu G, Xu X, Lv H, Yin Y, et al. Morphological characteristics and risk factors of myopic maculopathy in an older high myopia population-based on the new classification system (ATN). *Am J Ophthalmol*. (2019) 208:356–66. doi: 10.1016/j.ajo.2019.07.010
11. Jonas JB, Fang Y, Weber P, Ohno-Matsui K. Parapapillary gamma and delta zones in high myopia. *Retina*. (2017) 38:931–8. doi: 10.1097/IAE.0000000000001650
12. Takahashi H, Tanaka N, Shinohara K, Uramoto K, Yokoi T, Yoshida T, et al. Importance of paravascular vitreal adhesions for development of myopic macular retinoschisis detected by ultra-widefield OCT. *Ophthalmology*. (2020) 128:256–65. doi: 10.1016/j.ophtha.2020.06.063
13. Shimada N, Tanaka Y, Tokoro T, Ohno-Matsui K. Natural course of myopic traction Maculopathy and factors associated with progression or resolution. *Am J Ophthalmol*. (2013) 156:948–57. doi: 10.1016/j.ajo.2013.06.031
14. Sayanagi K, Ikuno Y, Gomi F, Tano Y. Retinal vascular microfolds in highly myopic eyes. *Am J Ophthalmol*. (2005) 139:658–63. doi: 10.1016/j.ajo.2004.11.025
15. Shimada N, Ohno-Matsui K, Nishimuta A, Moriyama M, Yoshida T, Tokoro T, et al. Detection of paravascular lamellar holes and other paravascular abnormalities by optical coherence tomography in eyes with high myopia. *Ophthalmology*. (2008) 115:708–17. doi: 10.1016/j.ophtha.2007.04.060
16. Ohno-Matsui K, Hayashi K, Tokoro T, Mochizuki M. Detection of paravascular retinal cysts before using OCT in a highly myopic patient. *Graefes Arch Clin Exp Ophthalmol*. (2006) 244:642–4. doi: 10.1007/s00417-005-0112-6
17. Yan Y, Wang Y, Yang Y, Xu L, Xu J, Wang Q, et al. Ten-year progression of myopic maculopathy: the Beijing eye study 2001–2011. *Ophthalmology*. (2018) 125:1253–63. doi: 10.1016/j.ophtha.2018.01.035
18. Gaucher D, Haouchine B, Tadayoni R, Massin P, Erginay A, Benhamou N, et al. Long-term follow-up of high myopic foveoschisis: natural course and surgical outcome. *Am J Ophthalmol*. (2007) 143:455–62. doi: 10.1016/j.ajo.2006.10.053
19. Sun CB, Liu Z, Xue AQ, Yao K. Natural evolution from macular retinoschisis to full-thickness macular hole in highly myopic eyes. *Eye*. (2010) 24:1787–91. doi: 10.1038/eye.2010.123
20. Shimada N, Ohno-Matsui K, Baba T, Futagami S, Tokoro T, Mochizuki M. Natural course of macular retinoschisis in highly myopic eyes without macular hole or retinal detachment. *Am J Ophthalmol*. (2006) 142:497–500. doi: 10.1016/j.ajo.2006.03.048
21. Parolini B, Palmieri M, Finzi A, Besozzi G, Lucente A, Nava U, et al. The new myopic traction maculopathy staging system. *Eur J Ophthalmol*. (2020) 1120672120930590. doi: 10.1177/1120672120930590. [Epub ahead of print].

22. Kamal-Salah R, Morillo-Sanchez MJ, Rius-Diaz F, Garcia-Campos JM. Relationship between paravascular abnormalities and foveoschisis in highly myopic patients. *Eye*. (2015) 29:280–5. doi: 10.1038/eye.2014.255
23. Li T, Wang X, Zhou Y, Feng T, Xiao M, Wang F, et al. Paravascular abnormalities observed by spectral domain optical coherence tomography are risk factors for retinoschisis in eyes with high myopia. *Acta ophthalmol*. (2018) 96:e515–23. doi: 10.1111/aos.13628
24. Liu HY, Hsieh YT, Yang CM. Paravascular abnormalities in eyes with idiopathic epiretinal membrane. *Graefes Arch Clin Exp Ophthalmol*. (2016) 254:1723–9. doi: 10.1007/s00417-016-3276-3

Conflict of Interest: The authors declare that the research was conducted in the absence of any commercial or financial relationships that could be construed as a potential conflict of interest.

frontiers in Medicine

ORIGINAL RESEARCH
published: 04 January 2022
doi: 10.3389/fmed.2021.671521

Clinical Characteristics and Early Visual Outcomes of Highly Myopic Cataract Eyes: The Shanghai High Myopia Study

Wenwen He[1,2,3,4†], *Yunqian Yao*[1,2,3,4†], *Keke Zhang*[1,2,3,4], *Yu Du*[1,2,3,4], *Jiao Qi*[1,2,3,4], *Yinglei Zhang*[1,2,3,4], *Shaohua Zhang*[1,2,3,4], *Zhennan Zhao*[1,2,3,4], *Lei Cai*[1,2,3,4], *Qi Fan*[1,2,3,4], *Yongxiang Jiang*[1,2,3,4], *Jin Yang*[1,2,3,4], *Xiangjia Zhu*[1,2,3,4*] and *Yi Lu*[1,2,3,4*]

[1] Department of Ophthalmology, Eye Institute, Eye & ENT Hospital, Fudan University, Shanghai, China, [2] NHC Key Laboratory of Myopia (Fudan University), Shanghai, China, [3] Key Laboratory of Myopia, Chinese Academy of Medical Sciences, Shanghai, China, [4] Shanghai Key Laboratory of Visual Impairment and Restoration, Shanghai, China

Purpose: To report ocular characteristics and early visual outcomes of highly myopic cataract eyes, and to analyze the risk factors of low vision.

Methods: A total of 2,027 eyes of 1,400 cataract patients with axial length (AL) ≥ 26 mm undergoing cataract surgery in Eye & ENT Hospital of Fudan University, who were registered in the Shanghai High Myopia Study, were analyzed. Routine pre-operative ophthalmic examinations were performed and macular scan of optical coherence tomography (OCT) were obtained. Macular complications, central foveal thickness (CFT) and subfoveal choroidal thickness (SFCT) were evaluated from OCT images. Ocular and surgical history and perioperative complications were also recorded. Uncorrected and best-corrected visual acuity (UCVA/BCVA) 1 month post-operatively and its influencing factors were evaluated.

Results: The average AL of all involved eyes was 29.52 ± 2.26 mm, and 39.7% of which were with an AL > 30 mm and 26.4% of which were with a corneal astigmatism more than 1.5 D. Nuclear cataract accounted for the largest proportion (70.6%). The rate of overall macular complications was 27.6%. Postoperative UCVA and BCVA were 0.70 ± 0.46 and 0.25 ± 0.32 logMAR, respectively. BCVA improved significantly after surgery (vs. $P < 0.001$) and affected by the elongation of AL ($P < 0.001$) and thinning of CFT and SFCT (both $P < 0.001$). The risk factors of post-operative low vision (BCVA < 20/66) were macular atrophy, lamellar macular hole, high corneal astigmatism, long AL, thin SFCT and junior surgeons, odds ratios ranging from 1.54 to 54.87 (all $P < 0.05$).

Conclusion: Cataract surgery could improve the VA of highly myopic eyes. Eye with macular complications, higher corneal astigmatism, longer AL, thinner SFCT, and who was treated by a junior surgeon, may have a high risk of low vision after surgery.

Keywords: highly myopic cataract, axial length, ocular characteristics, visual outcomes, risk factors

OPEN ACCESS

Edited by:
Chee Wai Wong, Singapore National Eye Center, Singapore

Reviewed by:
Wei Yan Ng, Singapore Health Services Pte Ltd, Singapore
Li Lian Foo, Singapore National Eye Center, Singapore

***Correspondence:**
Yi Lu
luyieent@126.com
Xiangjia Zhu
zhuxiangjia1982@126.com

†These authors have contributed equally to this work

Specialty section:
This article was submitted to Ophthalmology, a section of the journal Frontiers in Medicine

Received: *24 February 2021*
Accepted: *29 November 2021*
Published: *04 January 2022*

Citation:
He W, Yao Y, Zhang K, Du Y, Qi J, Zhang Y, Zhang S, Zhao Z, Cai L, Fan Q, Jiang Y, Yang J, Zhu X and Lu Y (2022) Clinical Characteristics and Early Visual Outcomes of Highly Myopic Cataract Eyes: The Shanghai High Myopia Study. Front. Med. 8:671521. doi: 10.3389/fmed.2021.671521

INTRODUCTION

High myopia is defined as myopia ≤ -6.00 diopters (D) or axial length (AL) ≥ 26 mm (1). The incidence of high myopia is increasing rapidly worldwide (2), especially in Asian areas (3, 4). At present, there are more than 500 million myopia patients in China alone, and nearly 100 million high myopia patients (5). Correspondingly, as the most common complication of high myopia, the incidence of highly myopic cataract is increasing year by year, and it accounts for 30% of total cataract surgeries in tertiary hospitals (6).

Highly myopic cataract surgery is relatively complex and very challenging for ophthalmologists because of its association with poor fundus conditions and the difficulty of estimating the visual outcome (7). Epidemiology shows that high myopia is related to education level (8), and it tends to develop cataract almost 10 years earlier than normal eyes (6, 9). Thus, these patients usually have high expectations for visual outcome of cataract surgery. However, the uncertainty of prognosis may lead to the contradiction between doctors and patients.

Modern cataract surgery has been proved to be safe and effective in treating highly myopic cataract (9–11). However, the previous studies were usually retrospective study with a small sample size (9, 11), which provided relatively weak clinical evidence. The Shanghai High Myopia Study is a hospital-based prospective cohort study, which continuously includes highly myopic and control patients scheduled for cataract surgery at the Eye & ENT Hospital of Fudan University since October 2015. All subjects underwent detailed pre-operative examinations and prospective follow-ups (7, 12–14). The purpose of this study is to summarize the pre-operative clinical characteristics and early visual outcomes of cataract surgery in a large amount of highly myopic cataract patients from the Shanghai High Myopia Study, and to analyze the risk factors of post-operative low vision. Our study aims to provide basis for treatment of this kind of patients, especially to help surgeons predict the risk of post-operative low vision before surgery, so as to be able to fully communicate with patients in the future.

METHODS

For this study, patients underwent cataract surgery with AL ≥ 26 mm of both eyes or the operated eye were included; excluded were those whose eyes had previous trauma, corneal transplantation, uveitis, diabetic retinopathy and other ocular conditions which could affect visual acuity except high myopia and its complications or previous refractive surgery history. Patients lost to follow-up were excluded from analysis. The Institutional Review Board of the Eye & ENT Hospital of Fudan University approved the protocol of the study, and it was registered at www.clinicaltrials.gov (accession number NCT03062085). All procedures adhered to the tenets of the Declaration of Helsinki, and informed consent was obtained from each patient before registration.

Pre-operative Examinations

Pre-operative examinations included the routine assessment of Snellen visual acuity, slit-lamp biomicroscopy, fundoscopy, non-contact tonometry (TX-20, Canon Inc., Japan), biomeasurement (IOLMaster 500 or IOLMaster 700, Carl Zeiss AG, Oberkochen, Germany), corneal topography (Pentacam HR, Oculus Inc., Wetzlar, Germany), B scans, and macular scan of optical coherence tomography (OCT, Zeiss Cirrus HD-OCT 5000; Carl Zeiss AG, Oberkochen, Germany). The following data were collected: age, gender, operative eye, visual acuity, intraocular pressure (IOP), AL, corneal curvature, cataract type (lens opacities classification system III, LOCS III grades), ocular and surgical history of the enrolled eye and systemic condition.

Macular Complications Evaluation

Macular complications, including foveal and extrafoveal retinalschisis (RS), epiretinal membrane (ERM), lamellar and full-thickness macular hole (LMH and FMH), choroidal neovascularization (CNV) or macular atrophy, were evaluated using OCT pre-operatively. Central foveal thickness (CFT) and subfoveal choroidal thickness (SFCT) were also measured and recorded by the same doctor (Dr. W.W.H).

Surgical Procedures

All patients underwent cataract extraction with or without intraocular lens (IOL) implantation. For the patients with IOL implantation, a foldable IOL was implanted in the capsular bag. Intraoperative complications were recorded, such as post capsular rupture. The surgeon who performed the surgery was also recorded and a surgeon with no more than 5 years of surgical training was considered as a junior surgeon.

Post-operative Follow-Up

Patients received 1 month follow-up after surgery. Postoperative examinations included assessment of Snellen visual acuity, manifest refraction, non-contact tonometry, fundoscopy, retinal photography (Optos-200Tx, Optos, Dunfermline, UK), Macular Integrity Assessment (MAIA) microperimeter system (Ceentervue, Padova, Italy), and an OCT macular scan (Zeiss Cirrus HD-OCT 5000; Carl Zeiss AG, Oberkochen, Germany). The outcome measures of interest were post-operative visual acuity and its influencing factors.

Statistical Analysis

Continuous variables were presented as the mean $\pm$ standard deviation (SD). Categorical variables were presented with numbers and percentages. Snellen visual acuity measurements were converted to logarithm of the minimum angle of resolution (logMAR) for statistical analyses, with counting fingers, hand motions and light perception corresponding to 1.98, 2.28, and 2.68, respectively. Because ocular characteristics and visual acuity is eye specific, analyses were run according to eye rather than patients. These were performed with all eyes combined by the generalized estimating equation method, which allows data from both eyes to be used while accounting for the correlation between the two eyes of a single patient, and analyses were

adjusted for age and gender, unless otherwise stated. *Post-hoc* least significant difference (LSD) test was performed for multiple comparisons. Comparisons between pre-operative and post-operative visual acuity were performed using paired *t*-test. The relationships between post-operative visual acuity and pre-operative characters were assessed with Pearson's correlation or Spearman's correlation. Post-operative best corrected visual acuity (BCVA) < 20/66 was defined as low vision, the risk factors for low vision were assessed with logistic regression. All analyses were conducted using SPSS software (version 23.0, IBM Inc.). A *P*-value of <0.05 was considered as statistically significant.

RESULTS

Baseline Characteristics

A total of 2,098 eyes from 1,448 patients were eligible and enrolled in this study. Forty-eight of these patients lost to follow-up. Finally, 2,027 eyes from 1,400 patients were able for analysis, including 601 males and 799 females.

Baseline characteristics and relevant ocular history of the included patients are summarized in **Table 1**. The average AL of the involved subjects was 29.52 ± 2.26 mm. Extremely high myopia (AL > 30 mm) accounted for 39.7% of all, and the maximum AL was 37.11 mm. Of these eyes, 535 (26.4%) had a corneal astigmatism more than 1.5 D, more of which were with-the-rule astigmatism. Among all the eyes, nuclear cataract accounted for the largest proportion (70.6%). In addition, previous refractive surgery occurred in 26 eyes (1.2%), while prior retinal detachment occurred in 59 eyes (2.9%).

Macular Complications in Highly Myopic Cataract Eyes

The rate of overall macular complications was 27.6% (560/2,027), and these complications were from high myopia, not from cataract surgery, because the OCT images were all obtained before surgery. ERM was the most common macular complication in highly myopic eyes, which occurred in 329 eyes (16.2%), followed by retinalschisis (185/2,027, 9.1%). The incidences of CNV or CNV related macular atrophy and macular hole were 8.7% (177/2,027) and 4.5% (91/2,027), respectively. The average CFT and SFCT were 226 ± 62 and 85 ± 63 μm, respectively.

We then divided all the subjects into four subgroups according to AL (AL: 26–28, 28–30, 30–32, >32 mm). The incidences of macular complications in each subgroup were summarized in **Table 2**. CFT and SFCT decreased significantly with the elongation of AL. SFCT had a more obvious decrease than CFT, as there were significant differences in SFCT between all paired subgroups (all $P < 0.01$), while no significant differences in CFT between the two subgroups with AL ≤ 30 mm and between the two subgroups with AL > 30 mm (both $P > 0.05$). The risk of overall macular complications increased significantly with the elongation of AL (all $P < 0.001$). Each different type of macular complications had the similar change with the overall rate according to AL except full-thickness macular hole, which were rare in all subgroups.

TABLE 1 | Baseline characteristics of highly myopic cataract patients.

Baseline characteristic	
Total eyes	2,027
Total patients	1,400
Age (years)	
Mean ± SD	61.48 ± 9.68
Range	18-88
Gender	
Males	601
Females	799
Operated eye	
Right	1,040
Left	987
AL (mm)	
Mean ± SD	29.52 ± 2.26
Range	26.00–37.11
26–28 mm	633 (31.2%)
28–30 mm	590 (29.1%)
30–32 mm	498 (24.6%)
>32 mm	306 (15.1%)
Corneal astigmatism (D)	
Mean ± SD	1.14 ± 0.77
Range	0.00–6.61
With-the-rule	942 (46.5%)
Against-the-rule	655 (32.3%)
0.0–1.5 D	1,492 (73.6%)
1.5–3.0 D	484 (23.9%)
>3.0 D	51 (2.5%)
IOP (mmHg)	
Mean ± SD	15.27 ± 3.42
Range	7.0–44.0
Cataract type	
Cortical	593 (29.3%)
Nuclear	1,431 (70.6%)
Posterior subcapsular	565 (27.9%)
Ocular and surgical history	
Glaucoma	34 (1.7%)
Prior retinal detachment	59 (2.9%)
Prior corneal laser surgery	17 (0.8%)
Prior ICL implantation	9 (0.4%)
Systemic condition	
High blood pressure	338 (24.1%)
Diabetes	91 (6.5%)

SD, standard deviation; AL, axial length; D, dioper; IOP, intraocualr pressure; ICL, implantable collamer lens.

Summary of Cataract Surgery in Highly Myopic Cataract Eyes

All of the involved subjects completed cataract surgery. Of these eyes, 2,016 eyes underwent phacoemulsification and the other 11 eyes received extracapsular cataract extraction due to nuclear opalescence grade no < 6 according to LOCSIII system. Types of IOL implanted were summarized in **Table 3**. Monofocal IOLs

TABLE 2 | Incidence of macular complications in highly myopic cataract eyes according to axial length.

Groups of AL	26–28 mm	28–30 mm	30–32 mm	>32 mm
mean AL (mm)	27.14 ± 0.76	29.02 ± 0.80	30.85 ± 0.81	33.24 ± 1.17
mean CFT (μm)	235 ± 49	242 ± 64	209 ± 61	208 ± 68
mean SFCT (μm)	138 ± 70	83 ± 56	55 ± 34	41 ± 20
No complications	542/633 eyes (85.6%)	431/590 eyes (73.1%)	317/498 eyes (63.6%)	177/306 eyes (57.8%)
With at least 1 complication	91/633 eyes (14.4%)	159/590 eyes (26.9%)	181/498 eyes (36.4%)	129/306 eyes (43.2%)
Macular complications				
OR (95% CI)	**1 –**	**2.09 (1.56–2.81)**	**3.50 (2.60–4.75)**	**5.45 (3.79–7.85)**
ERM	64/633 eyes (10.1%)	85/590 eyes (14.4%)	106/498 eyes (21.3%)	74/306 eyes (24.2%)
OR (95% CI)	**1 –**	**1.43 (1.01–2.02)**	**2.48 (1.76–3.51)**	**3.16 (2.13–4.68)**
Foveal RS	10/633 eyes (1.6%)	22/590 eyes (3.7%)	22/498 eyes (4.4%)	14/306 eyes (4.6%)
OR (95%CI)	**1 –**	**2.31 (1.06–5.06)**	**3.04 (1.44–6.42)**	**3.97 (1.77–8.89)**
Extrafoveal RS	9/633 eyes (1.4%)	42/590 eyes (7.1%)	48/498 eyes (9.6%)	18/306 eyes (5.8%)
OR (95% CI)	**1 –**	**4.64 (2.33–9.23)**	**6.74 (3.34–13.62)**	**5.98 (2.71–13.22)**
CNV (including CNV-related macular atrophy)	22/633 eyes (3.4%)	44/590 eyes (7.5%)	61/498 eyes (12.2%)	50/306 eyes (16.3%)
OR (95% CI)	**1 –**	**2.41 (1.48–3.94)**	**4.21 (2.49–7.11)**	**6.91 (3.80–12.57)**
LMH	16/633 eyes (2.5%)	24/590 eyes (4.1%)	27/498 eyes (5.4%)	15/306 eyes (4.9%)
OR (95% CI)	**1 –**	**1.55 (0.82–2.95)**	**2.14 (1.14–4.02)**	**2.26 (1.07–4.76)**
FMH	0/633 eyes (0%)	4/590 eyes (0.7%)	2/498 eyes (0.4%)	3/306 eyes (1.0%)
OR (95%CI)	**–**	**–**	**–**	**–**

AL, axial length; CFT, central foveal thickness; SFCT, subfoveal choroidal thickness; OR, odds ratio; CI, confidence interval; ERM, epiretinal membrane; RS, retinalschisis; CNV, choroidal neovascularization; LMH, lamella macular hole; FMH, full-thickness macular hole.

were the mostly used. Negative power IOL were used in 37 eyes (1.8%). Posterior capsular rupture (PCR) occurred in nineteen eyes (0.9%). There were 16 eyes without IOL implantation. Twelve of them were due to plano power need and with zonular weakness and poor fundus, and the other 4 were due to PCR.

Visual Outcomes of Highly Myopic Cataract Eyes

The mean post-operative UCVA and BCVA were 0.70 ± 0.46 and 0.25 ± 0.32 logMAR, respectively, and both improved significantly than pre-operative visual acuity (0.95 ± 0.56 logMAR). Proportions of eyes with different visual acuity before and after surgery are shown in **Figure 1**. Most patients got visual acuity between 20/40 and 20/20 (1,354/2,027 eyes, 66.8%) after cataract surgery. Fifteen eyes (0.7%) developed retinal tear at 1 month follow-up with laser barrier done, one of which had PCR during surgery, and no eye developed retinal detachment during follow-up.

Factors Influencing Post-operative VA in Highly Myopic Cataract Eyes

Table 4 lists the post-operative VA and refraction of each AL subgroup. The subgroup with AL > 32 mm had significantly worse post-operative UCVA than other subgroups (all $P < 0.05$), while post-operative BCVA became worse gradually in each subgroup (all $P < 0.001$). Postoperative myopia diopters were less in the subgroups of eyes with AL > 30 mm than the subgroups of eyes with AL ≤ 30 mm.

Among the 535 eyes with pre-operative corneal astigmatism more than 1.5 D, the average post-operative UCVA of the eyes with toric IOL implantation was significantly better than those eyes without toric IOL implantation after adjusting for age, gender and post-operative SE (0.52 ± 0.31 vs. 0.71 ± 0.48,

TABLE 3 | IOL used in highly myopic cataract eyes.

IOL types	Number of eyes (%)
Monofocal IOL	**1,951 (96.3%)**
Rayner 920H/970C	898 (44.3%)
MC X11 ASP	883 (43.6%)
AT LISA 409MP	96 (4.7%)
ZCB00	45 (2.2%)
SN60WF	6 (0.3%)
HOYA	19 (0.9%)
PC 525W Ergomax	4 (0.2%)
Monofocal toric IOL	**46 (2.3%)**
SN6ATX	14 (0.7%)
AT LISA 709M	32 (1.6%)
Multifocal IOL	**12 (0.6%)**
ZMB00	8 (0.4%)
AT LISA 839MP	4 (0.2%)
Multifocal toric IOL	**2 (0.1%)**
AT LISA 909M	2 (0.1%)
Without IOL	**16 (0.8%)**

$P = 0.001$). All the patients with toric IOL implantation did not require a second re-rotation surgery.

Eyes with macular complications had worse post-operative BCVA than those without (0.49 ± 0.44 vs. 0.16 ± 0.20, $P < 0.001$). Both CFT and SFCT had a negative correlation with the logMAR value of post-operative BCVA ($r = -0.331$, $P < 0.001$ and $r = -0.317$, $P < 0.001$).

Risk Factors for Post-operative Low Vision in Highly Myopic Cataract Eyes

Table 5 shows the logistic regression model of post-operative low vision (BCVA < 20/66) using generalized estimating equation method. CNV or CNV-related macular atrophy was the most important risk factor (OR = 54.87), followed by LMH, junior surgeons, higher corneal astigmatism, longer AL, and thinner SFCT.

DISCUSSION

Based on the epidemiology data, at least 500 million people worldwide are estimated to have high myopia, and this number would increase to one billion by 2,050 (2). In Asia area, the incidence of high myopia is much higher than elsewhere, from 2.6 to 9.1% (15, 16). Consequently, the prevalence of highly myopic cataract has also increased rapidly. However, because of the complexity of fundus conditions, it is very difficult to estimate the post-operative visual outcomes in these eyes. Therefore, to provide the evidence for clinic, we evaluated the clinical characteristics and 1-month post-operative outcomes of highly myopic cataract eyes in a large sample of 2,027 eyes from 1,400 patients. We found that cataract surgery could improve the visual acuity of highly myopic patients but the effect decreased with the elongation of axial length. Toric IOL may improve post-operative visual acuity of highly myopic cataract patients with over 1.5 D corneal astigmatism. Low vision with BCVA < 20/66 was found in 14.5% of all the eyes, and the risk factors of these eyes were CNV or CNV-related macular atrophy, LMH, junior surgeons, higher corneal astigmatism, longer AL, and thinner SFCT.

Our data show that modern cataract extraction with or without IOL implantation can be safe and effective in treating highly myopic cataract patients. Both UCVA and BCVA improved in all patients and the average post-operative BCVA was comparable with previous studies (9, 17). However, our study showed a better visual outcome in extremely high myopic eyes with AL > 30 mm than the previous study (0.55 ± 0.54 logMAR) (11), probably due to the short follow-up time. Previous studies reported high axial myopia as a risk factor for pseudophakic retinal detachment (18, 19). Although there was no retinal detachment in our 1 month follow-up, there were still 15 cases occurring new retinal tear, which may because that the poor retinal was pulled by the disturbance of the vitreous body caused by the perfusion fluid during cataract surgery. Thus, regular fundal examination follow-up is particularly important for cataract patients with high myopia, which can avoid the occurrence of serious retinal complications.

However, with the extension of AL, visual outcome became worse, especially the BCVA. This may be due to the significant increase of vision-threatening macular complications such us CNV with the elongation of AL, as well as we proved before. Besides, we also found SFCT decreased significantly with the elongation of axial length rather than CFT, indicating that choroidal atrophy was more significant than retinal atrophy with the extension of axial length in patients with high myopia. Previous studies also had proved that retinal sensitivity and visual acuity were directly correlated with SFCT and did not seem to be associated with CFT in highly myopic patients (20, 21), which were similar to our results of multiple analysis. This may be because in some cases of retinal atrophy combined with ERM, the CFT is thickened, but the SFCT is still thinner. Thus, along with longer AL, thinner SFCT could be a sensitive predictor of worse vision of highly myopic cataract patients. In addition, with the elongation of axial length, post-operative myopia diopters became less, which indicated that the hyperopia drift increased, since the target refraction was more myopia for eyes with longer axial length, which was consistent with our previous results (22, 23).

Interestingly, we found corneal astigmatism affected both UCVA and BCVA after cataract surgery in highly myopic eyes. Implantation of Toric IOL in eyes with over 1.5 D corneal astigmatism improved UCVA significantly than the non-toric monofocal IOL. However, we also found high myopia as a risk factor of rotational stability of toric IOL in previous research (24). Therefore, whether a toric IOL should be used for high myopia needs to weigh the degree of corneal astigmatism and capsular stability. According to previous studies, capsular tension ring and more stable IOL type such as plate-haptic toric IOL were recommended (25–27). At the same time, the high residual astigmatism is difficult to be completely corrected by glasses and may affect the BCVA and visual function.

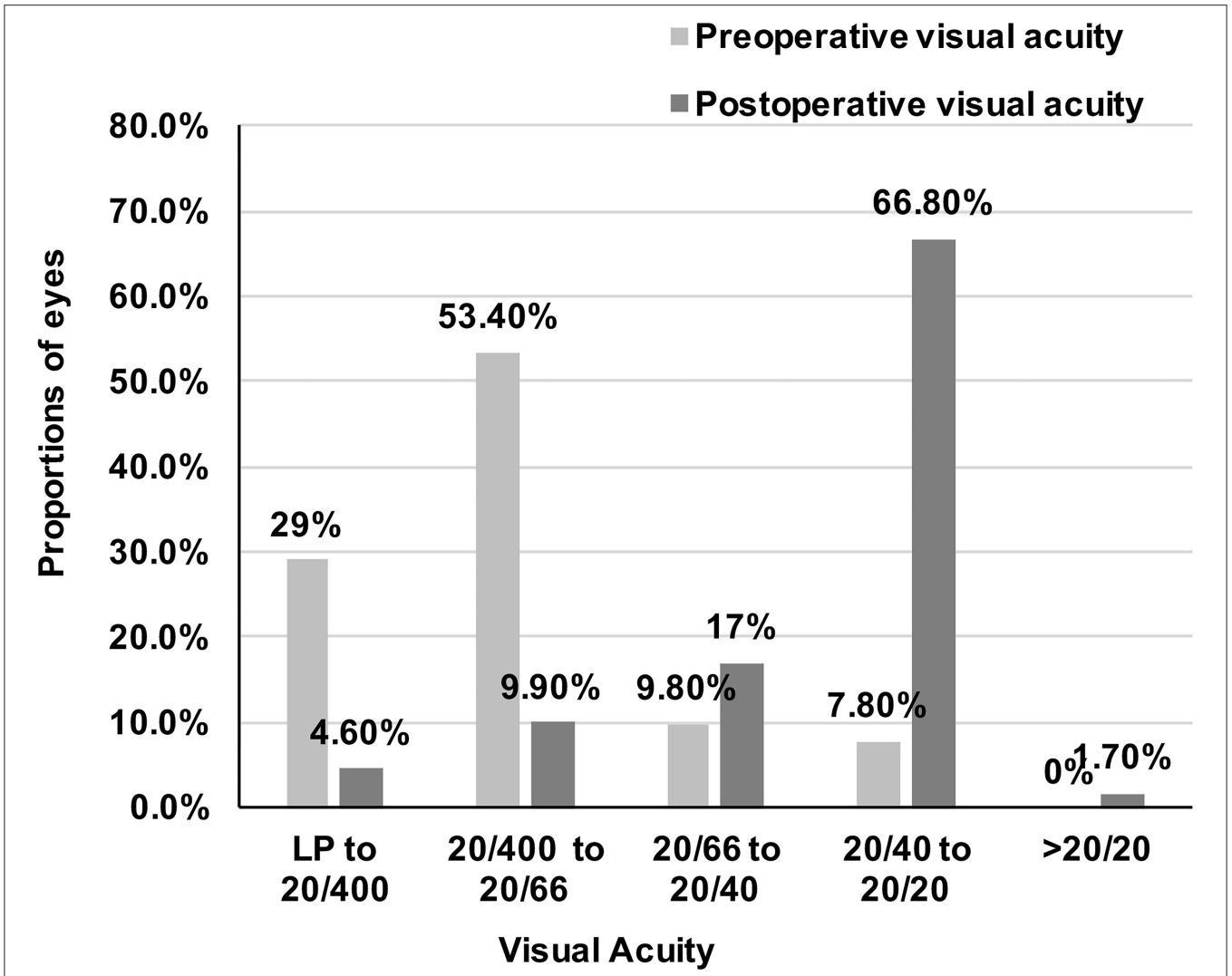

FIGURE 1 | Proportions of eyes with different visual acuity before and after surgery. Visual acuity of all patients significantly improved and most patients got visual acuity between 20/40 and 20/20 (1,354/2,027 eyes, 66.8%) after cataract surgery. LP, Light perception.

TABLE 4 | Visual and refraction outcomes of highly myopic cataract eyes in different subgroups of axial length.

Groups of AL	1: 26–28 mm	2: 28–30 mm	3: 30–32 mm	4: >32 mm
Pre-operative VA	0.78 ± 0.49	0.93 ± 0.53	1.02 ± 0.54	1.26 ± 0.61
Postoperative UCVA*	0.68 ± 0.48	0.70 ± 0.44	0.68 ± 0.44	0.75 ± 0.47
Postoperative BCVA†	0.17 ± 0.26	0.23 ± 0.30	0.30 ± 0.35	0.38 ± 0.37
Postoperative SE (D)#	−3.08 ± 1.54	−3.10 ± 1.54	−2.90 ± 1.34	−2.62 ± 2.56

VA, visual acuity; UCVA, uncorrected visual acuity; BCVA, best corrected visual acuity; SE, spherical equivalent; D, diopter.

**Significant difference was found between subgroup with AL > 32 mm and other subgroups (Generalized estimating equation method with post-hoc least significant difference test, P = 0.005, 0.036, and 0.001, respectively).*

† Post-operative BCVA became worse gradually in each subgroup (Generalized estimating equation method with post-hoc least significant difference test, all P < 0.001).

#Post-operative myopia diopters were less in the subgroups of eyes with AL > 30 mm than the subgroups of eyes with AL ≤ 30 mm (Generalized estimating equation method with post-hoc least significant difference test, Subgroup 1 vs. Subgroup 3, P = 0.023, Subgroup 1 vs. Subgroup 4, P = 0.004, Subgroup 2 vs. Subgroup 3, P = 0.037, Subgroup 2 vs. Subgroup 4, P = 0.007.

In addition, we found that CNV or CNV related maculor atrophy and LMH were the macular complications significantly associated with low vision after highly myopic cataract surgery. CNV or CNV related maculor atrophy is the most serious macular complication and affects VA most. Compared to LMH, FMH should have more threatening effect on VA. We also found

TABLE 5 | Logistic regression model of post-operative low vision in highly myopic cataract eyes.

Parameters	OR	95% CI	*P*-value
Age	1.01	0.99–1.04	0.438
Gender	0.993	0.65–1.51	0.974
Eye	0.671	0.44–1.03	0.065
AL	1.16	1.06–1.27	0.002
Corneal astigmatism	1.54	1.20–1.98	0.001
ERM	1.68	0.97–2.94	0.066
Foveal RS	1.83	0.75–4.43	0.183
Extrafoveal RS	1.48	0.74–3.99	0.271
CNV or CNV related maculor atrophy	54.87	33.36–90.23	<0.001
LMH	3.03	1.35–6.77	0.007
FMH	27.95	0.86–911.5	0.061
CFT	0.997	0.987–1.007	0.583
SFCT	0.987	0.978–0.996	0.003
RD history	2.3	0.70–7.61	0.171
Surgeons			
Expert	1	–	–
Senior	1.008	0.63–1.49	0.881
Junior	2.625	1.17–5.91	0.02

OR, odds ratio; AL, axial length; ERM, epiretinal membrane; RS, retinalschisis; CNV, choroidal neovascularization; LMH, lamella macular hole; FMH, full-thickness macular hole; CFT, central foveal thickness; SFCT, subfoveal choroidal thickness; RD, retinal detachment.

an OR as high as 27.95 of FMH to low vision. However, the patients we included simply underwent cataract surgery, and the patients with FMH often needed combined cataract and retinal surgery, so the eyes with FMH were rare in our study and there was no statistical significance in the multivariate analysis model.

Cataract surgery underwent by junior doctors was another risk factor of post-operative low vision of highly myopic patients. A large database study showed that greater surgeon experience was associated with lower complication rates in phacoemulsification cataract extraction and with a statistically significant improvement in UCVA (28), which was similar with our results. In our study, 14 of 19 cases with intraoperative posterior capsule rupture occurred in the operation of junior doctors, which may be the cause of poor visual outcome. Therefore, it is suggested that the complicated highly myopic cataract surgery should be performed by senior doctors with certain surgical and clinical experience.

However, there were still several limitations of our study. Forty-eight patients lost to follow-up and we did not include their data in the analysis, which may add to selected basis. In addition, our follow-up time frame of this study was short and we will show long term outcomes of these patients in the future.

In conclusion, our study suggests that cataract surgery could improve the VA of highly myopic eyes. For patients with corneal astigmatism more than 1.5 D before surgery, toric IOL implantation may be needed, but caution should be taken. With the extension of axial length in highly myopic cataract eyes, the incidence of macular complications increased, and the thickness of retina and choroid became thinner, which were correlated with worse BCVA. Multiple regression analysis confirmed that CNV or CNV-related macular atrophy, LMH, high astigmatism, long AL, thin SFCT, and junior surgeons were risk factors for low vision after the surgery.

DATA AVAILABILITY STATEMENT

The raw data supporting the conclusions of this article will be made available by the authors, without undue reservation.

ETHICS STATEMENT

The studies involving human participants were reviewed and approved by Institutional Review Board of the Eye & ENT Hospital of Fudan University, Shanghai, China. The patients/participants provided their written informed consent to participate in this study.

AUTHOR CONTRIBUTIONS

XZ and YL: study design and revising the manuscript. WH, YY, KZ, YD, JQ, YZ, SZ, ZZ, LC, QF, YJ, and JY: study performance. WH, YY, KZ, and YD: data collection and management. WH, YY, and KZ: data analysis and interpretation. WH: drafting the manuscript. All authors approved the manuscript.

FUNDING

Publication of this article was supported by research grants from the National Natural Science Foundation of China (81970780, 81900838, 81870642, and 81670835), the Outstanding Youth Medical Talents Program of Shanghai Health and Family Planning Commission (2017YQ011), the Science and Technology Innovation Action Plan of Shanghai Science and Technology Commission (19441900700 and 21S31904900), the National Key R&D Program of China (2018YFC0116800), Clinical Research Plan of Shanghai Shenkang Hospital Development Center (SHDC2020CR4078 and SHDC12019X08), the WIT120 Research Project of Shanghai (2018ZHYL0220), Clinical Research Project of Shanghai Health and Family Planning Committee (201840199) and the Shanghai Science and Technology Commission Research Project (18ZR1435700).

REFERENCES

1. Morgan IG, Ohno-Matsui K, Saw SM. Myopia. *Lancet.* (2012) 379:1739–48. doi: 10.1016/S0140-6736(12)60272-4

2. Holden BA, Fricke TR, Wilson DA, Jong M, Naidoo KS, Sankaridurg P, et al. Global prevalence of myopia and high myopia and temporal trends from 2000 through 2050. *Ophthalmology.* (2016) 123:1036–42. doi: 10.1016/j.ophtha.2016.01.006

3. Praveen MR, Vasavada AR, Jani UD, Trivedi RH, Choudhary PK. Prevalence of cataract type in relation to axial length in subjects with high myopia and emmetropia in an Indian population. *Am J Ophthalmol.* (2008) 145:176–81. doi: 10.1016/j.ajo.2007.07.043
4. Morgan IG, French AN, Ashby RS, Guo X, Ding X, He M, et al. The epidemics of myopia: aetiology and prevention. *Prog Retinal Eye Res.* (2018) 62:134–49. doi: 10.1016/j.preteyeres.2017.09.004
5. Sun J, Zhou J, Zhao P, Lian J, Zhu H, Zhou Y, et al. High prevalence of myopia and high myopia in 5060 Chinese university students in Shanghai. *Invest Ophthalmol Vis Sci.* (2012) 53:7504–9. doi: 10.1167/iovs.11-8343
6. Zhu XJ, Zhou P, Zhang KK, Yang J, Luo Y, Lu Y. Epigenetic regulation of alphaA-crystallin in high myopia-induced dark nuclear cataract. *PLoS ONE.* (2013) 8:e81900. doi: 10.1371/journal.pone.0081900
7. Zhu X, He W, Zhang S, Rong X, Fan Q, Lu Y. Dome-shaped macula: a potential protective factor for visual acuity after cataract surgery in patients with high myopia. *Br J Ophthalmol.* (2019) 103:1566–70. doi: 10.1136/bjophthalmol-2018-313279
8. Mountjoy E, Davies NM, Plotnikov D, Smith GD, Rodriguez S, Williams CE, et al. Education and myopia: assessing the direction of causality by mendelian randomisation. *BMJ.* (2018) 361:k2022. doi: 10.1136/bmj.k2022
9. Jeon S, Kim HS. Clinical characteristics and outcomes of cataract surgery in highly myopic Koreans. *Korean J Ophthalmol.* (2011) 25:84–9. doi: 10.3341/kjo.2011.25.2.84
10. Srinivasan B, Leung HY, Cao H, Liu S, Chen L, Fan AH. Modern phacoemulsification and intraocular lens implantation (refractive lens exchange) is safe and effective in treating high myopia. *Asia Pac J Ophthalmol.* (2016) 5:438–44. doi: 10.1097/APO.0000000000000241
11. Lam JK, Chan TC, Ng AL, Chow VW, Wong VW, Jhanji V. Outcomes of cataract operations in extreme high axial myopia. *Graefes Arch Clin Exp Ophthalmol.* (2016) 254:1811–7. doi: 10.1007/s00417-016-3414-y
12. Zhu X, He W, Du Y, Zhang K, Lu Y. Interocular Symmetry of Fixation, Optic Disc, and Corneal Astigmatism in Bilateral High Myopia: The Shanghai High Myopia Study. *Transl Vis Sci Technol.* (2019) 8:22. doi: 10.1167/tvst.8.1.22
13. Zhu X, He W, Zhang K, Zhang Y, Fan Q, Lu Y. Fixation Characteristics in Highly Myopic Eyes: the Shanghai High Myopia Study. *Sci Rep.* (2019) 9:6502. doi: 10.1038/s41598-019-42895-3
14. Zhu X, Qi J, He W, Zhang S, Zhang K, Lu Q, et al. Early transient intraocular pressure spike after cataract surgery in highly myopic cataract eyes and associated risk factors. *Br J Ophthalmol.* (2019) 104:1137–41. doi: 10.1136/bjophthalmol-2019-315117
15. Liu HH, Xu L, Wang YX, Wang S, You QS, Jonas JB. Prevalence and progression of myopic retinopathy in Chinese adults: the Beijing Eye Study. *Ophthalmology.* (2010) 117:1763–8. doi: 10.1016/j.ophtha.2010.01.020
16. Wong TY, Foster PJ, Hee J, Ng TP, Tielsch JM, Chew SJ, et al. Prevalence and risk factors for refractive errors in adult Chinese in Singapore. *Invest Ophthalmol Vis Sci.* (2000) 41:2486–94. Available online at: https://iovs.arvojournals.org/article.aspx?articleid=2162611
17. Cetinkaya S, Acir NO, Cetinkaya YF, Dadaci Z, Yener H, Saglam F. Phacoemulsification in eyes with cataract and high myopia. *Arquivos brasileiros de oftalmologia.* (2015) 78:286–9. doi: 10.5935/0004-2749.20150076
18. Daien V, Le Pape A, Heve D, Carriere I, Villain M. Incidence, risk factors, and impact of age on retinal detachment after cataract surgery in france: a national population study. *Ophthalmology.* (2015) 122:2179–85. doi: 10.1016/j.ophtha.2015.07.014
19. Lin JY, Ho WL, Ger LP, Sheu SJ. Analysis of factors correlated with the development of pseudophakic retinal detachment–a long-term study in a single medical center. *Graefes Arch Clin Exp Ophthalmol.* (2013) 251:459–65. doi: 10.1007/s00417-012-2043-3
20. Zaben A, Zapata M, Garcia-Arumi J. Retinal sensitivity and choroidal thickness in high myopia. *Retina.* (2015) 35:398–406. doi: 10.1097/IAE.0000000000000367
21. Ye J, Shen M, Huang S, Fan Y, Yao A, Pan C, et al. Visual acuity in pathological myopia is correlated with the photoreceptor myoid and ellipsoid zone thickness and affected by choroid thickness. *Invest Ophthalmol Vis Sci.* (2019) 60:1714–23. doi: 10.1167/iovs.18-26086
22. Rong X, He W, Zhu Q, Qian D, Lu Y, Zhu X. Intraocular lens power calculation in eyes with extreme myopia: Comparison of Barrett Universal II, Haigis, and Olsen formulas. *J Cataract Refract Surg.* (2019) 45:732–7. doi: 10.1016/j.jcrs.2018.12.025
23. Zhu X, He W, Sun X, Dai J, Lu Y. Fixation stability and refractive error after cataract surgery in highly myopic eyes. *Am J Ophthalmol.* (2016) 169:89–94. doi: 10.1016/j.ajo.2016.06.022
24. Zhu X, He W, Zhang K, Lu Y. Factors influencing 1-year rotational stability of AcrySof Toric intraocular lenses. *Br J Ophthalmol.* (2016) 100:263–8. doi: 10.1136/bjophthalmol-2015-306656
25. Tataru CP, Dogaroiu AC, Tataru CI, Dogaroiu C. Enhancing rotational stability of toric intraocular lenses using a type 2L Cionni capsular tension ring in patients with high myopia. *J Cataract Refract Surg.* (2019) 45:1219–21. doi: 10.1016/j.jcrs.2019.05.045
26. Vokrojová M, Havlíčková L, BroŽková M, Hlinomazová Z. Effect of capsular tension ring implantation on postoperative rotational stability of a toric intraocular lens. *J Refract Surg.* (2020) 36:186–92. doi: 10.3928/1081597X-20200120-01
27. Zhu X, Meng J, He W, Rong X, Lu Y. Comparison of the rotational stability between plate-haptic toric and C-loop haptic toric IOLs in myopic eyes. *J Cataract Refract Surg.* (2020) 46:1353–9. doi: 10.1097/j.jcrs.0000000000000259
28. Cox JT, Subburaman GB, Munoz B, Friedman DS, Ravindran RD. Visual acuity outcomes after cataract surgery: high-volume versus low-volume surgeons. *Ophthalmology.* (2019) 126:1480–9. doi: 10.1016/j.ophtha.2019.03.033

Conflict of Interest: The authors declare that the research was conducted in the absence of any commercial or financial relationships that could be construed as a potential conflict of interest.

frontiers in Medicine

ORIGINAL RESEARCH
published: 04 January 2022
doi: 10.3389/fmed.2021.670229

Multimodal Imaging-Based Phenotyping of a Singaporean Hospital-Based Cohort of High Myopia Patients

Kai Yuan Tey[1†], Quan V. Hoang[1,2,3†], Isabella Q. Loh[1], Yee Shan Dan[1], Qiu Ying Wong[1], Daryle Jason G. Yu[1], Vivi R. Yandri[1], Marcus Ang[1], Gemmy C. M. Cheung[1], Shu Yen Lee[1], Tien Yin Wong[1], SNEC Retina Group[1], Rachel S. Chong[1‡] and Chee Wai Wong[1‡]*

[1] Singapore Eye Research Institute, Singapore National Eye Centre, Duke-NUS Medical School, Singapore, Singapore,
[2] Department of Ophthalmology, Columbia University College of Physicians and Surgeons, New York, NY, United States,
[3] Department of Ophthalmology, Yong Loo Lin School of Medicine, National University of Singapore, Singapore, Singapore

OPEN ACCESS

Edited by:
Paris Tranos,
Ophthalmica Eye Institute, Greece

Reviewed by:
Alain Gaudric,
Université de Paris, France
Karim Mohamed-Noriega,
Autonomous University of Nuevo León, Mexico

***Correspondence:**
Quan V. Hoang
donny.hoang@singhealth.com.sg

[†]These authors have contributed equally to this work and share first authorship

[‡]These authors have contributed equally to this work

Specialty section:
This article was submitted to Ophthalmology, a section of the journal Frontiers in Medicine

Received: 20 February 2021
Accepted: 22 November 2021
Published: 04 January 2022

Citation:
Tey KY, Hoang QV, Loh IQ, Dan YS, Wong QY, Yu DJG, Yandri VR, Ang M, Cheung GCM, Lee SY, Wong TY, SNEC Retina Group, Chong RS and Wong CW (2022) Multimodal Imaging-Based Phenotyping of a Singaporean Hospital-Based Cohort of High Myopia Patients. Front. Med. 8:670229. doi: 10.3389/fmed.2021.670229

Purpose: To assess the effect of axial length (AL) on the prevalence of pathologic myopia (PM) and associated myopic features in a Singaporean hospital-based cohort of patient with high myopia (HM).

Methods: In total, 923 HM eyes from 495 individuals were recruited from the Myopic and Pathologic Eyes in Singapore (MyoPES) cohort and underwent ocular biometry, fundus photography, fundus autofluorescence, and swept-source optical coherence tomography (SS-OCT). Images were analyzed for the presence of myopic macular degeneration (MMD), myopic choroidal neovascularization (mCNV), myopic traction maculopathy (MTM), peripapillary atrophy (PPA), myopic tilted disc, posterior staphyloma (PS), dome-shaped macula (DSM), vitremacular adhesions (VMA), and the epiretinal membrane (ERM). Eyes were stratified into quartiles based on ALs to determine cut-off values to perform comparisons between shorter-length and longer-length groups. A χ^2-test was done to determine the difference in the prevalence of pathologies between groups.

Results: Overall, mean AL was 29.2 ± 2.2 mm (range 25.0–36.7 mm). Myopic macular degeneration, PPA, myopic tilted disc, and ERM have AL threshold of ≥27.5 mm, whereas MTM has an AL threshold of ≥29.0 mm. We found that there was a significantly higher prevalence of MMD (88.2 vs. 49.4%; $p < 0.001$), PPA (98.1 vs. 80.1%; $p < 0.001$), myopic tilted disc (72.7 vs. 50.2%; $p < 0.001$), and ERM (81.4 vs. 17.3%; $p = 0.003$) in eyes with AL ≥ 27.5 mm vs. eyes without AL <27.5 mm. Prevalence of MTM (34.7 vs. 32.1%; $p < 0.001$), mCNV (17.4 vs. 12.1%; $p = 0.03$), PS (43.4 vs. 34.7%; $p = 0.012$), DSM (21.3 vs. 13.2%; $p = 0.002$), and VMA (5.9 vs. 2.6%; $p = 0.014$) in eyes with AL ≥ 29.0 mm compared with AL < 29.0 mm.

Conclusion: Our study describes the overall prevalence of PM and related pathologies among patients with HM in our hospital-based cohort. Longer eyes even among HM

eyes had a significantly higher prevalence of PM-associated pathologies studied. This supports the premise that eyes with longer AL, even among HM eyes may be at greater risk of vision-threatening changes and therefore merit regular follow-up.

Keywords: high myopia, pathologic myopia, multimodal imaging, myopic macular degeneration, myopic traction maculopathy

INTRODUCTION

Myopia is the leading cause of distance refractive error in the world, affecting 1.89 billion of the global population in 2017 (1), and it is believed that this number will continue to grow due to the myopia boom as a result of a modern lifestyle (2). Mild-to-moderate myopia is a common condition, often due to axial elongation, that can be corrected with appropriate spectacles, contact lenses, and refractive surgery (3).

High myopia, on the other hand, due to excessive ocular elongation (4) can predispose the eye to a risk of permanent vision loss through the development of pathologic myopia (PM), which often manifests clinically as one or a combination of the following conditions: myopic macular degeneration (MMD) (5, 6), myopic choroidal neovascularization (mCNV), or myopic traction maculopathy (MTM) (6–12). While the WHO defines high myopia as spherical equivalent (SE) of five diopters (D) of myopia and above (13), definitions of high myopia vary in the current literature, with most defining high myopia as ≥5.0–8.0 D of myopia (14–16), or axial length (AL) 25–27 mm and above (17–20). High myopia is the second major cause of vision impairment worldwide, having affected approximately 2.8% (170 million) of the global population, with the highest prevalence in East and Southeast Asia, such as China, Japan, the Republic of Korea, and Singapore (2, 13). The prevalence of high myopia continues to grow rapidly, and it is estimated that by 2050, 9.8% (938 million) people globally will be highly myopic (HM) (16). Consequently, the prevalence of PM-related visual impairment is likely to rise in tandem with the prevalence of high myopia (21, 22).

In addition to PM, HM eyes are more likely to develop associated myopic pathologies, such as peripapillary atrophy (PPA) (23), myopic tilted disc (24), posterior staphyloma (PS) (25), dome-shaped macula (DSM) (26), vitreomacular adhesion (VMA) (27), and the epiretinal membrane (ERM) (28). Determining the characteristics of patients with HM at high risk of developing these pathologic changes is critical in guiding the optimal monitoring of patients with HM, so as to administer timely interventions to mitigate or prevent permanent visual loss (29).

In this study, we aimed to assess the prevalence of the aforementioned myopia-related pathologies in a cohort of hospital-based patients with HM using multimodal imaging, including widefield swept-source optical coherence tomography (SS-OCT) and fundus photography/autofluorescence. To further evaluate the impact of AL on PM (13, 30), we stratified patients into two groups based on a cut-off threshold derived from quartile analysis in the hopes of providing credence to an AL-based system to guide the frequency of clinical follow-up for patients with HM.

METHODS

We conducted a cross-sectional analysis of high myopes from the Myopic and Pathologic Eyes in Singapore (MyoPES) cohort. In brief, high myopes defined by an SE refractive error of ≥5.0 D of myopia and/or AL ≥ 25.0 mm in the study eye, and aged 18 years old and above were enrolled from the High Myopia clinic at the Singapore National Eye Centre, Singapore, from January 2017 to December 2018. The study was performed with approval from the SingHealth Institutional Review Board and in accordance with the Declaration of Helsinki. Written informed consent was obtained from all participants. Participants with any existing or previous ocular diseases in either eye that may confound measurements from SS-OCT, and fundus photography were excluded from the study. Such conditions included corneal opacities, uveitis, dense cataracts, vitreous hemorrhage, diabetic retinopathy/diabetic macular edema, central serous chorioretinopathy, previous retinal laser photocoagulation or photodynamic therapy, retinal dystrophies, and macular scarring from any cause other than myopic maculopathy, retinopathy due to any cause other than myopia, previous retinal vein or artery occlusion, and ocular ischemic syndrome.

All enrolled participants underwent the following investigations: (1) ocular biometry, (2) dilated retinal examination, (3) color fundus photography, (4) fundus autofluorescence, and (5) SS-OCT.

Image Acquisition and Assessment

Axial length was measured using Aladdin HW 3.0, Topcon (Topcon Medical Systems, Oakland, NJ, USA). Triton DRI OCT Plus (Topcon Medical Systems, Oakland, NJ, USA) was used to obtain both fundus photos and SS-OCT images after pupillary dilation. Two fields of each eye were photographed, with one centered at the optic disc and another centered at the fovea. For SS-OCT, images of the fovea, optic disc, vitreous, and sclera were obtained. Scans performed included fovea-centered 3D raster (12 × 9 mm), 3D disc (6 × 6 mm), and fovea-centered radial (diameter 12 mm) scans.

All images and scans obtained were assessed by two retinal specialists (QVH and CWW) for the presence of MMD that includes plus signs (such as mCNV), MTM, myopic tilted disc, PPA, PS, DSM, VMA, and ERM.

Specifically, fundus images were evaluated for the presence of the following: (1) MMD based on the international Meta Analyses of Pathologic Myopia (META-PM) classifications,

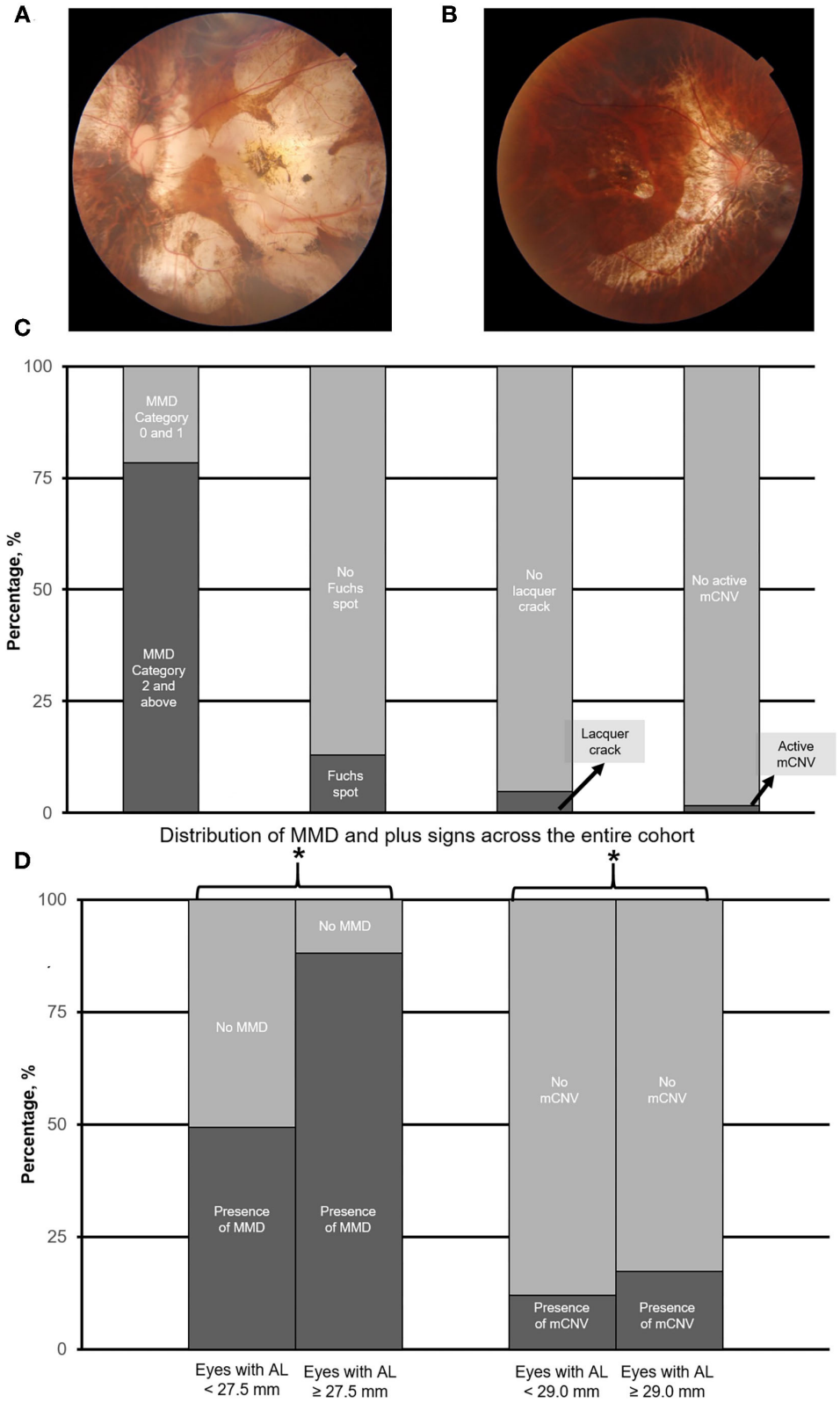

FIGURE 1 | (A) and **(B)** are the representative fundus photograph of a myopic macular degeneration (MMD) category 4, i.e., macular atrophy, and active myopic choroidal neovascularization (mCNV), respectively. Panel **(C)** shows the overall prevalence of myopic macular degeneration as assessed by the META-PM classification system. Panel **(D)** illustrates the prevalence of MMD (including plus signs), and mCNV in eyes with axial length (AL) 25.0–27.5 mm vs. with AL ≥ 27.5 mm, and AL 25.0–<29.0 mm vs. AL ≥ 29.0 mm, respectively. Asterisk (*) denotes statistical significance ($p < 0.05$).

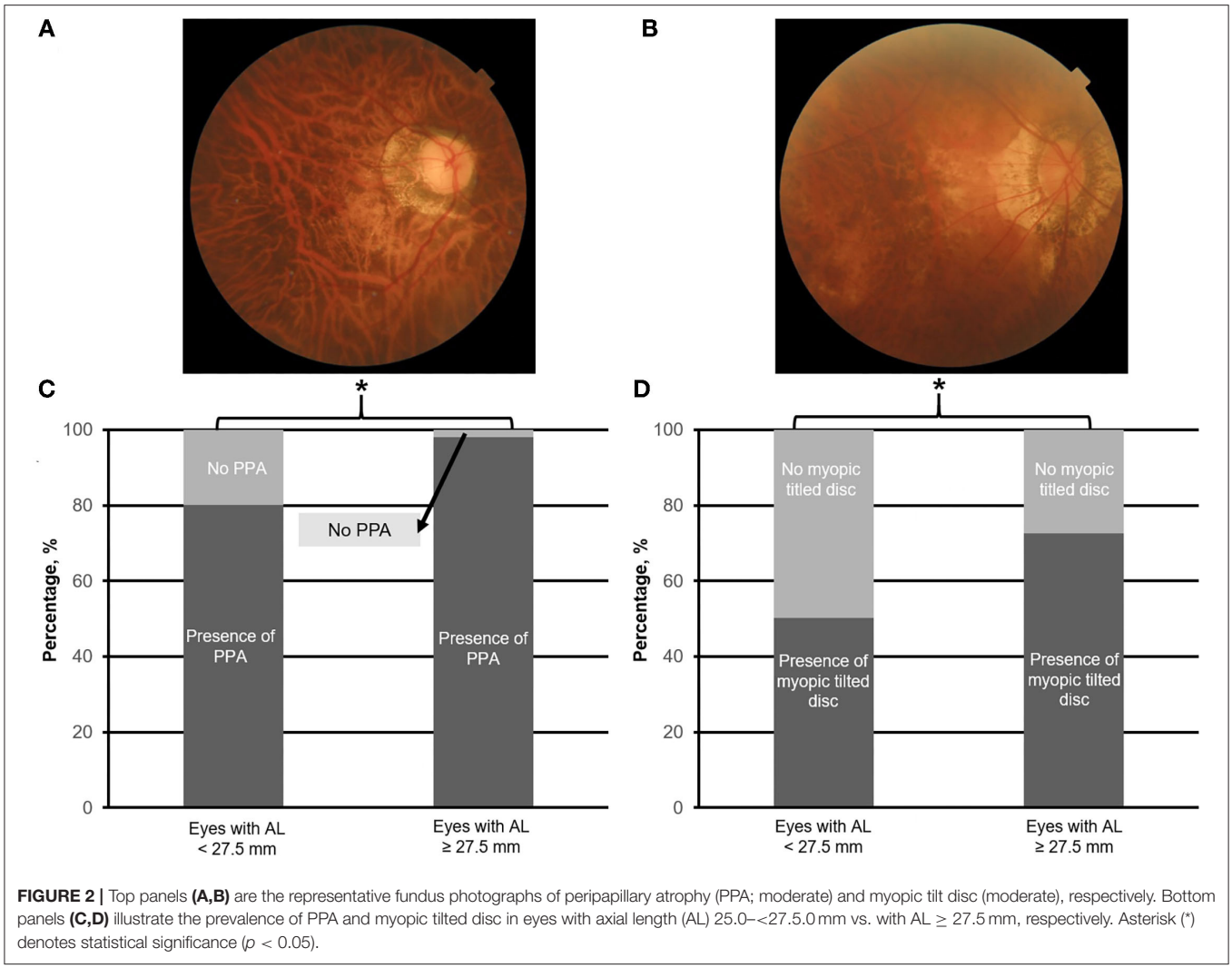

FIGURE 2 | Top panels **(A,B)** are the representative fundus photographs of peripapillary atrophy (PPA; moderate) and myopic tilt disc (moderate), respectively. Bottom panels **(C,D)** illustrate the prevalence of PPA and myopic tilted disc in eyes with axial length (AL) 25.0–<27.5.0 mm vs. with AL ≥ 27.5 mm, respectively. Asterisk (*) denotes statistical significance ($p < 0.05$).

where the presence of MMD was defined as META-PM MMD category 2 (diffuse atrophy) or worse (e.g., **Figure 1A**), or the presence of plus signs (e.g., lacquer cracks, mCNV, or Fuchs spots; **Figure 1B**) (6), (2) PPA (e.g., **Figure 2A**), and (3) myopic tilted disc (e.g., **Figure 2B**) defined as an optic disc with a ratio of minimal to maximal disc diameter of 0.75 or less and was assessed via the use of fundus photography (31). Given that Fuchs spot is considered a quiescent mCNV (32), and mCNV is one of the most commonly described features of PM (33), we included both active and quiescent forms in our prevalence of mCNV.

Swept-source optical coherence tomography scans were assessed for the presence of the following: (1) MTM (e.g., **Figures 3A–C**) defined by the presence of extrafoveal schisis, foveoschisis (with or without foveal detachment), or macular hole (partial/full-thickness macular hole, such as previously repaired macular hole) (10), (2) PS (e.g., **Figure 4A**) defined as an abrupt change in radius of curvature of the posterior sclera (34), (3) DSM (e.g., **Figure 4B**) defined as a hill-like appearance [an inward bludge of the retinal pigment epithelium (RPE)], greater than 50 μm on the most convex vertical or horizontal OCT sections above a presumed line tangent to the outer surface of the RPE, or at the bottom of the PS in HM eyes) (35), (4) VMA (e.g., **Figure 5A**), and (5) ERM (e.g., **Figure 5B**). In this analysis, we also included saddle-shaped macula (SSM, a hill-like surface present only in one meridian) (35) within the DSM group.

Outcome Measures and Statistical Analysis

IBM SPSS Statistics for Windows version 26 (IBM Corp., Armonk, NY, USA) was used for the statistical analysis in this study. Our cohort of 923 eyes was arranged in order of AL and divided into four equal groups based on quartiles. Specifically, the quartile 1 (Q1) group contained eyes with AL ranging from 25.0 to 27.4 mm, quartile 2 (Q2: AL 27.5–28.9 mm), quartile 3 (Q3: AL 29.0–30.7 mm), and lastly, group 4 contained quartile 4 (Q4: AL 30.8–36.7 mm). The χ^2-test was performed on adjacent quartiles (Q1 vs. Q2, Q2 vs. Q3, and Q3 vs. Q4) to screen for potential cut-off thresholds for significant differences in prevalence in pathologic findings as detailed above and instances where MMD and MTM (MMD+MTM), or MMD, MTM, and DSM (MMD+MTM+DSM) occurred concurrently.

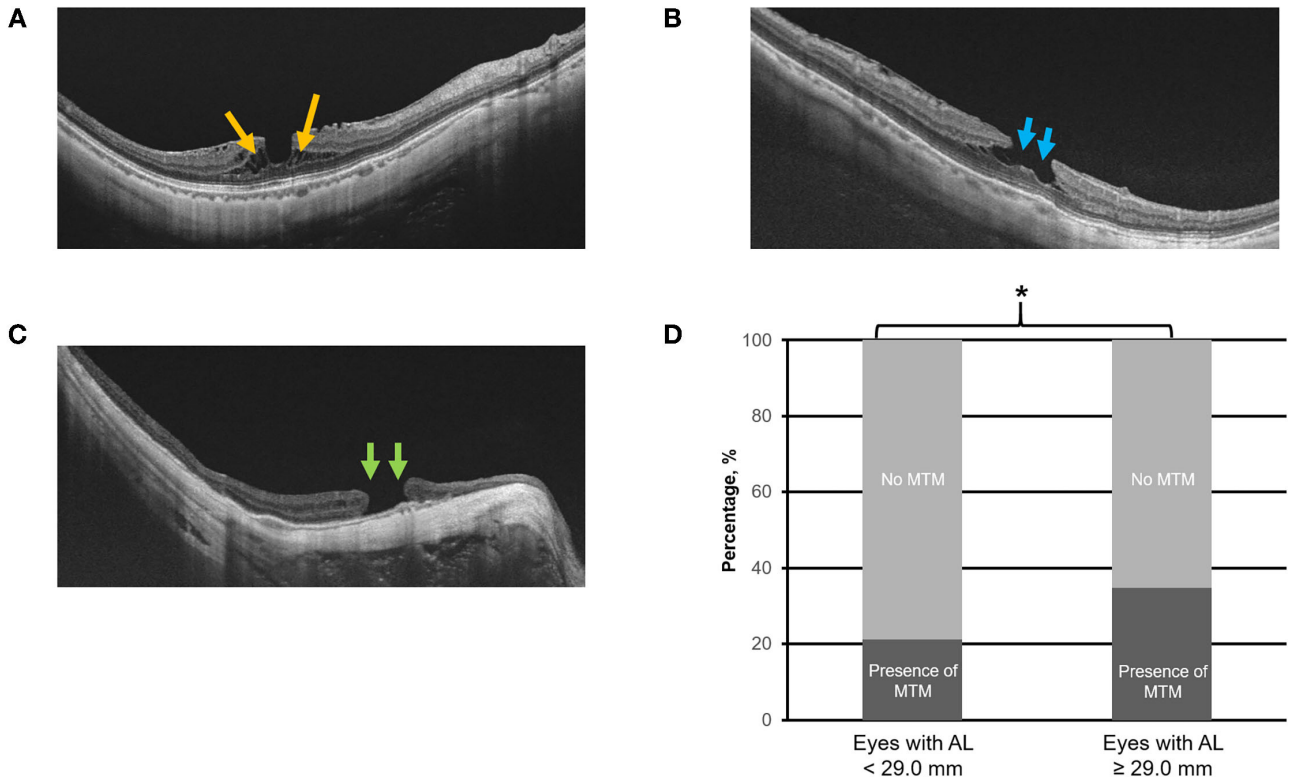

FIGURE 3 | Panels **(A–C)** are the representative swept-source optical coherence scans of myopic traction maculopathy (MTM), e.g., myopic foveoschisis **(A)**, a partial-thickness macular hole **(B)**, and a full-thickness macular hole **(C)**. Panel **(D)** illustrates the prevalence of MTM in eyes with axial length (AL) 25.0–<29.0 mm vs. with AL ≥ 29.0 mm. Asterisk (*) denotes statistical significance ($p < 0.05$). Yellow arrows denote the area of foveoschisis. Blue arrows denote a partial-thickness macular hole. Green arrows denote full-thickness macular hole.

Eyes were then stratified into two groups depending on the threshold identified above for various pathologies analyzed. For conditions in which two or more thresholds were identified, the lower threshold was employed. For conditions without a threshold identified, the Q2 cut-off (AL 29.0 mm) was employed. The mean differences in AL were analyzed with the independent *t*-test for between-groups comparison. Prevalence in each group of MMD, mCNV, MTM, PPA, myopic tilted disc, PS, ERM, DSM, VMA, and conditions occurring concurrently (such as MMD+MTM concurrently, and MMD+MTM+DSM concurrently) were compared using the χ^2-test. These tests were two-sided with statistical significance set at $p < 0.05$.

RESULTS

Overall, 495 subjects were included in the study. A total of 990 eyes were imaged: 923 eyes were included in the analysis after excluding 45 unilateral eyes with AL < 25.0 mm, and 22 eyes due to poor image signal or inability to obtain images. In total, 326 (65.9%) of included subjects were female, and the mean age was 61.7 ± 13.7 years old (range 19–91 years old). The overall mean AL was 29.2 ± 2.2 mm (range 25.0–36.7 mm).

Overall, there were 231 (25.0%) eyes in Q1, 231 (25.0%) eyes in Q2, 231 (25.0%) eyes in Q3, and 230 (25.0%) eyes in Q4. The mean ALs were 26.5 ± 0.6, 28.2 ± 0.5, 29.8 ± 0.5, and 32.3 ± 1.2 mm for Q1, Q2, Q3, and Q4, respectively. Characteristics of patients and a summary of the χ^2-test analysis are found in **Table 1**. In summary, the identified threshold for MMD, PPA, myopic tilted disc, ERM, and for concurrent MMD+MTM was AL ≥ 27.5 mm, whereas for MTM and for concurrent MMD+MTM+DSM, the threshold was AL ≥ 29.0 mm. The summary of the χ^2-test analysis based on the threshold identified is found in **Table 2**.

Prevalence of MMD

Of 923 eyes, 724 (78.4%) eyes were found to have the presence of MMD. Overall, 9 (1.0%) eyes were found to have no MMD, 206 (22.3%) eyes were found to have tessellated fundus (Category 1 MMD), 401 (43.4%) eyes had diffuse atrophy (Category 2), 168 (18.2%) eyes had patchy atrophy (Category 3), and 139 (15.1%) eyes had macular atrophy (Category 4). For plus signs, 120 (13.0%) patients had Fuchs spot, 43 (4.7%) patients had lacquer crack, and 16 (1.7%) patients had active mCNV. The overall prevalence of MMD is found in **Figure 1C**.

The threshold identified for MMD was AL ≥ 27.5 mm (Q1 vs. Q2; $\chi^2 = 24.5$; $p < 0.001$, **Table 1**). Specifically, the prevalence of MMD was significantly higher in eyes with AL ≥ 27.5 mm, with 610 (88.2%) of the eyes found to have the presence of MMD,

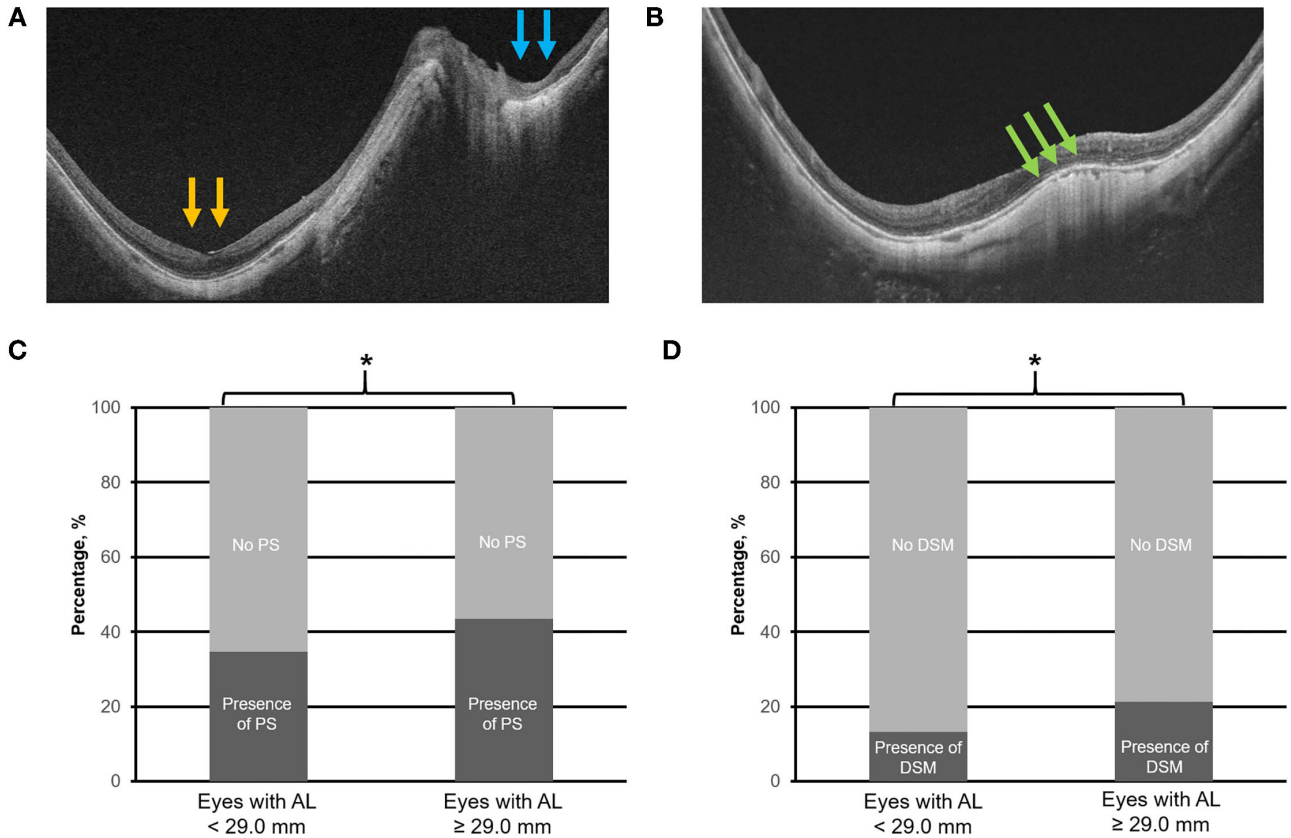

FIGURE 4 | Top panels **(A,B)** are the representative swept-source optical coherence tomography scans of posterior staphyloma (PS; compound type—macular PS as denoted by the yellow arrows, and peripapillary PS as denoted by the blue arrows) and dome-shaped macula (DSM), respectively. Bottom panels **(C,D)** illustrate the prevalence of PS and DSM in eyes with axial length (AL) 25.0–<29.0 mm vs. with AL ≥ 29.0 mm. Asterisk (*) denotes statistical significance ($p < 0.05$). Yellow and blue arrows denote abrupt changes in the radius of curvature of the posterior sclera. Green arrows denote the inward bulge of the retinal pigment epithelium line.

as compared to 114 (49.4%) in eyes <27.5 mm ($\chi^2 = 154.2$; $p < 0.001$; **Table 2**; **Figure 1D**). The prevalence of mCNV (active mCNV or Fuchs spot) was significantly higher in in eyes with AL ≥ 29.0 mm with 80 (17.4%) eyes found to have presence of mCNV, as compared to the 57 (12.1%) eyes of AL < 29.0 mm ($\chi^2 = 5.0$; $p = 0.03$; **Table 2**; **Figure 1D**).

Prevalence of MTM

Of the 923 images obtained, 259 (28.1%) eyes were found to have presence of MTM. The threshold identified for MTM was AL ≥ 29.0 mm (Q2 vs. Q3; $\chi^2 = 9.0$; $p = 0.003$, **Table 1**). Specifically, the prevalence of MTM was significantly higher in the in eyes with AL ≥ 29.0 mm with 160 (34.7%) eyes found to have MTM, as compared to the 99 (21.1%) eyes of AL < 29.0 mm ($\chi^2 = 55.8$; $p < 0.001$; **Table 2**; **Figure 3D**).

Prevalence of Other Associated Myopic Features

Overall, of the 923 images obtained, 864 (93.6%), 619 (67.1%), 363 (39.3%), 228 (24.7%), 160 (17.3%), and 39 (4.2%) eyes were found to have PPA, myopic tilted disc, PS, ERM, DSM, and VMA, respectively.

The identified threshold for PPA (Q1 vs. Q2; $\chi^2 = 32.4$; $p < 0.001$), myopic tilted disc (Q1 vs. Q2; $\chi^2 = 15.1$; $p < 0.001$), and ERM (Q1 vs. Q2; $\chi^2 = 6.1$; $p < 0.003$) was AL ≥ 27.5 mm (**Table 1**). The prevalence of PPA ($\chi^2 = 94.1$; $p < 0.001$; **Figure 2C**), myopic tilted disc ($\chi^2 = 39.6$; $p < 0.001$; **Figure 2D**), and ERM ($\chi^2 = 9.0$; $p < 0.001$; **Figure 5D**) was higher in eyes with AL ≥ 27.5 mm, as compared to eyes with AL < 27.5 mm (**Table 2**). The prevalence of PS ($\chi^2 = 6.3$; $p = 0.012$; **Figure 4C**), DSM ($\chi^2 = 9.9$; $p = 0.002$; **Figure 4D**), and VMA ($\chi^2 = 6.058$; $p = 0.014$; **Figure 5C**) was significantly higher in the eyes of AL ≥ 29.0 mm when compared to eyes with AL < 29.0 mm (**Table 2**).

When considering eyes with multiple concurrent myopic pathologic changes, 234 (25.4%) eyes had MMD and MTM (MMD+MTM) concurrently (**Figure 6A**), whereas 56 (6.1%) eyes had MMD, MTM, and DSM (MMD+MTM+DSM) concurrently (**Figure 6B**). The identified threshold for MMD+MTM AL ≥ 27.5 mm (Q1 vs. Q2; $\chi^2 = 8.9$; $p = 0.003$, **Table 1**), while the threshold for MMD+MTM+DSM was AL ≥ 29.0 mm (Q2 vs. Q3; $\chi^2 = 9.4$; $p = 0.002$, **Table 1**). Prevalence of MMD and MTM concurrently was higher in eyes with AL ≥ 27.5 mm, with 207 (30.0%) eyes displaying MMD+MTM concurrently as compared to eyes with AL < 27.5 mm, among

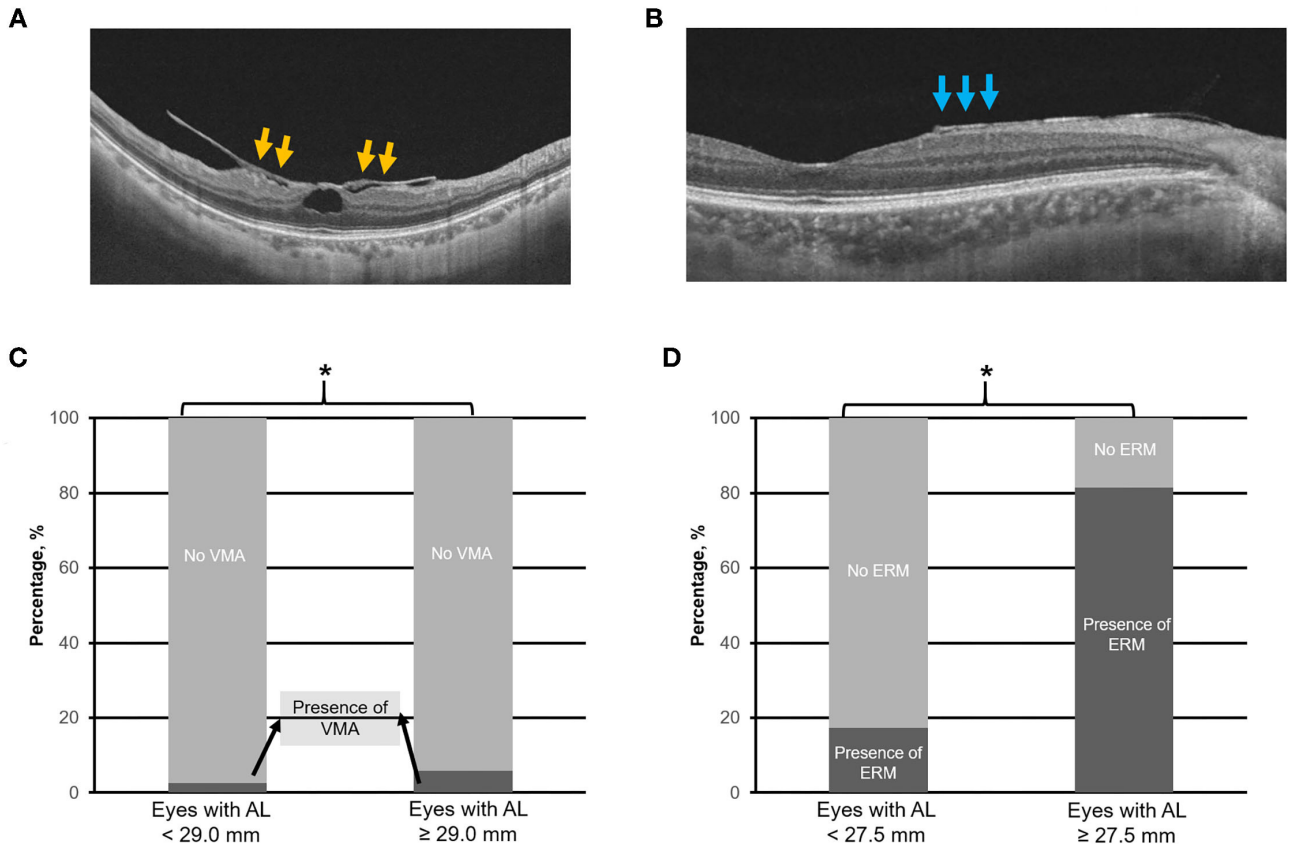

FIGURE 5 | Top panels **(A,B)** are the representative swept-source optical coherence tomography scans of vitreomacular adhesion (VMA) and the epiretinal membrane (ERM), respectively. Bottom panels **(C,D)** illustrate the prevalence of VMA and ERM in eyes with axial length (AL) 25.0–< 29.0 mm vs. with AL ≥ 29.0 mm, and AL 25.0–<27.5 mm vs. with AL ≥ 27.5 mm, respectively. Asterisk (*) denotes statistical significance ($p < 0.05$). Yellow arrows denote VMA. Blue arrows denote ERM.

which 27 (11.7%) eyes displayed MMD+MTM ($\chi^2 = 30.4$; $p < 0.001$, **Table 2**). Prevalence of MMD+MTM+DSM concurrently was significantly higher in eyes with AL ≥ 29.0 mm, with 43 (9.3%) found to have MMD+MTM+DSM concurrently, as compared to 13 (2.8%) eyes with AL < 29.0 mm ($\chi^2 = 17.2$; $p < 0.001$, **Table 2**).

DISCUSSION

In this study, we established the prevalence of MMD, MTM, and associated myopic features in a cohort of hospital-based patients with HM using multimodal imaging. Overall, we observed that even among HM eyes, i.e., AL ≥ 25.0 mm, longer eyes were associated with a higher prevalence of MMD, mCNV, MTM, and associated myopic features, namely, myopic tilted disc, PPA, PS, DSM, ERM, and VMA when compared to relatively shorter HM eyes. Our quartile analysis suggested an AL threshold above which the prevalence of certain myopic pathologies was significantly higher, namely, for MMD (AL ≥ 27.5 mm), MTM (AL ≥ 29.0 mm), PPA (AL ≥ 27.5 mm), myopic tilted disc (AL ≥ 27.5 mm), MMD+MTM concurrently (AL ≥ 27.5 mm), and MMD+MTM+DSM concurrently (AL ≥ 29.0 mm).

The presence of MMD in HM eyes has been well-described in the literature. The prevalence of MMD has been reported to be 1.3–6.0% in the general population (36–45). Specifically, the prevalence of MMD among subjects with HM was observed to be 25.3–71.4%, which varies depending on the population reported (36–45). In our study, we observed a prevalence of 78.4% among hospital-based subjects with HM, which is slightly higher than the upper end of the previously reported number. This is likely attributed to the fact that this cohort of patients (MyoPES cohort) was recruited from a tertiary referral center (Singapore National Eye Centre High Myopia Clinic, Singapore), which specifically looks after high myopes, in which a vast majority have PM as compared to population studies that involve subjects from the general population. In addition, although eyes from both groups were considered to be HM, we observed that long HM eyes (AL ≥ 27.5 mm) were found to have a higher prevalence of MMD (88.2 vs. 49.4%; $p < 0.001$). This finding is consistent with Choudhury et al.'s findings, which found that longer AL is an independent risk factor for MMD (46). Similarly, this finding is also supported by the Hisayama study (47), which established an association between AL elongation and the likelihood of MMD. While AL has been identified as an independent risk

TABLE 1 | Prevalence of pathologic changes in high myopia eyes stratified by axial length into quartiles.

					Overall					
Patients, *n* (number of eyes included)					495 (923)					
Females, *n* (%)					326 (65.9%)					
Mean age, years old (range)					61.7 ± 13.7 (19–93)					
Axial length, mm (range)					29.2 ± 2.2 (25.0–36.7)					
	Q1	**Q2**	**Q3**	**Q4**	**Q1 vs. Q2**		**Q2 vs. Q3**		**Q3 vs. Q4**	
n	231	231	231	230						
AL range	25.0–27.4	27.5–28.9	29.0–30.7	30.8–36.7						
Mean AL, mm	26.5 ± 0.6	28.2 ± 0.5	29.8 ± 0.5	32.3 ± 1.2						
	***n* (%)**	***n* (%)**	***n* (%)**	***n* (%)**	χ^2	***p***	χ^2	***p***	χ^2	***p***
MMD	114 (49.4)	166 (71.9)	214 (92.6)	230 (100.0)	24.5	**<0.001***	34.2	**<0.001***	17.6	**<0.001***
mCNV or Fuchs spot	22 (9.5)	34 (14.7)	39 (16.9)	41 (17.8)	2.9	0.87	0.4	0.524	0.1	0.789
MTM	41 (17.7)	58 (25.1)	88 (38.1)	72 (31.3)	3.7	0.054	9.0	**0.003***	2.3	0.126
PPA	185 (80.1)	224 (97.0)	229 (99.1)	226 (98.3)	32.4	**< 0.001 ***	2.8	0.092	0.7	0.408
Myopic tilted disc	116 (50.2)	157 (68.0)	162 (70.1)	184 (80.0)	15.1	**< 0.001***	0.3	0.615	6.0	**0.014***
PS	76 (32.9)	87 (37.7)	91 (39.4)	109 (47.4)	1.1	0.284	0.1	0.702	3.0	0.083
DSM	28 (12.1)	34 (14.7)	43 (18.6)	55 (23.9)	0.7	0.413	1.3	0.3	1.9	0.164
VMA	6 (2.6)	6 (2.6)	14 (6.1)	13 (5.6)	0	0.99	3.3	0.067	0.04	0.852
ERM	40 (17.3)	62 (26.8)	65 (28,1)	61 (26.5)	6.1	**0.014***	0.1	0.755	0.2	0.697
MMD+MTM	27 (11.7)	51 (22.1)	84 (36.4)	72 (31.3)	8.9	**0.003***	11.4	**0.001***	1.3	0.251
MMD+MTM+DSM	5 (2.2)	8 (3.5)	25 (10.8)	18 (7.8)	0.7	0.399	9.4	**0.002***	1.2	0.269

AL, axial length; DSM, dome-shaped macula; ERM, epiretinal membrane; mCNV, myopic choroidal neovascularization; MMD, myopic macular degeneration; MTM, myopic traction maculopathy; PPA, peripapillary atrophy; PS, posterior staphyloma; Q, Quartile; VMA, vitreomacular adhesion. Asterisks (*) and bold font represent statistical significance ($p < 0.05$).

TABLE 2 | Summary of the χ^2 analysis made between eyes with AL < 27.5 mm vs. AL ≥ 27.5 mm, and AL < 29.0 mm vs. AL ≥ 29.0 mm.

	Eyes with AL < 27.5 mm (*n* = 231)	**Eyes with AL ≥ 27.5 mm (*n* = 692)**	**Pearson chi-squared value**	***p*-values**
MMD, *n* (%)	114 (49.4)	610 (88.2)	154.2	<0.001*
PPA, *n* (%)	185 (80.1)	679 (98.1%)	94.1	<0.001*
Myopic tilted disc, *n* (%)	116 (50.2)	503 (72.7)	39.6	<0.001*
ERM, *n* (%)	40 (17.3)	188 (81.4)	9.0	0.003*
MMD+MTM, *n* (%)	27 (11.7)	207 (30.0)	30.4	<0.001*
	Eyes with AL < 29.0 mm (*n* = 462)	**Eyes with AL ≥ 29.0 mm (*n* = 461)**	**Pearson chi-squared value**	***p*-values**
mCNV (active mCNV and Fuchs spot), *n* (%)	57 (12.1)	80 (17.4)	5.0	**0.03***
MTM, *n* (%)	99 (21.1)	160 (34.7)	55.8	**<0.001***
PS, *n* (%)	163 (34.7)	200 (43.4)	6.3	**0.012***
DSM, *n* (%)	62 (13.2)	98 (21.3)	9.9	**0.002***
VMA, *n* (%)	12 (2.6)	27 (5.9)	6.1	**0.014***
MMD+MTM+DSM, *n* (%)	13 (2.8)	43 (9.3)	17.2	**<0.001***

AL, axial length; DSM, dome-shaped macula; ERM, epiretinal membrane; mCNV, myopic choroidal neovascularization; mm, millimeters; MMD, myopic macular degeneration; MTM, myopic traction maculopathy; PPA, peripapillary atrophy; PS, posterior staphyloma; VMA, vitreomacular adhesion. Asterisks (*) and bold font represent statistical significance ($p < 0.05$).

factor for MMD development (48), the exact mechanism of what drives the pathology is unknown. Ohsugi et al. previously reported that AL was the greatest in those with mCNV (49), thus suggesting that the presence of MMD could be mainly driven by AL elongation. Our study shared a similar observation, where the prevalence of mCNV (both active and quiescent forms) was found to be significantly higher in eyes with longer AL (≥27.5 mm). We found a significantly higher prevalence of MMD and mCNV in HM eyes with AL ≥ 27.5 mm, and therefore, it is important to monitor such patients more frequently vs. eyes <27.5 mm.

Overall, we observed an overall prevalence of 28.1% for the presence of MTM among our HM eyes, which was similar to what was reported by Panozzo and Mercanti

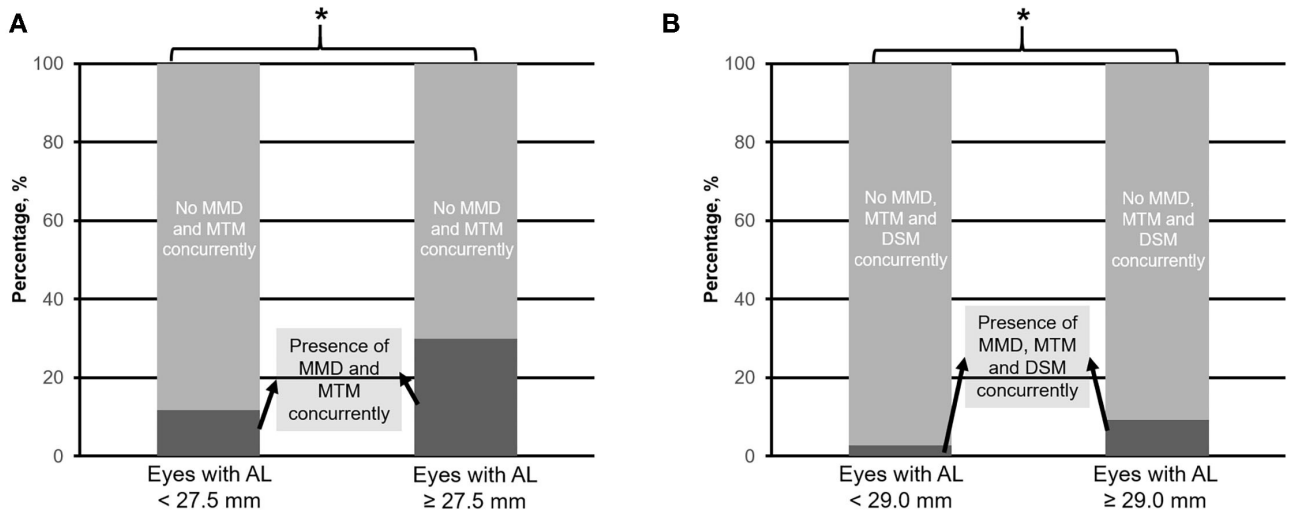

FIGURE 6 | Prevalence of myopic macular degeneration (MMD) and myopic macular traction maculopathy (MTM) concurrently **(A)**, and MMD, MTM plus dome-shaped macula (DSM) concurrently **(B)** in eyes with axial length (AL) 25.0–< 27.5 mm vs. with AL ≥ 27.5 mm, and 25.0–<29.0 mm vs. with AL ≥ 29.0 mm, respectively. Asterisk (*) denotes statistical significance ($p < 0.05$).

(34.4%) (9). Long AL has been a common theme in eyes with MTM (50, 51). In particular, we have found that the prevalence of MTM was significantly higher among eyes with extremely long AL, especially after the threshold AL of ≥ 29.0 mm. Similar observations were made by Xia et al. (50–54). Patients with MTM can have a prolonged subclinical phase in which they remain asymptomatic, and early changes can be difficult to diagnose on routine fundus examination (8). With OCT and an identified threshold, i.e., AL ≥ 29.0 mm, however, MTM can now be detected even in its early stages (55), enabling the timely diagnosis and treatment of patients at risk.

We also examined other pathological features that have been commonly described among HM eyes, as mentioned below. Peripapillary atrophy is more commonly seen in HM eyes (56, 57) and is an important feature to be identified given that it is not only a hallmark of HM but also an important factor for higher risk of glaucomatous damage (58). Myopic tilted disc and PS have also been reported to be progressive in nature in eyes with severe myopia (17, 59, 60). Axial length was identified as a risk factor for the presence of ERM (61), and similarly, DSM and VMA are conditions that are commonly seen in patients with HM (26, 27), and although these conditions alone might not affect visual function, they may increase the risk of developing further sight-threatening complications (26, 27). We found that the prevalence of PPA, myopic tilted disc, PS, DSM, ERM, and VMA was significantly higher in eyes with longer AL even among HM eyes. The association between the presence of these features and AL elongation has also been seen in other studies as well (26, 58, 62, 63). This suggests that AL elongation not only drives the pathogenic pathway of MMD and MTM but may in part lead to the development of these associated features as a by-product (24, 63–65). These patients should be followed up regularly with multimodal imaging for a comprehensive evaluation of these pathologies, and patients should be counseled about the symptoms of sight-threatening conditions, such as mCNV and MTM, to allow for early detection and appropriate interventions.

In this study, we also looked at the prevalence of accumulated eye conditions, namely, MMD+MTM concurrently and MMD+MTM+DSM concurrently. Overall, we found that MMD+MTM is of higher prevalence in eyes with AL ≥ 27.5 mm as compared to eyes with AL < 29.0 mm. Our study findings concur with our previous study where we found that eyes with MTM are at higher risk of developing MMD (12), as the tractional changes may lead to stretching of retinal layers, which may be associated with degenerative changes seen in MMD. In this study, we have further established the threshold where the prevalence of both events occurs concurrently, which is an AL of 27.5 mm. Similarly, we see a higher prevalence of MMD, MTM, and DSM occurring concurrently in eyes with AL ≥ 29.0 mm as compared to eyes with AL < 29.0 mm, and the implication of these findings would be interesting to be explored in a further longitudinal study.

The strengths of our study include the relatively large sample size with comprehensive multimodal imaging to accurately capture the prevalence of multiple HM-related pathologies. Our limitations include first, the cross-sectional design of our study precludes the analysis of incidence and causation. Ideally, a longitudinal study design would be preferred, although difficult in the context of a slowly progressive disease, such as MMD. Second, participants in our study are patients with HM recruited from a tertiary referral center, who are more likely to have worse pathology. Our results, therefore, may not be generalizable to the entire population of individuals with HM. Third, we are not able to establish the threshold of PS, DSM, and VMA, which is likely due to the relatively low prevalence of these phenotypes observed in our study group when subdivided into quartiles.Analyses of

these parameters did reach significance when subdivided into two groups (**Table 2**).

In conclusion, our study described the overall prevalence of PM (MMD and MTM) and associated myopic pathological features in a cohort of hospital-based patients with HM. We found that longer eyes are more likely to have MMD, PPA, myopic tilted disc, ERM, and chances of MMD and MTM concurrently if AL $\geq$ 27.5 mm, and mCNV, MTM, myopic tilted disc, PS, DSM, VMA and chances of MMD, MTM, and DSM concurrently if AL $\geq$ 29.0 mm. We recommend a relatively closer follow-up with multimodal imaging for the timely diagnosis and treatment of sight-threatening complications in these extremely myopic individuals.

DATA AVAILABILITY STATEMENT

The raw data supporting the conclusions of this article will be made available by the authors, without undue reservation.

ETHICS STATEMENT

The studies involving human participants were reviewed and approved by SingHealth Institutional Review Board. The patients/participants provided their written informed consent to participate in this study.

SNEC RETINA GROUP

Anna Cheng Sim Tan, Beau James Fenner, Choi Mun Chan, Ian Yew San Yeo, Kelvin Yi Chong Teo, Ranjana Mathur, Shaun Sebastian Sim, Wiryasaputra Shaan, Andrew Shih Hsiang Tsai, Chong Lye Ang, Ning Cheung, Ting Shu Wei Daniel, Doric Wen Kuan Wong, Edmund Yick Mun Wong, Gavin Siew Wei Tan, and Hyungtaek Rim.

AUTHOR CONTRIBUTIONS

QH and CW conceptualized and supervised the study and obtained the data. KT, IL, YD, QW, DY, and VY curated the data and conducted formal analysis of data. All authors wrote, reviewed, edited, and approved the manuscript.

FUNDING

This work was supported in part by the SingHealth-Duke-NUS Eye Academic Clinical Program Nurturing Clinician Scientist Scheme (NCSS/R1364/50/2016, CW, Singapore), the National Eye Institute/National Institutes of Health (Grant K08 EY023595, QH, USA), and the National Medical Research Council (Grant CSA/MOH-000151/2019, QH, Singapore). The funding organizations had no role in the design or conduct of this research.

REFERENCES

1. Holden BA, Wilson DA, Jong M, Sankaridurg P, Fricke TR, Smith EL, et al. Myopia: a growing global problem with sight-threatening complications. *Community Eye Health.* (2015) 28:35–35.
2. Dolgin E. The myopia boom. *Nature.* (2015). 519:276–8. doi: 10.1038/519276a
3. Maduka Okafor FC, Okoye OI, Eze BI. Myopia: a review of literature. *Niger J Med.* (2009) 18:134–8. doi: 10.4314/njm.v18i2.45051
4. Meng W, Butterworth J, Malecaze F, Calvas P. Axial length of myopia: a review of current research. *Ophthalmologica.* (2011) 225:127–34. doi: 10.1159/000317072
5. Samarawickrama C, Mitchell P, Tong L, Gazzard G, Lim L, Wong TY, et al. Myopia-related optic disc and retinal changes in adolescent children from Singapore. *Ophthalmology.* (2011) 118:2050–7. doi: 10.1016/j.ophtha.2011.02.040
6. Ohno-Matsui K, Kawasaki R, Jonas JB, Cheung GCM, Saw SM, Verhoeven VJM, et al. International photographic classification and grading system for myopic maculopathy. *Am J Ophthalmol.* (2015). 159:877.e7–83.e7. doi: 10.1016/j.ajo.2015.01.022
7. Chang L, Pan C-W, Ohno-Matsui K, Lin X, Cheung GCM, Gazzard G, et al. Myopia-related fundus changes in Singapore adults with high myopia. *Am J Ophthalmol.* (2013). 155:991.e1–9.e1. doi: 10.1016/j.ajo.2013.01.016
8. Shimada N, Tanaka Y, Tokoro T, Ohno-Matsui K. Natural course of myopic traction maculopathy and factors associated with progression or resolution. *Am J Ophthalmol.* (2013). 156:948.e1–57.e1. doi: 10.1016/j.ajo.2013.06.031
9. Panozzo G, Mercanti A. Optical coherence tomography findings in myopic traction maculopathy. *Arch Ophthalmol.* (2004) 122:1455–60. doi: 10.1001/archopht.122.10.1455
10. Shimada N, Ohno-Matsui K, Baba T, Futagami S, Tokoro T, Mochizuki M. Natural course of macular retinoschisis in highly myopic eyes without macular hole or retinal detachment. *Am J Ophthalmol.* (2006) 142:497–500. doi: 10.1016/j.ajo.2006.03.048
11. Hoang QV, Chen C-L, Garcia-Arumi J, Sherwood PR, Chang S. Radius of curvature changes in spontaneous improvement of foveoschisis in highly myopic eyes. *Brit J Ophthalmol.* (2016) 100:222–6. doi: 10.1136/bjophthalmol-2015-306628
12. Tey KY, Wong QY, Dan YS, Tsai ASH, Ting DSW, Ang M, et al. Association of aberrant posterior vitreous detachment and pathologic tractional forces with myopic macular degeneration. *Invest Ophthalmol Vis Sci.* (2021) 62:7–7. doi: 10.1167/iovs.62.7.7
13. Organisation WH. *The Impact of Myopia and High Myopia: Report of the Joint World Health Organization-Brien Holden Vision Institute Global Scientific Meeting on Myopia*. Geneva: University of New South Wales (2017).
14. Xu L, Wang Y, Wang S, Wang Y, Jonas JB. High myopia and glaucoma susceptibility: the Beijing eye study. *Ophthalmology.* (2007) 114:216–20. doi: 10.1016/j.ophtha.2006.06.050
15. Sun J, Zhou J, Zhao P, Lian J, Zhu H, Zhou Y, et al. High prevalence of myopia and high myopia in 5060 chinese university students in Shanghai. *Invest Ophthalmol Vis Sci.* (2012) 53:7504–9. doi: 10.1167/iovs.11-8343
16. Holden BA, Fricke TR, Wilson DA, Jong M, Naidoo KS, Sankaridurg P, et al. Global prevalence of myopia and high myopia and temporal trends from 2000 through 2050. *Ophthalmology.* (2016) 123:1036–42. doi: 10.1016/j.ophtha.2016.01.006
17. Saka N, Ohno-Matsui K, Shimada N, Sueyoshi S, Nagaoka N, Hayashi W, et al. Long-term changes in axial length in adult eyes with pathologic myopia. *Am J Ophthalmol.* (2010). 150:562.e1–8.e1. doi: 10.1016/j.ajo.2010.05.009
18. Jonas JB, Wang YX, Dong L, Guo Y, Panda-Jonas S. Advances in myopia research anatomical findings in highly myopic eyes. *Eye Vis (Lond).* (2020) 7:45. doi: 10.1186/s40662-020-00210-6
19. Bartol-Puyal FdA, Isanta C, Ruiz-Moreno Ó, Abadia B, Calvo P, Pablo L. Distribution of choroidal thinning in high myopia, diabetes mellitus, and aging: a swept-source OCT study. *J Ophthalmol.* (2019). 2019:3567813. doi: 10.1155/2019/3567813
20. Krzizok TH, Schroeder BU. Quantification of recti eye muscle paths in high myopia. *Strabismus.* (2003) 11:213–20. doi: 10.1076/stra.11.4.213.24306

21. Cho B-J, Shin JY Yu HG. Complications of pathologic myopia. *Eye Contact Lens.* (2016) 42:9–15. doi: 10.1097/ICL.0000000000000223
22. Saw S-M, Matsumura S, Hoang QV. Prevention and management of myopia and myopic pathology. *Invest Ophthalmol Vis Sci.* (2019) 60:488–99. doi: 10.1167/iovs.18-25221
23. Moon Y, Lim HT. Relationship between peripapillary atrophy and myopia progression in the eyes of young school children. *Eye.* (2020) 35:665–71. doi: 10.1038/s41433-020-0945-6
24. Park K-A, Park S-E, Oh SY. Long-term changes in refractive error in children with myopic tilted optic disc compared to children without tilted optic disc. *Invest Ophthalmol Vis Sci.* (2013) 54:7865–70. doi: 10.1167/iovs.13-12987
25. Ohno-Matsui K, Jonas JB. Posterior staphyloma in pathologic myopia. *Prog Retin Eye Res.* (2019) 70:99–109. doi: 10.1016/j.preteyeres.2018.12.001
26. Fang D, Zhang Z, Wei Y, Wang L, Zhang T, Jiang X, et al. The morphological relationship between dome-shaped macula and myopic retinoschisis: a cross-sectional study of 409 highly myopic eyes. *Invest Ophthalmol Vis Sci.* (2020) 61:19–19. doi: 10.1167/iovs.61.3.19
27. Liao D-Y, Liu J-H, Zheng Y-P, Shiu H-W, Wang J-M, Chao H-M, et al. OCT proves that vitreomacular adhesion is significantly more likely to develop vision-threatening retinal complications than vitreomacular separation. *BMC Ophthalmol.* (2020) 20:163. doi: 10.1186/s12886-020-01416-x
28. Sayanagi K, Ikuno Y, Gomi F, Tano Y. Retinal vascular microfolds in highly myopic eyes. *Am J Ophthalmol.* (2005) 139:658–63. doi: 10.1016/j.ajo.2004.11.025
29. Ang M, Wong CW, Hoang QV, Cheung GCM, Lee SY, Chia A, et al. Imaging in myopia: potential biomarkers, current challenges and future developments. *Br J Ophthalmol.* (2019) 103:855–62. doi: 10.1136/bjophthalmol-2018-312866
30. Ohno-Matsui K. What is the fundamental nature of pathologic myopia? *Retina.* (2017) 37:1043–8. doi: 10.1097/IAE.0000000000001348
31. How AC, Tan GS, Chan YH, Wong TTL, Seah SK, Foster PJ, et al. Population prevalence of tilted and torted optic discs among an adult Chinese population in Singapore: the Tanjong Pagar Study. *Arch Ophthalmol.* (2009) 127:894–9. doi: 10.1001/archophthalmol.2009.134
32. Wong TY, Ohno-Matsui K, Leveziel N, Holz FG, Lai TY Yu HG, et al. Myopic choroidal neovascularisation: current concepts and update on clinical management. *Br J Ophthalmol.* (2015) 99:289–96. doi: 10.1136/bjophthalmol-2014-305131
33. Zaour N, Luciani L, Petrella RJ. Prevalence, incidence and characteristics of patients with choroidal neovascularization secondary to pathologic myopia in a representative canadian cohort. *Value Health.* (2014) 17:A283–4. doi: 10.1016/j.jval.2014.03.1652
34. Spaide RF. Staphyloma: Part 1. In: Spaide RF, Ohno-Matsui K, Yannuzzi LA, editors. *Pathologic Myopia*. New York, NY: Springer New York. (2014) p. 167–6. doi: 10.1007/978-1-4614-8338-0_12
35. Ellabban AA, Tsujikawa A, Muraoka Y, Yamashiro K, Oishi A, Ooto S, et al. Dome-shaped macular configuration: longitudinal changes in the sclera and choroid by swept-source optical coherence tomography over two years. *Am J Ophthalmol.* (2014). 158:1062–70. doi: 10.1016/j.ajo.2014.08.006
36. He Y, Nie A, Pei J, Ji Z, Jia J, Liu H, et al. Prevalence and causes of visual impairment in population more than 50 years old: the Shaanxi Eye Study. *Medicine.* (2020) 99:e20109. doi: 10.1097/MD.0000000000020109
37. Wong YL, Sabanayagam C, Ding Y, Wong CW, Yeo ACH, Cheung YB, et al. Prevalence, risk factors, and impact of myopic macular degeneration on visual impairment and functioning among adults in Singapore. *Invest Ophthalmol Vis Sci.* (2018) 59:4603–13. doi: 10.1167/iovs.18-24032
38. Chen SJ, Cheng CY Li AF, Peng KL, Chou P, Chiou SH, Hsu WM. Prevalence and associated risk factors of myopic maculopathy in elderly Chinese: The Shihpai Eye Study. *Invest Ophthalmol Vis Sci.* (2012) 53:4868–73. doi: 10.1167/iovs.12-9919
39. Gao LQ, Liu W, Liang YB, Zhang F, Wang JJ, Peng Y, et al. Prevalence and characteristics of myopic retinopathy in a rural Chinese adult population: The Handan Eye Study. *Arch Ophthalmol.* (2011) 129:1199–204. doi: 10.1001/archophthalmol.2011.230
40. Liu HH, Xu L, Wang YX, Wang S, You QS, Jonas JB. Prevalence and progression of myopic retinopathy in Chinese adults: The Beijing Eye Study. *Ophthalmology.* (2010) 117:1763–8. doi: 10.1016/j.ophtha.2010.01.020
41. Miyazaki M, Kiyohara Y, Yoshida A, Iida M, Nose Y, Ishibashi T. The 5-year incidence and risk factors for age-related maculopathy in a general Japanese population: The Hisayama Study. *Invest Ophthalmol Vis Sci.* (2005) 46:1907–10. doi: 10.1167/iovs.04-0923
42. Mitchell P, Smith W, Attebo K, Wang JJ. Prevalence of age-related maculopathy in Australia. The Blue Mountains Eye Study. *Ophthalmology.* (1995) 102:1450–60. doi: 10.1016/S0161-6420(95)30846-9
43. Jonas JB, Weber P, Nagaoka N, Ohno-Matsui K. Glaucoma in high myopia and parapapillary delta zone. *PLoS ONE.* (2017) 12:e0175120. doi: 10.1371/journal.pone.0175120
44. Ueda E, Yasuda M, Fujiwara K, Hashimoto S, Ohno-Matsui K, Hata J, et al. Trends in the prevalence of myopia and myopic maculopathy in a Japanese population: the Hisayama Study. *Invest Ophthalmol Vis Sci.* (2019) 60:2781–6. doi: 10.1167/iovs.19-26580
45. Chen X, Zhou D, Shen J, Wu Y, Sun Q, Dong J, et al. Prevalence and causes of visual impairment in adults in Binhu District, Wuxi, China. *Med Sci Monit.* (2018) 24:317–23. doi: 10.12659/MSM.908218
46. Choudhury F, Meuer SM, Klein R, Wang D, Torres M, Jiang X, et al. Chinese American Eye Study Group (2018). Prevalence and Characteristics of Myopic Degeneration in an Adult Chinese American Population: The Chinese American Eye Study. *Am J Ophthalmol.* 187, 3496-42. doi: 10.1016/j.ajo.2017.12.010
47. Hashimoto S, Yasuda M, Fujiwara K, Ueda E, Hata J, Hirakawa Y, et al. Association between axial length and myopic maculopathy: The Hisayama Study. *Ophthalmol Retina.* (2019) 3:867–73. doi: 10.1016/j.oret.2019.04.023
48. Wong Y-L, Sabanayagam C, Wong C-W, Cheung Y-B, Man REK, Yeo AC-H, et al. Six-year changes in myopic macular degeneration in adults of the Singapore Epidemiology of Eye Diseases Study. *Invest Ophthalmol Vis Sci.* (2020) 61:14. doi: 10.1167/iovs.61.4.14
49. Ohsugi H, Ikuno Y, Shoujou T, Oshima K, Ohsugi E, Tabuchi H. Axial length changes in highly myopic eyes and influence of myopic macular complications in Japanese adults. *PLoS ONE.* (2017) 12:e0180851. doi: 10.1371/journal.pone.0180851
50. Matsumura S, Sabanayagam C, Wong CW, Tan C-S, Kuo A, Wong YL, et al. Characteristics of myopic traction maculopathy in myopic Singaporean adults. *Brit J Ophthalmol.* (2020) 105:531–7. doi: 10.1136/bjophthalmol-2020-316182
51. Xia H-J, Wang W-J, Chen FE, Wu Y, Cai Z-Y, Chen W, et al. Long-term follow-up of the fellow eye in patients undergoing surgery on one eye for treating myopic traction maculopathy. *J Ophthalmol.* (2016) 2016:2989086. doi: 10.1155/2016/2989086
52. Wu PC, Chen YJ, Chen YH, Chen C-H, Shin S-J, Tsai C-L, et al. Factors associated with foveoschisis and foveal detachment without macular hole in high myopia. *Eye.* (2009) 23:356–61. doi: 10.1038/sj.eye.6703038
53. Baba T, Ohno-Matsui K, Futagami S, Yoshida T, Yasuzumi K, Kojima A, et al. Prevalence and characteristics of foveal retinal detachment without macular hole in high myopia. *Am J Ophthalmol.* (2003) 135:338–42. doi: 10.1016/S0002-9394(02)01937-2
54. Grossniklaus HE, Green WR. Pathologic findings in pathologic myopia. *Retina.* (1992) 12:127–33. doi: 10.1097/00006982-199212020-00009
55. Konidaris V, Androudi S, Brazitikos P. Myopic traction maculopathy: study with spectral domain optical coherence tomography and review of the literature. *Hippokratia.* (2009) 13:110–3.
56. Jonas JB, Gusek GC, Naumann GO. Optic disk morphometry in high myopia. *Graefes Arch Clin Exp Ophthalmol.* (1988) 226:587–90. doi: 10.1007/BF02169209
57. Xu L, Li Y, Wang S, Wang Y, Wang Y, Jonas JB. Characteristics of highly myopic eyes: the Beijing Eye Study. *Ophthalmology.* (2007) 114:121–6. doi: 10.1016/j.ophtha.2006.05.071
58. Nonaka A, Hangai M, Akagi T, Mori S, Nukada M, Nakano N, et al. Biometric features of peripapillary atrophy beta in eyes with high myopia. *Invest Ophthalmol Vis Sci.* (2011) 52:6706–13. doi: 10.1167/iovs.11-7580
59. Hwang YH, Yoo C, Kim YY. Characteristics of peripapillary retinal nerve fiber layer thickness in eyes with myopic optic disc tilt and rotation. *J Glaucoma.* (2012) 21:394–400. doi: 10.1097/IJG.0b013e3182182567
60. Nakazawa M, Kurotaki J, Ruike H. Longterm findings in peripapillary crescent formation in eyes with mild or moderate myopia. *Acta Ophthalmol.* (2008) 86:626–9. doi: 10.1111/j.1600-0420.2007.01139.x

61. Cheung N, Tan SP, Lee SY, Cheung GCM, Tan G, Kumar N, et al. Prevalence and risk factors for epiretinal membrane: the Singapore Epidemiology of Eye Disease study. *Br J Ophthalmol.* (2017) 101:371–6. doi: 10.1136/bjophthalmol-2016-308563
62. Tay E, Seah SK, Chan SP, Lim ATH, Chew SJ, Foster PJ, et al. Optic disk ovality as an index of tilt and its relationship to myopia and perimetry. *Am J Ophthalmol.* (2005) 139:247–52. doi: 10.1016/j.ajo.2004.08.076
63. Igarashi-Yokoi T, Shinohara K, Fang Y, Ogata S, Yoshida T, Imanaka T, et al. Prognostic factors for axial length elongation and posterior staphyloma in adults with high myopia: a Japanese Observational Study. *Am J Ophthalmol.* (2020) 225:76–85. doi: 10.1016/j.ajo.2020.11.023
64. Lee KM, Choung H-K, Kim M, Oh S, Kim SH. Change of β-zone parapapillary atrophy during axial elongation: boramae myopia cohort study report 3. *Invest Ophthalmol Vis Sci.* (2018) 59:4020–30. doi: 10.1167/iovs.18-24775
65. Dormegny L, Liu X, Philippakis E, Tadayoni R, Bocskei Z, Bourcier T, et al. Evolution of dome-shaped macula is due to differential elongation of the eye predominant in the peri-dome region. *Am J Ophthalmol.* (2021) 224:18–29. doi: 10.1016/j.ajo.2020.11.013

Conflict of Interest: The authors declare that the research was conducted in the absence of any commercial or financial relationships that could be construed as a potential conflict of interest.

Advantages of publishing in Frontiers

OPEN ACCESS
Articles are free to read for greatest visibility and readership

FAST PUBLICATION
Around 90 days from submission to decision

HIGH QUALITY PEER-REVIEW
Rigorous, collaborative, and constructive peer-review

TRANSPARENT PEER-REVIEW
Editors and reviewers acknowledged by name on published articles

Frontiers
Avenue du Tribunal-Fédéral 34
1005 Lausanne | Switzerland

Visit us: www.frontiersin.org
Contact us: frontiersin.org/about/contact

REPRODUCIBILITY OF RESEARCH
Support open data and methods to enhance research reproducibility

DIGITAL PUBLISHING
Articles designed for optimal readership across devices

FOLLOW US
@frontiersin

IMPACT METRICS
Advanced article metrics track visibility across digital media

EXTENSIVE PROMOTION
Marketing and promotion of impactful research

LOOP RESEARCH NETWORK
Our network increases your article's readership